Time-Domain Analysis of Sensor-to-Sensor Transmissibility Operators with Application to Fault Detection

by

Khaled F. Aljanaideh

A dissertation submitted in partial fulfillment
of the requirements for the degree of
Doctor of Philosophy
(Aerospace Engineering)
in The University of Michigan
2015

Doctoral Committee:

Professor Dennis S. Bernstein, Chair
Assistant Professor James R. Forbes
Professor Daniel J. Inman
Professor Jerome P. Lynch

وما بكم من نعمة فمن الله

© Khaled F. Aljanaideh 2015

All Rights Reserved

To my parents and my lovely wife

ACKNOWLEDGEMENTS

First of all, I would like to thank my advisor, Professor Dennis S. Bernstein for all of his guidance and support during the past five years. Also, I would like to thank my committee members Professor James R. Forbes, Professor Daniel J. Inman, and Professor Jerome P. Lynch for their helpful comments and suggestions, which greatly improved this work.

I am very grateful to my friends and colleagues at the University of Michigan: Ahmad Almutady, Anas Domi, Khaled AlAshmouny, Amjad Abu Jbara, Mahmoud Azzouny, Amr Alaa Eldin Ibrahim, Samer Kadous, Uros Kalabic, Rohit Gupta, Marco Ceze, Asad A. Ali, Jin Yan, Yousaf Rahman, Ray Yu, Ahmad Ansari, Shicong Dai, Ankit Goel. Thanks to Antai Xie for helping me with the acoustic experiment in Section 4.6 of this dissertation and thanks to Francois Hogan for helping me with the vibrating plate example in Section 4.5 of this dissertation.

I would like to thank Professor Johan Schoukens and others from Vrije Universiteit Brussel (VUB) for the one-month system identification summer course at VUB, Brussels, Belgium.

Finally, I would like to thank my family. Very special thanks goes to my parents for their love, support, and encouragement. My wife Hala for her love, patience, and support and my baby to come. My siblings Fadi, Saeb, Mohammad, Barah, Omar, and Ahmad, and my cousin Nabil. My nieces Dana, Razan, and Liana, and my nephews Yaman, Ghaith, Mohammad, Ahmad, Tamim, Omar, Karam, and Khaled. I am very grateful for the love and support I am surrounded by from all of you.

TABLE OF CONTENTS

LIST OF FIGURES

Figure

LIST OF APPENDICES

Appendix

ABSTRACT

Time-Domain Analysis of Sensor-to-Sensor Transmissibility Operators with Application to Fault Detection

by

Khaled F. Aljanaideh

Chair: Dennis S. Bernstein

In some applications, multiple measurements are available, but the driving input that gives rise to those outputs may be unknown. This raises the question as to whether it is possible to model the response of a subset of sensors based on the response of the remaining sensors without knowledge of the driving input. To address this issue, we develop time-domain sensor-to-sensor models that account for nonzero initial conditions. The sensor-to-sensor model is in the form of a transmissibility operator, that is, a rational function of the differentiation operator. What is essential in defining the transmissibility operator is that it must be independent of both the initial condition and inputs of the underlying system, which is assumed to be time-invariant. The development is carried out for both single-input, single-output and multi-input, multi-output transmissibility operators. These time-domain sensor-to-sensor models can be used for diagnostics and output prediction.

We show that transmissibility operators may be unstable, noncausal, and of unknown order. Therefore, to facilitate system identification, we consider a class of

models that can approximate transmissibility operators with these properties. This class of models consists of noncausal finite impulse response models based on a truncated Laurent expansion. These models are shown to approximate the Laurent expansion inside the annulus between the asymptotically stable pole of largest modulus and the unstable pole of smallest modulus. By delaying the measured pseudo output relative to the measured pseudo input, the identified finite impulse response model is a noncausal approximation of the transmissibility operator. The causal (backward-shift) part of the Laurent expansion is asymptotically stable since all of its poles are zero, while the noncausal (forward-shift) part of the Laurent expansion captures the unstable and noncausal components of the transmissibility operator.

This dissertation also develops a time-domain framework for both single-input, single-output and multi-input, multi-output transmissibilities that account for nonzero initial conditions for both force-driven and displacement-driven structures. We show that motion transmissibilities in force-driven and displacement-driven structures are equal when the locations of the forces and prescribed displacements are identical.

CHAPTER 1

Introduction

The traditional concept of input-output modeling distinguishes between inputs that evoke response and outputs that capture the response. In some applications, multiple measurements are available, but the driving input that gives rise to those outputs may be unknown. This raises the question as to whether it is possible to model the response of a subset of sensors based on the response of the remaining sensors without knowledge of the driving input. Since the “transfer function” between sensors does not arise as the forced response of a state space model, a sensor-to-sensor “transfer function” is not a transfer function in the usual sense. Therefore, we adopt the terminology *pseudo transfer function* (PTF) and *transmissibility operator* to refer to a dynamic model relating sensor signals, which are called the *pseudo input* and *pseudo output* [1–3]. Models of this type are widely used in structural modeling and health monitoring [4–12]. In structural vibration analysis, a transmissibility is a relation between a pair of sensor measurements of the same type, for example, displacements, accelerations, or forces [13].

In the most common setup, the transmissibility involves the motion of the point at which the force is prescribed. A more general notion of transmissibility arises in the case where neither of the displacement measurements coincides with the location of the applied force. This situation is of interest in applications where the applied force is unknown. Except for the case where one of the measurements is located at a node of a mode, the resulting transmissibility captures information about only the zeros (anti-resonances) in the structural response, and thus information about the modal resonances is not included in the model.

The potential usefulness of transmissibilities for applications such as damage detection [14–16] has led to increased interest in their properties. In [8, 17, 18], transmissibilities are used to update modal models, while computation and identification of transmissibilities is discussed in [11, 19, 20]. Transmissibilities are used in [21] to analyze the effects of structural coupling. Multi-input, multi-output (MIMO) transmissibilities are considered in [22], while the effect of distributed forces is analyzed in [20]. Finally, transmissibilities play a role in "operational modal analysis" [17, 23], which assumes stationary excitation.

While the transmissibility literature is extensive, a common feature is that transmissibilities are modeled in the frequency domain [7, 8, 11, 14, 17, 18, 22, 24–26]. A transmissibility is not a transfer function in the usual sense, however, since neither sensor captures the input driving the system except in the special case that one of the sensors measures the driving input. Consequently, a transmissibility does not have a state space realization with physically meaningful states.

Transmissibility estimates are traditionally obtained using frequency-domain methods [7, 8, 11, 14, 17, 18, 22, 24–26], which are based on the assumption that the response of the system consists entirely of the forced response and thus the free response is zero. For asymptotically stable systems, the free response decays exponentially, which suggests that measurements of the forced response can be obtained by using only data obtained after the free response is approximately zero. However, as shown in the following example, at the time at which data collection begins, a nonzero initial condition can degrade the accuracy of frequency-domain identification.

Example 1.1. Consider the discrete-time asymptotically stable system $\mathcal{S}$ with the state-space realization

$$A = \begin{bmatrix} -0.5 & 0.2 \\ 0 & 0.7 \end{bmatrix}, \quad B = \begin{bmatrix} 4 \\ 1 \end{bmatrix}, \quad C = [1.25 \quad -3], \quad D = 0. \tag{1.1}$$

Let $x(k) \in \mathbb{R}^2$ be the state vector and thus $x(0)$ is the initial state. Let $u_0 \in \mathbb{R}^{1\times N}$ be a realization of a stationary white random process with the gaussian distribution $\mathcal{N}(0,1)$. Define the input $u \triangleq [u_0\ u_0] \in \mathbb{R}^{1\times 2N}$, that is, u is formed by repeating u_0. Consider zero initial conditions, that is, $x(0) = 0$, and define $y(k) \triangleq Cx(k)$. If we split $y \in \mathbb{R}^{1\times 2N}$ into two halves, then the first half of y is the response of $\mathcal{S}$ due to the input u_0 and the zero initial condition $x(0)$, while the second half of y is the response of $\mathcal{S}$ due to the input u_0 and the possibly nonzero initial condition $x(N)$. Figure 1.1 shows a plot of the difference $y(k) - y(k+N)$, where $k = 0, \ldots, N-1$ and $N = 500$ time steps for a given realization u_0. Note that despite the initial condition $x(0) = 0$, the difference $y(k) - y(k+N)$ is not zero due to the fact that $x(N)$, which is the initial state when data collection begins at time $k = N$, is not zero.

Next, define $Y_{N,L} \triangleq [y(N) \ \cdots \ y(N+L-1)] \in \mathbb{R}^{1\times L}$ and $U_{N,L} \triangleq [u(N) \ \cdots \ u(N+L-1)] \in \mathbb{R}^{1\times L}$, and define $M_L \triangleq 2^p$, where p is the smallest integer such that $2^p \geq L$. For all $j = 1, \ldots, M_L$, let $\mathcal{S}(e^{\jmath\theta_j})$ be the frequency response of $\mathcal{S}$ at frequency θ_j. Moreover, for all $j = 1, \ldots, M_L$, let

$$\hat{S}_{N,L}(e^{\jmath\theta_j}) \triangleq \frac{1}{r}\sum_{i=1}^{r} \hat{S}_{N,L,i}(e^{\jmath\theta_j}), \tag{1.2}$$

where r is the number of experiments and $\hat{S}_{N,L,i}(e^{\jmath\theta_j})$ is the estimated value of $\mathcal{S}(e^{\jmath\theta_j})$ obtained from the i^{th} experiment using either frequency-domain or time-domain identification. For frequency-domain identification, $\hat{S}_{N,L,i}(e^{\jmath\theta_j})$ is obtained by finding the ratio of the cross power spectral density of $Y_{N,L}$ and $U_{N,L}$ to the power spectral density of $U_{N,L}$ for the i^{th} experiment. For time-domain identification, $\hat{S}_{N,L,i}(e^{\jmath\theta_j})$ is obtained

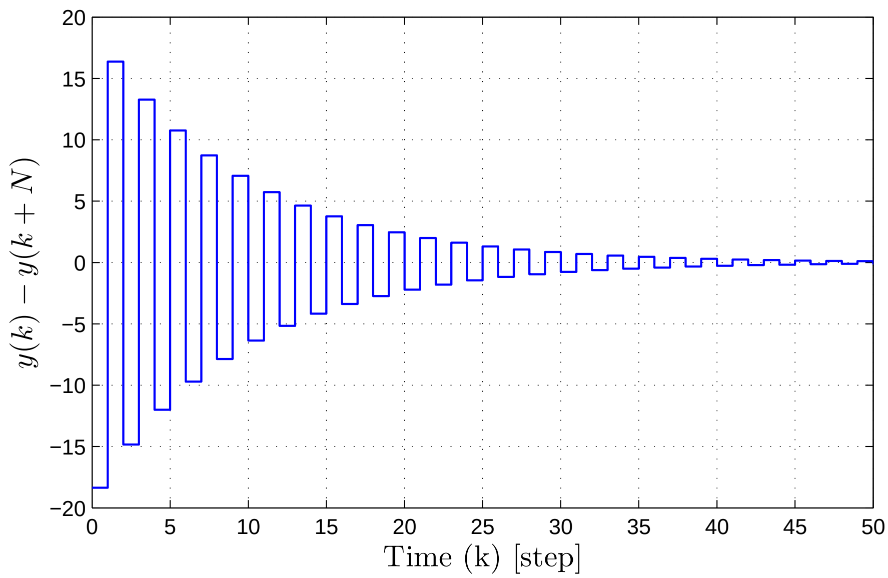

Figure 1.1: Plot of the difference $y(k) - y(k+N)$ for the system $\mathcal{S}$ with the realization (1.1), where $k = 0, \ldots, 50$, $N = 500$, $u = [u_0\ u_0]$ is the input, and $x(0) = 0$ is the initial state. This plot shows that the difference $y(k) - y(k+N)$ is not zero due to the fact that $x(N)$, which is the initial state of the system when we start collecting data at time $k = N$, is not zero.

by finding the frequency response of the estimated model obtained using least squares identification with the time-domain data $U_{N,L}$ and $Y_{N,L}$. Define the error

$$e_{N,L} \triangleq \left(\sum_{j=1}^{M_L} \left(|\mathcal{S}(e^{\jmath\theta_j})| - |\hat{\mathcal{S}}_{N,L}(e^{\jmath\theta_j})| \right)^2 \right)^{1/2}. \tag{1.3}$$

Figure 1.2 shows a plot of $e_{N,L}$ when using time-domain identification with $L = 10,000$ time steps and N varies from 1 to 1000. Moreover, Figure 1.2 shows a plot of $e_{N,L}$ when using frequency-domain identification with $L = 10,000$ and $L = 100,000$ time steps and N varies from 1 to 1000. The initial condition is $x(0) = [1000\ 1000]^{\mathrm{T}}$. Note from Figure 1.2 that the frequency response function (FRF) estimates obtained using time-domain identification are much better than the FRF estimates obtained using frequency-domain identification. Moreover, although we are using noise-free data, Figure 1.2 shows that waiting for the free response to decay does not help the

FRF estimates obtained using frequency-domain identification to converge to the true values. This is partly due to the nonzero initial condition $x(N)$, which occurs at the instant that data collection begins, and thus corrupts the estimates when using finite data sets. On the other hand, Figure 1.2 shows that the FRF estimates obtained using time-domain identification are not affected by the nonzero initial conditions. It can be seen that the significance of the transients depends on the magnitude of the initial state relative to the magnitude of the state under stationary conditions. ■

Another issue with frequency-domain identification techniques is leakage errors,

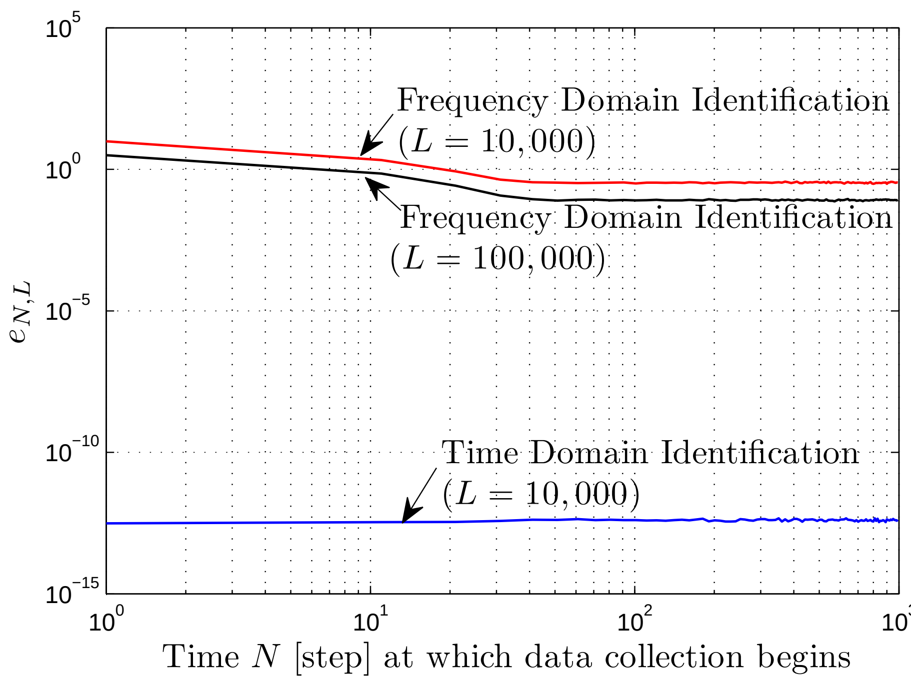

Figure 1.2: Plot of $e_{N,L}$ using time-domain identification with $L = 10,000$ time steps and frequency-domain identification with $L = 10,000$ and $L = 100,000$ time steps, N varies from 1 to 1000, and $r = 100$ experiments. The initial condition is $x(0) = [1000\ 1000]^{\mathrm{T}}$. Note that the FRF estimates obtained using time-domain identification are much better than the FRF estimates obtained using frequency-domain identification. Moreover, waiting for the free response to decay does not help the FRF estimates obtained using frequency-domain identification to converge to the true values, whereas the FRF estimates obtained using time-domain identification are not affected by the nonzero initial conditions.

which are unavoidable in the case of aperiodic random excitations [27]. Theorem 2.6 in [27] shows that leakage errors decrease as the number of samples increases, but it is not guaranteed that the leakage errors are small for finite data sets. Example 2.7 in [27] shows that leakage errors can be interpreted as a transient effect, that is, as the effect of a nonzero initial condition. Leakage errors can be avoided by using periodic excitation and measurements of an integer number of periods, which cannot be achieved if the excitation signal cannot be specified.

The goal of the present dissertation is to develop sensor-to-sensor models that account for nonzero initial conditions and thus are necessarily defined in the time domain. These models, which we call transmissibility operators, are rational functions of the differentiation operator. Accordingly, a transmissibility operator defines a differential equation involving the sensor signals. The internal state of the underlying input-output system loses its meaning within the context of a transmissibility operator. What is essential in defining the transmissibility operator, however, is that it must be independent of both the initial condition and inputs of the underlying system, which is assumed to be time-invariant.

The development of time-domain transmissibility models requires special attention to the cancellation of poles in the underlying structural model as well as the role of the initial conditions. The resulting model is not an input-output model in the usual sense, and therefore the notions of free and forced response do not apply. These issues were considered in [1, 28, 29] in terms of PTFs. The present dissertation goes beyond these papers by providing a significantly more detailed and rigorous treatment of transmissibility operators, including complete proofs.

Transmissibility operators are developed in this dissertation within the context of continuous-time, linear, time-invariant systems. We show that a transmissibility operator that relates sensor signals can be defined independently of the initial condition and inputs. This operator is a rational function of the differential operator, and thus represents a differential equation. However, the transmissibility operator cannot be defined in terms of the Laplace variable "s," due to the nonzero initial condition. This observation is a key conceptual contribution of this dissertation.

Transmissibility operators contain information about the zeros of the system and not the poles. Therefore, a nonminimum-phase zero in the pseudo-input channel of a transmissibility operator yields an unstable transmissibility operator. Moreover, if the pseudo-output channel of a transmissibility operator has more zeros than the pseudo-input channel, then the transmissibility operator is improper, and thus noncausal. However, neither instability nor causality has the usual meaning associated with transfer functions. Nevertheless, to facilitate system identification, we consider a class of models that can approximate transmissibility operators that may be unstable, noncausal, and of unknown order. This class of models consists of noncausal finite impulse response (FIR) models based on a truncated Laurent expansion. The causal (backward-shift) part of the Laurent expansion is asymptotically stable since all of its poles are zero, while the noncausal (forward-shift) part of the Laurent expansion captures the unstable and noncausal components of the transmissibility operator [30].

Linear systems inside a closed loop are similar to transmissibilities in several aspects, namely, they can be stable or unstable, of unknown order, and have bounded input and bounded output. Therefore, noncausal FIR models can be also used to identify linear systems inside a closed loop. A noncausal FIR model that approximates the Laurent series of an unstable plant involves both positive and negative powers of the Z-transform variable z. The negative powers approximate the stable part of the plant outside of a disk (that is, inside a punctured plane), whereas the positive powers approximate the unstable part of the plant inside a disk. Inside the common region, which is an annulus, the Laurent series represents a noncausal model, as evidenced by the positive powers of z.

To identify an unstable plant inside a stabilizing feedback loop, the measured output can be delayed relative to the measured input to obtain an FIR model that is a noncausal approximation of the unstable plant. The transfer function of this noncausal FIR model approximates the Laurent series of the plant inside the maximal annulus of analyticity lying between the smallest disk containing the asymptotically stable poles and the smallest punctured plane containing the unstable poles.

One of the contributions of the present dissertation is a fully justified treatment of closed-loop identification of unstable plants using noncausal FIR models. This work presents analysis and proofs that connect the Laurent series of a transfer function and an associated noncausal FIR model. These results are developed in the context of identifying noncausal models and are needed to establish a rigorous connection between the estimated noncausal FIR model and the impulse response of the system.

The theoretical basis for this work is given by Theorem 2, which provides necessary and sufficient conditions under which the coefficients of the Laurent series are square summable. Most importantly, Theorem 2 shows that there is exactly one maximal annulus corresponding to which the coefficients of the Laurent series are bounded. This fact suggests that the objective of identifying the unstable system G in closed loop by estimating the coefficients of a Laurent series of G is meaningful only for the Laurent series corresponding to this special annulus, since otherwise the unidentified (that is, truncated) coefficients are unbounded. For unstable plants, the Markov parameters, which are the coefficients of the Laurent series in the maximal punctured plane, are unbounded. For unstable plants, however, the Laurent series in the special annulus (as opposed to the punctured plane) has terms involving positive powers of z, which represent a noncausal model. The coefficients of the negative powers of z are Markov parameters of the stable part of the transfer function.

1.1 Current Fault Detection Techniques and the Proposed Approach

Different fault detection techniques have been introduced in the literature [31–44]. In some cases, health monitoring can be assessed by exciting the system in a controlled manner, using a plant model and observer to predict the response, and by comparing the measured response to the prediction [34, 35, 45–50]. This approach, known as active fault detection, is based on residual generation. In contrast, passive fault detection detects faults by analyzing the sensors signals alone and searching for anomalies [51–58].

In this dissertation we focus on a technique for fault detection called *sensor-to-sensor identification* (S2SID). S2SID is neither active nor passive as defined above. Instead, S2SID takes advantage of freely available and unknown external (ambient) excitation to identify a sensor-to-sensor model (i.e. a PTF or a transmissibility operator), which is independent of the excitation signal. In the presence of subsequent unknown external excitation, the identified PTF is used to compute sensor-to-sensor residuals, which are used to detect and diagnose faults in sensors or systems dynamics. The sensor-to-sensor residual is the discrepancy between the predicted sensor output (based on the PTF) and the actual measurements.

The novel feature of this approach is the way external excitation is taken advantage of to identify a PTF between sensor signals. In particular, the external excitation, whether it is provided by the environment or by actuators, need not be measured or precisely controlled. Consequently, freely available ambient noise (such as flow around an aircraft wing) can play a useful role in PTF identification. Most importantly, the identified PTF is independent of the excitation; this means that the PTF identified using one data set can be used for fault detection with a different data set; for both data sets, the external excitation can be completely unknown.

The ability to take advantage of unknown external excitation along with the fact that the PTF is independent of that excitation gives the method considerable flexibility in practice by alleviating the need for a known or controlled excitation. This feature is the key benefit of the proposed approach relative to residual-based fault-detection methods that require known external excitation.

Excitation-free techniques for fault detection were also used in [1, 14–16, 28, 29, 59–61]. Transmissibility estimates obtained using frequency-domain methods were used for fault detection in [14–16]. As we showed before, this approach ignores the effect of nonzero initial conditions and requires periodic excitations to avoid leakage errors. These issues are avoided in the present dissertation by developing a time-domain framework for transmissibilities that accounts for nonzero initial conditions and is independent of both the initial condition and inputs of the underlying system. Discrete-time PTFs were developed in [1, 28, 29] and a μ-Markov model is used to identify them. A fault is detected if a sudden change in the identified Markov parameters of the PTF occurs. Excitation-free fault detection was also used in [59–61], where a SISO autoregressive model with exogenous input (ARX) between a pair of sensors is identified to detect spike faults in wireless sensor networks. The approaches in [1, 28, 29, 59–61] do not consider the possible noncausal relationships between different sensors. Moreover, underestimating or overestimating the order of the μ-Markov or ARX models may yield inaccurate estimates, which can affect the fault detection process. We show that the proposed approach circumvents the above issues by using noncausal FIR models to identify PTFs.

1.2 Contributions

In the following, we list the major contributions of this dissertation.

- We develop a time-domain framework for MIMO transmissibilities that accounts for nonzero initial conditions as well as cancellation of the common factor occurring in the underlying state space model. We show that transmissibility operators are independent of both the initial condition and inputs of the underlying system, which is assumed to be time-invariant [62].

- We show that transmissibility operators may be unstable, noncausal, and of unknown order. We show that noncausal FIR models can be used to approximate transmissibility operators and unstable systems in closed loop. Noncausal FIR models are used for closed-loop identification of unstable systems [30].

- Transmissibility operators can be effectively used for fault detection and output prediction when the excitation signal is unknown. Application to health monitoring of aircraft sensors [63], and the dynamics of acoustic systems are considered.

- We derive continuous time-domain models for transmissibility operators in force-driven and displacement-driven structures. We show that motion transmissibilities in force-driven and displacement-driven structures are equal when the locations of the forces and prescribed displacements are identical [64].

1.3 Dissertation Outline

The dissertation is organized as follows. We develop a time-domain framework for transmissibilities in Chapter 2. We show that transmissibility operators are independent of both the initial condition and inputs of the underlying system, which is assumed to be time-invariant. The cancellation of a common factor that appears in the numerator and denominator of the transmissibility operator is discussed. SISO and MIMO transmissibility operators are illustrated by examples.

In Chapter 3 we use noncausal FIR models for closed-loop identification of unstable systems. In this chapter we first motivate the use of noncausal FIR models for identifying systems of unknown order. Then, we provide analysis of the Laurent series of a rational function and the connection to noncausal FIR models. We show the identification architecture using least squares (LS), instrumental variables (IV), and prediction error methods (PEM). Numerical examples are presented to compare noncausal FIR models to infinite impulse response (IIR) models for identification of unstable systems in closed loop. A procedure to estimate the order of the system from its identified noncausal FIR model is shown. Then we show how to construct an IIR model of the system from its identified noncausal FIR model.

Chapter 4 shows that noncausal FIR models can be used to approximate transmissibility operators. A procedure to estimate the number of unknown excitations using only output measurements is presented. Moreover, PEMs with noncausal FIR models are used to identify transmissibility operators. The NASA Generic Transport Model (GTM) [65, 66] is used to simulate the fully nonlinear aircraft dynamics for data generation and rate-gyro measurements are used along with sideslip-angle measurements to construct a transmissibility operator. We then use the transmissibility operator for health monitoring of the aircraft gyros. The case of gyro drift and deadzone nonlinearity are considered as illustrative examples. Next, we consider an experimental setup consists of a drum with two speakers and four microphones. Each speaker is an actuator, and each microphone is a sensor that measures the acoustic response at its location. Two plastic pieces are placed inside the drum, and these can be removed during operation to emulate changes to the system. A transmissibility operator is constructed from the four microphones and is used for health monitoring of the dynamics of the drum.

Chapter 5 discusses transmissibilities in force-driven and displacement-driven structures. We derive time-domain models for transmissibility operators in force-driven and displacement-driven structures. We show the equality of motion transmissibilities in force-driven and displacement-driven structures with identical inputs and outputs when the force and prescribed motion are applied to the same location. We introduce examples for both lumped and distributed systems.

Chapter 6 considers the problem of identifying a SISO PTF for a two-output Hammerstein system. We identify the Markov parameters of this PTF and compare them to the Markov parameters of the PTF constructed from the same system without the Hammerstein nonlinearities [67].

Finally, conclusions and future work are presented in Chapter 7.

CHAPTER 2

Time-Domain Analysis of Sensor-to-Sensor Transmissibility Operators

2.1 Introduction

Transmissibility operators are developed in the present chapter within the context of continuous-time, linear, time-invariant systems. We show that a transmissibility operator that relates sensor signals can be defined independently of the initial condition and inputs. This operator is a rational function of the differential operator, and thus represents a differential equation. However, the transmissibility operator cannot be defined in terms of the Laplace variable "s," due to the nonzero initial condition. This observation is a key conceptual contribution of this dissertation.

A feature of the transmissibility operator is the presence of a common factor in its numerator and denominator. One of the main technical contributions of this dissertation is a proof that this factor can be canceled; without such a proof, such cancellation can potentially exclude solutions of the transmissibility differential equation and render it invalid. Since this proof is lengthy, several technical lemmas are sequestered in the appendices. An earlier version of the proof was introduced in [68] in terms of discrete-time SISO PTFs. In the present dissertation the proof is extended to cover the continuous-time MIMO case.

The contents of this chapter are as follows. In Section 2.2 we derive a time-domain model for MIMO transmissibility operators. In Section 2.3 we discuss the cancellation of a common factor that appears in the numerator and denominator of the transmissibility operator. SISO and MIMO transmissibility operators are illustrated in Section 2.4. Finally, we present conclusions in Section 2.5.

2.2 Time-Domain Transmissibility Operator

Consider the MIMO linear system

$$\dot{x}(t) = Ax(t) + Bu(t), \tag{2.1}$$

$$x(0) = x_0, \tag{2.2}$$

$$y(t) = Cx(t) + Du(t), \tag{2.3}$$

where $A \in \mathbb{R}^{n\times n}, B \in \mathbb{R}^{n\times m}, C \in \mathbb{R}^{p\times n}$, $D \in \mathbb{R}^{p\times m}$ and $p > m$. No assumptions are made about the controllability of (A, B) or the observability of (A, C). Let

$$C = \begin{bmatrix} C_{\rm i} \\ C_{\rm o} \end{bmatrix}, \quad D = \begin{bmatrix} D_{\rm i} \\ D_{\rm o} \end{bmatrix}, \tag{2.4}$$

where $C_{\rm i} \in \mathbb{R}^{m\times n}, C_{\rm o} \in \mathbb{R}^{(p-m)\times n}, D_{\rm i} \in \mathbb{R}^{m\times m}$, and $D_{\rm o} \in \mathbb{R}^{(p-m)\times m}$. Then,

$$y_{\rm i}(t) \triangleq C_{\rm i}x(t) + D_{\rm i}u(t) \in \mathbb{R}^m, \tag{2.5}$$

$$y_{\rm o}(t) \triangleq C_{\rm o}x(t) + D_{\rm o}u(t) \in \mathbb{R}^{p-m}, \tag{2.6}$$

$$y(t) \triangleq \begin{bmatrix} y_{\rm i}(t) \\ y_{\rm o}(t) \end{bmatrix} \in \mathbb{R}^p. \tag{2.7}$$

The goal is to obtain a transmissibility function relating $y_{\rm i}$ and $y_{\rm o}$ that is independent of both the initial condition x_0 and the input u. As a first attempt at obtaining such a function, assuming $m = 1$ and $p = 2$ and letting $b \in \mathbb{R}^n$, $c_{\rm i}, c_{\rm o} \in \mathbb{R}^{1\times n}$, and $d_{\rm i}, d_{\rm o} \in \mathbb{R}$, we consider the system

$$\dot{x}(t) = Ax(t) + bu(t), \tag{2.8}$$

$$y_{\rm i}(t) = c_{\rm i}x(t) + d_{\rm i}u(t), \tag{2.9}$$

$$y_{\rm o}(t) = c_{\rm o}x(t) + d_{\rm o}u(t). \tag{2.10}$$

Transforming (2.9) and (2.10) to the Laplace domain yields

$$\hat{y}_{\rm i}(s) = c_{\rm i}(sI - A)^{-1}x_0 + [c_{\rm i}(sI - A)^{-1}b + d_{\rm i}]\hat{u}(s), \tag{2.11}$$

$$\hat{y}_{\rm o}(s) = c_{\rm o}(sI - A)^{-1}x_0 + [c_{\rm o}(sI - A)^{-1}b + d_{\rm o}]\hat{u}(s), \tag{2.12}$$

respectively, and thus

$$\frac{\hat{y}_{\rm o}(s)}{\hat{y}_{\rm i}(s)} = \frac{c_{\rm o}(sI - A)^{-1}x_0 + [c_{\rm o}(sI - A)^{-1}b + d_{\rm o}]\hat{u}(s)}{c_{\rm i}(sI - A)^{-1}x_0 + [c_{\rm i}(sI - A)^{-1}b + d_{\rm i}]\hat{u}(s)}. \tag{2.13}$$

Note that, if x_0 is zero, then $\hat{u}(s)$ can be cancelled in (2.13), and $\hat{y}_{\rm o}(s)$ and $\hat{y}_{\rm i}(s)$ are related by a transmissibility that is independent of the input. However, if x_0 is not zero, then $\hat{u}(s)$ cannot be canceled in (2.13).

Alternatively, we consider a time-domain analysis using the differentiation operator $\mathbf{p} = {\rm d}/{\rm d}t$ instead of the Laplace variable s. Multiplying (2.5), (2.6) by $\det(\mathbf{p}I - A)$, where $\mathbf{p}I$ denotes $\mathrm{diag}(\mathbf{p}, \ldots, \mathbf{p})$, and using the fact that

$$\det(\mathbf{p}I - A)I_n = \mathrm{adj}(\mathbf{p}I - A)(\mathbf{p}I - A) \tag{2.14}$$

yields the differential equation

$$\begin{aligned}
\det(\mathbf{p}I - A)y_{\mathrm{i}}(t) &= C_{\mathrm{i}}\det(\mathbf{p}I - A)I_n x(t) + D_{\mathrm{i}}\det(\mathbf{p}I - A)u(t) \\
&= C_{\mathrm{i}}\mathrm{adj}(\mathbf{p}I - A)(\mathbf{p}I - A)x(t) + D_{\mathrm{i}}\det(\mathbf{p}I - A)u(t) \\
&= C_{\mathrm{i}}\mathrm{adj}(\mathbf{p}I - A)(\dot{x}(t) - Ax(t)) + D_{\mathrm{i}}\det(\mathbf{p}I - A)u(t) \\
&= [C_{\mathrm{i}}\mathrm{adj}(\mathbf{p}I - A)B + D_{\mathrm{i}}\det(\mathbf{p}I - A)]u(t). \qquad (2.15)
\end{aligned}$$

Similarly,

$$\det(\mathbf{p}I - A)y_{\mathrm{o}}(t) = [C_{\mathrm{o}}\mathrm{adj}(\mathbf{p}I - A)B + D_{\mathrm{o}}\det(\mathbf{p}I - A)]u(t). \qquad (2.16)$$

For convenience, we define

$$G_{\mathrm{i}}(\mathbf{p}) \triangleq C_{\mathrm{i}}(\mathbf{p}I - A)^{-1}B + D_{\mathrm{i}} \in \mathbb{R}^{m\times m}(\mathbf{p}), \qquad (2.17)$$

$$G_{\mathrm{o}}(\mathbf{p}) \triangleq C_{\mathrm{o}}(\mathbf{p}I - A)^{-1}B + D_{\mathrm{o}} \in \mathbb{R}^{(p-m)\times m}(\mathbf{p}), \qquad (2.18)$$

and rewrite (2.15), (2.16) as

$$y_{\mathrm{i}}(t) = G_{\mathrm{i}}(\mathbf{p})u(t), \quad y_{\mathrm{o}}(t) = G_{\mathrm{o}}(\mathbf{p})u(t), \qquad (2.19)$$

respectively, which are interpreted as the differential equations (2.15), (2.16), respectively. Note that (2.19) includes both the free response due to x_0 and the forced response due to u. In the subsequent analysis, we omit the argument "t" where no ambiguity can arise.

Defining

$$\Gamma_{\rm i}(\mathbf{p}) \stackrel{\triangle}{=} C_{\rm i}\mathrm{adj}(\mathbf{p}I - A)B + D_{\rm i}\delta(\mathbf{p}) \in \mathbb{R}^{m\times m}[\mathbf{p}], \tag{2.20}$$

$$\Gamma_{\rm o}(\mathbf{p}) \stackrel{\triangle}{=} C_{\rm o}\mathrm{adj}(\mathbf{p}I - A)B + D_{\rm o}\delta(\mathbf{p}) \in \mathbb{R}^{(p-m)\times m}[\mathbf{p}], \tag{2.21}$$

$$\delta(\mathbf{p}) \stackrel{\triangle}{=} \det(\mathbf{p}I - A), \tag{2.22}$$

we can rewrite (2.15), (2.16) as

$$\delta(\mathbf{p})y_{\rm i} = \Gamma_{\rm i}(\mathbf{p})u, \tag{2.23}$$

$$\delta(\mathbf{p})y_{\rm o} = \Gamma_{\rm o}(\mathbf{p})u, \tag{2.24}$$

respectively. Multiplying (2.23) by $\mathrm{adj}\,\Gamma_{\rm i}(\mathbf{p})$ from the left yields

$$\delta(\mathbf{p})\,\mathrm{adj}\,\Gamma_{\rm i}(\mathbf{p})y_{\rm i} = [\mathrm{adj}\,\Gamma_{\rm i}(\mathbf{p})]\,\Gamma_{\rm i}(\mathbf{p})u = \det\Gamma_{\rm i}(\mathbf{p})u. \tag{2.25}$$

Next, multiplying (2.24) by $\det\Gamma_{\rm i}(\mathbf{p})$ yields

$$[\det\Gamma_{\rm i}(\mathbf{p})]\,\delta(\mathbf{p})y_{\rm o} = [\det\Gamma_{\rm i}(\mathbf{p})]\,\Gamma_{\rm o}(\mathbf{p})u. \tag{2.26}$$

Substituting the left hand side of (2.25) in (2.26) yields

$$\delta(\mathbf{p})\det\Gamma_{\rm i}(\mathbf{p})y_{\rm o} = \delta(\mathbf{p})\Gamma_{\rm o}(\mathbf{p})\,\mathrm{adj}\,\Gamma_{\rm i}(\mathbf{p})y_{\rm i}. \tag{2.27}$$

In the case $m = 1$ and $p = 2$, (2.27) becomes

$$\delta(\mathbf{p})\Gamma_{\rm i}(\mathbf{p})y_{\rm o} = \delta(\mathbf{p})\Gamma_{\rm o}(\mathbf{p})y_{\rm i}. \tag{2.28}$$

Definition 1. Assume that $\Gamma_{\rm i}(\mathbf{p})$ is nonsingular. Then, the *transmissibility operator* from $y_{\rm i}$ to $y_{\rm o}$ is the operator

$$\mathcal{T}(\mathbf{p}) \triangleq \frac{\delta(\mathbf{p})}{\delta(\mathbf{p})\det\Gamma_{\rm i}(\mathbf{p})}\Gamma_{\rm o}(\mathbf{p})\mathrm{adj}\,\Gamma_{\rm i}(\mathbf{p}). \tag{2.29}$$

Note that (2.29) is independent of the input u and the initial condition x_0. Using (2.29), the differential equation (2.27) can be written as

$$y_{\rm o} = \mathcal{T}(\mathbf{p})y_{\rm i}. \tag{2.30}$$

Since $\Gamma_{\rm i}(\mathbf{p})$ is nonsingular, (2.29) can be written as

$$\mathcal{T}(\mathbf{p}) = \frac{\delta(\mathbf{p})}{\delta(\mathbf{p})}\Gamma_{\rm o}(\mathbf{p})\Gamma_{\rm i}{}^{-1}(\mathbf{p}). \tag{2.31}$$

Unlike common factors in the complex number s, common factors in the differentiation operator $\mathbf{p}$ cannot always be canceled. In particular, the following examples show that canceling common factors may exclude solutions of the original differential equation.

Example 2.2.1. Consider the signals $y_{\rm i}(t) = t + 1$ and $y_{\rm o}(t) = t + 5$. Operating on $y_{\rm i}(t)$ and $y_{\rm o}(t)$ with $\mathbf{p}$ yields $\mathbf{p}y_{\rm i}(t) = \dot{y}_{\rm i}(t) = 1 = \dot{y}_{\rm o}(t) = \mathbf{p}y_{\rm o}(t)$. Hence $\mathbf{p}y_{\rm i} = \mathbf{p}y_{\rm o}$. However, $y_{\rm i} \neq y_{\rm o}$. ■

Example 2.2.2. Consider the signals $y_{\rm i}(t) = 1$ and $y_{\rm o}(t) = 1 + e^{-t}$. Operating on $y_{\rm i}(t)$ and $y_{\rm o}(t)$ with $\mathbf{p} + 1$ yields $(\mathbf{p} + 1)y_{\rm i}(t) = \dot{y}_{\rm i}(t) + y_{\rm i}(t) = 1 = \dot{y}_{\rm o}(t) + y_{\rm o}(t) = (\mathbf{p} + 1)y_{\rm o}(t)$. Hence $(\mathbf{p} + 1)y_{\rm i} = (\mathbf{p} + 1)y_{\rm o}$. However, $y_{\rm i} \neq y_{\rm o}$. ■

Despite Examples 2.2.1 and 2.2.2, we show in Section 2.3 that the common factor $\delta(\mathbf{p})$ in (2.29) can be canceled without excluding any solutions of (2.25).

2.3 Cancellation of the Common Factor $\delta(\mathbf{p})$

We now show that (2.27) holds if and only if (2.27) holds with the factor $\delta(\mathbf{p})$ cancelled. Since sufficiency is immediate, the goal of this section is to prove necessity. This result allows us to reduce the order of $\mathcal{T}(\mathbf{p})$ without excluding any solutions of (2.27).

Theorem 1. $y_{\rm i}$ and $y_{\rm o}$ satisfy

$$\det \Gamma_{\rm i}(\mathbf{p}) y_{\rm o} = \Gamma_{\rm o}(\mathbf{p}) \mathrm{adj}\, \Gamma_{\rm i}(\mathbf{p}) y_{\rm i}. \tag{2.32}$$

Proof. Let

$$B = \begin{bmatrix} b_1 & \cdots & b_m \end{bmatrix}, \quad C_{\rm i} = \begin{bmatrix} c_{{\rm i},1} \\ \vdots \\ c_{{\rm i},m} \end{bmatrix}, \quad C_{\rm o} = \begin{bmatrix} c_{{\rm o},1} \\ \vdots \\ c_{{\rm o},p-m} \end{bmatrix},$$

where, for all $i \in \{1, \ldots, m\}$, $b_i \in \mathbb{R}^n$ and $c_{{\rm i},i} \in \mathbb{R}^{1\times n}$, and, for all $j \in \{1, \ldots, p-m\}$, $c_{{\rm o},j} \in \mathbb{R}^{1\times n}$. Moreover, for all $i, j \in \{1, \ldots, m\}$, let

$$c_{{\rm i},i} \mathrm{adj}(\mathbf{p} I_n - A) b_j + D_{{\rm i},i,j} \delta(\mathbf{p}) = \sum_{k=0}^{n} \mu_{i,j,k} \mathbf{p}^k,$$

where $D_{\mathrm{i},i,j}$ is the (i,j) entry of D_{i}. Then, we can write

$$\Gamma_{\mathrm{i}}(\mathbf{p}) = \begin{bmatrix} \sum_{i=0}^{n} \mu_{1,1,i}\mathbf{p}^i & \cdots & \sum_{i=0}^{n} \mu_{1,m,i}\mathbf{p}^i \\ \vdots & \ddots & \vdots \\ \sum_{i=0}^{n} \mu_{m,1,i}\mathbf{p}^i & \cdots & \sum_{i=0}^{n} \mu_{m,m,i}\mathbf{p}^i \end{bmatrix}$$

$$= \begin{bmatrix} \mu_{1,1}(\mathbf{p}) & \cdots & \mu_{1,m}(\mathbf{p}) \\ \vdots & \ddots & \vdots \\ \mu_{m,1}(\mathbf{p}) & \cdots & \mu_{m,m}(\mathbf{p}) \end{bmatrix}, \tag{2.33}$$

where, for all $i,j \in \{1,\ldots,m\}$, $\mu_{i,j}(\mathbf{p}) \triangleq \sum_{k=0}^{n} \mu_{i,j,k}\mathbf{p}^k$. Then, it follows from (2.33) that

$$\operatorname{adj}\Gamma_{\mathrm{i}}(\mathbf{p}) = \begin{bmatrix} T_{1,1}(\mathbf{p}) & \cdots & T_{m,1}(\mathbf{p}) \\ \vdots & \cdots & \vdots \\ T_{1,m}(\mathbf{p}) & \cdots & T_{m,m}(\mathbf{p}) \end{bmatrix}, \tag{2.34}$$

where

$$T_{i,j}(\mathbf{p}) \triangleq (-1)^{i+j} \det \Gamma_{\mathrm{i}_{[i,j]}}(\mathbf{p}),$$

and $\Gamma_{\mathrm{i}_{[i,j]}}(\mathbf{p}) \in \mathbb{R}^{(m-1)\times(m-1)}[\mathbf{p}]$ denotes $\Gamma_{\mathrm{i}}(\mathbf{p})$ with the i^{th} row and j^{th} column removed.

For all $i \in \{1,\ldots,p-m\}$ and $j \in \{1,\ldots,m\}$, let

$$c_{\mathrm{o},i}\mathrm{adj}(\mathbf{p}I_n - A)b_j + D_{\mathrm{o},i,j}\delta(\mathbf{p}) = \sum_{k=0}^{n} \nu_{i,j,k}\mathbf{p}^k,$$

where $D_{\mathrm{o},i,j}$ is the (i,j) entry of D_o. Then, we can write

$$\Gamma_\mathrm{o}(\mathbf{p}) = \begin{bmatrix} \sum_{i=0}^{n} \nu_{1,1,i}\mathbf{p}^i & \cdots & \sum_{i=0}^{n} \nu_{1,m,i}\mathbf{p}^i \\ \vdots & \ddots & \vdots \\ \sum_{i=0}^{n} \nu_{p-m,1,i}\mathbf{p}^i & \cdots & \sum_{i=0}^{n} \nu_{p-m,m,i}\mathbf{p}^i \end{bmatrix} = \begin{bmatrix} \nu_{1,1}(\mathbf{p}) & \cdots & \nu_{1,m}(\mathbf{p}) \\ \vdots & \cdots & \vdots \\ \nu_{p-m,1}(\mathbf{p}) & \cdots & \nu_{p-m,m}(\mathbf{p}) \end{bmatrix}, \tag{2.35}$$

where, for all $i \in \{1,\ldots,p-m\}$ and $j \in \{1,\ldots,m\}$, $\nu_{i,j}(\mathbf{p}) \triangleq \sum_{k=0}^{n} \nu_{i,j,k}\mathbf{p}^k$.

Let $u = \begin{bmatrix} u_1 & \cdots & u_m \end{bmatrix}^\mathrm{T}$. Define

$$y_\mathrm{i} \triangleq \begin{bmatrix} y_{\mathrm{i},1} & \cdots & y_{\mathrm{i},m} \end{bmatrix}^\mathrm{T}, \quad y_\mathrm{o} \triangleq \begin{bmatrix} y_{\mathrm{o},1} & \cdots & y_{\mathrm{o},p-m} \end{bmatrix}^\mathrm{T}.$$

Multiplying (2.23) by $\operatorname{adj}\Gamma_\mathrm{i}(\mathbf{p})$ yields

$$\delta(\mathbf{p})\operatorname{adj}\Gamma_\mathrm{i}(\mathbf{p})y_\mathrm{i} = \det\Gamma_\mathrm{i}(\mathbf{p})u.$$

Therefore, for all $i \in \{1,\ldots,m\}$, we have

$$\delta(\mathbf{p})\sum_{j=1}^{m} T_{j,i}(\mathbf{p})y_{\mathrm{i},j} = \det\Gamma_\mathrm{i}(\mathbf{p})u_i. \tag{2.36}$$

Using (2.35), for all $k \in \{1,\ldots,p-m\}$, (2.24) implies that

$$\delta(\mathbf{p})y_{\mathrm{o},k} = \sum_{i=1}^{m} \nu_{k,i}(\mathbf{p})u_i. \tag{2.37}$$

Note that, for all $k \in \{1, \ldots, p-m\}$ and all $t \geq 0$,

$$y_{\mathrm{o},k,\mathrm{forced}}(t) = \sum_{i=1}^{m} y_{\mathrm{o},k,i,\mathrm{forced}}(t), \tag{2.38}$$

where, for all $k \in \{1, \ldots, p-m\}$ and all $i \in \{1, \ldots, m\}$,

$$y_{\mathrm{o},k,i,\mathrm{forced}}(t) \triangleq \int_0^t c_{\mathrm{o},k} e^{A(t-\tau)} b_i u_i(\tau) \mathrm{d}\tau + D_{\mathrm{o},k,i} u_i(t).$$

Moreover, note that, for all $t \geq 0$,

$$y_{\mathrm{o},k,\mathrm{free}}(t) = c_{\mathrm{o},k} e^{At} x_0 = \sum_{i=1}^{m} y_{\mathrm{o},k,i,\mathrm{free}}(t), \tag{2.39}$$

where

$$y_{\mathrm{o},k,i,\mathrm{free}}(t) \triangleq \frac{1}{m} c_{\mathrm{o},k} e^{At} x_0. \tag{2.40}$$

For all $k \in \{1, \ldots, p-m\}$ and all $i \in \{1, \ldots, m\}$, define

$$y_{\mathrm{o},k,i} \triangleq y_{\mathrm{o},k,i,\mathrm{free}} + y_{\mathrm{o},k,i,\mathrm{forced}}.$$

Then, $y_{\mathrm{o},k,i}$ satisfies

$$\delta(\mathbf{p}) y_{\mathrm{o},k,i} = \nu_{k,i}(\mathbf{p}) u_i. \tag{2.41}$$

Since

$$y_{\mathrm{o},k} = y_{\mathrm{o},k,\mathrm{free}} + y_{\mathrm{o},k,\mathrm{forced}}, \tag{2.42}$$

it follows from (2.38), (2.39), and (2.42) that

$$y_{\mathrm{o},k} = \sum_{i=1}^{m} y_{\mathrm{o},k,i}. \tag{2.43}$$

Multiplying (2.36) by $\nu_{k,i}(\mathbf{p})$ and multiplying (2.41) by $\det \Gamma_{\mathrm{i}}(\mathbf{p})$ yields

$$\delta(\mathbf{p})\nu_{k,i}(\mathbf{p}) \sum_{j=1}^{m} T_{j,i}(\mathbf{p}) y_{\mathrm{i},j} = \nu_{k,i}(\mathbf{p}) \det \Gamma_{\mathrm{i}}(\mathbf{p}) u_i, \tag{2.44}$$

$$\delta(\mathbf{p}) \det \Gamma_{\mathrm{i}}(\mathbf{p}) y_{\mathrm{o},k,i} = \nu_{k,i}(\mathbf{p}) \det \Gamma_{\mathrm{i}}(\mathbf{p}) u_i. \tag{2.45}$$

Comparing (2.44) and (2.45) yields

$$\delta(\mathbf{p})\nu_{k,i}(\mathbf{p}) \sum_{j=1}^{m} T_{j,i}(\mathbf{p}) y_{\mathrm{i},j} = \delta(\mathbf{p}) \det \Gamma_{\mathrm{i}}(\mathbf{p}) y_{\mathrm{o},k,i}, \tag{2.46}$$

which represents a SISO relationship between $y_{\mathrm{o},k,i}$ and $\sum_{j=1}^{m} T_{j,i}(\mathbf{p}) y_{\mathrm{i},j}$ due to the input u_i with the free response given by (2.40). Therefore, Lemma A.5 in Appendix A implies that

$$\nu_{k,i}(\mathbf{p}) \sum_{j=1}^{m} T_{j,i}(\mathbf{p}) y_{\mathrm{i},j} = \det \Gamma_{\mathrm{i}}(\mathbf{p}) y_{\mathrm{o},k,i}, \tag{2.47}$$

which indicates that $\delta(\mathbf{p})$ can be cancelled from (2.46) without excluding any solutions.

Using (2.34) and (2.35) we have

$$\Gamma_{\mathrm{o}}(\mathbf{p}) \operatorname{adj} \Gamma_{\mathrm{i}}(\mathbf{p}) = \begin{bmatrix} \sum_{i=1}^{m} \nu_{1,i}(\mathbf{p})\, T_{1,i}(\mathbf{p}) & \cdots & \sum_{i=1}^{m} \nu_{1,i}(\mathbf{p})\, T_{m,i}(\mathbf{p}) \\ \vdots & \cdots & \vdots \\ \sum_{i=1}^{m} \nu_{p-m,i}(\mathbf{p})\, T_{1,i}(\mathbf{p}) & \cdots & \sum_{i=1}^{m} \nu_{p-m,i}(\mathbf{p})\, T_{m,i}(\mathbf{p}) \end{bmatrix}. \tag{2.48}$$

Using (2.43), (2.47), and (2.48) yields

$$\Gamma_{\mathrm{o}}(\mathbf{p})\,[\operatorname{adj}\Gamma_{\mathrm{i}}(\mathbf{p})]\,y_{\mathrm{i}} = \begin{bmatrix} \displaystyle\sum_{i=1}^{m}\sum_{j=1}^{m}\nu_{1,i}(\mathbf{p})T_{j,i}(\mathbf{p})y_{\mathrm{i},j} \\ \vdots \\ \displaystyle\sum_{i=1}^{m}\sum_{j=1}^{m}\nu_{p-m,i}(\mathbf{p})T_{j,i}(\mathbf{p})y_{\mathrm{i},j} \end{bmatrix}$$

$$= \begin{bmatrix} \displaystyle\sum_{i=1}^{m}\det\Gamma_{\mathrm{i}}(\mathbf{p})y_{\mathrm{o},1,i} \\ \vdots \\ \displaystyle\sum_{i=1}^{m}\det\Gamma_{\mathrm{i}}(\mathbf{p})y_{\mathrm{o},p-m,i} \end{bmatrix}$$

$$= \det\Gamma_{\mathrm{i}}(\mathbf{p})y_{\mathrm{o}}. \qquad \square$$

Theorem 1 implies that we can redefine $\mathcal{T}(\mathbf{p})$ in (2.30) as

$$\mathcal{T}(\mathbf{p}) \stackrel{\triangle}{=} \Gamma_{\mathrm{o}}(\mathbf{p})\Gamma_{\mathrm{i}}^{-1}(\mathbf{p}). \tag{2.49}$$

Note that each entry of $\mathcal{T}(\mathbf{p})$ is a rational operator that is not necessarily proper and whose numerator and denominator are not necessarily coprime.

Consider the case $m = 1$ and $p = 2$. Then, using (2.49), the SISO transmissibility from y_{i} to y_{o} is

$$\mathcal{T}(\mathbf{p}) = \frac{\Gamma_{\mathrm{o}}(\mathbf{p})}{\Gamma_{\mathrm{i}}(\mathbf{p})} = \frac{C_{\mathrm{o}}\operatorname{adj}(\mathbf{p}I - A)B + D_{\mathrm{o}}\delta(\mathbf{p})}{C_{\mathrm{i}}\operatorname{adj}(\mathbf{p}I - A)B + D_{\mathrm{i}}\delta(\mathbf{p})}, \tag{2.50}$$

which can be interpreted as the differential equation

$$\Gamma_{\mathrm{i}}(\mathbf{p})y_{\mathrm{o}} = \Gamma_{\mathrm{o}}(\mathbf{p})y_{\mathrm{i}}. \tag{2.51}$$

2.4 Examples

Example 2.4.1. Consider the mass-spring system in Figure 2.1, where f is the input force, q_1 and q_2 are the displacements of m_1 and m_2, respectively, and (2.1) holds with

$$x \triangleq \begin{bmatrix} q_1 & q_2 & \dot{q}_1 & \dot{q}_2 \end{bmatrix}^{\mathrm{T}}, \quad A \triangleq \begin{bmatrix} 0_{2\times 2} & I_2 \\ \Omega & 0_{2\times 2} \end{bmatrix}, \tag{2.52}$$

$$\Omega \triangleq \begin{bmatrix} -\frac{k_1+k_2}{m_1} & \frac{k_2}{m_1} \\ \frac{k_2}{m_2} & -\frac{k_2}{m_2} \end{bmatrix}, \quad b = \begin{bmatrix} 0 & 0 & \frac{1}{m_1} & 0 \end{bmatrix}^{\mathrm{T}}. \tag{2.53}$$

For the transmissibility from $y_{\mathrm{i}} = q_1$ to $y_{\mathrm{o}} = q_2$, we have

$$C_{\mathrm{i}} = \begin{bmatrix} 1 & 0 & 0 & 0 \end{bmatrix}, C_{\mathrm{o}} = \begin{bmatrix} 0 & 1 & 0 & 0 \end{bmatrix}. \tag{2.54}$$

Using (2.20), (2.21), and (2.22) it follows that

$$\Gamma_{\mathrm{i}}(\mathbf{p}) = C_{\mathrm{i}}\mathrm{adj}\,(\mathbf{p}I_n - A)B = \frac{m_2\mathbf{p}^2 + k_2}{m_1 m_2}, \tag{2.55}$$

$$\Gamma_{\mathrm{o}}(\mathbf{p}) = C_{\mathrm{o}}\mathrm{adj}\,(\mathbf{p}I_n - A)B = \frac{k_2}{m_1 m_2}, \tag{2.56}$$

$$\delta(\mathbf{p}) = \mathbf{p}^4 + \frac{k_2 m_1 + (k_1+k_2)m_2}{m_1 m_2}\mathbf{p}^2 + \frac{k_1 k_2}{m_1 m_2}, \tag{2.57}$$

respectively. Therefore, we have

$$\delta(\mathbf{p})q_1 = \Gamma_{\mathrm{i}}(\mathbf{p})f, \tag{2.58}$$

$$\delta(\mathbf{p})q_2 = \Gamma_{\mathrm{o}}(\mathbf{p})f. \tag{2.59}$$

Multiplying (2.58) and (2.59) by $\Gamma_{\rm o}(\mathbf{p})$ and $\Gamma_{\rm i}(\mathbf{p})$, respectively, yields

$$\delta(\mathbf{p})\Gamma_{\rm o}(\mathbf{p})q_1 = \Gamma_{\rm i}(\mathbf{p})\Gamma_{\rm o}(\mathbf{p})f, \tag{2.60}$$

$$\delta(\mathbf{p})\Gamma_{\rm i}(\mathbf{p})q_2 = \Gamma_{\rm i}(\mathbf{p})\Gamma_{\rm o}(\mathbf{p})f. \tag{2.61}$$

Comparing (2.60) and (2.61) yields

$$\delta(\mathbf{p})\Gamma_{\rm o}(\mathbf{p})q_1 = \delta(\mathbf{p})\Gamma_{\rm i}(\mathbf{p})q_2, \tag{2.62}$$

in accordance with (2.28). Moreover, Theorem 1 and (2.51) imply that

$$\Gamma_{\rm o}(\mathbf{p})q_1 = \Gamma_{\rm i}(\mathbf{p})q_2. \tag{2.63}$$

Alternatively, note that the equation of motion for m_2 is given by

$$m_2\mathbf{p}^2q_2 + k_2(q_2 - q_1) = 0. \tag{2.64}$$

Solving (2.64) for q_1 yields

$$q_1 = \frac{m_2\mathbf{p}^2 + k_2}{k_2}q_2. \tag{2.65}$$

Hence, (2.55), (2.56), and (2.65) imply

$$\begin{aligned}\Gamma_{\rm o}(\mathbf{p})y_{\rm i} &= \frac{k_2}{m_1m_2}q_1 = \frac{k_2}{m_1m_2}\frac{m_2\mathbf{p}^2 + k_2}{k_2}q_2\\ &= \frac{m_2\mathbf{p}^2 + k_2}{m_1m_2}q_2 = \Gamma_{\rm i}(\mathbf{p})y_{\rm o},\end{aligned} \tag{2.66}$$

which confirms (2.51) directly without using Theorem 1. Thus, $y_\mathrm{o} = \mathcal{T}(\mathbf{p})y_\mathrm{i}$ where

$$\mathcal{T}(\mathbf{p}) = \frac{\Gamma_\mathrm{o}(\mathbf{p})}{\Gamma_\mathrm{i}(\mathbf{p})} = \frac{k_2}{m_2\mathbf{p}^2 + k_2}. \qquad \blacksquare$$

Example 2.4.2. Consider the MIMO system

$$x = \begin{bmatrix} x_1 \\ x_2 \\ x_3 \end{bmatrix}, \quad A = \begin{bmatrix} -1 & 1 & 0 \\ 0 & -1 & 1 \\ 0 & 0 & -1 \end{bmatrix}, \tag{2.67}$$

$$B = \begin{bmatrix} 1 & 0 \\ 0 & 1 \\ 1 & 1 \end{bmatrix}, \quad C = \begin{bmatrix} 1 & 0 & 0 \\ 0 & 1 & 0 \\ 0 & 0 & 1 \end{bmatrix}, \quad D = \begin{bmatrix} 1 & 0 \\ 0 & 0 \\ 0 & 0 \end{bmatrix}, \tag{2.68}$$

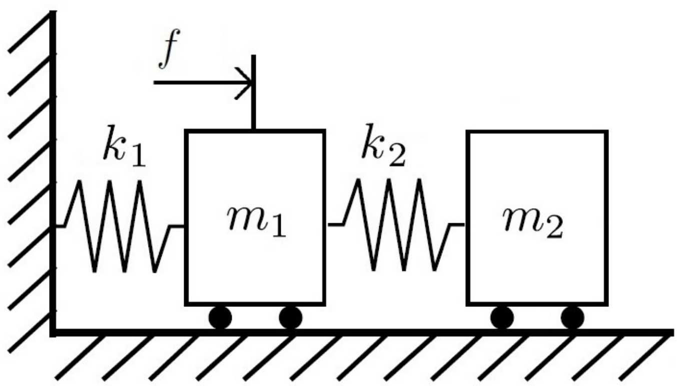

Figure 2.1: Mass-spring system for Example 2.4.1, where f is the input force and the outputs y_i and y_o are the displacements q_1 and q_2 of m_1 and m_2, respectively.

$u = [u_1\ u_2]^{\mathrm{T}}$, $y_{\mathrm{i}} = [x_1 + u_1\ \ x_2]^{\mathrm{T}}$, and $y_{\mathrm{o}} = x_3$. Hence, $m = 2, p = 3$, and

$$C_{\mathrm{i}} = \begin{bmatrix} 1 & 0 & 0 \\ 0 & 1 & 0 \end{bmatrix}, \quad C_{\mathrm{o}} = \begin{bmatrix} 0 & 0 & 1 \end{bmatrix}, \tag{2.69}$$

$$D_{\mathrm{i}} = \begin{bmatrix} 1 & 0 \\ 0 & 0 \end{bmatrix}, \quad D_{\mathrm{o}} = \begin{bmatrix} 0 & 0 \end{bmatrix}. \tag{2.70}$$

It follows from (2.22) that $\delta(\mathbf{p}) = \mathbf{p}^3 + 3\mathbf{p}^2 + 3\mathbf{p} + 1$. Using (2.20) we have

$$\begin{aligned} \Gamma_{\mathrm{i}}(\mathbf{p}) &= C_{\mathrm{i}}\mathrm{adj}(\mathbf{p}I - A)B + \delta(\mathbf{p})D_{\mathrm{i}} \\ &= \begin{bmatrix} (\mathbf{p}+1)^2(\mathbf{p}+2)+1 & \mathbf{p}+2 \\ \mathbf{p}+1 & (\mathbf{p}+1)(\mathbf{p}+2) \end{bmatrix}. \end{aligned} \tag{2.71}$$

Moreover, (2.21) implies that

$$\begin{aligned} \Gamma_{\mathrm{o}}(\mathbf{p}) &= C_{\mathrm{o}}\mathrm{adj}\,(\mathbf{p}I - A)B + \delta(\mathbf{p})D_{\mathrm{o}} \\ &= \begin{bmatrix} (\mathbf{p}+1)^2 & (\mathbf{p}+1)^2 \end{bmatrix}. \end{aligned} \tag{2.72}$$

Hence, using (2.49) we have

$$\begin{aligned} \mathcal{T}(\mathbf{p}) &= \Gamma_{\mathrm{o}}(\mathbf{p})\Gamma_{\mathrm{i}}^{-1}(\mathbf{p}) \\ &= \frac{1}{(\mathbf{p}+1)^3(\mathbf{p}+2)^2}\begin{bmatrix} (\mathbf{p}+1)^4 & (\mathbf{p}+1)^3(\mathbf{p}^2+3\mathbf{p}+1) \end{bmatrix}. \end{aligned} \tag{2.73}$$

It follows from (2.30) that

$$(\mathbf{p}+1)^3(\mathbf{p}+2)^2 x_3 = (\mathbf{p}+1)^4 x_1 + (\mathbf{p}+1)^3(\mathbf{p}^2+3\mathbf{p}+1)x_2, \tag{2.74}$$

that is,

$$x_3^{(5)} + 7x_3^{(4)} + 19x_3^{(3)} + 25\ddot{x}_3 + 16\dot{x}_3 + 4x_3 = x_1^{(4)} + 4x_1^{(3)} + 6\ddot{x}_1 + 4\dot{x}_1 + x_1 \\ + x_2^{(5)} + 6x_2^{(4)} + 13x_2^{(3)} + 13\ddot{x}_2 + 6\dot{x}_2 + x_2. \tag{2.75}$$

To confirm (2.32), substituting x, A, and B from (2.67) and (2.68) and u into (2.1) yields

$$\mathbf{p}x_1 = -x_1 + x_2 + u_1, \tag{2.76}$$

$$\mathbf{p}x_2 = -x_2 + x_3 + u_2, \tag{2.77}$$

$$\mathbf{p}x_3 = -x_3 + u_1 + u_2. \tag{2.78}$$

Using (2.76)–(2.78) note that

$$\begin{aligned} \det \Gamma_{\mathrm{i}}(\mathbf{p}) y_{\mathrm{o}} &= (\mathbf{p}+1)^3(\mathbf{p}+2)^2 x_3 \\ &= (\mathbf{p}+1)^3\big((\mathbf{p}+2)x_3 + (\mathbf{p}+2)(\mathbf{p}+1)x_3\big) \\ &= (\mathbf{p}+1)^3\big((\mathbf{p}+2)x_3 + (\mathbf{p}+2)(u_1+u_2)\big) \\ &= (\mathbf{p}+1)^3\big((\mathbf{p}+2)(x_3+u_2) + (\mathbf{p}+2)u_1\big) \\ &= (\mathbf{p}+1)^3\big((\mathbf{p}+2)(\mathbf{p}+1)x_2 + (\mathbf{p}+2)u_1\big) \\ &= (\mathbf{p}+1)^3\big(x_2 + u_1 + (\mathbf{p}+1)u_1 + ((\mathbf{p}+2)(\mathbf{p}+1)-1)x_2\big) \\ &= (\mathbf{p}+1)^3\big((\mathbf{p}+1)(x_1+u_1) + (\mathbf{p}^2+3\mathbf{p}+1)x_2\big) \\ &= \Gamma_{\mathrm{o}}(\mathbf{p}) \operatorname{adj} \Gamma_{\mathrm{i}}(\mathbf{p}) y_{\mathrm{i}}. \end{aligned} \tag{2.79}$$

Hence, y_{i} and y_{o} satisfy (2.32) in accordance with Theorem 1. Moreover, multiplying (2.79) by $\delta(\mathbf{p})$ shows that y_{i} and y_{o} satisfy (2.27). ■

Example 2.4.3. Consider the mass-spring system in Figure 2.2, where f is the input force, q_1, q_2, q_3 are the displacements of m_1, m_2, m_3, respectively, and (2.1) holds with

$$x \triangleq \begin{bmatrix} q_1 & q_2 & q_3 & \dot{q}_1 & \dot{q}_2 & \dot{q}_3 \end{bmatrix}^{\mathrm{T}}, \quad A \triangleq \begin{bmatrix} 0_{3\times3} & I_3 \\ \Omega & 0_{3\times3} \end{bmatrix}, \tag{2.80}$$

$$\Omega \triangleq \begin{bmatrix} -\frac{k_{01}+k_{12}+k_{13}}{m_1} & \frac{k_{12}}{m_1} & \frac{k_{13}}{m_1} \\ \frac{k_{12}}{m_2} & -\frac{k_{12}+k_{23}}{m_2} & \frac{k_{23}}{m_2} \\ \frac{k_{13}}{m_3} & \frac{k_{23}}{m_3} & -\frac{k_{13}+k_{23}}{m_3}, \end{bmatrix}, \tag{2.81}$$

$$B = \begin{bmatrix} 0 & 0 & 0 & \frac{1}{m_1} & 0 & 0 \end{bmatrix}^{\mathrm{T}}. \tag{2.82}$$

For $i = 1, 2, 3$, define

$$y_i \triangleq C_i x, \tag{2.83}$$

where

$$C_1 \triangleq e_{1,6}^{\mathrm{T}}, \quad C_2 \triangleq e_{2,6}^{\mathrm{T}}, \quad C_3 \triangleq e_{3,6}^{\mathrm{T}}, \tag{2.84}$$

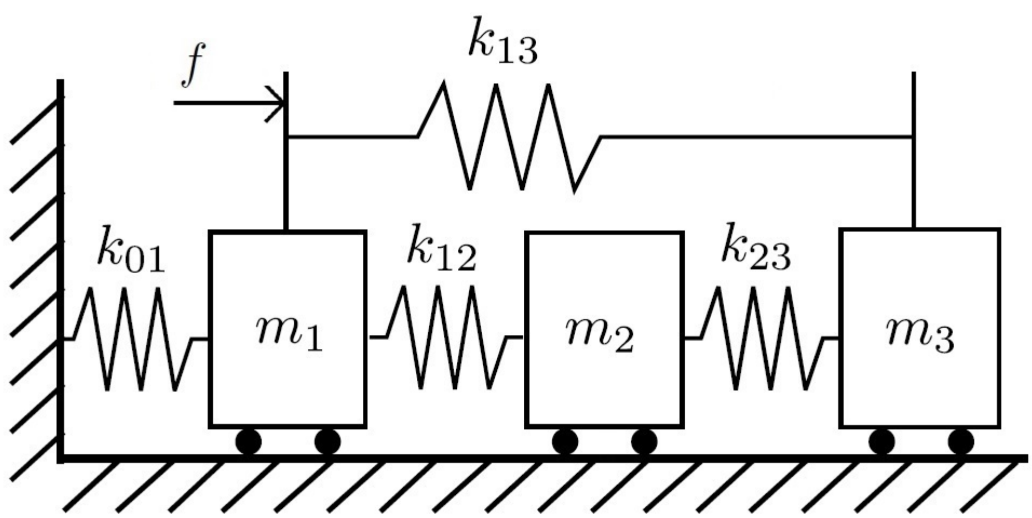

Figure 2.2: Mass-spring system for Example 2.4.3, where f is the input force and the outputs y_1, y_2, and y_3 are the displacements q_1, q_2, and q_3 of m_1, m_2, and m_3, respectively.

and $e_{i,n} \in \mathbb{R}^n$ is the i^{th} unit vector. Then,

$$y_1 = C_1 x = q_1, \tag{2.85}$$

$$y_2 = C_2 x = q_2, \tag{2.86}$$

$$y_3 = C_3 x = q_3. \tag{2.87}$$

Define

$$\begin{aligned}\Gamma_1(\mathbf{p}) &\triangleq C_1 \mathrm{adj}\,(\mathbf{p}I_n - A)B \\ &= \frac{m_2 m_3 \mathbf{p}^4 + (m_3(k_{12}+k_{23}) + m_2(k_{13}+k_{23}))\,\mathbf{p}^2 + k}{m_1 m_2 m_3},\end{aligned} \tag{2.88}$$

$$\Gamma_2(\mathbf{p}) \triangleq C_2 \mathrm{adj}\,(\mathbf{p}I_n - A)B = \frac{k_{12} m_3 \mathbf{p}^2 + k}{m_1 m_2 m_3}, \tag{2.89}$$

$$\Gamma_3(\mathbf{p}) \triangleq C_3 \mathrm{adj}\,(\mathbf{p}I_n - A)B = \frac{k_{13} m_2 \mathbf{p}^2 + k}{m_1 m_2 m_3}, \tag{2.90}$$

where $k \triangleq k_{12}k_{13} + k_{12}k_{23} + k_{13}k_{23}$. Next, let $\mathcal{T}_{j,i}(\mathbf{p})$ be the transmissibility whose pseudo input is q_i and whose pseudo output is q_j, where $i, j \in \{1, 2, 3\}$. Therefore, using (2.50)

$$\begin{aligned}\mathcal{T}_{2,1}(\mathbf{p}) &= \frac{\Gamma_2(\mathbf{p})}{\Gamma_1(\mathbf{p})} \\ &= \frac{k_{12} m_3 \mathbf{p}^2 + k}{m_2 m_3 \mathbf{p}^4 + (m_3(k_{12}+k_{23}) + m_2(k_{13}+k_{23}))\,\mathbf{p}^2 + k},\end{aligned} \tag{2.91}$$

$$\begin{aligned}\mathcal{T}_{3,1}(\mathbf{p}) &= \frac{\Gamma_3(\mathbf{p})}{\Gamma_1(\mathbf{p})} \\ &= \frac{k_{13} m_2 \mathbf{p}^2 + k}{m_2 m_3 \mathbf{p}^4 + (m_3(k_{12}+k_{23}) + m_2(k_{13}+k_{23}))\,\mathbf{p}^2 + k},\end{aligned} \tag{2.92}$$

$$\mathcal{T}_{3,2}(\mathbf{p}) = \frac{\Gamma_3(\mathbf{p})}{\Gamma_2(\mathbf{p})} = \frac{k_{13} m_2 \mathbf{p}^2 + k}{k_{12} m_3 \mathbf{p}^2 + k} \tag{2.93}$$

are the transmissibilities from q_1 to q_2, q_1 to q_3, and q_2 to q_3, respectively. Note that

$$q_2 = \mathcal{T}_{2,1}(\mathbf{p})q_1, \tag{2.94}$$

$$q_3 = \mathcal{T}_{3,2}(\mathbf{p})q_2, \tag{2.95}$$

and thus

$$q_3 = \mathcal{T}_{3,2}(\mathbf{p})\mathcal{T}_{2,1}(\mathbf{p})q_1 = \mathcal{T}_{3,1}(\mathbf{p})q_1, \tag{2.96}$$

that is,

$$q_3 = \frac{\Gamma_3(\mathbf{p})}{\Gamma_2(\mathbf{p})}\frac{\Gamma_2(\mathbf{p})}{\Gamma_1(\mathbf{p})}q_1 = \frac{\Gamma_3(\mathbf{p})}{\Gamma_1(\mathbf{p})}q_1, \tag{2.97}$$

which shows that $\Gamma_2(\mathbf{p})$ can be cancelled. ■

2.5 Conclusions

This chapter developed a time-domain framework for MIMO transmissibilities that accounts for nonzero initial conditions as well as cancellation of the common factor occurring in the underlying state space model. A natural extension of these models is to the discrete-time case to facilitate system identification [28].

CHAPTER 3

Closed-Loop Identification of Unstable Systems Using Noncausal FIR Models

3.1 Introduction

Identification of a plant operating inside a closed loop is motivated by the need to monitor plant changes without opening the loop [69–71]. This need is unavoidable when the controlled plant is open-loop unstable, in which case opening the loop for identification is prohibited. Even for plants that are asymptotically stable, opening the loop for identification may not be feasible due to operational constraints. In these cases, identification must rely on sensor-actuator data obtained under normal operating conditions, although in some cases it may be possible to inject additional signals to enhance persistency and signal amplitude relative to noise levels.

In addition to the fact that closed-loop identification constrains the feasible inputs, output noise and process noise inside the feedback loop are correlated with the control input. Although knowledge of this correlation may be useful for system identification, this information is usually not available in practice, and decorrelation techniques are needed [72–74]. In [75, 76] an IIR model is used with prediction error methods (PEM) to identify unstable systems in closed loop. Assuming that the output noise and process noise are uncorrelated with the exogenous signal, applying PEM with either the true system order or an overestimated system order guarantees that the estimated transfer function converges to the true transfer function as the number of samples used for identification tends to infinity [75]. However, for a finite data set, overestimating the system order can yield poor transfer function estimates.

If the plant order is unknown, then an initial overestimate of the order can be used with PEM, and a refined estimate can be obtained from Ho-Kalman realization theory [77] and its implementation in terms of the singular value decomposition of the Hankel matrix [78]. Although this approach, which requires estimates of the Markov (impulse response) parameters, is sensitive to noise, heuristics can be used to improve its accuracy [79–83].

By constructing a predictor, PEM identification minimizes the difference between the predicted output and the measured output to obtain an estimate of the transfer function. If the predictor is unstable, which is the case when output-error and Box-Jenkins model structures are used to identify unstable systems in closed loop [84], the prediction error may be large, which leads to erroneous transfer function estimates. This issue can be mitigated by using modified output-error and Box-Jenkins models as in [84], where the predictor is constrained to be stable. However, this constraint complicates the search algorithm [84].

An alternative approach to PEM identification of unstable plants is discussed in [85], where an output-error model structure is considered. In this case the predictor is decomposed into stable and unstable parts, which correspond to causal and noncausal filters, respectively. Since output-error models are a special type of IIR models, this approach requires an estimate of the order of the system. However, as discussed above, if the estimated order is incorrect, then the transfer function estimates may have poor accuracy. In addition, identifying the noncausal part of the model requires time-reversing the signal and thus is confined to offline identification. Moreover, the approaches used in [85] and [84] require a priori knowledge of whether the system is stable or unstable.

Noncausal filtering was also used in [86] in a two-step projection method to identify systems in closed loop with nonlinear feedback. A noncausal FIR model is first used with linear least mean squares optimization to identify the causal closed-loop system from the exogenous signal to the control input. Then, the identified model is used with the exogenous signal to compute the predicted control input, which is then compared with the output of the closed-loop system to identify the plant using an IIR model. The role of the noncausal FIR model in [86] is restricted to approximating the Wiener smoother, which relates the exogenous signal to the control input.

Instrumental variables can also be used to identify unstable systems in closed loop, where the instruments consist of samples of either the exogenous signal or a prefiltered version of the exogenous signal [72, 87]. Subspace methods can also be used to identify linear systems in closed loop [88, 89].

The usefulness of Markov parameters for estimating the order of an IIR system suggests consideration of a finite impulse response model structure, whose numerator coefficients are its Markov parameters and all of whose poles are zero. Although physical systems are rarely FIR, an FIR model can approximate an asymptotically stable, IIR system [90–92]. An advantage of FIR models for system identification is that the Markov parameters of an FIR model are given explicitly, and thus can be used directly in Ho-Kalman realization to estimate the system order and construct an IIR model. Most importantly, the FIR model structure is independent of the system poles and zeros, and thus no prior estimate of the plant order is needed.

Noncausal FIR controllers are used for tracking problems where the command signal is known in advance. In particular, a noncausal FIR feedforward controller is obtained by truncating the Laurent series of the unstable inverse of a nonminimum-phase plant; the resulting controller provides approximate plant inversion without unstable pole-zero cancellation [93–97].

A noncausal FIR model that approximates the Laurent series of an unstable plant involves both positive and negative powers of the Z-transform variable z. The negative powers approximate the asymptotically stable part of the plant outside of a disk (that is, inside a punctured plane), whereas the positive powers approximate the unstable part of the plant inside a disk. Inside the common region, which is an annulus, the Laurent series represents a noncausal model, as evidenced by the positive powers of z.

To identify an unstable plant operating inside a stabilizing feedback loop, the measured output can be delayed relative to the measured input to obtain an FIR model that is a noncausal approximation of the unstable plant. The transfer function of this noncausal FIR model approximates the Laurent series of the plant inside the maximal annulus of analyticity lying between the smallest disk containing the asymptotically stable poles and the smallest punctured plane containing the unstable poles.

Although advantages of noncausal filters were observed in [85] and [76], a complete justification is lacking. One of the contributions of the present chapter is thus to use the Laurent expansion of a rational transfer function to further justify the use of these models in system identification. The contribution of the present chapter is thus a detailed treatment of closed-loop identification of unstable plants using noncausal FIR models. This work presents analysis and proofs that connect the Laurent series of a transfer function and an associated noncausal FIR model. These results are needed to establish a rigorous connection between the estimated noncausal FIR model and the impulse response of the system. Unlike the noncausal output-error models identified in [85], noncausal FIR models can be identified online. Moreover, unlike the approaches of [85] and [84], noncausal FIR models do not require knowledge of whether the system is stable or unstable.

3.2 Motivation for FIR Models in System Identification

The first challenge in identifying a linear system of unknown order using an IIR model structure is the need to estimate the order of the system. To illustrate this problem, we estimate the order n of the system by identifying an IIR model of order n_{mod}, where n_{mod} varies from 1 to an upper bound $n_{\mathrm{mod,max}}$ for n. For each value of n_{mod}, we use the identified IIR model of order n_{mod} and the measured input and output data to calculate the one-step predicted output. Then we compute the residual between the one-step predicted output and the measured output. The estimated order of the system is considered to be the value of n_{mod} for which no significant improvement in the residual occurs for values greater than n_{mod}. As the following example shows, this approach may fail.

Example 3.2.1. Consider the asymptotically stable transfer function

$$G(z) = \frac{(z^2+0.16)(z-0.3)(z+0.3)}{(z+0.8)(z+0.7)(z+0.6)(z-0.7)(z-0.6)(z^2+0.25)} \tag{3.1}$$

with input u and output y_0, where u is a realization of a zero-mean, unit-variance white random process. Let y be the output obtained by adding zero-mean white gaussian output noise to y_0 with a signal-to-noise ratio of 10.

We use PEM with an IIR model of order n_{mod}, where $1 \le n_{\mathrm{mod}} \le 20$, to identify G using 100 independent realizations of $10,000$ samples of u and y. For each value of n_{mod}, let $\varepsilon_{y,\ell,n_{\mathrm{mod}}}$, where ℓ is the number of samples be the averaged error in the one-step predicted output obtained from each experiment using PEM with an IIR model of order n_{mod}. Figure 3.1 shows $\varepsilon_{y,\ell,n_{\mathrm{mod}}}$ for $n_{\mathrm{mod}} = 1,\ldots,20$. Note from Figure 3.1 that $n_{\mathrm{mod}} = 3$ gives the least value of $\varepsilon_{y,\ell,n_{\mathrm{mod}}}$. Therefore, the estimated order of (3.1) using PEM with an IIR model is 3. However, the true order is $n = 7$. Moreover, note from Figure 3.1 that $\varepsilon_{y,\ell,n_{\mathrm{mod}}}$ increases for values of $n_{\mathrm{mod}} > 7$. That is, overestimating n degrades $\varepsilon_{y,\ell,n_{\mathrm{mod}}}$.

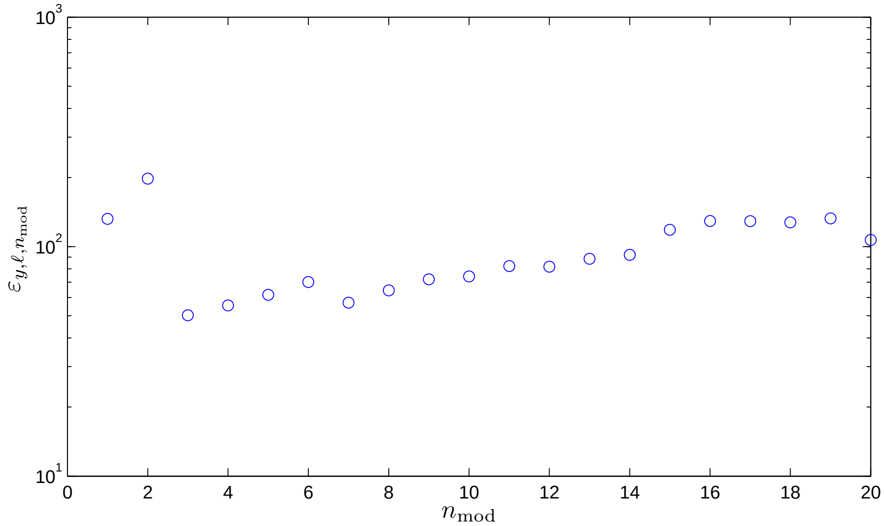

Figure 3.1: Plot of $\varepsilon_{y,\ell,n_{\mathrm{mod}}}$ for Example 3.2.1, where $n_{\mathrm{mod}} = 1,\ldots,20$. Note that $n_{\mathrm{mod}} = 3$ gives the least value of $\varepsilon_{y,\ell,n_{\mathrm{mod}}}$. Hence, the estimated order of (3.1) using PEM with an IIR model is 3. However, the order of G is $n = 7$. Moreover, note that $\varepsilon_{y,\ell,n_{\mathrm{mod}}}$ increases for values of $n_{\mathrm{mod}} > 7$. That is, overestimating n degrades $\varepsilon_{y,\ell,n_{\mathrm{mod}}}$.

Next, we use PEM with an FIR model of order μ, where $1 \leq \mu \leq 50$, to identify G using 100 independent realizations of $10,000$ samples of u and y. For each value of μ, let $\varepsilon_{y,\ell,\mu}$ be the averaged error in the one-step predicted output obtained from each experiment using PEM with an FIR model of order μ. Figure 3.2 shows that $\varepsilon_{y,\ell,\mu}$ decreases monotonically as μ increases for values of μ less than 30, with no significant improvement in $\varepsilon_{y,\ell,\mu}$ for larger values of μ.

We now use the coefficients of the FIR model of G to estimate the order of G. Once the order of G is estimated, Ho-Kalman realization can be used to construct an IIR model of G from its estimated Markov parameters. Beginning with an initial estimate $\hat{n} \geq n$, we construct the Markov block-Hankel matrix

$$\mathcal{H}(H) \triangleq \begin{bmatrix} H_1 & \cdots & H_{\hat{n}} \\ \vdots & \ddots & \vdots \\ H_{\hat{n}} & \cdots & H_{2\hat{n}-1} \end{bmatrix}, \tag{3.2}$$

where $H \triangleq \begin{bmatrix} H_0 & \cdots & H_{2\hat{n}-1} \end{bmatrix}$ is a vector of Markov parameters of G. For all $\hat{n} \geq n$, the rank of $\mathcal{H}(H)$ is equal to the McMillan degree of G. We thus compute the singular values of $\mathcal{H}(H)$ and look for a large decrease in the singular values. For noise-free data, a large decrease in the singular values is evident. However, in the presence of noise, the large decrease in the singular values disappears, and thus the problem of estimating the model order becomes difficult [80].

Let $\hat{H} \triangleq \begin{bmatrix} \hat{H}_0 & \cdots & \hat{H}_{2\hat{n}-1} \end{bmatrix}$ be the vector of estimated Markov parameters. To estimate the order of G using $\hat{H}$, the nuclear-norm minimization technique given in [79, 80] considers the optimization problem

$$\underset{\bar{H}(\gamma)}{\text{minimize}} \, \|\mathcal{H}(\bar{H}(\gamma))\|_{\mathrm{N}} \tag{3.3}$$

subject to

$$\|\bar{H}(\gamma) - \hat{H}\|_{\mathrm{F}} \leq \gamma, \tag{3.4}$$

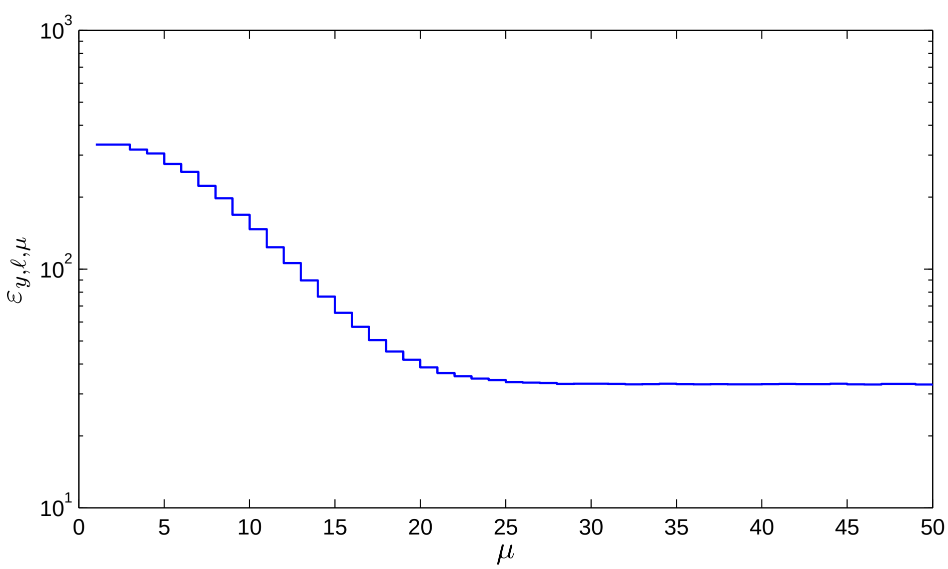

Figure 3.2: Plot of $\varepsilon_{y,\ell,\mu}$ for Example 3.2.1, where $\mu = 1, \ldots, 50$. Note that $\varepsilon_{y,\ell,\mu}$ decreases monotonically as μ increases for values of μ less than 30 and no significant improvement in $\varepsilon_{y,\ell,\mu}$ for larger values of μ.

where $\|\cdot\|_{\mathrm{N}}$ is the nuclear norm, which is the sum of the singular values, $\|\cdot\|_{\mathrm{F}}$ is the Frobenius norm, γ is varied over a range of small positive numbers, and $\bar{H}(\gamma) \in \mathbb{R}^{1\times(2\hat{n}-1)}$ is the optimization parameter vector. For each value of γ, we solve the optimization problem (3.3), (3.4), and then construct the Markov block-Hankel matrix $\mathcal{H}(\bar{H}(\gamma))$ and compute its singular values. The singular values of $\mathcal{H}(\bar{H}(\gamma))$ that are robust to changes in γ provide an estimate of the McMillan degree of G.

Figure 3.3 shows the singular values of $\mathcal{H}(\bar{H}(\gamma))$ versus γ, where $\hat{H}$ in (3.4) is the vector of Markov parameters of the identified model of (3.1) obtained using PEM with an IIR model of order $n_{\mathrm{mod}} = 20$ averaged over 100 independent realizations. Note from Figure 3.3 that 5 singular values of $\mathcal{H}(\bar{H}(\gamma))$ are robust to the change in γ, which yields 5 as the estimated order of G. However, the order of G is $n = 7$.

Figure 3.4 shows the singular values of the Hankel matrix $\mathcal{H}(\bar{H}(\gamma))$ versus γ, where $\hat{H}$ in (3.4) is the vector of estimated Markov parameters obtained from the identified model using PEM with an FIR model of order $\mu = 50$ averaged over 100 independent realizations. Figure 3.4 shows that 7 singular values of $\mathcal{H}(\bar{H}(\gamma))$ are robust to the change in γ, which correctly yields 7 as the estimated order of G.

Figure 3.5 shows the error $|G(e^{\jmath\theta}) - \hat{G}(e^{\jmath\theta})|$ in the frequency response of the estimated model versus frequency θ, where $\hat{G}$ is either the estimated IIR model of order $n_{\mathrm{mod}} = 5$ or the estimated FIR model of order $\mu = 50$, each averaged over 100 independent realizations. Note that the estimated FIR model gives a better estimate of the frequency response than the estimated IIR model. ■

Example 3.2.2. Consider the unstable transfer function

$$G(z) = \frac{(z^2+0.16)(z-0.3)(z+0.3)}{(z+0.6)(z-0.7)(z^2+0.25)(z-1.6)(z-1.7)(z-1.8)} \tag{3.5}$$

with the realization

$$A = \begin{bmatrix} 0.2000 & 2.000 & 0.7200 & -0.2999 & -0.2088 & -0.2156 & -0.0941 \\ 1 & 0 & 0 & 0 & 0 & 0 & 0 \\ 0 & 1 & 0 & 0 & 0 & 0 & 0 \\ 0 & 0 & 1 & 0 & 0 & 0 & 0 \\ 0 & 0 & 0 & 1 & 0 & 0 & 0 \\ 0 & 0 & 0 & 0 & 1 & 0 & 0 \\ 0 & 0 & 0 & 0 & 0 & 1 & 0 \end{bmatrix}, B = \begin{bmatrix} 1 \\ 0 \\ 0 \\ 0 \\ 0 \\ 0 \\ 0 \end{bmatrix}, \tag{3.6}$$

$$C = \begin{bmatrix} 0 & 0 & 1 & 0 & 0.0700 & 0 & -0.0144 \end{bmatrix}, \quad D = 0, \tag{3.7}$$

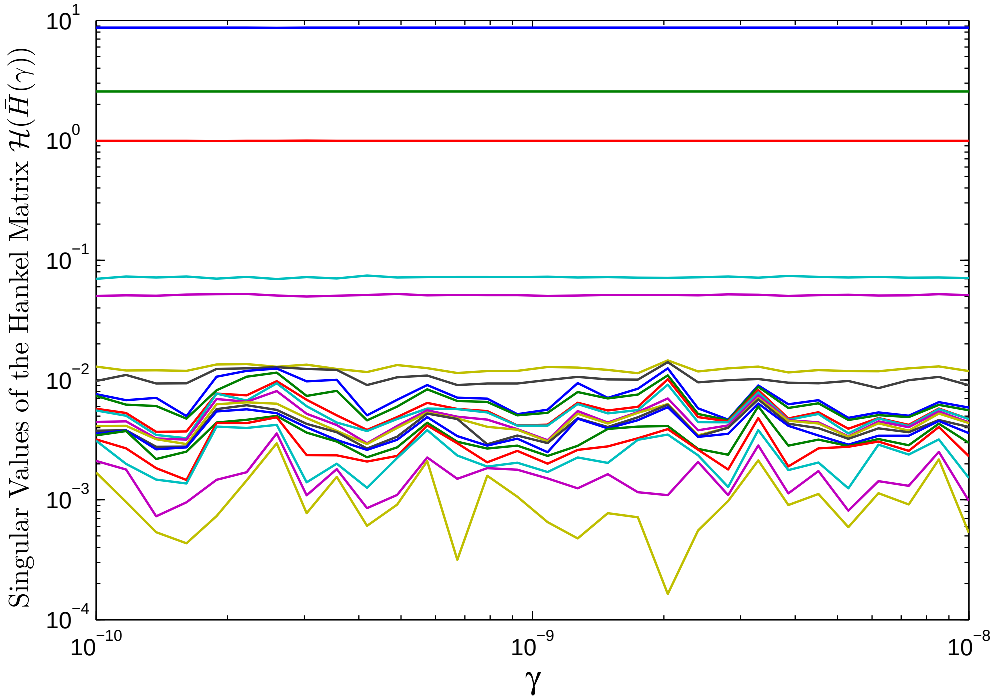

Figure 3.3: Example 3.2.1. Plot of the singular values of $\mathcal{H}(\bar{H}(\gamma))$ versus γ, where $\hat{H}$ in (3.4) is the vector of Markov parameters of the identified model of (3.1) obtained using PEM with an IIR model of order $n_{\rm mod} = 20$ averaged over 100 independent realizations. This figure shows that 5 singular values of the Hankel matrix $\mathcal{H}(\bar{H}(\gamma))$ are robust to the change in γ, which suggests that the estimated order of G is 5, where the order of G is $n = 7$.

stabilized by an LQR controller with $Q = I_7$ and $R = 1$, where I_7 is the 7×7 identity matrix, and thus

$$K = \begin{bmatrix} 0.3337 & 1.7995 & 0.6122 & -0.3158 & -0.2112 & -0.2001 & -0.0862 \end{bmatrix}. \tag{3.8}$$

Figure 3.6 shows the closed-loop control system, where A, B, C are given by (3.6), (3.7), x is the state vector, K is the LQR gain given by (3.8), c is the exogenous signal, v is the process noise, and u_0 and y_0 are the measured input and output signals, respectively. The plant G given by (3.5) is unstable and the closed-loop system is internally stable.

Let the exogenous signal c of the closed-loop system shown in Figure 3.6 be a

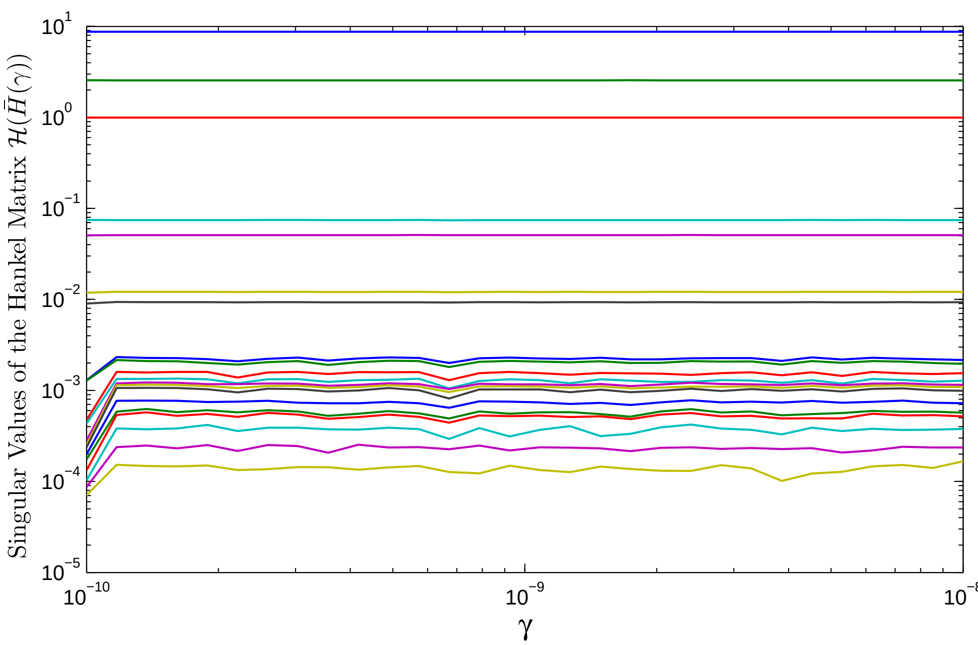

Figure 3.4: Example 3.2.1. Plot of the singular values of $\mathcal{H}(\bar{H}(\gamma))$ versus γ, where $\hat{n} = 20$ and $\hat{H}$ in (3.4) is the vector of Markov parameters obtained using PEM with an FIR model of order $\mu = 50$ averaged over 100 independent realizations. Note that 7 singular values of $\mathcal{H}(\bar{H}(\gamma))$ are robust to the change in γ, which correctly yields 7 as the estimated order of G.

realization of a zero-mean, unit-variance white random process and let the process noise v be a white noise signal added to u_0 with a signal-to-noise ratio of 10. We use u_0 and y_0 to identify G.

We use PEM with an IIR model of order $n_{\rm mod}$, where $1 \leq n_{\rm mod} \leq 20$, to identify G using 100 independent realizations of $10,000$ samples of u_0 and y_0. For each value

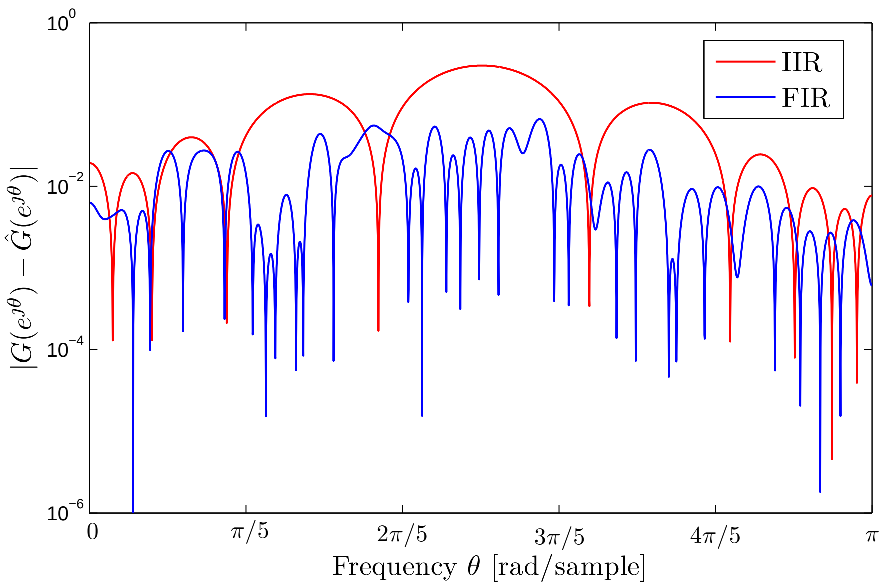

Figure 3.5: Example 3.2.1. Error in the frequency response of the estimated IIR model of order $n_{\rm mod} = 5$ and the estimated FIR model of order $\mu = 50$, each averaged over 100 independent realizations. Note that the estimated FIR model gives a better estimate of the frequency response than the estimated IIR model.

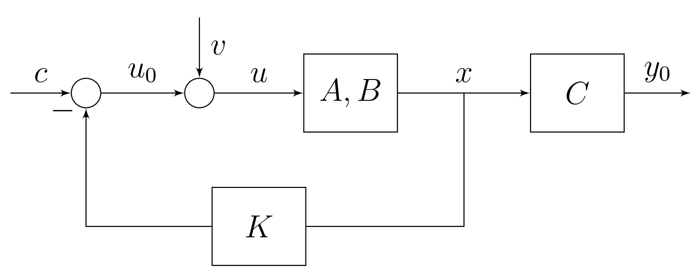

Figure 3.6: Discrete-time closed-loop control system, where A, B, C are given by (3.6), (3.7) x is the state vector, K is the LQR gain vector, c is the zero-mean, unit-variance white exogenous signal, v is a white noise signal with signal-to-noise ratio of 10, and u_0 and y_0 are the measured input and output, respectively. The plant G given by (3.5) is unstable and the closed-loop system is internally stable.

of n_{mod}, let $\varepsilon_{y_0,\ell,n_{\mathrm{mod}}}$ be the averaged error in the one-step predicted output obtained from each experiment using PEM with an IIR model of order n_{mod}. Figure 3.7 shows that $n_{\mathrm{mod}} = 5$ gives the least value of $\varepsilon_{y_0,\ell,n_{\mathrm{mod}}}$. However, the order of G is $n = 7$. Moreover, note from Figure 3.7 that $\varepsilon_{y_0,\ell,n_{\mathrm{mod}}}$ increases for values of $n_{\mathrm{mod}} > 7$, that is, overestimating n degrades the one-step prediction error.

Figure 3.8 shows the singular values of $\mathcal{H}(\bar{H}(\gamma))$ versus γ, where $\hat{H}$ in (3.4) is the vector of Markov parameters of the identified model of (3.5) obtained using PEM with an IIR model of order $n_{\mathrm{mod}} = 20$ averaged over 100 independent realizations. Note from Figure 3.8 that 5 singular values of $\mathcal{H}(\bar{H}(\gamma))$ are robust to the change in γ, which yields 5 as the estimated order of G. However, the order of G is $n = 7$.

Next, we use PEM with an FIR model of order μ to identify G using 100 independent realizations of $10,000$ samples of u_0 and y_0. For each value of μ let $\varepsilon_{y_0,\ell,\mu}$ be the averaged error in the one-step predicted output obtained from each experiment using PEM with an FIR model of order μ. Figure 3.9 shows $\varepsilon_{y_0,\ell,\mu}$ for the estimated

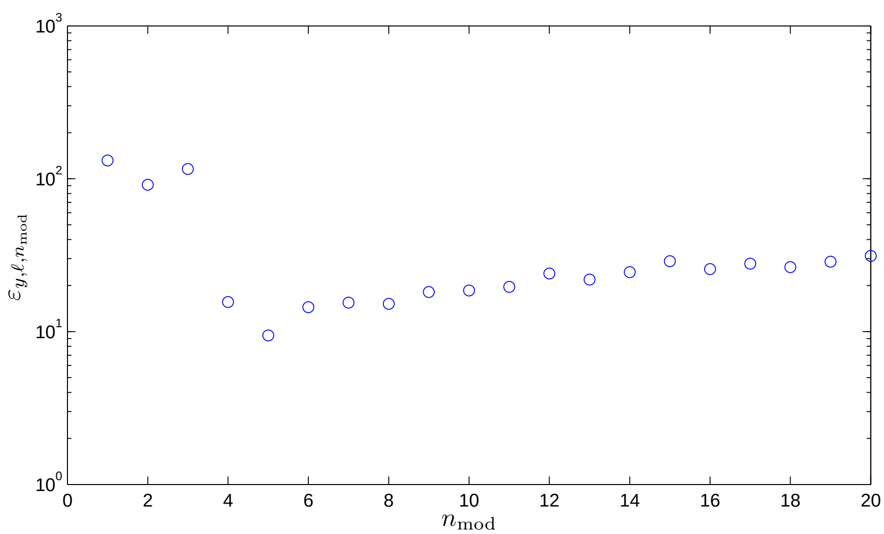

Figure 3.7: Plot of $\varepsilon_{y_0,\ell,n_{\mathrm{mod}}}$ for Example 3.2.2, where $n_{\mathrm{mod}} = 1,\ldots,20$. Note that $n_{\mathrm{mod}} = 5$ gives the least value of $\varepsilon_{y_0,\ell,n_{\mathrm{mod}}}$. Hence, the estimated order of (3.5) using PEM with an IIR model is 5. However, the order of G is $n = 7$. Note that $\varepsilon_{y_0,\ell,n_{\mathrm{mod}}}$ increases for values of $n_{\mathrm{mod}} > 7$, that is, overestimating n degrades the one-step prediction error.

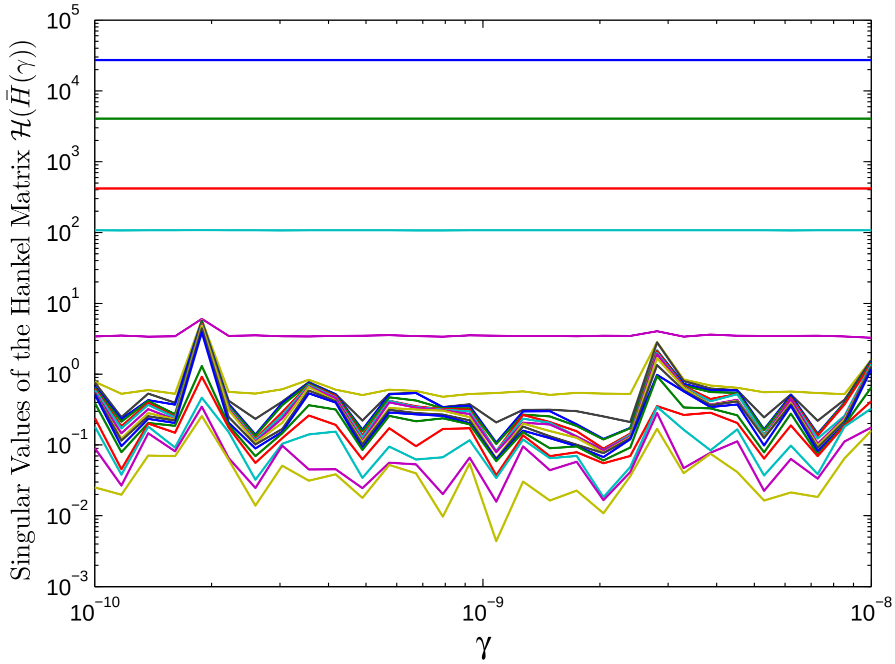

Figure 3.8: Example 3.2.2. Plot of the singular values of $\mathcal{H}(\bar{H}(\gamma))$ versus γ, where $\hat{H}$ in (3.4) is the vector of Markov parameters of the identified model of (3.5) obtained using PEM with an IIR model of order $n_{\rm mod} = 20$ averaged over 100 independent realizations. This figure shows that 5 singular values of the Hankel matrix $\mathcal{H}(\bar{H}(\gamma))$ are robust to the change in γ, which suggests that the estimated order of G is 5, where the order of G is $n = 7$.

FIR model of order $\mu = 1, \ldots, 50$, and the estimated FIR model of order $\mu = 2d$, where the output y_0 is delayed d steps and $d = 1, \ldots, 25$. Note that the FIR model with delay, which is noncausal, gives significantly lower values of $\varepsilon_{y_0,\ell,\mu}$ than the FIR model with no delay. Moreover, note that for the FIR model with delay $\varepsilon_{y_0,\ell,\mu}$ decreases monotonically as μ increases for values of μ less than 32 and no significant improvement in $\varepsilon_{y_0,\ell,\mu}$ for values of μ greater than 32. Moreover, increasing the FIR model order does not degrade the one-step prediction error.

Figure 3.10 shows the error $|G(e^{\jmath\theta}) - \hat{G}(e^{\jmath\theta})|$ in the frequency response of the estimated model versus θ, where θ is the frequency and $\hat{G}$ is either the estimated IIR model of order $n_{\rm mod} = 5$, the estimated FIR model of order $\mu = 50$, or the estimated FIR model of order $\mu = 50$ with the output y_0 delayed $d = 25$ steps, each averaged over 100 independent realizations. Note that the FIR model with delay, which is noncausal, gives the least error in frequency response of G. ■

The justification for the use of noncausal FIR models will be developed in the following sections.

3.3 Preliminaries

For $\rho > 0$, let $\mathbb{D}(\rho) \triangleq \{z \in \mathbb{C} : |z| < \rho\}$ be the open disk in the complex plane centered at the origin with radius ρ. Also, for $\rho \geq 0$, let $\mathbb{P}(\rho) \triangleq \{z \in \mathbb{C} : |z| > \rho\}$ be the open punctured plane centered at the origin with inner radius ρ. Moreover, for $0 \leq \rho_1 < \rho_2$, let $\mathbb{A}(\rho_1, \rho_2) \triangleq \{z \in \mathbb{C} : \rho_1 < |z| < \rho_2\} = \mathbb{P}(\rho_1) \cap \mathbb{D}(\rho_2)$ be the open

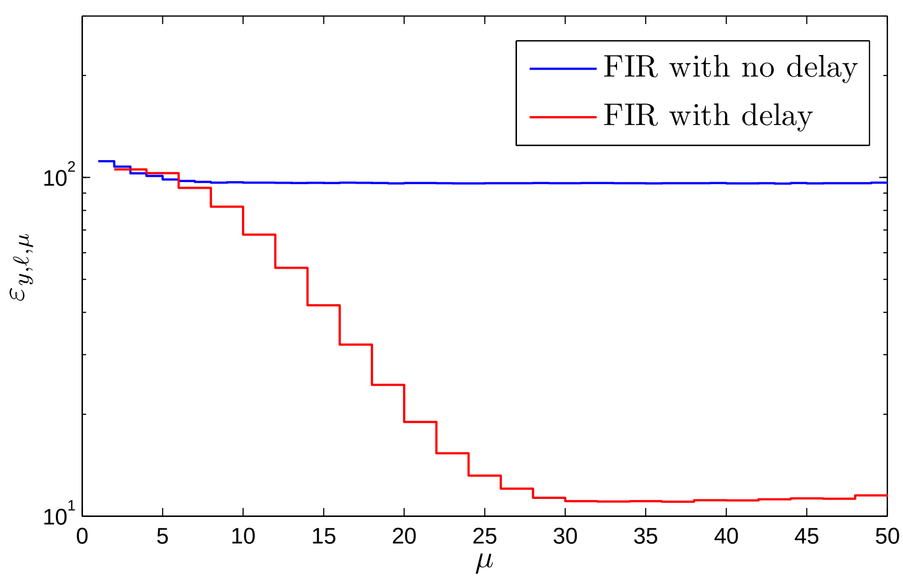

Figure 3.9: Plot of $\varepsilon_{y_0,\ell,\mu}$ for Example 3.2.2 for the estimated FIR model of order $\mu = 1, \ldots, 50$, and the estimated FIR model of order $\mu = 2d$, where the output y_0 is delayed d steps and $d = 1, \ldots, 25$. Note that the FIR model with delay, which is noncausal, gives significantly lower values of $\varepsilon_{y_0,\ell,\mu}$ than the FIR model with no delay. Moreover, note that for the FIR model with delay $\varepsilon_{y_0,\ell,\mu}$ decreases as μ increases for values of μ less than 32 and no significant improvement in $\varepsilon_{y_0,\ell,\mu}$ for values of μ greater than 32. Moreover, increasing the FIR model order does not degrade the one-step prediction error.

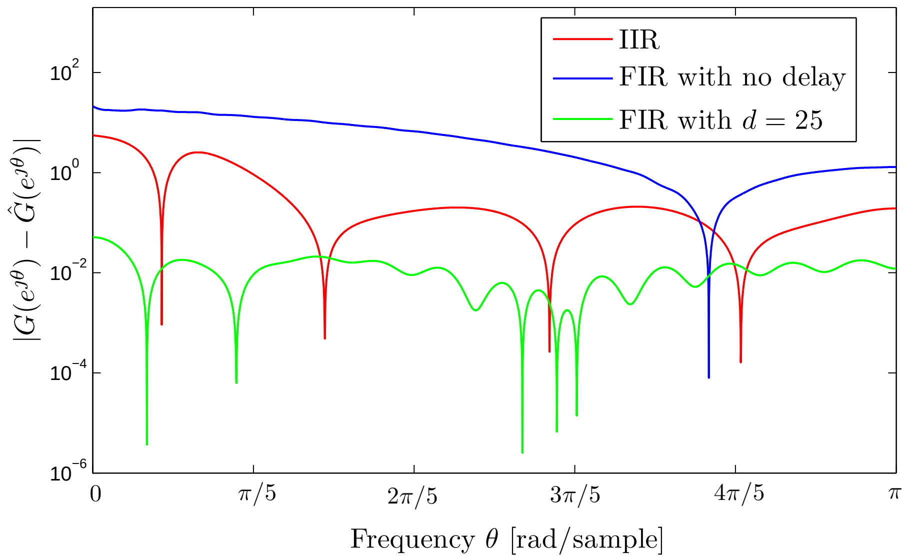

Figure 3.10: Example 3.2.2. Error in the frequency response of the estimated IIR model of order $n_{\mathrm{mod}} = 5$, the estimated FIR model of order $\mu = 50$, and the estimated FIR model of order $\mu = 50$ with the output y_0 delayed $d = 25$ steps, each averaged over 100 independent realizations. Note that the FIR model with $d = 25$ delay steps, which is noncausal, gives the least error in frequency response.

annulus in the complex plane centered at the origin with inner radius ρ_1 and outer radius ρ_2.

Recall [98, p. 168] that if the rational function $g(z)$ is analytic in the open annulus $\mathbb{A}(\rho_1, \rho_2)$, then $g(z)$ has a unique, absolutely convergent Laurent series in $\mathbb{A}(\rho_1, \rho_2)$ of the form

$$g(z) = \sum_{i=-\infty}^{\infty} h_i z^i. \tag{3.9}$$

If $\rho_2 = \infty$, then g is analytic in the punctured plane $\mathbb{P}(\rho_1)$ and, if g is proper, then, for all $i > 0$, $h_i = 0$ in (3.9). If $\rho_1 = 0$ and g has no pole at zero, then g is analytic in the disk $\mathbb{D}(\rho_2)$ and, for all $i < 0$, $h_i = 0$ in (3.9). In this case, (3.9) is a power series that converges absolutely in $\mathbb{D}(\rho_2)$ and diverges at every point in $\mathbb{P}(\rho_2)$ [98, p. 138].

Definition 2. Let $0 \leq \rho_1 < \rho_2$ and let g be a rational function. If $\rho_1 > 0$, then the open annulus $\mathbb{A}(\rho_1, \rho_2)$ is *maximal* with respect to g if g is analytic in $\mathbb{A}(\rho_1, \rho_2)$ and, for all $\varepsilon_1 \in [0, \rho_1)$ and $\varepsilon_2 \geq 0$, not both zero, g is not analytic in $\mathbb{A}(\rho_1 - \varepsilon_1, \rho_2 + \varepsilon_2)$. If $\rho_1 = 0$, then the open disk $\mathbb{D}(\rho_2)$ is maximal with respect to g if g is analytic in $\mathbb{D}(\rho_2)$ and, for all $\varepsilon > 0$, g is not analytic in $\mathbb{D}(\rho_2 + \varepsilon)$.

For convenience, the term maximal open annulus may also refer to an open disk or an open punctured plane.

Consider the system

$$x(k+1) = Ax(k) + Bu(k), \tag{3.10}$$

$$y(k) = Cx(k) + Du(k), \tag{3.11}$$

where $A \in \mathbb{R}^{n \times n}$, $B \in \mathbb{R}^{n \times m}$, $C \in \mathbb{R}^{l \times n}$, $D \in \mathbb{R}^{l \times m}$. Assume that (A, B) is controllable and (A, C) is observable. Let G be the $l \times m$ transfer matrix corresponding to (A, B, C, D). The i^{th} Markov parameter H_i of G, which is given by

$$H_i \triangleq \begin{cases} D, & i = 0, \\ CA^{i-1}B, & i \geq 1, \end{cases} \tag{3.12}$$

is independent of the realization (3.10), (3.11) of G. Let $\rho(A)$ denote the spectral radius of A.

Proposition 1. $\{H_i\}_{i=0}^{\infty}$ are the coefficients of the Laurent series of G in $\mathbb{P}(\rho(A))$, that is, for all $z \in \mathbb{P}(\rho(A))$,

$$G(z) = \sum_{i=0}^{\infty} H_i z^{-i}. \tag{3.13}$$

Proof. For all $|z| > \rho(A)$,

$$\begin{aligned} G(z) &= C(zI - A)^{-1}B + D \\ &= C(I - z^{-1}A)^{-1}Bz^{-1} + D \\ &= C\sum_{i=0}^{\infty} z^{-i-1}A^{i}B + D \\ &= \sum_{i=1}^{\infty} CA^{i-1}Bz^{-i} + D \\ &= \sum_{i=0}^{\infty} H_i z^{-i}. \end{aligned} \qquad \square$$

Next, we define the reflected transfer matrix G_{ref} to be the transfer matrix obtained by replacing z in $G(z)$ by z^{-1}, that is, $G_{\mathrm{ref}}(z) \triangleq G(z^{-1})$.

Proposition 2. Assume that A is nonsingular. Then G_{ref} is proper, and $(A^{-1}, -A^{-1}B, CA^{-1}, D - CA^{-1}B)$ is a minimal realization of G_{ref}.

Proof. Note that

$$\begin{aligned} G_{\mathrm{ref}}(z) &= C(z^{-1}I - A)^{-1}B + D \\ &= C\big(A(z^{-1}A^{-1} - I)\big)^{-1}B + D \\ &= -CA^{-1}(zI - A^{-1})^{-1}A^{-1}B + D - CA^{-1}B. \end{aligned}$$

Now, assume that (A, B) is controllable. Since A is nonsingular, it follows that

$$\operatorname{rank}\left(\begin{bmatrix} -A^{-1}B & -A^{-2}B & \cdots & -A^{-n}B \end{bmatrix}\right)$$
$$= \operatorname{rank}\left(-A^{-n}\begin{bmatrix} A^{n-1}B & A^{n-2}B & \cdots & B \end{bmatrix}\right) = n.$$

Likewise, (A, C) observable implies that (A^{-1}, CA^{-1}) is observable.

To prove the converse, replace (A, B, C, D) with $(A^{-1}, -A^{-1}B, CA^{-1}, D-CA^{-1}B)$.

□

Definition 3. The *spectral radius* $\rho(G)$ *of* G is the spectral radius of A.

Definition 4. Assume that A is nonsingular. Then, the *inner spectral radius* $\rho_{\text{inner}}(A)$ of A is defined as

$$\rho_{\text{inner}}(A) \triangleq \frac{1}{\rho(A^{-1})}.$$

Furthermore, the *inner spectral radius* $\rho_{\text{inner}}(G)$ *of* G is the inner spectral radius of A.

Proposition 3. Assume that zero is not a pole of G. Then,

$$\rho_{\text{inner}}(G_{\text{ref}}) = \frac{1}{\rho(G)}, \quad \rho(G_{\text{ref}}) = \frac{1}{\rho_{\text{inner}}(G)}. \tag{3.14}$$

Proof. Assume that (A, B, C, D) is a minimal realization of $G(z)$. Then A is nonsingular and Proposition 2 implies that $(A^{-1}, -A^{-1}B, CA^{-1}, D - CA^{-1}B)$ is a minimal realization of G_{ref}. It follows that

$$\rho_{\text{inner}}(G_{\text{ref}}) = \rho_{\text{inner}}(A^{-1}) = \frac{1}{\rho(A)} = \frac{1}{\rho(G)}.$$

Similarly,

$$\rho(G_{\text{ref}}) = \rho(A^{-1}) = \frac{1}{\rho_{\text{inner}}(A)} = \frac{1}{\rho_{\text{inner}}(G)}.$$ □

Definition 5. G is *strongly unstable* if it has no poles in the closed unit disk.

Proposition 4. G is strongly unstable if and only if G_{ref} is asymptotically stable.

Proof. The result follows directly from Proposition 3. □

3.4 Analysis of the Laurent Series

Throughout this section, let G be a proper $l \times m$ rational function with minimal realization (A, B, C, D). If A is nonsingular, then the Markov parameters of G_{ref} are given by

$$\tilde{H}_i \triangleq \begin{cases} D - CA^{-1}B, & i = 0, \\ -CA^{-i-1}B, & i \geq 1. \end{cases} \tag{3.15}$$

Therefore, if A is nonsingular, then Proposition 1 and Proposition 3 imply that the Laurent series of $G_{\rm ref}$ in $\mathbb{P}(\rho(G_{\rm ref})) = \mathbb{P}(\rho(A^{-1})) = \mathbb{P}(1/\rho(A))$ is given by

$$G_{\rm ref}(z) = \sum_{i=0}^{\infty} \tilde{H}_i z^{-i}. \tag{3.16}$$

The following result shows that (3.15) provides the coefficients of the power series for G in the maximal disk.

Proposition 5. Assume that zero is not a pole of G. Then, for all $z \in \mathbb{D}(\rho_{\rm inner}(G))$,

$$G(z) = \sum_{i=0}^{\infty} \tilde{H}_i z^{i}, \tag{3.17}$$

where $\tilde{H}_i$ are the Markov parameters of $G_{\rm ref}$ given by (3.15).

Proof. Replacing $z \in \mathbb{P}(\rho(G_{\rm ref})) = \mathbb{P}(1/\rho_{\rm inner}(G))$ in (3.16) by $z^{-1} \in \mathbb{D}(\rho_{\rm inner}(G))$ and using the fact that, for all $z \in \mathbb{P}(\rho(G_{\rm ref})), G_{\rm ref}(1/z) = G(z)$ yields (3.17). □

Using partial fractions, G can be represented as

$$G = G_{\rm s} + G_{\rm u} + D, \tag{3.18}$$

where the strictly proper transfer functions $G_{\rm s}$ and $G_{\rm u}$ are asymptotically stable and strongly unstable, respectively. Defining $\rho_{\rm s} \triangleq \rho(G_{\rm s})$, Proposition 1 implies that $G_{\rm s}$ is analytic in $\mathbb{P}(\rho_{\rm s})$ with the Laurent series

$$G_{\rm s}(z) = \sum_{i=1}^{\infty} H_{{\rm s}_i} z^{-i}, \tag{3.19}$$

where, for all $i \geq 0$, $H_{{\rm s}_i}$ is the $i^{\rm th}$ Markov parameter of $G_{\rm s}$. Next, note that zero is not a pole of $G_{\rm u}$. Hence, defining $\rho_{\rm u} \triangleq \rho_{\rm inner}(G_{\rm u})$, $G_{\rm u}$ is analytic in $\mathbb{D}(\rho_{\rm u})$ with the power series

$$G_{\mathrm{u}}(z) = \sum_{i=0}^{\infty} H_{\mathrm{u}_{-i}} z^i, \tag{3.20}$$

where, by Proposition 5, $H_{\mathrm{u}_{-i}}$ is the i^{th} Markov parameter of $G_{\mathrm{u,ref}}$. Rewriting (3.20) as

$$G_{\mathrm{u}}(z) = \sum_{i=-\infty}^{0} H_{\mathrm{u}_i} z^{-i}, \tag{3.21}$$

it follows from (3.18), (3.19), and (3.21) that G is analytic in the annulus $\mathbb{A}(\rho_{\mathrm{s}}, \rho_{\mathrm{u}})$ with the Laurent series

$$G(z) = \sum_{i=-\infty}^{\infty} L_i z^{-i}, \tag{3.22}$$

where

$$L_i \triangleq \begin{cases} H_{\mathrm{u}_i}, & i < 0, \\ H_{\mathrm{u}_0} + D, & i = 0, \\ H_{\mathrm{s}_i}, & i > 0. \end{cases} \tag{3.23}$$

Note that the Laurent series of G in $\mathbb{A}(\rho_{\mathrm{s}}, \rho_{\mathrm{u}})$ given by (3.22) is different from the Laurent series (3.13) of G in $\mathbb{P}(\rho(G))$ given by (3.13). Furthermore, both $D = G(\infty)$ and $H_{\mathrm{u}_0} = G_{\mathrm{u,ref}}(\infty)$ may be nonzero as illustrated by the following examples.

Example 3.4.1. Let

$$G(z) = \frac{(z-1)(z-0.5)}{(z-2)(z-3)}.$$

Then, $D = G(\infty) = 1$, and

$$G_{\mathrm{s}}(z) = 0, \quad G_{\mathrm{u}}(z) = \frac{3.5z - 5.5}{(z-2)(z-3)}, \quad G_{\mathrm{u,ref}}(z) = \frac{-5.5z^2 + 3.5z}{(1-2z)(1-3z)},$$

and thus $H_{\mathrm{u}_0} = G_{\mathrm{u,ref}}(\infty) = -\frac{11}{12}$. ■

Example 3.4.2. Let

$$G(z) = \frac{1}{(z-0.5)(z-1.5)}.$$

Then, $D = G(\infty) = 0$,

$$G_{\rm s}(z) = \frac{-1}{z-0.5}, \quad G_{\rm u}(z) = \frac{1}{z-1.5}, \quad G_{\rm u,ref}(z) = \frac{z}{-1.5z+1},$$

and thus $H_{{\rm u}_0} = G_{\rm u,ref}(\infty) = -\frac{2}{3}$. ■

Assume that G has no poles on the unit circle. Let d and r be positive integers, and define the FIR truncations $G_{{\rm s},r}$ and $G_{{\rm u},d}$ of $G_{\rm s}(z)$ and $G_{\rm u}(z^{-1})$, respectively, by

$$G_{{\rm s},r}(z) \triangleq \sum_{i=1}^{r} H_{{\rm s}_i} z^{-i}, \quad G_{{\rm u},d}(z^{-1}) \triangleq \sum_{i=0}^{d} H_{{\rm u}_{-i}} z^{-i}, \tag{3.24}$$

where $H_{{\rm s}_i}$ and $H_{{\rm u}_{-i}}$ are defined by (3.23). Note that

$$G_{{\rm s},r}(z) = \sum_{i=1}^{r} L_i z^{-i}, \quad G_{{\rm u},d}(z) = \sum_{i=0}^{d} L_{-i} z^{i} = \sum_{i=-d}^{0} L_i z^{-i}. \tag{3.25}$$

Now, define the improper rational function $G_{r,d}(z)$ by

$$G_{r,d} \triangleq G_{{\rm s},r} + G_{{\rm u},d} + D, \tag{3.26}$$

where $G_{{\rm s},r}(z)$ and $G_{{\rm u},d}(z)$ are the causal and noncausal components of $G_{r,d}$, respectively. Hence, for all $z \neq 0$,

$$G_{r,d}(z) = \sum_{i=-d}^{r} L_i z^{-i}. \tag{3.27}$$

3.5 Necessary and Sufficient Conditions for Boundedness of the Laurent Series Coefficients

Throughout this section, let G be an $l \times m$ proper rational function. Let $||\cdot||_{\mathrm{F}}$ denote the Frobenius norm.

For asymptotically stable and strongly unstable transfer functions, the following result, which is used in the proof of Theorem 2, concerns boundedness of the coefficients of the Laurent series of a rational function.

Lemma 1. The following statements hold:

i) Assume that zero is not a pole of G. If the coefficients (3.15) of the power series (3.17) of G in $\mathbb{D}(\rho_{\mathrm{inner}}(G))$ are bounded, then $\rho_{\mathrm{inner}}(G) \geq 1$.

ii) If the coefficients (3.12) of the Laurent series (3.13) of G in $\mathbb{P}(\rho(G))$ are bounded, then $\rho(G) \leq 1$.

Proof.

i) It follows from [98, p. 142] that the radius of convergence of the power series (3.17) of G in $\mathbb{D}(\rho_{\mathrm{inner}}(G))$ is given by $\rho_{\mathrm{inner}} = \frac{1}{\limsup_{i\to\infty} |\tilde{H}_i|^{1/i}}$. Define the positive number $M \triangleq \sup_i |\tilde{H}_i|$. Then

$$\rho_{\mathrm{inner}}(G) = \frac{1}{\limsup_{i\to\infty} |\tilde{H}_i|^{1/i}} \geq \frac{1}{\lim_{i\to\infty} M^{1/i}} = 1.$$

ii) Assume that zero is not a pole of G_{ref}. Proposition 5 implies that the power series of G_{ref} in $\mathbb{D}(\rho_{\mathrm{inner}}(G_{\mathrm{ref}}))$ is given by (3.17), where the coefficients of the power series of $G_{\rm ref}$ in $\mathbb{D}(\rho_{\rm inner}(G_{\rm ref}))$ are the Markov parameters of $(G_{\rm ref})_{\rm ref} = G$, which are given by (3.12). It follows from [98, p. 142] that the radius of convergence of the power series of $G_{\rm ref}$ in $\mathbb{D}(\rho_{\rm inner}(G_{\rm ref}))$ is given by $\rho_{\rm inner} = \frac{1}{\limsup_{i\to\infty}|H_i|^{1/i}}$. Define the positive number $M \triangleq \sup_i |H_i|$. Then

$$\frac{1}{\rho(G)} = \rho_{\rm inner}(G_{\rm ref}) = \frac{1}{\limsup_{i\to\infty}|H_i|^{1/i}} \geq \frac{1}{\lim_{i\to\infty} M^{1/i}} = 1.$$

Now assume that $G_{\rm ref}$ has m poles at zero. Then $G_{\rm ref}$ can be written as

$$G_{\rm ref}(z) = \frac{1}{z^m} G_{{\rm ref},0}(z), \tag{3.28}$$

where $G_{{\rm ref},0}$ has no poles at zero. Note that the factor $\frac{1}{z^m}$ shifts the indices of the power series coefficients of (3.28) but otherwise leaves them unchanged. Applying the above argument for $G_{{\rm ref},0}$ thus yields $\rho(G) \leq 1$. □

The following result shows that there is a unique maximal annulus for which the coefficients of the Laurent series of G are bounded.

Theorem 2. Let $\rho_2 > \rho_1 \geq 0$, and assume that $\mathbb{A}(\rho_1, \rho_2)$ is maximal with respect to G. Then the following statements are equivalent:

i) The coefficients of the Laurent series of G in $\mathbb{A}(\rho_1, \rho_2)$ are square summable.

ii) The coefficients of the Laurent series of G in $\mathbb{A}(\rho_1, \rho_2)$ converge to zero.

iii) The coefficients of the Laurent series of G in $\mathbb{A}(\rho_1, \rho_2)$ are bounded.

iv) $\rho_1 < 1 < \rho_2$.

Proof. $i)$ implies $ii)$ and $ii)$ implies $iii)$ are immediate. To show that $iii)$ implies $iv)$ assume that the coefficients of the Laurent series of G in $\mathbb{A}(\rho_1, \rho_2)$ are bounded. Decompose G as $G = G_{\rm i} + G_{\rm o} + D$, where all of the poles of $G_{\rm i}$ are contained in $\mathbb{D}(\rho_1)$ and all of the poles of $G_{\rm o}$ are contained in $\mathbb{P}(\rho_2)$. Suppose $\rho_1 < \rho_2 < 1$ and $\mathbb{A}(\rho_1, \rho_2)$ is maximal. Then $\rho_{\rm inner}(G_{\rm o}) < 1$, and thus $i)$ of Lemma 1 implies that the coefficients of the Laurent series of $G_{\rm o}$, and thus the coefficients of the Laurent series of G, are unbounded. Now suppose that $1 < \rho_1 < \rho_2$ and $\mathbb{A}(\rho_1, \rho_2)$ is maximal. Then $\rho(G_{\rm i}) > 1$, and thus $ii)$ of Lemma 1 implies that the coefficients of the Laurent series of $G_{\rm i}$, and thus G, are unbounded. Therefore, $\rho_1 < 1 < \rho_2$.

To show that $iv)$ implies $i)$ assume that $\rho_1 < 1 < \rho_2$ and consider the Laurent series of G in $\mathbb{A}(\rho_1, \rho_2)$ given by (3.22), where $\{L_i\}_{i=-\infty}^{\infty}$ is given by (3.23). Then, $f : [0, \infty) \to \mathbb{C}$ defined by $f(\theta) \triangleq G(e^{\jmath\theta})$ is continuous and periodic. By Parseval's theorem, the coefficients of the Fourier series of f are square summable. Since, on the unit circle, the Laurent series of G given by (3.22) is identical to the Fourier series of f, it follows that $\{L_i\}_{i=-\infty}^{\infty}$ is square summable. $\square$

Theorem 2 applies to rational functions that have no poles on the unit circle. If this is not the case, let $\rho_{\rm s} < \alpha < 1$ be such that G has no poles on the circle $|z| = \alpha$. Consider the decomposition

$$G = G_{{\rm i},\alpha} + G_{{\rm o},\alpha} + D, \tag{3.29}$$

where all poles of $G_{{\rm i},\alpha}$ are contained in $\mathbb{D}(\alpha)$, all poles of $G_{{\rm o},\alpha}$ are contained in $\mathbb{P}(\alpha)$, and $D = G(\infty)$. Using (3.22), we have

$$G_\alpha(z) \triangleq G(\alpha z) = \sum_{i=-\infty}^{\infty} L_i(\alpha z)^{-i} = \sum_{i=-\infty}^{\infty} \alpha^{-i} L_i z^{-i} = \sum_{i=-\infty}^{\infty} L_{\alpha,i} z^{-i}, \tag{3.30}$$

where, for all i,

$$L_{\alpha,i} \triangleq \alpha^{-i} L_i. \tag{3.31}$$

Let $\rho_{\rm s} < \alpha < 1$, and assume that G has no poles on the circle $|z| = \alpha$. Therefore, G_α has no poles on the unit circle. Theorem 2 can now be applied to G_α in $\mathbb{A}(\frac{\rho_{\rm s}}{\alpha}, \frac{\rho_{\rm u}}{\alpha})$ and (3.31) can be used to compute the coefficients of the Laurent series of G in $\mathbb{A}(\rho_{\rm s}, \rho_{\rm u})$.

3.6 Noncausal Closed-Loop Identification

Consider the closed-loop system in Figure 3.11 consisting of the MIMO, discrete-time transfer function G of order n and the discrete-time controller C. We assume that the closed-loop system is internally asymptotically stable, although no assumptions are made about the stability of G except that G has no poles on the unit circle. However, this restriction can be avoided by using (3.30).

Using the Laurent series (3.22) of G in $\mathbb{A}(\rho_{\rm s}, \rho_{\rm u})$, the output of G can be written as

$$y_0(k) = \sum_{j=-\infty}^{k} L_j u(k-j), \tag{3.32}$$

where $u(k) = 0$ for all $k < 0$. Note that the terms corresponding to $j < 0$ represent

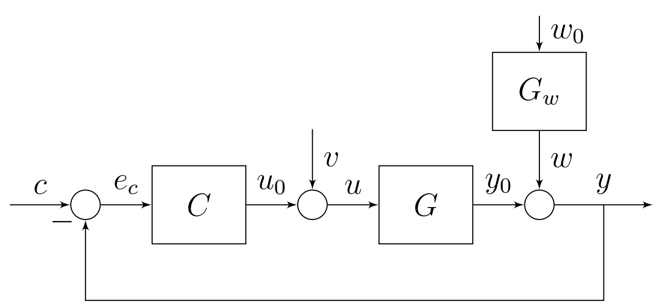

Figure 3.11: Discrete-time closed-loop control system, where C is the controller, G is the plant, v and w_0 are white noise signals, and G_w is the output noise model. The plant G may be unstable, and the closed-loop system is assumed to be internally stable.

the noncausal component of the model. Thus, for all $k \geq 0$, (3.32) can be represented as

$$y_0(k) = y_{0,r,d}(k) + e_{r,d}(k), \tag{3.33}$$

where the noncausal FIR model output $y_{0,r,d}(k)$ is defined as

$$y_{0,r,d}(k) \triangleq \sum_{j=-d}^{\min\{r,k\}} L_j u(k-j), \tag{3.34}$$

and the *output error* at time k is defined by

$$e_{r,d}(k) \triangleq y_0(k) - y_{0,r,d}(k), \tag{3.35}$$

which is the difference between the true output and the noncausal FIR model output at time k. Using (3.32) and (3.34) it follows that, for all $k \geq 0$,

$$\lim_{r,d\to\infty} y_{0,r,d}(k) = \sum_{j=-\infty}^{k} L_j u(k-j) = y_0(k). \tag{3.36}$$

Therefore, for all $k \geq 0$,

$$\lim_{r,d\to\infty} e_{r,d}(k) = y_0(k) - \lim_{r,d\to\infty} y_{0,r,d}(k) = 0. \tag{3.37}$$

It follows from (3.34) that computing the output at time k requires the inputs $u(k-r), \ldots, u(k+d)$. That is, to identify a noncausal FIR model we delay the measured output data by d steps and then perform identification between the input and delayed output, as we show next.

Let c, v, and w_0 be realization of the zero-mean stationary white random processes $\mathcal{C}, \mathcal{V}$, and $\mathcal{W}_0$, respectively, and let w be a realization of the stationary colored random process $\mathcal{W}$. We assume that $\mathcal{C}, \mathcal{W}_0$, and $\mathcal{V}$ are mutually independent and ergodic, that is, their statistical properties can be determined from a single, sufficiently long realization.

Let u and y denote measurements of the input u_0 and output y_0, respectively, that is, for all $k \geq 0$,

$$u(k) = u_0(k) + v(k), \tag{3.38}$$

$$y(k) = y_0(k) + w(k). \tag{3.39}$$

Note that (3.33) can be expressed as

$$y_0(k) = \theta_{r,d}\phi_{r,d}(k) + e_{r,d}(k), \tag{3.40}$$

where

$$\theta_{r,d} \triangleq \left[\begin{array}{ccc} L_{-d} & \cdots & L_r \end{array} \right], \quad \phi_{r,d}(k) \triangleq \left[\begin{array}{ccc} u(k+d) & \cdots & u(k-r) \end{array} \right]^{\mathrm{T}}.$$

Moreover, for all $k \geq 0$

$$y(k) = \theta_{r,d}\phi_{r,d}(k) + w(k) + e_{r,d}(k). \tag{3.41}$$

3.6.1 Noncausal Closed-Loop Identification Using Least Squares

The least squares (LS) estimate $\hat{\theta}^{\mathrm{LS}}_{r,d,\ell}$ of $\theta_{r,d}$ is given by

$$\hat{\theta}^{\mathrm{LS}}_{r,d,\ell} = \underset{\bar{\theta}_{r,d}}{\arg\min} \left\| \Psi_{y,\ell} - \bar{\theta}_{r,d}\Phi_{\mu,\ell} \right\|_{\mathrm{F}}, \tag{3.42}$$

where $\bar{\theta}_{r,d} \in \mathbb{R}^{l \times \mu m}$,

$$\Psi_{y,\ell} \triangleq \left[\begin{array}{ccc} y(r) & \cdots & y(\ell-d) \end{array} \right], \quad \Phi_{\mu,\ell} \triangleq \left[\begin{array}{ccc} \phi_{r,d}(r) & \cdots & \phi_{r,d}(\ell-d) \end{array} \right],$$

$\mu \triangleq r + d + 1$, and ℓ is the number of samples. It follows from (3.42) that the least squares estimate $\hat{\theta}^{\rm LS}_{r,d,\ell}$ of $\theta_{r,d}$ satisfies

$$\Psi_{y,\ell}\Phi^{\rm T}_{\mu,\ell} = \hat{\theta}^{\rm LS}_{r,d,\ell}\Phi_{\mu,\ell}\Phi^{\rm T}_{\mu,\ell}. \tag{3.43}$$

Note that

$$\Psi_{y,\ell} = \Psi y_{0,\ell} + \Psi_{w,\ell}, \quad \Psi_{y_0,\ell} = \theta_{r,d}\Phi_{\mu,\ell} + \Psi_{e_{r,d},\ell}, \quad \Phi_{\mu,\ell} = \Phi_{\mu_0,\ell} + \Phi_{v,\ell}, \tag{3.44}$$

where

$$\begin{aligned}
\Psi_{y_0,\ell} &\triangleq \begin{bmatrix} y_0(r) & \cdots & y_0(\ell-d) \end{bmatrix}, \quad \Psi_{w,\ell} \triangleq \begin{bmatrix} w(r) & \cdots & w(\ell-d) \end{bmatrix}, \\
\Phi_{\mu_0,\ell} &\triangleq \begin{bmatrix} \phi_{0_{r,d}}(r) & \cdots & \phi_{0_{r,d}}(\ell-d) \end{bmatrix}, \quad \phi_{0_{r,d}}(k) \triangleq \begin{bmatrix} u_0(k+d) & \cdots & u_0(k-r) \end{bmatrix}^{\rm T}, \\
\Phi_{v,\ell} &\triangleq \begin{bmatrix} \phi_{v_{r,d}}(r) & \cdots & \phi_{v_{r,d}}(\ell-d) \end{bmatrix}, \quad \phi_{v_{r,d}}(k) \triangleq \begin{bmatrix} v(k+d) & \cdots & v(k-r) \end{bmatrix}^{\rm T}.
\end{aligned}$$

Then, (3.43) becomes

$$\theta_{r,d}\Phi_{\mu,\ell}\Phi^{\rm T}_{\mu,\ell} + \Psi_{w,\ell}\Phi^{\rm T}_{\mu,\ell} + \Psi_{e_{r,d},\ell}\Phi^{\rm T}_{\mu,\ell} = \hat{\theta}^{\rm LS}_{r,d,\ell}\Phi_{\mu,\ell}\Phi^{\rm T}_{\mu,\ell}, \tag{3.45}$$

where

$$\Psi_{e_{r,d},\ell} \triangleq \begin{bmatrix} e_{r,d}(r) & \cdots & e_{r,d}(\ell-d) \end{bmatrix}.$$

Note from Figure 3.11 that u can be written as

$$u(k) = G_{u,c}(z)c(k) + G_{u,v}(z)v(k) + G_{u,w_0}(z)w_0(k), \tag{3.46}$$

where $G_{u,c}$, $G_{u,v}$, and G_{u,w_0} are the asymptotically stable closed loop transfer functions from c, v, and w_0 to u, respectively. It follows from (3.46) that we can write

$$\mathcal{U}(k) = G_{u,c}(z)\mathcal{C}(k) + G_{u,v}(z)\mathcal{V}(k) + G_{u,w_0}(z)\mathcal{W}_0(k). \tag{3.47}$$

Since $\mathcal{C}$, $\mathcal{V}$, and $\mathcal{W}_0$ are ergodic processes and $\mathcal{U}$ is the output of a linear time-invariance (LTI) system whose inputs are ergodic, then (3.47) implies that $\mathcal{U}$ is also ergodic. Similarly, we can show that $\mathcal{W}$, $\mathcal{Y}_0$, and $\mathcal{Y}$ are ergodic.

Dividing (3.45) by ℓ and taking the limit as ℓ tends to infinity yields

$$\theta_{r,d} \lim_{\ell\to\infty} \frac{1}{\ell}\Phi_{\mu,\ell}\Phi_{\mu,\ell}^{\mathrm{T}} + \lim_{\ell\to\infty} \frac{1}{\ell}\Psi_{w,\ell}\Phi_{\mu,\ell}^{\mathrm{T}} + \lim_{\ell\to\infty} \frac{1}{\ell}\Psi_{e_{r,d},\ell}\Phi_{\mu,\ell}^{\mathrm{T}} \overset{\mathrm{wp1}}{=} \lim_{\ell\to\infty} \frac{1}{\ell}\hat{\theta}_{r,d,\ell}^{\mathrm{LS}}\Phi_{\mu,\ell}\Phi_{\mu,\ell}^{\mathrm{T}}, \tag{3.48}$$

where $\lim_{\ell\to\infty} \frac{1}{\ell}\Phi_{\mu,\ell}\Phi_{\mu,\ell}^{\mathrm{T}}$, $\lim_{\ell\to\infty} \frac{1}{\ell}\Psi_{w,\ell}\Phi_{\mu,\ell}^{\mathrm{T}}$, and $\lim_{\ell\to\infty} \frac{1}{\ell}\Psi_{e_{r,d},\ell}\Phi_{\mu,\ell}^{\mathrm{T}}$ exist due to ergodicity conditions.

Define

$$Q \triangleq \lim_{\ell\to\infty} \frac{1}{\ell}\Phi_{\mu,\ell}\Phi_{\mu,\ell}^{\mathrm{T}}. \tag{3.49}$$

Therefore, (3.48) can be written as

$$\theta_{r,d}Q + \lim_{\ell\to\infty} \frac{1}{\ell}\Psi_{w,\ell}\Phi_{\mu,\ell}^{\mathrm{T}} + \lim_{\ell\to\infty} \frac{1}{\ell}\Psi_{e_{r,d},\ell}\Phi_{\mu,\ell}^{\mathrm{T}} \overset{\mathrm{wp1}}{=} \lim_{\ell\to\infty} \hat{\theta}_{r,d,\ell}^{\mathrm{LS}}Q. \tag{3.50}$$

Taking the limit as r and d tend to infinity, (3.50) becomes

$$\lim_{r,d\to\infty} \theta_{r,d}Q + \lim_{r,d\to\infty}\lim_{\ell\to\infty} \frac{1}{\ell}\Psi_{w,\ell}\Phi_{\mu,\ell}^{\mathrm{T}} + \lim_{r,d\to\infty}\lim_{\ell\to\infty} \frac{1}{\ell}\Psi_{e_{r,d},\ell}\Phi_{\mu,\ell}^{\mathrm{T}} \overset{\mathrm{wp1}}{=} \lim_{r,d\to\infty}\lim_{\ell\to\infty} \hat{\theta}_{r,d,\ell}^{\mathrm{LS}}Q. \tag{3.51}$$

It follows from (3.37) that

$$\lim_{r,d\to\infty}\lim_{\ell\to\infty} \frac{1}{\ell}\Psi_{e_{r,d},\ell}\Phi_{\mu,\ell}^{\mathrm{T}} \overset{\mathrm{wp1}}{=} 0_{l\times\mu m}. \tag{3.52}$$

Therefore, (3.51) becomes

$$\lim_{r,d\to\infty}\lim_{\ell\to\infty}\frac{1}{\ell}\Psi_{w,\ell}\Phi_{\mu,\ell}^{\mathrm{T}} \overset{\mathrm{wp1}}{=} \left(\lim_{r,d\to\infty}\lim_{\ell\to\infty}\hat{\theta}_{r,d,\ell}^{\mathrm{LS}} - \lim_{r,d\to\infty}\theta_{r,d}\right)Q. \tag{3.53}$$

Since w and u are realizations of correlated processes, then $\lim_{r,d\to\infty}\lim_{\ell\to\infty}\frac{1}{\ell}\Psi_{w,\ell}\Phi_{\mu,\ell}^{\mathrm{T}}$ is not zero. Therefore, (3.53) implies that $(\lim_{r,d\to\infty}\lim_{\ell\to\infty}\hat{\theta}_{r,d,\ell}^{\mathrm{LS}} - \lim_{r,d\to\infty}\theta_{r,d})Q$ is not zero, which implies that $\lim_{r,d\to\infty}\lim_{\ell\to\infty}\hat{\theta}_{r,d,\ell}^{\mathrm{LS}} - \lim_{r,d\to\infty}\theta_{r,d}$ is not in the left null space of Q, and thus is not zero. Therefore, $\hat{\theta}_{r,d,\ell}^{\mathrm{LS}}$ is not a consistent estimator of $\theta_{r,d}$.

3.6.2 Noncausal Closed-Loop Identification Using the Basic Instrumental Variables Method

The basic instrumental variables (BIV) method [72] is used with an FIR model to identify the transfer function G shown in Figure 3.11 by modifying (3.43) [72, 99]. A typical choice of the vector of instrumental variables for closed-loop identification is to use samples of the exogenous signal c [87]. Let $\phi_{c,r,d}(k)$ denote the vector of instrumental variables, that is,

$$\phi_{c,r,d}(k) \triangleq \begin{bmatrix} c(k+d) & \cdots & c(k-r) \end{bmatrix}^{\mathrm{T}} \in \mathbb{R}^{\mu m}. \tag{3.54}$$

We then modify (3.43) as

$$\Psi_{y,\ell}\Phi_{c,\mu,\ell}^{\mathrm{T}} = \hat{\theta}_{r,d,\ell}^{\mathrm{IV}}\Phi_{\mu,\ell}\Phi_{c,\mu,\ell}^{\mathrm{T}}, \tag{3.55}$$

where

$$\Phi_{c,\mu,\ell} \triangleq \begin{bmatrix} \phi_{c,r,d}(r) & \cdots & \phi_{c,r,d}(\ell-d) \end{bmatrix}. \tag{3.56}$$

Then, (3.55) becomes

$$\theta_{r,d}\Phi_{\mu_0,\ell}\Phi_{c,\mu,\ell}^{\mathrm{T}} + \theta_{r,d}\Phi_{v,\ell}\Phi_{c,\mu,\ell}^{\mathrm{T}} + \Psi_{w,\ell}\Phi_{c,\mu,\ell}^{\mathrm{T}} + \Psi_{e_{r,d},\ell}\Phi_{c,\mu,\ell}^{\mathrm{T}} = \hat{\theta}_{r,d,\ell}^{\mathrm{IV}}\Phi_{\mu_0,\ell}\Phi_{c,\mu,\ell}^{\mathrm{T}} + \hat{\theta}_{r,d,\ell}^{\mathrm{IV}}\Phi_{v,\ell}\Phi_{c,\mu,\ell}^{\mathrm{T}}. \tag{3.57}$$

Since $\mathcal{C}, \mathcal{W}_0$, and $\mathcal{V}$ are ergodic processes, (3.57) implies

$$\begin{aligned}\theta_{r,d}\lim_{\ell\to\infty}\frac{1}{\ell}\Phi_{\mu_0,\ell}\Phi_{c,\mu,\ell}^{\mathrm{T}} + \theta_{r,d}\lim_{\ell\to\infty}\frac{1}{\ell}\Phi_{v,\ell}\Phi_{c,\mu,\ell}^{\mathrm{T}} + \lim_{\ell\to\infty}\frac{1}{\ell}\Psi_{w,\ell}\Phi_{c,\mu,\ell}^{\mathrm{T}} + \lim_{\ell\to\infty}\frac{1}{\ell}\Psi_{e_{r,d},\ell}\Phi_{c,\mu,\ell}^{\mathrm{T}} \\ \overset{\mathrm{wp1}}{=} \lim_{\ell\to\infty}\frac{1}{\ell}\hat{\theta}_{r,d,\ell}^{\mathrm{IV}}\Phi_{\mu_0,\ell}\Phi_{c,\mu,\ell}^{\mathrm{T}} + \lim_{\ell\to\infty}\frac{1}{\ell}\hat{\theta}_{r,d,\ell}^{\mathrm{IV}}\Phi_{v,\ell}\Phi_{c,\mu,\ell}^{\mathrm{T}}.\end{aligned} \tag{3.58}$$

Using (3.58), consistency of the estimated Markov parameters holds if $\Phi_{c,\mu,\ell}$ satisfies the following assumptions

A1) $\lim_{\ell\to\infty}\frac{1}{\ell}\Phi_{\mu_0,\ell}\Phi_{c,\mu,\ell}^{\mathrm{T}}$ is nonsingular.

A2) $\lim_{\ell\to\infty}\frac{1}{\ell}\Psi_{w,\ell}\Phi_{c,\mu,\ell}^{\mathrm{T}} \overset{\mathrm{wp1}}{=} 0_{l\times\mu m}$.

A3) $\lim_{\ell\to\infty}\frac{1}{\ell}\Phi_{v,\ell}\Phi_{c,\mu,\ell}^{\mathrm{T}} \overset{\mathrm{wp1}}{=} 0_{\mu m\times\mu m}$.

The vector of instrumental variables is constructed from the exogenous signal data, which is a realization of a stationary white random process and satisfies A1) [87]. Next, note that

$$\begin{aligned}\lim_{\ell\to\infty}\frac{1}{\ell}\Psi_{w,\ell}\Phi_{c,\mu,\ell}^{\mathrm{T}} &= \lim_{\ell\to\infty}\frac{1}{\ell}\begin{bmatrix} w(r) & \cdots & w(\ell-d)\end{bmatrix}\begin{bmatrix} c(r+d) & \ldots & c(0) \\ \vdots & \ldots & \vdots \\ c(\ell) & \ldots & c(\ell-r-d)\end{bmatrix} \\ &= \lim_{\ell\to\infty}\frac{1}{\ell}\begin{bmatrix} \sum_{i=r}^{\ell-d} w(i)c(i+d) & \cdots & \sum_{i=r}^{\ell-d} w(i)c(r-i)\end{bmatrix} \\ &\overset{\mathrm{wp1}}{=} \begin{bmatrix} \mathbb{E}\left[\mathcal{W}(k)\mathcal{C}(k+d)\right] & \cdots & \mathbb{E}\left[\mathcal{W}(k)\mathcal{C}(r-k)\right]\end{bmatrix} = 0_{l\times\mu m},\end{aligned} \tag{3.59}$$

where the last equality follows from the assumptions that $\mathcal{W}$ and $\mathcal{C}$ are independent processes and $\mathcal{C}$ is zero-mean. Similarly, we can show that

$$\lim_{\ell\to\infty}\frac{1}{\ell}\Phi_{v,\ell}\Phi_{c,\mu,\ell}^{\mathrm{T}} = 0_{\mu m\times\mu m}. \tag{3.60}$$

Then, it follows from (3.59) and (3.60) that the choice of the instrumental variables satisfies A2) and A3). Moreover, using (3.59) and (3.60), (3.58) becomes

$$\theta_{r,d}\left[\lim_{\ell\to\infty}\frac{1}{\ell}\Phi_{\mu_0,\ell}\Phi_{c,\mu,\ell}^{\mathrm{T}}\right]+\lim_{\ell\to\infty}\frac{1}{\ell}\Psi_{e_{r,d},\ell}\Phi_{\mu,\ell}^{\mathrm{T}} \overset{\text{wp1}}{=} \lim_{\ell\to\infty}\hat{\theta}_{r,d,\ell}^{\mathrm{IV}}\left[\lim_{\ell\to\infty}\frac{1}{\ell}\Phi_{\mu_0,\ell}\Phi_{c,\mu,\ell}^{\mathrm{T}}\right]. \tag{3.61}$$

Taking the limit of (3.61) as r and d tend to infinity and using (3.53) and assumption A1), (3.61) becomes

$$\lim_{r,d\to\infty}\lim_{\ell\to\infty}\hat{\theta}_{r,d,\ell}^{\mathrm{IV}} \overset{\text{wp1}}{=} \lim_{r,d\to\infty}\theta_{r,d}. \tag{3.62}$$

We choose r and d to be sufficiently large such that $\lim_{\ell\to\infty}\frac{1}{\ell}\Psi_{e_{r,d},\ell}\Phi_{\mu,\ell}^{\mathrm{T}}$ is negligible.

3.6.3 Noncausal Closed-Loop Identification Using the Extended Instrumental Variables Method

The extended instrumental variables (XIV) method generalizes the basic instrumental variables method by prefiltering the sampled data of the instrumental variables [72, 87]. That is, in (3.55) we replace $\Phi_{c,\mu,\ell}$ by

$$\Phi_{\tilde{c},\mu,\ell} \triangleq L(z)\Phi_{c,\mu,\ell}, \tag{3.63}$$

where $L(z)$ is an asymptotically stable filter. Using the same argument used above to show consistency for the basic instrumental variables method, consistency of the estimated Markov parameters of XIV denoted by $\hat{\theta}_{r,d,\ell}^{\mathrm{XIV}}$, holds if $\Phi_{\tilde{c},\mu,\ell}$ satisfies the assumptions

B1) $\lim_{\ell\to\infty}\frac{1}{\ell}\Phi_{\mu_0,\ell}\Phi_{\tilde{c},\mu,\ell}^{\mathrm{T}}$ is nonsingular.

B2) $\lim_{\ell\to\infty} \frac{1}{\ell}\Psi_{w,\ell}\Phi^{\mathrm{T}}_{\tilde{c},\mu,\ell} \overset{\mathrm{wp1}}{=} 0_{l\times\mu m}$.

B3) $\lim_{\ell\to\infty} \frac{1}{\ell}\Phi_{v,\ell}\Phi^{\mathrm{T}}_{\tilde{c},\mu,\ell} \overset{\mathrm{wp1}}{=} 0_{\mu m\times\mu m}$.

3.6.4 Noncausal Closed-Loop Identification Using Prediction Error Methods

Let $\hat{G}_\ell(\mathbf{q})$ and $\hat{G}_{w,\ell}(\mathbf{q})$ be estimates of $G(\mathbf{q})$ and $G_w(\mathbf{q})$, respectively, obtained with ℓ samples of input and output data, and assume that $G_w(\mathbf{q})$ and $\hat{G}_{w,\ell}(\mathbf{q})$ are square and nonsingular. Note that y in Figure 3.11 can be written as

$$y(k) = G(\mathbf{q})u(k) + G_w(\mathbf{q})w_0(k). \tag{3.64}$$

Then, the one-step predictor of (3.64) is defined by [100]

$$y(k|\hat{G}_\ell, \hat{G}_{w,\ell}) \overset{\triangle}{=} \hat{G}^{-1}_{w,\ell}(\mathbf{q})\hat{G}_\ell(\mathbf{q})u(k) + (1 - \hat{G}^{-1}_{w,\ell}(\mathbf{q}))y(k). \tag{3.65}$$

Define the prediction error

$$\varepsilon(k|\hat{G}_\ell, \hat{G}_{w,\ell}) \overset{\triangle}{=} y(k) - y(k|\hat{G}_\ell, \hat{G}_{w,\ell}). \tag{3.66}$$

Using (3.64) and (3.65), (3.66) can be written as

$$\begin{aligned}
\varepsilon(k|\hat{G}_\ell, \hat{G}_{w,\ell}) &= y(k) - \hat{G}^{-1}_{w,\ell}(\mathbf{q})\hat{G}_\ell(\mathbf{q})u(k) - (1 - \hat{G}^{-1}_{w,\ell}(\mathbf{q}))y(k) \\
&= \hat{G}^{-1}_{w,\ell}(\mathbf{q})(y(k) - \hat{G}_\ell(\mathbf{q})u(k)) \\
&= \hat{G}^{-1}_{w,\ell}(\mathbf{q})\Big((G(\mathbf{q}) - \hat{G}_\ell(\mathbf{q}))u(k) + G_w(\mathbf{q})w_0(k)\Big) \\
&= \hat{G}^{-1}_{w,\ell}(\mathbf{q})\Big((G(\mathbf{q}) - \hat{G}_\ell(\mathbf{q}))u(k) + (G_w(\mathbf{q}) - \hat{G}_{w,\ell}(\mathbf{q}))w_0(k)\Big) + w_0(k).
\end{aligned} \tag{3.67}$$

Assume that G, G_w, and G_w^{-1} have no poles on the unit circle. Then G, G_w, and G_w^{-1} are analytic in the maximal annulus that contains the unit circle with the Laurent series given by (3.22) for G and with the Laurent series

$$G_w(z) = \sum_{i=-\infty}^{\infty} M_i z^{-i}, \tag{3.68}$$

$$G_w^{-1}(z) = \sum_{i=-\infty}^{\infty} N_i z^{-i}, \tag{3.69}$$

for G_w and G_w^{-1}, respectively, in the maximal annulus that contains the unit circle, where for all i, $M_i, N_i \in \mathbb{R}^{l\times l}$. Define

$$\mathcal{H}(\mathbf{q}, \theta_{r,d}) \triangleq \sum_{i=-d}^{r} L_i \mathbf{q}^{-i}, \quad \mathcal{H}(\mathbf{q}, \theta_{M,r,d}) \triangleq \sum_{i=-d}^{r} M_i \mathbf{q}^{-i}, \quad \mathcal{H}(\mathbf{q}, \theta_{N,r,d}) \triangleq \sum_{i=-d}^{r} N_i \mathbf{q}^{-i}, \tag{3.70}$$

$$\theta_{r,d} \triangleq \begin{bmatrix} L_{-d} & \cdots & L_r \end{bmatrix}, \ \theta_{M,r,d} \triangleq \begin{bmatrix} M_{-d} & \cdots & M_r \end{bmatrix}, \ \theta_{N,r,d} \triangleq \begin{bmatrix} N_{-d} & \cdots & N_r \end{bmatrix}, \tag{3.71}$$

where $\theta_{r,d} \in \mathbb{R}^{l\times \mu m}$, and $\theta_{M,r,d}, \theta_{N,r,d} \in \mathbb{R}^{l\times \mu l}$. Note from (3.34) and (3.70) that

$$y_{0,r,d}(k) = \mathcal{H}(\mathbf{q}, \theta_{r,d})u(k). \tag{3.72}$$

Therefore, (3.35) implies that

$$\begin{aligned} e_{r,d}(k) &= y_0(k) - \mathcal{H}(\mathbf{q}, \theta_{r,d})u(k) \\ &= G(\mathbf{q})u(k) - \mathcal{H}(\mathbf{q}, \theta_{r,d})u(k). \end{aligned} \tag{3.73}$$

Moreover, define

$$
\begin{aligned}
e_{w,r,d}(k) &\stackrel{\triangle}{=} w(k) - \mathcal{H}(\mathbf{q}, \theta_{M,r,d}) w_0(k) \\
&= G_w(\mathbf{q}) w_0(k) - \mathcal{H}(\mathbf{q}, \theta_{M,r,d}) w_0(k).
\end{aligned} \tag{3.74}
$$

Therefore, (3.73) and (3.74) imply, respectively, that

$$
G(\mathbf{q}) u(k) = \mathcal{H}(\mathbf{q}, \theta_{r,d}) u(k) + e_{r,d}(k), \tag{3.75}
$$

$$
G_w(\mathbf{q}) w_0(k) = \mathcal{H}(\mathbf{q}, \theta_{M,r,d}) w_0(k) + e_{w,r,d}(k). \tag{3.76}
$$

Let

$$
\mathcal{H}(\mathbf{q}, \hat{\theta}_{r,d,\ell}) \stackrel{\triangle}{=} \hat{G}_\ell(\mathbf{q}) = \sum_{i=-d}^{r} \hat{L}_{i,\ell} \mathbf{q}^{-i}, \quad \hat{\theta}_{r,d,\ell} \stackrel{\triangle}{=} \left[\begin{array}{ccc} \hat{L}_{-d,\ell} & \cdots & \hat{L}_{r,\ell} \end{array} \right], \tag{3.77}
$$

$$
\mathcal{H}(\mathbf{q}, \hat{\theta}_{M,r,d,\ell}) \stackrel{\triangle}{=} \hat{G}_{w,\ell}(\mathbf{q}) = \sum_{i=-d}^{r} \hat{M}_{i,\ell} \mathbf{q}^{-i}, \quad \hat{\theta}_{M,r,d,\ell} \stackrel{\triangle}{=} \left[\begin{array}{ccc} \hat{M}_{-d,\ell} & \cdots & \hat{M}_{r,\ell} \end{array} \right], \tag{3.78}
$$

$$
\mathcal{H}(\mathbf{q}, \hat{\theta}_{N,r,d,\ell}) \stackrel{\triangle}{=} \hat{G}_{w,\ell}^{-1}(\mathbf{q}) = \sum_{i=-d}^{r} \hat{N}_{i,\ell} \mathbf{q}^{-i}, \quad \hat{\theta}_{N,r,d,\ell} \stackrel{\triangle}{=} \left[\begin{array}{ccc} \hat{N}_{-d,\ell} & \cdots & \hat{N}_{r,\ell} \end{array} \right], \tag{3.79}
$$

where $\hat{\theta}_{r,d,\ell} \in \mathbb{R}^{l \times \mu m}$ and $\hat{\theta}_{M,r,d,\ell}, \hat{\theta}_{N,r,d,\ell} \in \mathbb{R}^{l \times \mu l}$. Then, using (3.75)–(3.79), (3.67) can be rewritten as

$$
\begin{aligned}
\varepsilon(k|\hat{\theta}_{r,d,\ell}, \hat{\theta}_{M,r,d,\ell}, \hat{\theta}_{N,r,d,\ell}) \stackrel{\triangle}{=} & \mathcal{H}(\mathbf{q}, \hat{\theta}_{N,r,d,\ell}) \Big[(\mathcal{H}(\mathbf{q}, \theta_{r,d}) - \mathcal{H}(\mathbf{q}, \hat{\theta}_{r,d,\ell})) u(k) \\
& + (\mathcal{H}(\mathbf{q}, \theta_{M,r,d}) - \mathcal{H}(\mathbf{q}, \hat{\theta}_{M,r,d,\ell})) w_0(k) + e_{r,d}(k) + e_{w,r,d}(k) \Big] + w_0(k) \\
= & \mathcal{H}(\mathbf{q}, \hat{\theta}_{N,r,d,\ell}) \Big[T^{\mathrm{T}}(\mathbf{q}, \hat{\theta}_{r,d,\ell}, \hat{\theta}_{M,r,d,\ell}) \xi(k) + e_{r,d}(k) + e_{w,r,d}(k) \Big] + w_0(k),
\end{aligned} \tag{3.80}
$$

where

$$T(\mathbf{q},\hat{\theta}_{r,d,\ell},\hat{\theta}_{M,r,d,\ell}) \triangleq \begin{bmatrix} \mathcal{H}(\mathbf{q},\theta_{r,d}) - \mathcal{H}(\mathbf{q},\hat{\theta}_{r,d,\ell}) \\ \mathcal{H}(\mathbf{q},\theta_{M,r,d}) - \mathcal{H}(\mathbf{q},\hat{\theta}_{M,r,d,\ell}) \end{bmatrix}, \quad \xi(k) \triangleq \begin{bmatrix} u(k) \\ w_0(k) \end{bmatrix}. \tag{3.81}$$

Define

$$\hat{\theta}_\ell \triangleq \lim_{r,d\to\infty} \hat{\theta}_{r,d,\ell}, \quad \hat{\theta}_{M,\ell} \triangleq \lim_{r,d\to\infty} \hat{\theta}_{M,r,d,\ell}, \quad \hat{\theta}_{N,\ell} \triangleq \lim_{r,d\to\infty} \hat{\theta}_{N,r,d,\ell}, \tag{3.82}$$

$$\varepsilon(k|\hat{\theta}_\ell,\hat{\theta}_{M,\ell},\hat{\theta}_{N,\ell}) \triangleq \lim_{r,d\to\infty} \varepsilon(k|\hat{\theta}_{r,d,\ell},\hat{\theta}_{M,r,d,\ell},\hat{\theta}_{N,r,d,\ell}), \tag{3.83}$$

$$T(\mathbf{q},\hat{\theta},\hat{\theta}_{M,\ell}) \triangleq \lim_{r,d\to\infty} T(\mathbf{q},\hat{\theta}_{r,d,\ell},\hat{\theta}_{M,r,d,\ell}) = \begin{bmatrix} \mathcal{H}(\mathbf{q},\theta) - \mathcal{H}(\mathbf{q},\hat{\theta}_\ell) \\ \mathcal{H}(\mathbf{q},\theta_M) - \mathcal{H}(\mathbf{q},\hat{\theta}_{M,\ell}) \end{bmatrix}. \tag{3.84}$$

Note from (3.68) and (3.70) that

$$\lim_{r,d\to\infty} \mathcal{H}(\mathbf{q},\theta_{M,r,d}) = G_w(\mathbf{q}), \tag{3.85}$$

which implies that

$$\lim_{r,d\to\infty} e_{w,r,d}(k) = G_w(\mathbf{q})w_0(k) - \lim_{r,d\to\infty} \mathcal{H}(\mathbf{q},\theta_{M,r,d})w_0(k) = 0. \tag{3.86}$$

Using (3.37) and (3.82)–(3.86), taking the limit of (3.80) as r and d tend to infinity yields

$$\varepsilon(k|\hat{\theta}_\ell,\hat{\theta}_{M,\ell},\hat{\theta}_{N,,\ell}) = \mathcal{H}(\mathbf{q},\hat{\theta}_{N,\ell})T^{\mathrm{T}}(\mathbf{q},\hat{\theta}_\ell,\hat{\theta}_{M,\ell})\xi(k) + w_0(k). \tag{3.87}$$

Next, define the cost function

$$V(\ell,\hat{\theta}_\ell,\hat{\theta}_{M,\ell},\hat{\theta}_{N,\ell}) \triangleq \frac{1}{\ell}\sum_{k=1}^{\ell} \|\varepsilon(k|\hat{\theta}_\ell,\hat{\theta}_{M,\ell},\hat{\theta}_{N,\ell})\|_2^2. \tag{3.88}$$

Define

$$\hat{\theta} \triangleq \lim_{\ell\to\infty} \hat{\theta}_\ell, \quad \hat{\theta}_M \triangleq \lim_{\ell\to\infty} \hat{\theta}_{M,\ell}, \quad \hat{\theta}_N \triangleq \lim_{\ell\to\infty} \hat{\theta}_{N,\ell}, \tag{3.89}$$

which are independent of the data due to ergodicity. Define

$$\bar{V}(\hat{\theta}, \hat{\theta}_M, \hat{\theta}_N) \triangleq \lim_{\ell\to\infty} V(\ell, \hat{\theta}_\ell, \hat{\theta}_{M,\ell}, \hat{\theta}_{N,\ell}). \tag{3.90}$$

Using Parseval's theorem, (3.90) becomes

$$\bar{V}(\hat{\theta}, \hat{\theta}_M, \hat{\theta}_N) = \frac{1}{2\pi} \int_{-\pi}^{\pi} \Phi_\varepsilon(\omega) \mathrm{d}\omega, \tag{3.91}$$

where using (3.87), the spectrum of ε is given by

$$\Phi_\varepsilon(\omega) \triangleq \mathcal{H}(e^{\jmath\omega}, \hat{\theta}_N) T^{\mathrm{T}}(e^{\jmath\omega}, \hat{\theta}, \hat{\theta}_M) \Phi_\xi(\omega) T(e^{-\jmath\omega}, \hat{\theta}, \hat{\theta}_M) \mathcal{H}^{\mathrm{T}}(e^{-\jmath\omega}, \hat{\theta}_N) + \lambda_{w_0}, \tag{3.92}$$

$\mathcal{H}(e^{\jmath\omega}, \hat{\theta}_N)$ and $T(e^{\jmath\omega}, \hat{\theta}, \hat{\theta}_M)$ are the discrete-time Fourier transforms of $\mathcal{H}(\mathbf{q}, \hat{\theta}_N)$ and $T(\mathbf{q}, \hat{\theta}, \hat{\theta}_M)$, respectively,

$$\Phi_\xi(\omega) \triangleq \begin{bmatrix} \Phi_u(\omega) & \Phi_{u,w_0}(\omega) \\ \Phi_{w_0,u}(\omega) & \lambda_{w_0} \end{bmatrix} \tag{3.93}$$

is the spectrum of ξ, Φ_u is the spectrum of u, λ_{w_0} is the variance of w_0, and Φ_{u,w_0} and $\Phi_{w_0,u}$ are the cross-power spectra between u and w_0.

Note from (3.84) and (3.92) that $T(e^{\jmath\omega}, \hat{\theta}, \hat{\theta}_M) = T(e^{\jmath\omega}, \theta, \theta_M)$ is the global minimizer of (3.92), which implies that the PEM estimates $\hat{\theta}_\ell^{\mathrm{PEM}}$ and $\hat{\theta}_{M,\ell}^{\mathrm{PEM}}$ of θ and θ_M, respectively, converge to the true values as ℓ tends to infinity, that is,

$$\lim_{\ell\to\infty} \hat{\theta}_\ell^{\mathrm{PEM}} = \theta, \quad \lim_{\ell\to\infty} \hat{\theta}_{M,\ell}^{\mathrm{PEM}} = \theta_M. \tag{3.94}$$

We choose r and d to be sufficiently large such that $e_{r,d}(k)$ and $e_{w,r,d}(k)$ are negligible for all $k \geq 1$.

3.7 Numerical Examples

To identify a noncausal FIR model of a transfer function G in the closed-loop system shown in Figure 3.11 we delay the measured output data by d steps and then apply the identification methods discussed in the previous section using the input data and delayed output data. A nonzero estimate of the noncausal component of the identified FIR model indicates that G may have at least one unstable pole; otherwise G is asymptotically stable.

We assume that the exogenous signal c in Figure 3.11 is a realization of a stationary white random process $\mathcal{C}$ with the Gaussian pdf $\mathcal{N}(0,1)$. Moreover, we assume that the intermediate signal u is measured. In the first example in this section we assume noise-free data, that is, $v(k) = 0$ and $w(k) = 0$ for all $k \geq 0$ and we use least squares to identify a baseline model. These examples illustrate the role of the noncausal terms in the identified model. The second example in this section compares the accuracy of the identified model obtained using least squares, instrumental variables techniques, and prediction error methods for both IIR and noncausal FIR models in the presence of noise.

Example 3.1. Consider the unstable MIMO system

$$G(z) = \begin{bmatrix} G_{1,1}(z) & G_{1,2}(z) \\ G_{2,1}(z) & G_{2,2}(z) \end{bmatrix} \triangleq \frac{1}{z^2 - 2z + 0.35} \begin{bmatrix} -z + 6.3 & 5z - 11.9 \\ 4z - 14 & -12z + 26 \end{bmatrix}, \quad (3.95)$$

with the realization

$$A = \begin{bmatrix} 1.5 & 0.2 \\ 2 & 0.5 \end{bmatrix}, \quad B = \begin{bmatrix} 1 & -1 \\ -1 & 3 \end{bmatrix}, \quad C = \begin{bmatrix} 1 & 2 \\ 0 & -4 \end{bmatrix}, \quad D = 0_{2\times 2}. \qquad (3.96)$$

Consider the LQR controller with $Q = 2I_2$ and $R = I_2$, where I_2 is the 2×2 identity matrix, and thus

$$K = \begin{bmatrix} 2.5446 & 0.4259 \\ 1.3095 & 0.2707 \end{bmatrix}. \qquad (3.97)$$

Let $r = 25$ and $d = 25$. Figure 3.12 shows the true and identified Laurent series coefficients of G in $\mathbb{A}(\rho_{\rm s}, \rho_{\rm u})$, where $\rho_{\rm s} \approx 0.1938$ and $\rho_{\rm u} \approx 1.8062$. Note that the impulse response of G has both causal and noncausal components, where the causal components are due to the stable part of G and the noncausal components are due to the unstable part of G. ■

Example 3.2. Consider the 7^{th}-order unstable but not strongly unstable transfer

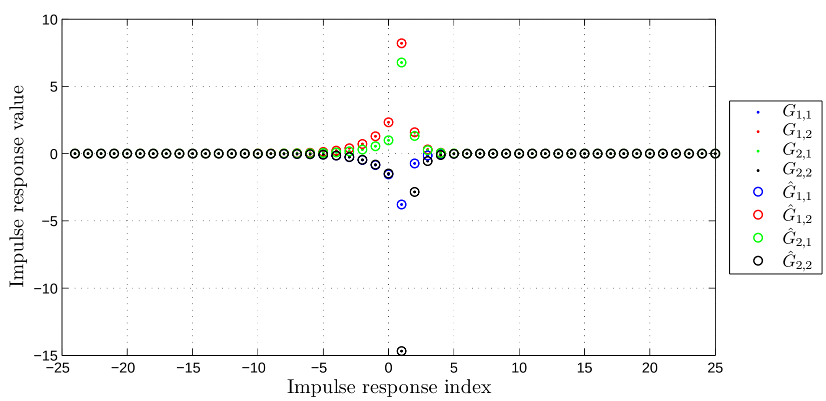

Figure 3.12: G is the MIMO system (3.95), $r = 25$, and $d = 25$ output-delay steps. The entries of the true impulse response of G are shown in dot markers and the entries of the identified impulse response of G are shown in circle markers. Note that the impulse response of G has both causal and noncausal components.

function

$$G(z) = \frac{(z^2+0.16)(z-0.3)(z+0.3)}{(z+0.7)(z+0.6)(z^2+0.25)(z-1.8)(z-1.7)(z-1.6)} \tag{3.98}$$

and the LQR controller with weighting matrices $Q = I_7$ and $R = 1$, and thus

$$K = \begin{bmatrix} 3.5197 & -3.1272 & -3.0739 & 2.0825 & 1.0096 & 0.7134 & 0.4997 \end{bmatrix}. \tag{3.99}$$

We set $r = 50$ and $d = 50$. Let v in Figure 3.6 be a realization of a zero-mean white gaussian random process with signal-to-noise ratio of 10. Let $\hat{G}_{\mathrm{LS},\ell}$, $\hat{G}_{\mathrm{IV},\ell}$, and $\hat{G}_{\mathrm{PEM},\ell}$ of order n_{mod} be the identified IIR models using LS, IV, and PEM, respectively, where ℓ samples are used for identification. To perform the identification using IV and PEM we use the Matlab functions `iv4(data,'na',`n_{mod}`,'nb',`n_{mod}`)` and `pem(data,`n_{mod}`)`, respectively. We use (3.27) to find the noncausal FIR truncations of $\hat{G}_{\mathrm{LS},\ell}$, $\hat{G}_{\mathrm{IV},\ell}$, and $\hat{G}_{\mathrm{PEM},\ell}$, then we compute the error in the Markov parameters estimates defined by

$$\delta_\ell \triangleq \frac{1}{50}\sum_{i=1}^{50} ||\theta_{r,d} - \hat{\theta}_{r,d,\ell,i}||_2, \tag{3.100}$$

where $\hat{\theta}_{r,d,\ell,i}$ is the vector of coefficients of the noncausal FIR truncation of $\hat{G}_{\mathrm{LS},\ell}$, $\hat{G}_{\mathrm{IV},\ell}$, or $\hat{G}_{\mathrm{PEM},\ell}$ obtained from the i^{th} experiment.

Next, we consider a noncausal FIR model with $r = 50$ and $d = 50$, and we estimate the vector of Markov parameters for 50 independent realizations. We compute the error in the Markov parameters estimates using (3.100), where $\hat{\theta}_{r,d,\ell,i}$ in (3.100) is the estimate of the vector of Markov parameters obtained from the i^{th} experiment using LS, IV, or PEM.

Figure 3.13 shows δ_ℓ for LS, IV, and PEM with IIR and noncausal FIR models for $\ell = 10,000$ samples, where the order n_{mod} of the IIR model changes between 1 and 20 and the order of the noncausal FIR model is fixed at $r = 50$ and $d = 50$. Figure 3.13

shows that FIR models give better estimates than IIR models for all $1 \leq n_{\rm mod} \leq 20$.

In the next section, we show that the estimated parameters of the noncausal FIR model can be used to estimate the order of the system, which in turn can be used with PEM to make the IIR estimates more accurate.

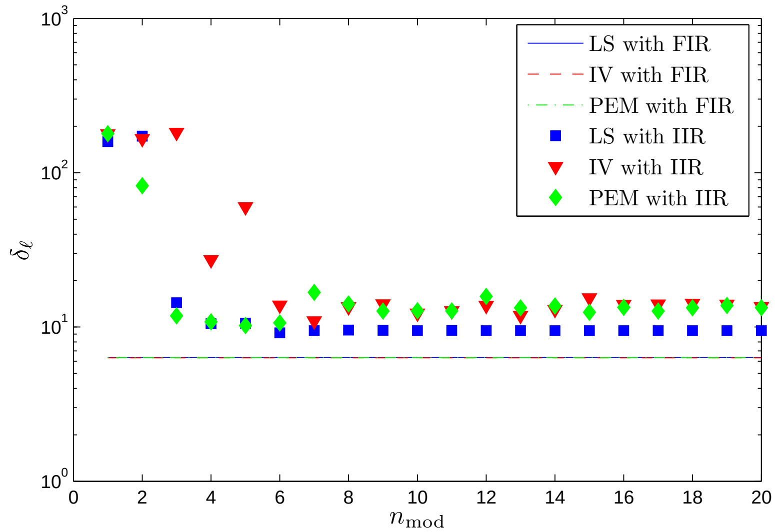

Figure 3.13: $G(z)$ given by (3.98) is an unstable but not strongly unstable transfer function, $r = 50$, $d = 50$ output-delay steps, $\ell = 10,000$ samples, and v in Figure 3.6 is a realization of a zero-mean white gaussian random process with signal-to-noise ratio of 10. This plot shows that FIR models give better coefficient estimates than IIR models for all $1 \leq n_{\rm mod} \leq 20$.

3.8 Reconstructing G from its Noncausal FIR Model

In order to reconstruct G from its noncausal FIR model we reconstruct the stable and unstable parts of G separately using the eigensystem realization algorithm (ERA) [78]. Then, we obtain G by adding these two terms together as in (3.18). Singular values of the Hankel matrix can be used to estimate the model orders $n_{\rm s}$ of $G_{\rm s}$ and $n_{\rm u}$ of $G_{\rm u}$. We begin with initial estimates $\hat{n}_{\rm s} \geq n_{\rm s}$ and $\hat{n}_{\rm u} \geq n_{\rm u}$. For $G_{\rm s}$, we set $r = 2\hat{n}_{\rm s} - 1$ and $d = 0$ and obtain the Markov parameters of $G_{\rm s}$ using the identification methods discussed above. On the other hand, for $G_{\rm u}$, we set $r = 0$ and $d = 2\hat{n}_{\rm u} - 1$ and obtain the Markov parameters of $G_{\mathrm{u}}(z^{-1})$ using the identification methods discussed above. Then, we construct the Markov block-Hankel matrix

$$\mathcal{H}(H_{\mathrm{s}}) \triangleq \begin{bmatrix} H_{\mathrm{s},1} & \cdots & H_{\mathrm{s},\hat{n}_{\mathrm{s}}} \\ \vdots & \ddots & \vdots \\ H_{\mathrm{s},\hat{n}_{\mathrm{s}}} & \cdots & H_{\mathrm{s},2\hat{n}_{\mathrm{s}}-1} \end{bmatrix}, \tag{3.101}$$

where

$$H_{\mathrm{s}} \triangleq \begin{bmatrix} H_{\mathrm{s},0} & \cdots & H_{\mathrm{s},2\hat{n}_{\mathrm{s}}-1} \end{bmatrix}, \tag{3.102}$$

and $\mathcal{H}(\cdot)$ is a linear mapping that constructs a Markov block-Hankel matrix from the components of the vector H_{s} except for $H_{\mathrm{s},0}$. The rank of $\mathcal{H}(H_{\mathrm{s}})$ is equal to the McMillan degree of G_{s}. Similarly, for $G_{\mathrm{u}}(z^{-1})$ we construct the Markov block-Hankel matrix

$$\mathcal{H}(H_{\mathrm{u}}) \triangleq \begin{bmatrix} H_{\mathrm{u},-2\hat{n}_{\mathrm{u}}+2} & \cdots & H_{\mathrm{u},-\hat{n}_{\mathrm{u}}+1} \\ \vdots & \ddots & \vdots \\ H_{\mathrm{u},-\hat{n}_{\mathrm{u}}+1} & \cdots & H_{\mathrm{u},0} \end{bmatrix}, \tag{3.103}$$

where

$$H_{\mathrm{u}} \triangleq \begin{bmatrix} H_{\mathrm{u},-2\hat{n}_{\mathrm{u}}+1} & \cdots & H_{\mathrm{u},0} \end{bmatrix}. \tag{3.104}$$

Note that $\mathcal{H}(\cdot)$ constructs a Markov block-Hankel matrix from the components of the vector H_{u} except for $H_{\mathrm{u},-2\hat{n}_{\mathrm{u}}+1}$. The rank of $\mathcal{H}(H_{\mathrm{u}})$ is equal to the McMillan degree of $G_{\mathrm{u}}(z^{-1})$.

We compute the singular values of $\mathcal{H}(H_{\mathrm{s}})$ and $\mathcal{H}(H_{\mathrm{u}})$ and look for a large decrease in the singular values. For noise-free data, a large decrease in the singular values is evident. However, even with a small amount of noise, the large decrease in the singular values disappears and thus the problem of estimating the model order becomes difficult [80].

The nuclear-norm minimization technique given in [79, 80] provides a heuristic optimization approach to this problem. Let $\hat{H}_{\rm s}$ be the vector of of estimated Markov parameters, where

$$\hat{H}_{\rm s} \triangleq \left[\begin{array}{ccc} \hat{H}_{{\rm s},0} & \cdots & \hat{H}_{{\rm s},2\hat{n}-1} \end{array} \right]. \tag{3.105}$$

To estimate the model order of $G_{\rm s}$ we solve the optimization problem

$$\underset{\bar{H}_{\rm s}(\gamma_{\rm s})}{\rm minimize} \|\mathcal{H}(\bar{H}_{\rm s}(\gamma_{\rm s}))\|_{\rm N} \tag{3.106}$$

subject to

$$\|\bar{H}_{\rm s}(\gamma_{\rm s}) - \hat{H}_{\rm s}\|_{\rm F} \leq \gamma_{\rm s}, \tag{3.107}$$

where $\gamma_{\rm s}$ is varied over a range of small positive numbers. For each value of $\gamma_{\rm s}$, we solve the optimization problem (3.106), (3.107), and then we construct the Markov block-Hankel matrix $\mathcal{H}(\bar{H}_{\rm s}(\gamma_{\rm s}))$ and compute its singular values. The singular values of $\mathcal{H}(\bar{H}_{\rm s}(\gamma_{\rm s}))$ that are robust to the change in $\gamma_{\rm s}$ provide an estimate of the McMillan degree of $G_{\rm s}$. Finally, we use ERA to construct the estimate $\hat{G}_{\rm s}(z)$ of $G_{\rm s}(z)$.

Similarly, let $\hat{H}_{\rm u}$ be the vector of of estimated Markov parameters, where

$$\hat{H}_{\rm u} \triangleq \left[\begin{array}{ccc} \hat{H}_{{\rm u},0} & \cdots & \hat{H}_{{\rm u},2\hat{n}-1} \end{array} \right]. \tag{3.108}$$

To estimate the model order of $G_{\rm u}$ we solve the optimization problem

$$\underset{\bar{H}_{\rm u}(\gamma_{\rm u})}{\rm minimize} \|\mathcal{H}(\bar{H}_{\rm u}(\gamma_{\rm u}))\|_{\rm N} \tag{3.109}$$

subject to

$$\|\bar{H}_{\rm u}(\gamma_{\rm u}) - \hat{H}_{\rm u}\|_{\rm F} \leq \gamma_{\rm u}, \tag{3.110}$$

where $\gamma_{\rm u}$ is varied over a range of small positive numbers. For each value of $\gamma_{\rm u}$, we solve the optimization problem (3.109), (3.110), and then we construct the Markov block-Hankel matrix $\mathcal{H}(\bar{H}_{\rm u}(\gamma_{\rm u}))$ and compute its singular values. The singular values of $\mathcal{H}(\bar{H}_{\rm u}(\gamma_{\rm u}))$ that are robust to the change in $\gamma_{\rm u}$ provide an estimate of the McMillan degree of $G_{\rm u}$. Finally, we use ERA to construct the estimate $\hat{G}_{\rm u}(z^{-1})$ of $G_{\rm u}(z^{-1})$.

The following example illustrates this method.

Example 3.3. Consider the system (3.98). We use c in Figure 3.6 to be a realization of the stationary white random process $\mathcal{C}$ with the Gaussian pdf $\mathcal{N}(0,1)$. Let v be a white noise signal with signal-to-noise ratio of 10. We set $r = 25$, $d = 25$, and $\ell = 5000$ points and then we identify a noncausal FIR model of G. The estimated Markov parameters are averaged over 100 experiments.

To choose the model order for $G_{\rm s}(z)$, we set $\hat{n}_{\rm s} = 10$ and we solve the optimization problem (3.106), (3.107) for a range of $\gamma_{\rm s}$ from 10^{-10} to 10^{-8}. For each value of $\gamma_{\rm s}$, we find the optimal $\hat{H}_{\rm s}(\gamma_{\rm s})$, and then we construct the Markov block-Hankel matrix $\mathcal{H}(\hat{H}_{\rm s}(\gamma_{\rm s}))$ and compute its singular values.

Figure 3.14 shows the singular values of the Hankel matrix $\mathcal{H}(\hat{H}_{\rm s}(\gamma_{\rm s}))$ versus $\gamma_{\rm s}$. Figure 3.14 shows that 4 singular values of $\mathcal{H}(\bar{H}_{\rm s}(\gamma_{\rm s}))$ are robust to the change in $\gamma_{\rm s}$, which correctly yields 4 as the estimated order of $G_{\rm s}$. Using ERA we obtain

$$\hat{G}_{\rm s}(z) = \frac{0.07241z^3 + 0.02234z^2 + 0.01606z - 0.00113}{z^4 + 1.3020z^3 + 0.7590z^2 + 0.3697z + 0.08392}. \tag{3.111}$$

Similarly, for $G_{\rm u}(z^{-1})$, we set $\hat{n}_{\rm u} = 10$ and we solve the optimization problem (3.109), (3.110) for a range of $\gamma_{\rm u}$ from 10^{-10} to 10^{-8}. For each value of $\gamma_{\rm u}$, we find the optimal $\hat{H}_{\rm u}(\gamma_{\rm u})$, and then we construct the Markov block-Hankel matrix $\mathcal{H}(\hat{H}_{\rm u}(\gamma_{\rm u}))$ and compute its singular values. Figure 3.15 shows the singular values of the Hankel matrix $\mathcal{H}(\hat{H}_{\rm u}(\gamma_{\rm s}))$ versus $\gamma_{\rm u}$. Figure 3.15 shows that 3 singular values of $\mathcal{H}(\bar{H}_{\rm u}(\gamma_{\rm u}))$ are robust to the change in $\gamma_{\rm u}$, which correctly yields 3 as the estimated order of $G_{\rm u}$.

Using ERA we obtain

$$\hat{G}_{\mathrm{u}}(z^{-1}) = \frac{0.0096z^3 - 0.0898z^2 + 0.0147z - 0.00002}{z^3 - 1.7680z^2 + 1.0400z - 0.2028}, \tag{3.112}$$

that is,

$$\hat{G}_{\mathrm{u}}(z) = \frac{0.00002z^3 - 0.0147z^2 + 0.0898z - 0.0096}{0.2028z^3 - 1.0400z^2 + 1.7680z - 1}. \tag{3.113}$$

It follows that the estimate $\hat{G}$ of G is

$$\begin{aligned}\hat{G}_{\mathrm{ERA}}(z) &= \hat{G}_{\mathrm{s}}(z) + \hat{G}_{\mathrm{u}}(z)\\ &= \frac{0.0001z^7 - 0.0001z^6 - 0.0006z^5 + 1.0070z^4 + 0.0018z^3 + 0.1573z^2 - 0.0694z + 0.0016}{z^7 - 3.8249z^6 + 2.8011z^5 + 2.8991z^4 - 1.6149z^3 - 0.9494z^2 - 1.0912z - 0.4138}.\end{aligned} \tag{3.114}$$

Figure 3.16 shows the difference between the bode plots of G and the estimates $\hat{G}_{\mathrm{ERA}}$, $\hat{G}_{\mathrm{IIR}}$ obtained using PEM with an IIR model with order $n_{\mathrm{mod}} = 5$, and $\hat{G}_{r,d}$ obtained using PEM with a noncausal FIR model with $r = 25$ and $d = 25$. Note that the noncausal FIR estimate, $\hat{G}_{r,d}$ yields the smallest error in the estimated frequency response of G. ■

3.9 Conclusions

In this chapter we used noncausal FIR models for closed-loop identification of open-loop-unstable plants. To identify the noncausal model we delayed the measured output relative to the measured input. We found that the identified FIR model approximates the Laurent series of the plant inside the annulus of analyticity lying between the disk of stable poles and the punctured plane of unstable poles. We presented examples to compare the accuracy of the identified model obtained using least squares, instrumental variables methods, and prediction error methods for both IIR and noncausal FIR models under arbitrary noise that is fed back into the loop.

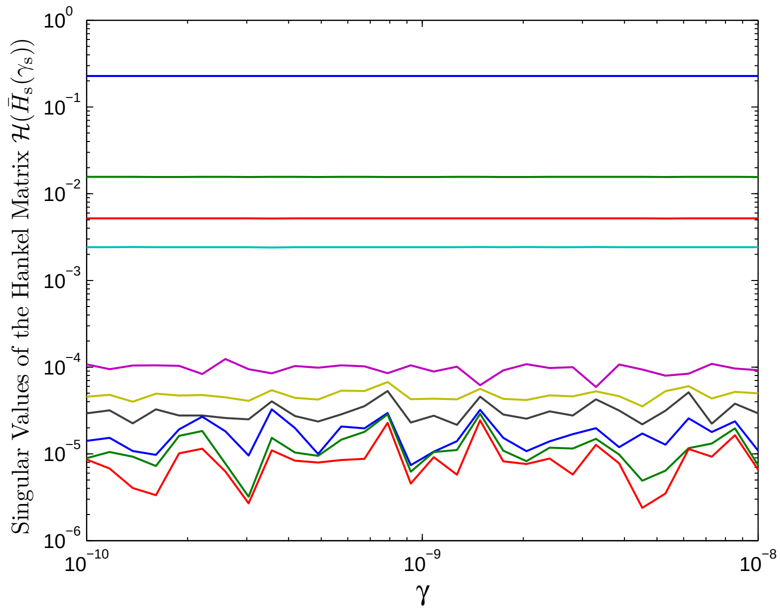

Figure 3.14: Plot of the singular values of $\mathcal{H}(\bar{H}(\gamma_s))$ versus γ_s, where $\hat{n}_s = 10$ and $\hat{H}_s$ in (3.107) is the vector of Markov parameters obtained using PEM with a noncausal FIR model of order $r = 25$ and $d = 25$, averaged over 100 independent realizations. Note that 4 singular values of $\mathcal{H}(\bar{H}(\gamma_s))$ are robust to the change in γ_s, which correctly yields 4 as the estimated order of G_s.

Numerical examples showed that for systems with unknown order, using noncausal FIR models for identification gives better estimates than using IIR models with an overestimated or underestimated model order. We used nuclear norm minimization technique to estimate the orders of the asymptotically stable and unstable parts of the plant, which can be used to improve the identification accuracy for IIR systems. Finally, we reconstructed an IIR model of the system from its stable and unstable parts using the eigensystem realization algorithm.

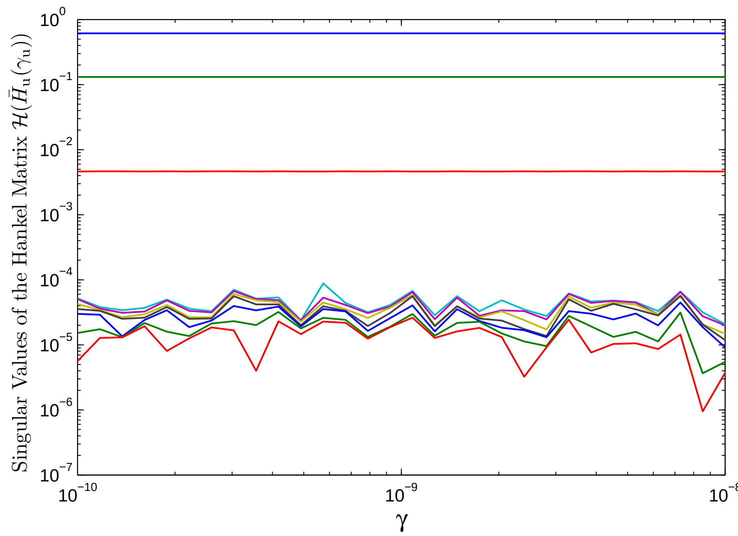

Figure 3.15: Plot of the singular values of $\mathcal{H}(\bar{H}(\gamma_{\mathrm{u}}))$ versus γ_{u}, where $\hat{n}_{\mathrm{u}} = 10$ and H in (3.110) is the vector of Markov parameters obtained using PEM with a noncausal FIR model of order $r = 25$ and $d = 25$ averaged over 100 independent realizations. Note that 3 singular values of $\mathcal{H}(\bar{H}(\gamma_{\mathrm{u}}))$ are robust to the change in γ_{u}, which correctly yields 3 as the estimated order of G_{u}.

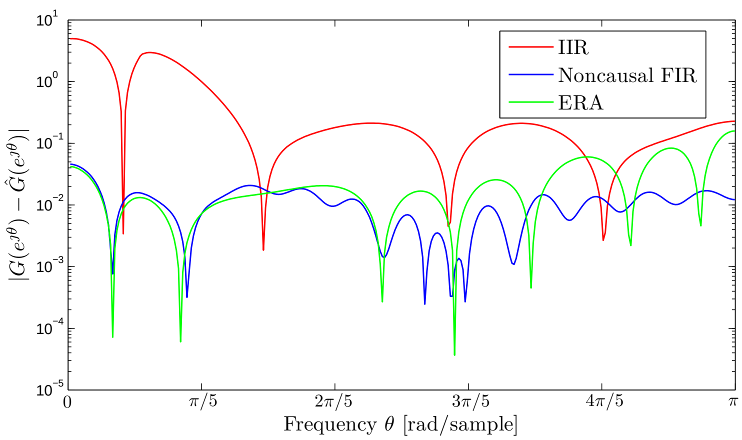

Figure 3.16: Bode plots of $G - \hat{G}_{\mathrm{IIR}}$ (red), $G - \hat{G}_{\mathrm{FIR}}$ (blue), and $G - \hat{G}_{\mathrm{ERA}}$ (green). Note that the noncausal FIR estimate $\hat{G}_{r,d}$ yields the smallest error in the estimated frequency response of G.

CHAPTER 4

Application to Health Monitoring of Aircraft Sensors and Acoustic Systems

4.1 Introduction

In the present chapter we use noncausal FIR models with prediction error methods to identify transmissibility operators. Then, we use the identified transmissibility operators for rate-gyro health monitoring in aircraft and to detect changes in the dynamics of a vibrating plate and an acoustic system.

The NASA Generic Transport Model (GTM) [65, 66] is used to simulate the fully nonlinear aircraft dynamics for data generation. In particular, we excite the aircraft by using the ailerons, elevator, and rudder, and we use rate-gyro measurements along with sideslip-angle measurements to construct a 1×3 transmissibility operator. We then use the transmissibility operator for health monitoring by computing the resulting one-step residual. The case of gyro drift is considered as an illustrative example.

Next, we consider simulating a vibrating plate with clamped-free-free-free (CFFF) boundary conditions. Three actuators and five sensors are placed on the plate. Measurements from the five sensors are used to construct a 1×1, 1×2, 1×3, and 1×4 transmissibility operators. We then use these transmissibility operators to estimate the number of excitations acting on the plate and to detect changes in the dynamics of the plate by computing the resulting one-step residual.

Next, we consider an experimental setup consisting of a drum with two speakers and four microphones. Each speaker is an actuator, and each microphone is a sensor that measures the acoustic response at its location. Two plastic pieces are placed inside the drum, and these can be removed during operation to emulate changes to the system. Measurements from the four microphones are used to construct a 1×1, 1×2, and 1×3 transmissibility operators. We then use these transmissibility operators to estimate the number of excitations acting on the system and to detect changes in the dynamics of the system by computing the resulting one-step residual.

4.2 Noncausal FIR Approximation of Transmissibility Operators

Expression (2.49) shows that a transmissibility operator contains information about the zeros of the system and not the poles. Therefore, a nonminimum-phase zero in the pseudo-input channel of a transmissibility operator yields an unstable transmissibility operator. Moreover, if the pseudo-output channel of a transmissibility operator has more zeros than the pseudo-input channel, then the transmissibility operator is improper, and thus noncausal. However, neither instability nor causality has the usual meaning associated with transfer functions. Nevertheless, to facilitate system identification, we consider a class of models that can approximate transmissibility operators that may be unstable, noncausal, and of unknown order. This class of models consists of noncausal FIR models based on a truncated Laurent expansion. The causal (backward-shift) part of the Laurent expansion is asymptotically stable since all of its poles are zero, while the noncausal (forward-shift) part of the Laurent expansion captures the unstable and noncausal components of the transmissibility operator [30].

Let $\mathcal{T}(\mathbf{q})$ be the discrete-time transmissibility operator whose pseudo input is $y_{\rm i}$ and whose pseudo output is $y_{\rm o}$, that is,

$$y_{\rm o}(k) = \mathcal{T}(\mathbf{q}) y_{\rm i}(k). \tag{4.1}$$

It follows from [30] that the truncated Laurent expansion

$$\mathcal{T}(\mathbf{q}, \theta_{r,d}) \stackrel{\triangle}{=} \sum_{i=-d}^{r} H_i \mathbf{q}^{-i} \tag{4.2}$$

is a noncausal FIR approximation of $\mathcal{T}(\mathbf{q})$, where r and d are positive integers, $H_{-d}, \ldots, H_r \in \mathbb{R}^{(p-m)\times m}$ are coefficients of the Laurent expansion of the rational function $\mathcal{T}$ in an annulus that contains the unit circle, and

$$\theta_{r,d} \stackrel{\triangle}{=} [\ H_{-d} \quad \ldots \quad H_r\ ] \in \mathbb{R}^{(p-m)\times(r+d+1)m}. \tag{4.3}$$

Using (4.2), the one-step predicted output is given by

$$y_{\rm o}(k|\theta_{r,d}) \stackrel{\triangle}{=} \mathcal{T}(\mathbf{q}, \theta_{r,d}) y_{\rm i}(k) = \sum_{i=-d}^{r} H_i y_{\rm i}(k-i). \tag{4.4}$$

4.3 Identification of Transmissibility Operators Using Noncausal FIR models with Prediction Error Methods

To identify transmissibility operators that are possibly unstable, improper, and of unknown order, we use noncausal FIR models with prediction error methods (PEM) [75].

For each choice of transmissibility coefficients

$$\bar{\theta}_{r,d} \stackrel{\triangle}{=} [\ \bar{H}_{-d} \quad \cdots \quad \bar{H}_r\ ] \in \mathbb{R}^{(p-m)\times(r+d+1)m}, \tag{4.5}$$

it follows that

$$\mathcal{T}(\mathbf{q},\bar{\theta}_{r,d}) = \sum_{i=-d}^{r} \bar{H}_i \mathbf{q}^{-i}. \tag{4.6}$$

The residual of the transmissibility $\mathcal{T}(\mathbf{q},\bar{\theta}_{r,d})$ at time k is defined to be the one-step prediction error

$$\begin{aligned} e(k|\bar{\theta}_{r,d}) &\triangleq y_{\mathrm{o}}(k) - y_{\mathrm{o}}(k|\bar{\theta}_{r,d}) \\ &= y_{\mathrm{o}}(k) - \mathcal{T}(\mathbf{q},\bar{\theta}_{r,d}) y_{\mathrm{i}}(k) \\ &= y_{\mathrm{o}}(k) - \sum_{i=-d}^{r} \bar{H}_i y_{\mathrm{i}}(k-i). \end{aligned} \tag{4.7}$$

The accuracy of $\bar{\theta}_{r,d}$ is measured by the performance metric

$$V(\bar{\theta}_{r,d},\ell) \triangleq \frac{1}{\ell-d-r+1} \sum_{k=r}^{\ell-d} \|e(k|\bar{\theta}_{r,d})\|_2^2, \tag{4.8}$$

where$\|\cdot\|_2$ is the Euclidean norm and $\ell+1$ is the number of data samples. Then, the PEM estimate $\hat{\theta}_{r,d,\ell}$ of $\theta_{r,d}$ is given by

$$\hat{\theta}_{r,d,\ell} \triangleq \arg\min_{\bar{\theta}_{r,d}} V(\bar{\theta}_{r,d},\ell), \tag{4.9}$$

where

$$\hat{\theta}_{r,d,\ell} \triangleq [\ \hat{H}_{-d,\ell} \quad \cdots \quad \hat{H}_{r,\ell}\ ] \in \mathbb{R}^{(p-m)\times(r+d+1)m}. \tag{4.10}$$

It follows from (4.7) that the residual of the identified transmissibility $\mathcal{T}(\mathbf{q},\hat{\theta}_{r,d,\ell})$ at time k is given by

$$\begin{aligned} e(k|\hat{\theta}_{r,d,\ell}) &= y_{\rm o}(k) - y_{\rm o}(k|\hat{\theta}_{r,d,\ell}) \\ &= y_{\rm o}(k) - \mathcal{T}(\mathbf{q}, \hat{\theta}_{r,d,\ell}) y_{\rm i}(k) \\ &= y_{\rm o}(k) - \sum_{i=-d}^{r} \hat{H}_{i,\ell} y_{\rm i}(k-i). \end{aligned} \tag{4.11}$$

For all $r \le k \le \ell - w - d$, define

$$E(k|\hat{\theta}_{r,d,\ell}, w) \triangleq \sqrt{\sum_{i=k}^{w+k} e^2(i|\hat{\theta}_{r,d,\ell})} \tag{4.12}$$

to be the norm of the residual of the rectangular data window of size $w+1$ starting at time step k. Expressions (4.11) and (4.12) measure the accuracy of the transmissibility from $y_{\rm i}$ to $y_{\rm o}$ for the estimate $\hat{\theta}_{r,d,\ell}$ of $\theta_{r,d}$. The identification data set used to obtain (4.9) is different from the validation data set used to compute (4.11) and (4.12).

Constructing a meaningful transmissibility operator requires knowledge of the number m of independent disturbances acting on the system. Since m may be unknown, we estimate m using the following procedure. Let $\hat{m} \in \{1, \ldots, p-1\}$ and define $\hat{p} \triangleq p - \hat{m}$. We use PEM with a noncausal FIR model to identify a transmissibility operator with $\hat{m}$ pseudo inputs and $\hat{p}$ pseudo outputs. For each identified transmissibility operator we compute the residual using (4.11). The estimated number of disturbances is the value of $\hat{m}$ at which a sharp drop occurs in the norm of the residual. If a sharp drop is not obvious, then the estimated number of disturbances is the smallest value of $\hat{m}$ for which no sizable improvement is obtained for larger values of $\hat{m}$. Redundant sensors can then be removed or retained for possible benefits in terms of the accuracy of the identified transmissibility operators.

4.4 Application to Aircraft Sensor Health Monitoring

To apply transmissibility operators to aircraft sensor health monitoring, we consider the NASA GTM model [65, 66], which is a fully nonlinear model with aerodynamic lookup tables. GTM includes sensor models that can be modified to emulate sensor faults.

Let $\delta\beta$ denote the sideslip angle in degrees, and let $\omega \stackrel{\triangle}{=} [\omega_x \ \omega_y \ \omega_z]^{\mathrm{T}}$ be the angular velocity of the aircraft relative to the Earth resolved in the aircraft frame, where ω_x, ω_y, and ω_z are measured by rate gyros in degrees per second. Define $\mathcal{T}(\mathbf{q})$ to be the 1×3 transmissibility operator whose pseudo input is $y_{\mathrm{i}} \stackrel{\triangle}{=} [\omega_x \ \omega_y \ \delta\beta]^{\mathrm{T}}$ and whose pseudo output is $y_{\mathrm{o}} \stackrel{\triangle}{=} \omega_z$, that is,

$$\omega_z(k) = \mathcal{T}(\mathbf{q}) \begin{bmatrix} \omega_x(k) \\ \omega_y(k) \\ \delta\beta(k) \end{bmatrix}. \tag{4.13}$$

We set the sampling time $T_{\mathrm{s}} = 0.01$ sec, and we assume that sampled data is available for $t \in [0, 500]$ sec, that is, $0 \le k \le 50,000$ steps. Let $\delta a, \delta e$, and δr denote the aileron, elevator, and rudder deflections, respectively. For all $0 \le k \le 50,000$ let $\delta a = \sin(\Omega k T_{\mathrm{s}})$ deg, $\delta e = \sin(\Omega k T_{\mathrm{s}} + 45)$ deg, and $\delta r = \cos(\Omega k T_{\mathrm{s}})$ deg, where $\Omega = 30$ deg/sec. Physically, the displacements of the ailerons, elevator, and rudder are sinusoidal with an amplitude of 1 deg and a period of 12 sec. We consider the following initial GTM trim conditions: Level flight, altitude = 8000.00 ft, equivalent airspeed = 89.18 kt, true airspeed = 100.58 kt, alpha = 3.00 deg, beta = 0 deg, gamma = 0 deg, roll = 0.066 deg, pitch = 3.00 deg, yaw = 45.00 deg, ground track = 45.00 deg, elevator = 2.70 deg, throttle = 22.84%.

To emulate sensor noise we add zero-mean white noise with SNR of 50 to all identification and validation measurements of ω_x, ω_y, ω_z, and $\delta\beta$. We use PEM with a noncausal FIR model with $r = 50$ and $d = 50$, along with identification data for $2,500 \le k \le 20,000$ steps to obtain the identified transmissibility $\mathcal{T}(\mathbf{q}, \hat{\theta}_{r,d,\ell})$ of $\mathcal{T}(\mathbf{q})$. Figure 4.1 shows the Markov (impulse response) parameters of $\mathcal{T}(\mathbf{q}, \hat{\theta}_{r,d,\ell})$ from each pseudo input ω_x, ω_y, and $\delta\beta$ to the pseudo output ω_z. Data for $20,000 < k \le 50,000$ is used for validation. Figure 4.2 shows ω_z and its one-step prediction $\hat{\omega}_z \triangleq \mathcal{T}(\mathbf{q}, \hat{\theta}_{r,d,\ell})[\omega_x \ \omega_y \ \delta\beta]^{\mathrm{T}}$ for $28,000 \le k \le 28,500$, that is, for $t \in [280, 285]$ sec.

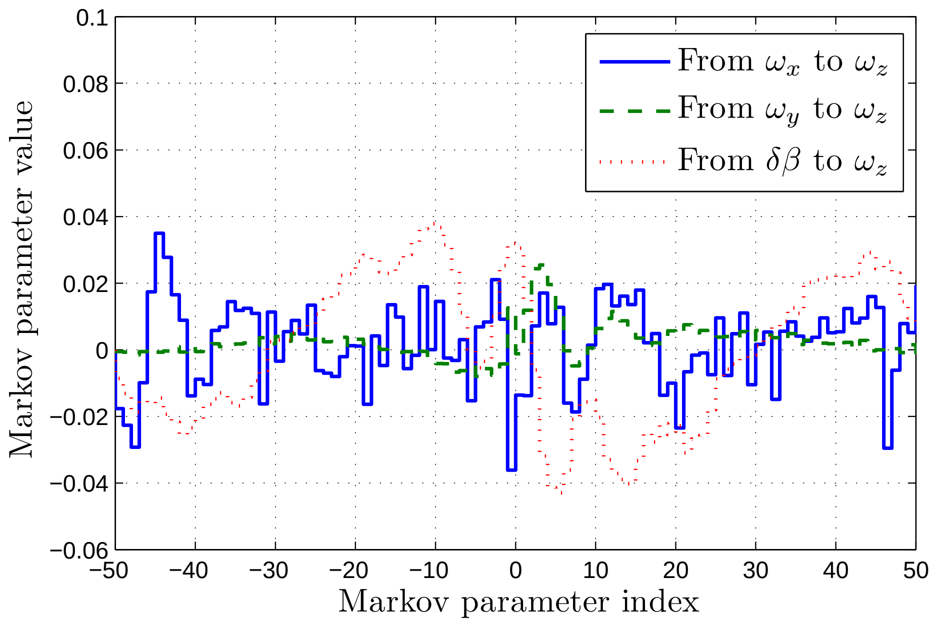

Figure 4.1: Entries of the estimated Markov parameters $\hat{\theta}_{r,d,\ell}$ of $\mathcal{T}(\mathbf{q}, \theta_{r,d})$ from each pseudo input ω_x, ω_y, and $\delta\beta$ to the pseudo output ω_z.

Next, we consider the case where a ramp-like drift with a slope of 0.05 deg/sec^2 is added to measurements of either ω_x, ω_y, or ω_z starting at $t = 300$ sec. Measurements of ω_x, ω_y, ω_z, and $\delta\beta$ are used with the identified transmissibility operator $\mathcal{T}(\mathbf{q}, \hat{\theta}_{r,d,\ell})$ to generate the residual using (4.11). Figure 4.3 shows $E(k|\hat{\theta}_{r,d,\ell}, w)$ for all $2,500 \le k \le 50,000 - w - d$ for $w = 1000$ steps, where a ramp-like drift is added to measurements of either ω_x, ω_y, or ω_z. Figure 4.3 shows that the residual levels increase after $t = 300$ sec, which indicates that, in all three cases, at least one of the sensors is faulty. However, we cannot conclude from Figure 4.3 which sensor is faulty.

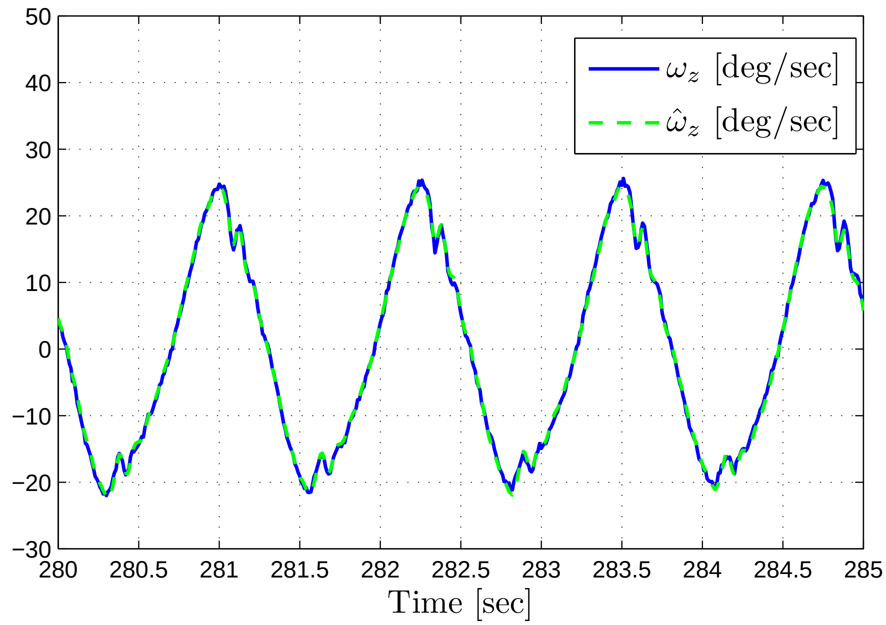

Figure 4.2: For the aircraft example, this plot shows measurements of ω_z and the computed one-step prediction $\hat{\omega}_z$ under healthy sensor conditions with SNR of 50 for both the pseudo inputs and the pseudo output.

Next, we consider the case where a deadzone nonlinearity is applied to measurements of either ω_x, ω_y, or ω_z starting at $t = 300$ sec. Measurements of ω_x, ω_y, ω_z, and $\delta\beta$ are used with the identified transmissibility operator $\mathcal{T}(\mathbf{q}, \hat{\theta}_{r,d,\ell})$ to generate the residual using (4.11). Figure 4.4 shows $E(k|\hat{\theta}_{r,d,\ell}, w)$ for all $2,500 \leq k \leq 50,000 - w - d$ for $w = 1000$ steps, where a ramp-like drift is added to measurements of either ω_x, ω_y, or ω_z. Figure 4.4 shows that the residual levels increase after $t = 300$ sec, which indicates that, in all three cases, at least one of the sensors is faulty. However, we cannot conclude from Figure 4.4 which sensor is faulty.

Similar results can be shown for other types of faults, such as magnitude saturation, rate saturation, and jam.

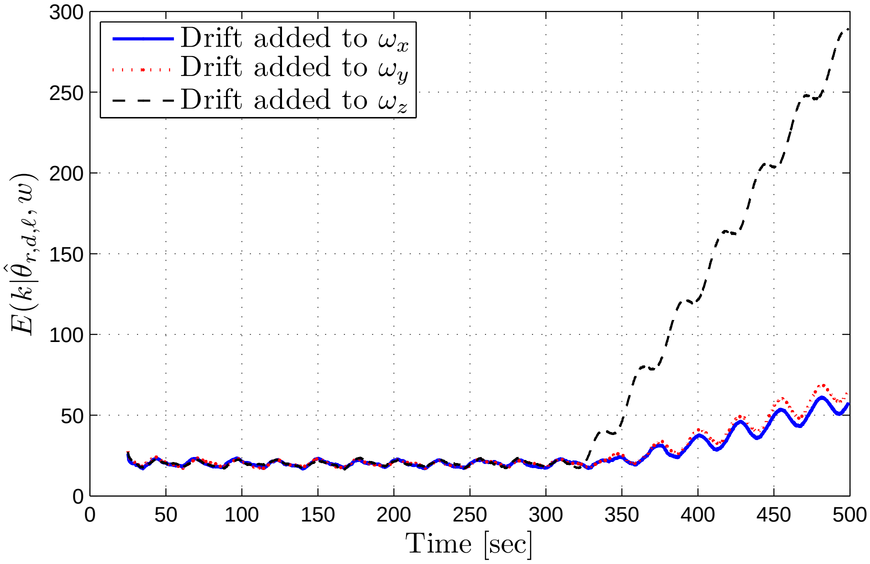

Figure 4.3: For the aircraft example, this plot shows $E(k|\hat{\theta}_{r,d,\ell}, w)$ for $w = 1000$ steps, where a ramp-like drift is added to measurements of either ω_x, ω_y, or ω_z. Note that the residual levels increase after $t = 300$ sec, which indicates that, in all three cases, at least one of the sensors is faulty. However, we cannot conclude from Figure 4.3 which sensor is faulty.

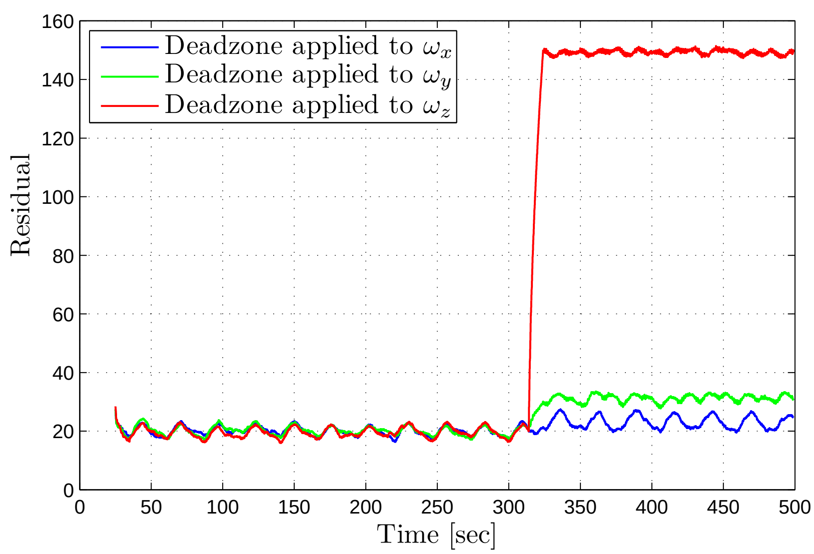

Figure 4.4: For the aircraft example, this plot shows $E(k|\hat{\theta}_{r,d,\ell}, w)$ for $w = 1000$ steps, where a deadzone nonlinearity is applied to either ω_x, ω_y, or ω_z. Note that the residual levels increase after $t = 300$ sec, which indicates that, in all three cases, at least one of the sensors is faulty. However, we cannot conclude from Figure 4.4 which sensor is faulty.

4.5 Application to a Vibrating Plate

Consider the rectangular aluminum plate shown in Figure 4.5 with length a, width b, height h, and clamped-free-free-free (CFFF) boundary conditions. The equations of motion are derived using a Lagrangian formulation with the kinetic energy and potential energy expressions developed in [101, pp. 242–243]. Using Rayleigh-Ritz discretization [101, pp. 247–253], assuming a nine-degree-of-freedom model of the plate an approximation of the vertical displacement at (x, y) at time t is given by

$$w(x, y, t) \triangleq \sum_{i=1}^{3} \sum_{j=1}^{3} x^{i+1} y^{j-1} q_{i,j}(t), \tag{4.14}$$

where $q_{i,j}$ are generalized coordinates [102].

Let $a = 5$ m, $b = 1$ m, and $h = 0.01$ m. Let $u_i(t)$ be the force acting at $(x_{\mathrm{a}_i}, y_{\mathrm{a}_i})$ at time t and $y_i(t)$ be the measured displacement in the vertical direction at $(x_{\mathrm{s}_i}, y_{\mathrm{s}_i})$ at time t. Let $u_1(t) = 600 \sin(5t)$ N, $u_2(t) = 500 \sin(10t)$ N, and $u_3(t) = 300 \sin(20t)$ N. Let $(x_{\mathrm{a}_1}, y_{\mathrm{a}_1}) = (0.3, 0.3), (x_{\mathrm{a}_2}, y_{\mathrm{a}_2}) = (1, 1)$, $(x_{\mathrm{a}_3}, y_{\mathrm{a}_3}) = (4, 0.25)$, $(x_{\mathrm{s}_1}, y_{\mathrm{s}_1}) = (0.5, 0.1), (x_{\mathrm{s}_2}, y_{\mathrm{s}_2}) = (1, 0.5)$, $(x_{\mathrm{s}_3}, y_{\mathrm{s}_3}) = (2, 0.8), (x_{\mathrm{s}_4}, y_{\mathrm{s}_4}) = (3, 0.6)$, and $(x_{\mathrm{s}_5}, y_{\mathrm{s}_5}) = (3, 0.75)$ as shown in Figure 4.5.

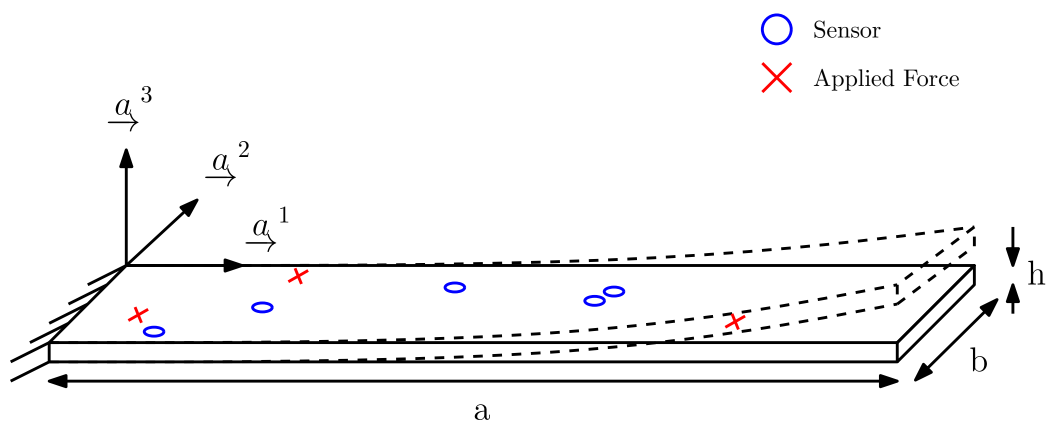

Figure 4.5: A rectangular plate with length a, width b, height h, and clamped-free-free-free (CFFF) boundary conditions. The unit vectors $\underset{\rightarrow}{a}^1$, $\underset{\rightarrow}{a}^2$, and $\underset{\rightarrow}{a}^3$ correspond to the x, y, and z directions, respectively.

For all $i = 1, \ldots, 5$, let y_i be the measurement of $w(x_{\mathrm{s}_i}, y_{\mathrm{s}_i}, t)$. Moreover, for all $i = 1, \ldots, 4$ let $Y_i \triangleq [y_1 \ \ldots \ y_i]^{\mathrm{T}} \in \mathbb{R}^i$, and $\mathcal{T}_i(\mathbf{p})$ be the transmissibility whose pseudo input is Y_i and whose pseudo output is y_5. Suppose that all measurements are noise free. We assume that data is available for $1 \leq k \leq 20,000$. We use PEM with a noncausal FIR model with $r = 25$, $d = 25$, and the first $\ell = 2000$ data points to obtain the identified transmissibilities $\mathcal{T}_i(\mathbf{q}^{-1}, \hat{\theta}_{r,d,\ell})$ of $\mathcal{T}_i(\mathbf{p})$ for all $i = 1, \ldots, 4$.

Figure 4.6 shows $E(k|\hat{\theta}_{r,d,\ell}, w)$ for $\mathcal{T}_i(\mathbf{q}^{-1}, \hat{\theta}_{r,d,\ell})$, where $i = 1, \ldots, 4$ and $w = 1000$ steps. Note that using additional input sensors for the transmissibility reduces the level of $E(k|\hat{\theta}_{r,d,\ell}, w)$. Moreover, note that the level of $E(k|\hat{\theta}_{r,d,\ell}, w)$ does not change significantly when three or four pseudo inputs are used for the transmissibility operator, which implies that three disturbances are acting on the system.

Next, we add zero-mean white noise with the gaussian pdf $\mathcal{N}(0, 1)$ to y_i for all

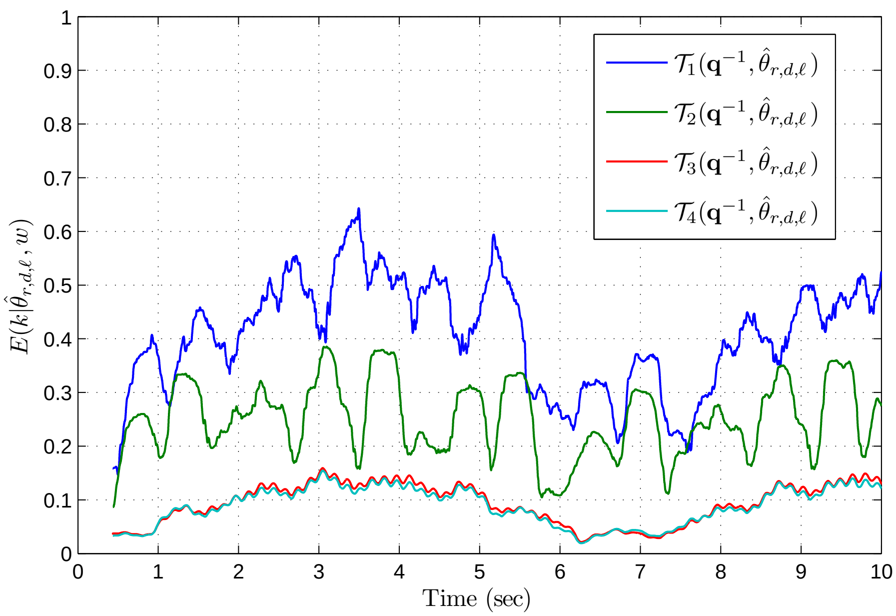

Figure 4.6: For the vibrating plate shown in Figure 4.5, this plot shows $E(k|\hat{\theta}_{r,d,\ell}, w)$ for $\mathcal{T}_i(\mathbf{q}^{-1}, \hat{\theta}_{r,d,\ell})$, where $i = 1, \ldots, 4$ and $w = 1000$ steps and no noise is added to the measurements. Note that using additional input sensors reduces the level of $E(k|\hat{\theta}_{r,d,\ell}, w)$. This plot implies that three disturbances are acting on the system.

i with the same SNR varying from 1 to 100. We assume that data is available for $1 \le k \le 20,000$. We use PEM with a noncausal FIR model with $r = 25$, $d = 25$, and the first $\ell = 2000$ data points to obtain the identified transmissibility $\mathcal{T}_i(\mathbf{q}^{-1}, \hat{\theta}_{r,d,\ell})$ for all $i = 1, \ldots, 4$. Figure 4.7 shows a plot of the norm of the residual of $\mathcal{T}_i(\mathbf{q}^{-1}, \hat{\theta}_{r,d,\ell})$ for all $i = 1, \ldots, 4$. Note from Figure 4.7 that using more input sensors reduces the norm of the residual. Moreover, note that the level of the norm of the residual does not change when three or four pseudo inputs are used for the transmissibility operator, which implies that three disturbances are acting on the system.

To emulate changes occurring in the plate, suppose that at $t = 5$ sec the Young's modulus of the plate starts to decrease. We use PEM with a noncausal FIR model with $r = 25$, $d = 25$, and the first $\ell = 2000$ data points to obtain the identified transmissibilities $\mathcal{T}_i(\mathbf{q}^{-1}, \hat{\theta}_{r,d,\ell})$ for all $i = 1, \ldots, 4$. Figure 4.8 shows the norm of the residual for $\mathcal{T}_i(\mathbf{q}^{-1}, \hat{\theta}_{r,d,\ell})$, where $i = 1, \ldots, 4$ and $w = 1000$ steps. Note that after $t = 5$ sec the residual level increases due to the change in the dynamics of the plate.

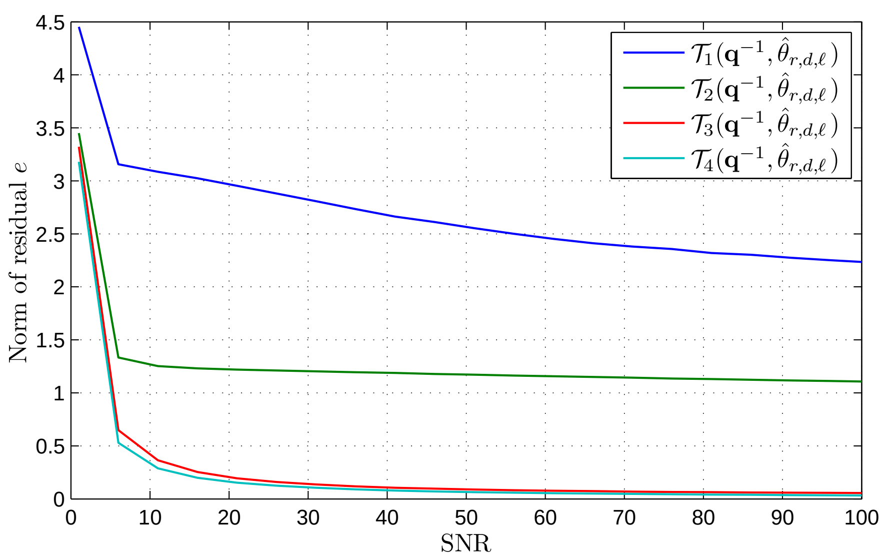

Figure 4.7: For the vibrating plate shown in Figure 4.5, this plot shows the norm of the residual of $\mathcal{T}_i(\mathbf{q}^{-1}, \hat{\theta}_{r,d,\ell})$ for $i = 1, \ldots, 4$ where zero-mean white noise with the gaussian pdf $\mathcal{N}(0, 1)$ is added to y_i for all i with the same SNR varying from 1 to 100. Note that using additional input sensors reduces the norm of the residual.

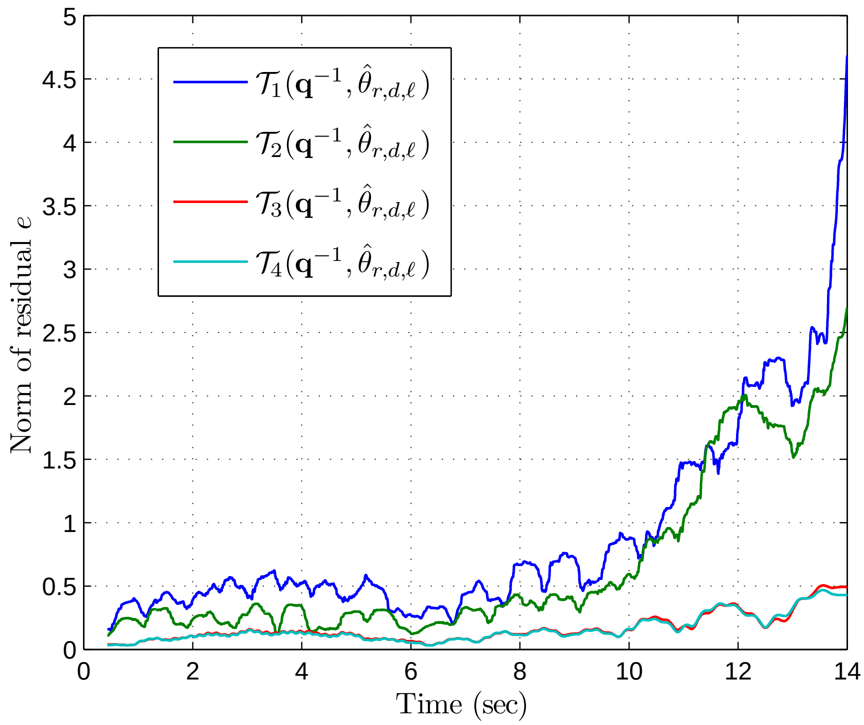

Figure 4.8: For the vibrating plate shown in Figure 4.5, this plot shows $E(k|\hat{\theta}_{r,d,\ell}, w)$ of $\mathcal{T}_i(\mathbf{q}^{-1}, \hat{\theta}_{r,d,\ell})$ for $i = 1, \ldots, 4$ for $w = 1000$ steps. Note that after $t = 5$ sec the residual level increases due to the change in the dynamics of the plate.

4.6 Application to an Acoustic System

In order to investigate the ability of transmissibility operators to detect changes in the dynamics of an acoustic system, we consider the experimental setup shown in Figure 4.9. The setup consists of a drum with two speakers w_1 and w_2 and four microphones mic_1–mic_4. Each speaker is an actuator, and each microphone is a sensor that measures the acoustic response at its location. Two plastic pieces are placed inside the drum, and these can be removed during operation to emulate changes to the system. All actuator signals are generated using MATLAB and sent to the speakers through a data acquisition card. The sampling rate is chosen to be 1000 Hz.

Let u_1 and u_2 be the measurements of the signals of the speakers w_1 and w_2, respectively, and let y_1–y_4 be the measurements obtained by the sensors mic_1–mic_4, respectively.

For $i = 1, 2, 3$, let $Y_i \triangleq [y_1 \ \dots \ y_i]^{\mathrm{T}} \in \mathbb{R}^i$ and let $\mathcal{T}_i$ be the transmissibility whose pseudo input is Y_i and whose pseudo output is y_4. We assume that data is available for $1 \le k \le 30,000$.

Suppose that the system is operating under healthy conditions, and suppose that w_1 and w_2 are driven with realizations of a bandlimited white noise with bandwidth of 500 Hz. We use PEM with a noncausal FIR model with $r = 25$, $d = 25$, and the first

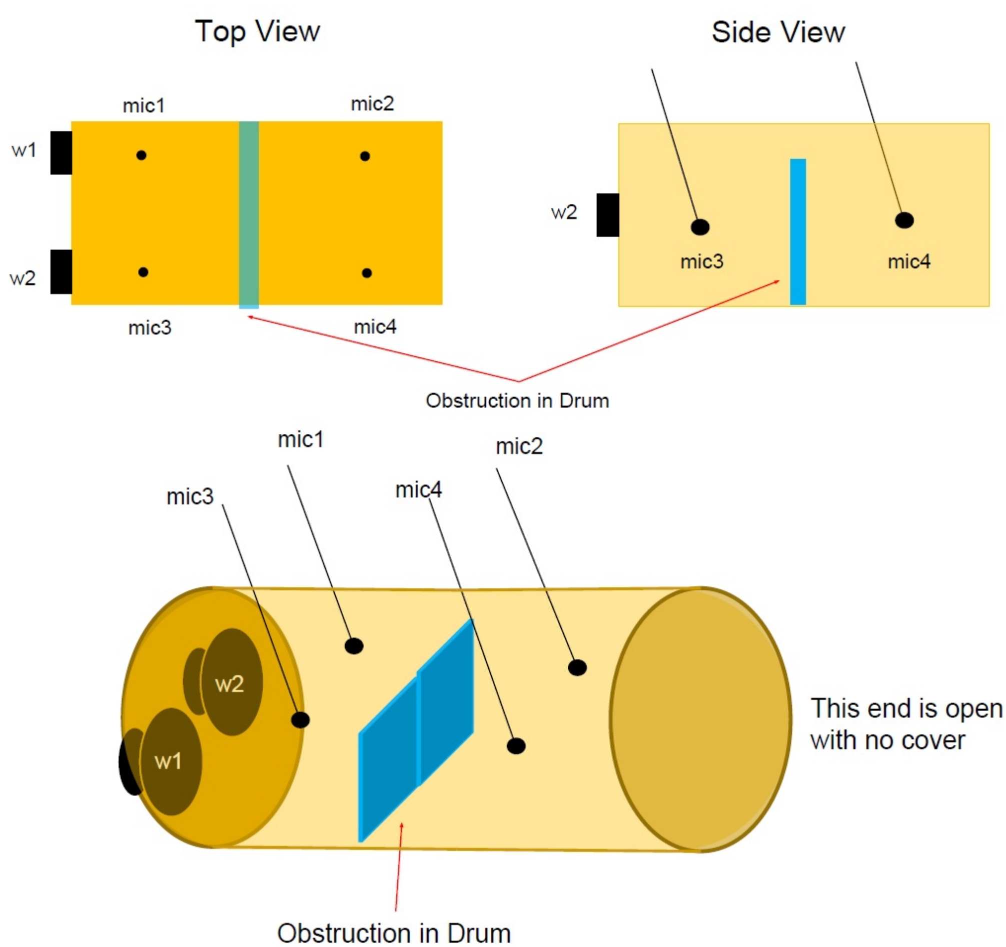

Figure 4.9: Experimental setup. The setup consists of a drum with two speakers w_1 and w_2 and four microphones mic_1–mic_4. Each speaker is an actuator and each microphone is a sensor measures the acoustic response at its location. Two plastic pieces are placed inside the drum (shown in blue) and can be removed during operation to emulate changes to the system.

$\ell = 10,000$ samples to obtain the identified transmissibilities $\mathcal{T}_i(\mathbf{q}^{-1}, \hat{\theta}_{r,d,\ell})$ of $\mathcal{T}_i(\mathbf{p})$ for $i = 1, 2, 3$. Figure 4.10 shows $E(k|\hat{\theta}_{r,d,\ell}, w)$ for $\mathcal{T}_i(\mathbf{q}^{-1}, \hat{\theta}_{r,d,\ell})$, where $w = 1000$ steps and $i = 1, 2, 3$. Note from Figure 4.10 that $\mathcal{T}_2(\mathbf{q}^{-1}, \hat{\theta}_{r,d,\ell})$ gives significantly lower residual than $\mathcal{T}_1(\mathbf{q}^{-1}, \hat{\theta}_{r,d,\ell})$, where $\mathcal{T}_3(\mathbf{q}^{-1}, \hat{\theta}_{r,d,\ell})$ produces no significant benefit compared to $\mathcal{T}_2(\mathbf{q}^{-1}, \hat{\theta}_{r,d,\ell})$. This suggests that the number of excitations acting on the system is two. Figure 4.11 shows y_4 and the computed one-step prediction $\hat{y}_4 \triangleq \mathcal{T}_3(\mathbf{q}^{-1}, \hat{\theta}_{r,d,\ell})[y_1\ y_2\ y_3]^{\mathrm{T}}$ for $15,000 \le k \le 15,300$, that is, for $t \in [15, 15.3]$ sec.

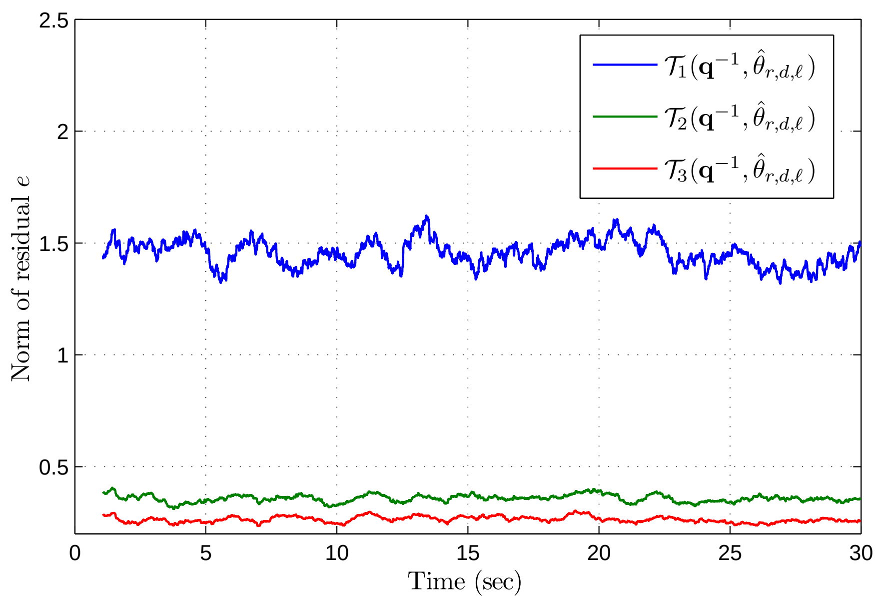

Figure 4.10: For the acoustic system shown in Figure 4.9 operating under healthy conditions, w_1 and w_2 are driven with realizations of a bandlimited white noise with bandwidth of 500 Hz. This plot shows $E(k|\hat{\theta}_{r,d,\ell}, w)$ for $\mathcal{T}_i(\mathbf{q}^{-1}, \hat{\theta}_{r,d,\ell})$, where $w = 1000$ steps and $i = 1, 2, 3$. Note that $\mathcal{T}_2(\mathbf{q}^{-1}, \hat{\theta}_{r,d,\ell})$ gives significantly lower residual than $\mathcal{T}_1(\mathbf{q}^{-1}, \hat{\theta}_{r,d,\ell})$ and $\mathcal{T}_3(\mathbf{q}^{-1}, \hat{\theta}_{r,d,\ell})$ produces no benefit compared to $\mathcal{T}_2(\mathbf{q}^{-1}, \hat{\theta}_{r,d,\ell})$. This suggests that the number of excitations acting on the system is two.

Next, suppose that the system is operating under healthy conditions, and suppose that w_1 is driven with a realization of a bandlimited white noise with bandwidth of 500 Hz and w_2 is not operating. We use PEM with a noncausal FIR model with $r = 25$, $d = 25$, and the first $\ell = 10,000$ samples to obtain the identified transmissibilities

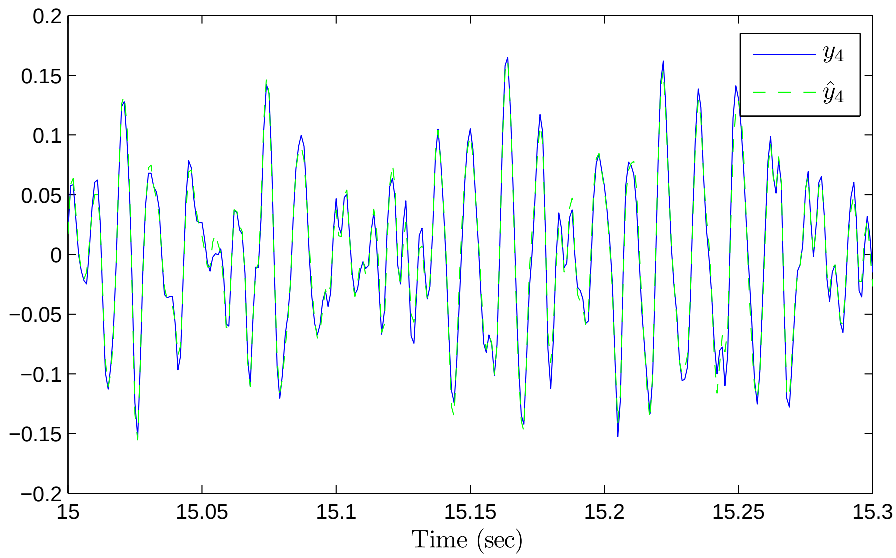

Figure 4.11: For the acoustic system shown in Figure 4.9 operating under healthy conditions, w_1 and w_2 are driven with realizations of a bandlimited white noise with bandwidth of 500 Hz. This plot shows the measurements of y_4 and the computed one-step prediction $\hat{y}_4$.

$\mathcal{T}_i(\mathbf{q}^{-1}, \hat{\theta}_{r,d,\ell})$ of $\mathcal{T}_i(\mathbf{p})$ for $i = 1, 2, 3$. Figure 4.12 shows $E(k|\hat{\theta}_{r,d,\ell}, w)$ for $\mathcal{T}_i(\mathbf{q}^{-1}, \hat{\theta}_{r,d,\ell})$, where $w = 1000$ steps and $i = 1, 2, 3$. Note from Figure 4.12 that $\mathcal{T}_2(\mathbf{q}^{-1}, \hat{\theta}_{r,d,\ell})$ gives significantly lower residual than $\mathcal{T}_1(\mathbf{q}^{-1}, \hat{\theta}_{r,d,\ell})$ and $\mathcal{T}_3(\mathbf{q}^{-1}, \hat{\theta}_{r,d,\ell})$ gives slightly lower residual than $\mathcal{T}_2(\mathbf{q}^{-1}, \hat{\theta}_{r,d,\ell})$. This shows the potential benefits of sensor redundancy.

Suppose that the two speakers are operating simultaneously and suppose that $u_1(t) = \sin(100\pi t)$ and $u_2(t) = \sin(120\pi t)$. We use PEM with a noncausal FIR model with $r = 25$, $d = 25$, and the first $\ell = 5{,}000$ samples to obtain the identified transmissibilities $\mathcal{T}_i(\mathbf{q}^{-1}, \hat{\theta}_{r,d,\ell})$ of $\mathcal{T}_i(\mathbf{p})$ for $i = 1, 2, 3$. At approximately $t = 10$ sec and $t = 21$ sec the first and second plastic pieces are removed. Data for $5{,}000 < k \leq 30{,}000$ is used for validation. Figure 4.13 shows $E(k|\hat{\theta}_{r,d,\ell}, w)$ for $\mathcal{T}_i(\mathbf{q}^{-1}, \hat{\theta}_{r,d,\ell})$, where $w = 1000$ steps and $i = 1, 2, 3$. Note from Figure 4.13 the changes in $E(k|\hat{\theta}_{r,d,\ell}, w)$ at approximately $t = 10$ sec and at $t = 21$ sec due to the change in the dynamics of the drum.

4.7 Conclusions

An estimate of the transmissibility operator between pairs or sets of sensors can be used to detect sensor faults in the presence of unknown external excitation. The ability to detect sensor faults by exploiting the presence of unknown external excitation is the key difference between this approach and techniques based on residual generation. In particular, the transmissibility operator is a relationship between pairs or sets of sensors that is independent of the time history of the external excitation.

Transmissibility-based fault detection depends on various assumptions. In particular, this approach assumes that the plant itself does not change between the identification and validation data sets and that the location of the external excitation does not change. By using the estimated transmissibility operator, the residual

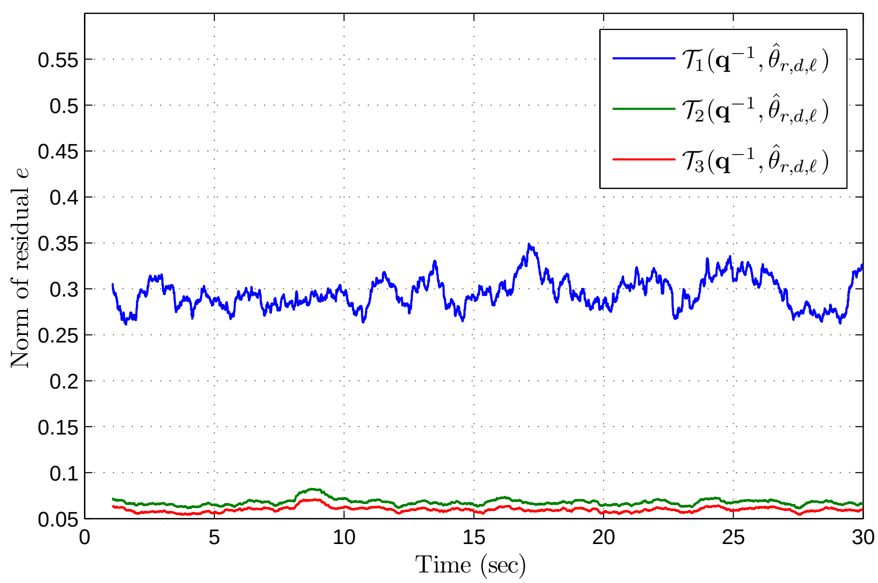

Figure 4.12: For the acoustic system shown in Figure 4.9 operating under healthy conditions, w_1 is driven with a realization of a bandlimited white noise with bandwidth of 500 Hz and w_2 is not operating. This plot shows $E(k|\hat{\theta}_{r,d,\ell}, w)$ for $\mathcal{T}_i(\mathbf{q}^{-1}, \hat{\theta}_{r,d,\ell})$, where $w = 1000$ steps and $i = 1, 2, 3$. Note that $\mathcal{T}_2(\mathbf{q}^{-1}, \hat{\theta}_{r,d,\ell})$ gives significantly lower residual than $\mathcal{T}_1(\mathbf{q}^{-1}, \hat{\theta}_{r,d,\ell})$. However, $\mathcal{T}_3(\mathbf{q}^{-1}, \hat{\theta}_{r,d,\ell})$ produces no benefit compared to $\mathcal{T}_2(\mathbf{q}^{-1}, \hat{\theta}_{r,d,\ell})$. This shows the potential benefits of sensor redundancy.

between pairs or sets of sensors can be used to detect a sensor failure or a change in the dynamics of a system. Moreover, the characteristic shape of the residual can be used to infer the type of sensor failure. However, this approach does not identify which sensor has failed. This problem is left for future research.

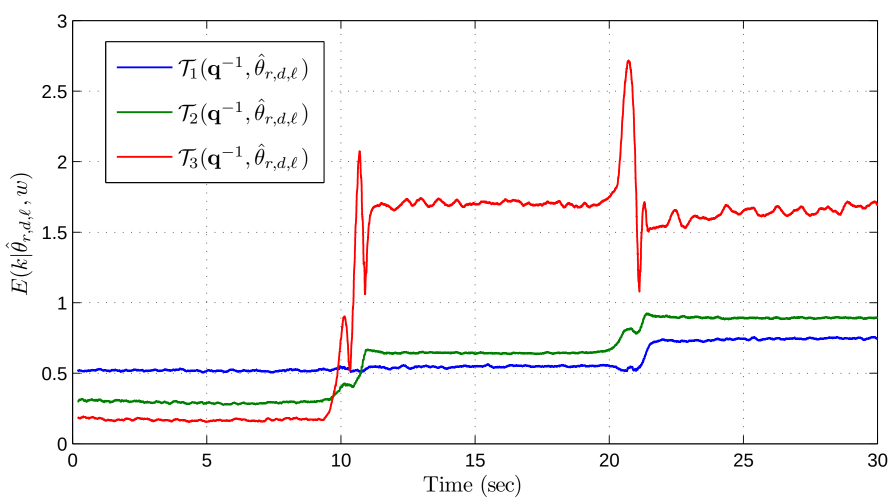

Figure 4.13: For the acoustic system shown in Figure 4.9 with $u_1(t) = \sin(100\pi t)$ and $u_2(t) = \sin(120\pi t)$, this plot shows $E(k|\hat{\theta}_{r,d,\ell}, w)$ for $\mathcal{T}_i(\mathbf{q}^{-1}, \hat{\theta}_{r,d,\ell})$, where $w = 1000$ steps, $i = 1, 2, 3$ and at approximately $t = 10$ sec and $t = 21$ sec the first and second plastic pieces are removed. Note the changes in $E(k|\hat{\theta}_{r,d,\ell}, w)$ at approximately $t = 10$ sec and at $t = 21$ sec due to the change in the drum dynamics.

CHAPTER 5

Time-Domain Analysis of Motion Transmissibilities in Force-Driven and Displacement-Driven Structures

5.1 Introduction

Structural vibration is most commonly modeled as the displacement, velocity, or acceleration response to a force input. Assuming that the dynamics are linear, lumped models of structural vibration with multiple degrees of freedom typically have the form of matrix differential equations with inertia, damping, and stiffness coefficients [103]. In the frequency domain, these force-driven outputs are modeled by compliance, admittance, and inertance transfer functions, respectively. Alternatively, a transfer function can relate displacements at different locations on a structure. The resulting transfer function is called a *motion transmissibility* [24, 25]. Velocity and acceleration signals can also be considered instead of displacements. These concepts extend directly to rotational variables, where "torque" replaces "force."

It is also possible to define a force transmissibility, and the relationship between force and motion transmissibilities is discussed in [26, 104]. In the present chapter, force transmissibility is not considered, and the term "transmissibility" refers to motion transmissibility.

Motivated by the advantages of time-domain identification techniques over frequency-domain identification techniques, in this chapter we develop a time-domain framework for SISO and MIMO transmissibilities that accounts for nonzero initial conditions for both force-driven and displacement-driven structures.

The contents of the chapter are as follows. In Section 5.2 and Section 5.3 we derive SISO and MIMO time-domain models for transmissibility operators in force-driven structures, respectively. In Section 5.4 we consider displacement-driven structures, while in Section 5.5 and Section 5.6 we derive SISO and MIMO time-domain models for transmissibility operators in displacement-driven structures, respectively. In Section 5.7 we show the equality of transmissibilities of force-driven and displacement-driven structures with identical inputs and outputs when the force and prescribed motion are applied to the same location. We introduce examples in Section 5.8. Finally, we present conclusions in Section 5.9.

5.2 SISO Transmissibilities in Force-Driven Structures

Consider a lumped force-driven structure (FDS) consisting of masses $m_1, \ldots, m_n$ connected by springs modeled by

$$M\ddot{q}(t) + Kq(t) = f_b(t), \tag{5.1}$$

where $M \overset{\triangle}{=} \operatorname{diag}(m_1, \ldots, m_n) \in \mathbb{R}^{n\times n}$ is the positive-definite mass matrix, $K \in \mathbb{R}^{n\times n}$ is the positive-definite stiffness matrix, $q(t) \overset{\triangle}{=} \begin{bmatrix} q_1(t) & \cdots & q_n(t) \end{bmatrix}^{\mathrm{T}} \in \mathbb{R}^n$ is the vector of mass displacements, and $f_b(t) \overset{\triangle}{=} bu(t) = \begin{bmatrix} f_1(t) & \cdots & f_n(t) \end{bmatrix}^{\mathrm{T}} \in \mathbb{R}^n$ is the vector of forces, where $b \in \mathbb{R}^n$ is a nonzero vector, $u(t)$ is a scalar force, and $f_i(t)$ is the force applied to the i^{th} mass. Let $c \in \mathbb{R}^{1\times n}$ be nonzero and consider the scalar output

$$q_{c|bu} \overset{\triangle}{=} cq, \tag{5.2}$$

where $q_{c|bu}$ denotes the output cq with the driving force bu. Note that $q_{e_{i,n}^{\mathrm{T}}|bu} = e_{i,n}^{\mathrm{T}} q = q_i$, where $e_{i,n} \in \mathbb{R}^n$ is the i^{th} unit vector.

Next, let $w_{\mathrm{i}}, w_{\mathrm{o}} \in \mathbb{R}^{1\times n}$ and define

$$y_{\mathrm{i}} \stackrel{\triangle}{=} q_{w_{\mathrm{i}}|bu} = w_{\mathrm{i}} q, \tag{5.3}$$

$$y_{\mathrm{o}} \stackrel{\triangle}{=} q_{w_{\mathrm{o}}|bu} = w_{\mathrm{o}} q. \tag{5.4}$$

The goal is to obtain a transmissibility function relating y_{i} and y_{o} that is independent of the initial conditions $q(0)$ and $\dot{q}(0)$ as well as the input u. As a first attempt at obtaining such a function, transforming (5.1) to the Laplace domain yields

$$(s^2 M + K)\hat{q}(s) - sMq(0) - M\dot{q}(0) = b\hat{u}(s), \tag{5.5}$$

where $\hat{q}(s)$ and $\hat{u}(s)$ are the Laplace transforms of $q(t)$ and $u(t)$, respectively. Therefore,

$$\hat{q}(s) = (s^2M + K)^{-1} b\hat{u}(s) + (s^2M + K)^{-1} M(sq(0) + \dot{q}(0)). \tag{5.6}$$

It follows from (5.3), (5.4), and (5.6) that the Laplace transforms of y_{i} and y_{o} are given by

$$\hat{y}_{\mathrm{i}}(s) = w_{\mathrm{i}}(s^2M + K)^{-1} b\hat{u}(s) + w_{\mathrm{i}}(s^2M + K)^{-1} M(sq(0) + \dot{q}(0)), \tag{5.7}$$

$$\hat{y}_{\mathrm{o}}(s) = w_{\mathrm{o}}(s^2M + K)^{-1} b\hat{u}(s) + w_{\mathrm{o}}(s^2M + K)^{-1} M(sq(0) + \dot{q}(0)), \tag{5.8}$$

respectively, and thus

$$\frac{\hat{y}_{\mathrm{o}}(s)}{\hat{y}_{\mathrm{i}}(s)} = \frac{w_{\mathrm{o}}(s^2M + K)^{-1} b\hat{u}(s) + w_{\mathrm{o}}(s^2M + K)^{-1} M(sq(0) + \dot{q}(0))}{w_{\mathrm{i}}(s^2M + K)^{-1} b\hat{u}(s) + w_{\mathrm{i}}(s^2M + K)^{-1} M(sq(0) + \dot{q}(0))}. \tag{5.9}$$

Note that, if $q(0)$ and $\dot{q}(0)$ are zero, then $\hat{u}(s)$ can be cancelled in (5.9), and $\hat{y}_{\mathrm{o}}(s)$ and $\hat{y}_{\mathrm{i}}(s)$ are related by a transmissibility that is independent of the input. However, if either $q(0)$ or $\dot{q}(0)$ is not zero, then $\hat{u}(s)$ cannot be canceled in (5.9), and an input-independent transmissibility cannot be obtained.

Alternatively, we consider a time-domain analysis using the differentiation operator $\mathbf{p} = \mathrm{d}/\mathrm{d}t$ instead of the Laplace variable s. It follows that (5.1) can be written as

$$(\mathbf{p}^2 M + K)q(t) = bu(t). \tag{5.10}$$

Multiplying (5.3) by the polynomial $\delta(\mathbf{p}) \overset{\triangle}{=} \det(\mathbf{p}^2 M + K)$ and using the fact that

$$\delta(\mathbf{p})I_n = \mathrm{adj}(\mathbf{p}^2 M + K)(\mathbf{p}^2 M + K) \tag{5.11}$$

yields the differential equation

$$\begin{aligned}\delta(\mathbf{p})y_{\mathrm{i}}(t) &= w_{\mathrm{i}}\delta(\mathbf{p})I_n q(t)\\ &= w_{\mathrm{i}}\mathrm{adj}(\mathbf{p}^2 M + K)(\mathbf{p}^2 M + K)q(t)\\ &= w_{\mathrm{i}}\mathrm{adj}(\mathbf{p}^2 M + K)(M\ddot{q}(t) + Kq(t))\\ &= w_{\mathrm{i}}\mathrm{adj}(\mathbf{p}^2 M + K)bu(t). \end{aligned}\tag{5.12}$$

Similarly,

$$\delta(\mathbf{p})y_{\mathrm{o}}(t) = w_{\mathrm{o}}\mathrm{adj}(\mathbf{p}^2 M + K)bu(t). \tag{5.13}$$

For convenience, we define the notation

$$G_{w_{\mathrm{i}},b}(\mathbf{p}) \overset{\triangle}{=} w_{\mathrm{i}}(\mathbf{p}^2 M + K)^{-1}b, \tag{5.14}$$

$$G_{w\mathrm{o},b}(\mathbf{p}) \overset{\triangle}{=} w_{\mathrm{o}}(\mathbf{p}^2 M + K)^{-1}b. \tag{5.15}$$

Using (5.14), (5.15) we can rewrite (5.12), (5.13) as

$$y_{\rm i}(t) = G_{w_{\rm i},b}(\mathbf{p})u(t), \tag{5.16}$$

$$y_{\rm o}(t) = G_{w_{\rm o},b}(\mathbf{p})u(t), \tag{5.17}$$

respectively. Note that (5.16), (5.17) are interpreted as the differential equations (5.12), (5.13), respectively.

Note that (5.7), (5.8), (5.16), and (5.17) include the free response due to $q(0)$ and $\dot{q}(0)$ as well as the forced response due to u. In the subsequent analysis, we omit the argument "t" where no ambiguity can arise.

Define the polynomials

$$\eta_{\rm o}(\mathbf{p}) \triangleq w_{\rm o}\text{adj}(\mathbf{p}^2 M + K)b, \tag{5.18}$$

$$\eta_{\rm i}(\mathbf{p}) \triangleq w_{\rm i}\text{adj}(\mathbf{p}^2 M + K)b. \tag{5.19}$$

If $G_{w_{\rm i},b}$ and $G_{w_{\rm o},b}$ are obtained from minimal state-space realizations, then $\delta(\mathbf{p})$ is coprime relative to both $\eta_{\rm i}(\mathbf{p})$ and $\eta_{\rm o}(\mathbf{p})$. Moreover, it follows from (5.14)–(5.17) that

$$y_{\rm i} = G_{w_{\rm i},b}(\mathbf{p})u = \frac{\eta_{\rm i}(\mathbf{p})}{\delta(\mathbf{p})}u, \tag{5.20}$$

$$y_{\rm o} = G_{w_{\rm o},b}(\mathbf{p})u = \frac{\eta_{\rm o}(\mathbf{p})}{\delta(\mathbf{p})}u. \tag{5.21}$$

Next, it follows from (5.20) and (5.21) that

$$\eta_{\rm o}(\mathbf{p})\delta(\mathbf{p})y_{\rm i} = \eta_{\rm o}(\mathbf{p})\eta_{\rm i}(\mathbf{p})u,$$

$$\eta_{\rm i}(\mathbf{p})\delta(\mathbf{p})y_{\rm o} = \eta_{\rm i}(\mathbf{p})\eta_{\rm o}(\mathbf{p})u,$$

and thus

$$\eta_{\rm i}(\mathbf{p})\delta(\mathbf{p})y_{\rm o} = \eta_{\rm o}(\mathbf{p})\delta(\mathbf{p})y_{\rm i}. \tag{5.22}$$

Definition 6. The *transmissibility operator* from $y_{\rm i}$ to $y_{\rm o}$ is the operator

$$\mathcal{T}^{\rm F}{}_{w_{\rm o},w_{\rm i}|b}(\mathbf{p}) \triangleq \frac{\delta(\mathbf{p})\eta_{\rm o}(\mathbf{p})}{\delta(\mathbf{p})\eta_{\rm i}(\mathbf{p})}. \tag{5.23}$$

Hence, (5.22) can be written as

$$y_{\rm o} = \mathcal{T}^{\rm F}{}_{w_{\rm o},w_{\rm i}|b}(\mathbf{p})y_{\rm i}. \tag{5.24}$$

Note that (5.23) is independent of the input u. Because (5.23) is expressed in terms of the differentiation operator $\mathbf{p}$ and not the complex number s, it is a time-domain model of the differential equation (5.22) and thus it accounts for nonzero initial conditions. However, (5.23) is not a transfer function. In the case $q(0) = 0$ and $\dot{q}(0) = 0$, it follows from (5.9) that $\mathbf{p}$ in (5.24) can be replaced by s to obtain

$$\hat{y}_{\rm o}(s) = \mathcal{T}^{\rm F}{}_{w_{\rm o},w_{\rm i}|b}(s)\hat{y}_{\rm i}(s), \tag{5.25}$$

where $\mathcal{T}^{\rm F}{}_{w_{\rm o},w_{\rm i}|b}(s)$ is a possibly improper rational function. However, if $q(0)$ or $\dot{q}(0)$ is not zero, then $\mathbf{p}$ cannot be replaced by s in (5.24).

Unlike common factors in the complex number s, common factors in the differentiation operator $\mathbf{p}$ cannot always be cancelled, as shown in Examples 2.2.1 and 2.2.2.

Despite Examples 2.2.1 and 2.2.2, the following theorem shows that the common factor $\delta(\mathbf{p})$ in (5.23) can be cancelled without excluding any solutions of (5.22).

Theorem 3. y_i and y_o satisfy

$$y_\mathrm{o} = \frac{\eta_\mathrm{o}(\mathbf{p})}{\eta_\mathrm{i}(\mathbf{p})} y_\mathrm{i}. \tag{5.26}$$

Proof. See [62]. □

It follows from Theorem 3 that

$$y_\mathrm{o} = \mathcal{T}^\mathrm{F}_{w_\mathrm{o},w_\mathrm{i}|b}(\mathbf{p}) y_\mathrm{i}, \tag{5.27}$$

where the transmissibility operator in (5.23) is redefined as

$$\mathcal{T}^\mathrm{F}_{w_\mathrm{o},w_\mathrm{i}|b}(\mathbf{p}) \triangleq \frac{\eta_\mathrm{o}(\mathbf{p})}{\eta_\mathrm{i}(\mathbf{p})} = \frac{w_\mathrm{o}\mathrm{adj}(\mathbf{p}^2 M + K)b}{w_\mathrm{i}\mathrm{adj}(\mathbf{p}^2 M + K)b}. \tag{5.28}$$

Note that $\mathcal{T}^\mathrm{F}_{w_\mathrm{o},w_\mathrm{i}|b}(\mathbf{p})$ is not necessarily proper, and the polynomials $w_\mathrm{o}\mathrm{adj}(\mathbf{p}^2 M + K)b$ and $w_\mathrm{i}\mathrm{adj}(\mathbf{p}^2 M + K)b$ are not necessarily coprime.

5.3 MIMO Transmissibilities in Force-Driven Structures

Consider the lumped MIMO force-driven structure

$$M\ddot{q}(t) + Kq(t) = F_B(t), \tag{5.29}$$

where M, K, and q are as defined in (5.1), and

$$F_B \triangleq Bu(t), \tag{5.30}$$

where

$$B \triangleq \begin{bmatrix} b_1 & \cdots & b_m \end{bmatrix}, \quad u(t) \triangleq \begin{bmatrix} u_1(t) & \cdots & u_m(t) \end{bmatrix}^{\mathrm{T}}, \tag{5.31}$$

and, for all $i \in \{1, \ldots, m\}$, $b_i \in \mathbb{R}^n$ and u_i is a scalar force.

Consider p outputs for (5.29). Let $W_{\mathrm{i}} \in \mathbb{R}^{m\times n}, W_{\mathrm{o}} \in \mathbb{R}^{(p-m)\times n}$ and define

$$y_{\mathrm{i}} \triangleq q_{W_{\mathrm{i}}|Bu} = W_{\mathrm{i}}q \in \mathbb{R}^m, \tag{5.32}$$

$$y_{\mathrm{o}} \triangleq q_{W_{\mathrm{o}}|Bu} = W_{\mathrm{o}}q \in \mathbb{R}^{p-m}. \tag{5.33}$$

The goal is to obtain a transmissibility function relating y_{i} and y_{o} that is independent of both the initial conditions $q(0)$ and $\dot{q}(0)$, as well as the input u.

Multiplying (5.32), (5.33) by $\delta(\mathbf{p})$ and following the procedure used to derive (5.12), (5.13) yields

$$\delta(\mathbf{p})y_{\mathrm{i}} = W_{\mathrm{i}}\mathrm{adj}(\mathbf{p}^2M + K)Bu, \tag{5.34}$$

$$\delta(\mathbf{p})y_{\mathrm{o}} = W_{\mathrm{o}}\mathrm{adj}(\mathbf{p}^2M + K)Bu. \tag{5.35}$$

For convenience, we define

$$G_{W_{\mathrm{i}},B}(\mathbf{p}) \triangleq W_{\mathrm{i}}(\mathbf{p}^2M + K)^{-1}B, \tag{5.36}$$

$$G_{W_{\mathrm{o}},B}(\mathbf{p}) \triangleq W_{\mathrm{o}}(\mathbf{p}^2M + K)^{-1}B, \tag{5.37}$$

and rewrite (5.34), (5.35) as

$$y_{\mathrm{i}} = G_{W_{\mathrm{i}},B}(\mathbf{p})u, \quad y_{\mathrm{o}} = G_{W_{\mathrm{o}},B}(\mathbf{p})u, \tag{5.38}$$

respectively, which are interpreted as the differential equations (5.34), (5.35), respectively. Note that (5.38) includes the free response due to $q(0)$ and $\dot{q}(0)$ as well as the forced response due to u.

Defining the polynomial matrices

$$\Gamma_{\mathrm{i}}(\mathbf{p}) \triangleq W_{\mathrm{i}}\mathrm{adj}(\mathbf{p}^2 M + K)B \in \mathbb{R}^{m\times m}[\mathbf{p}], \tag{5.39}$$

$$\Gamma_{\mathrm{o}}(\mathbf{p}) \triangleq W_{\mathrm{o}}\mathrm{adj}(\mathbf{p}^2 M + K)B \in \mathbb{R}^{(p-m)\times m}[\mathbf{p}], \tag{5.40}$$

we can rewrite (5.34), (5.35) as

$$\delta(\mathbf{p})y_{\mathrm{i}} = \Gamma_{\mathrm{i}}(\mathbf{p})u, \tag{5.41}$$

$$\delta(\mathbf{p})y_{\mathrm{o}} = \Gamma_{\mathrm{o}}(\mathbf{p})u, \tag{5.42}$$

respectively. Multiplying (5.41) by $\mathrm{adj}\,\Gamma_{\mathrm{i}}(\mathbf{p})$ from the left yields

$$\delta(\mathbf{p})\,\mathrm{adj}\,\Gamma_{\mathrm{i}}(\mathbf{p})y_{\mathrm{i}} = [\mathrm{adj}\,\Gamma_{\mathrm{i}}(\mathbf{p})]\,\Gamma_{\mathrm{i}}(\mathbf{p})u = \det\Gamma_{\mathrm{i}}(\mathbf{p})u. \tag{5.43}$$

Next, multiplying (5.42) by $\det\Gamma_{\mathrm{i}}(\mathbf{p})$ yields

$$[\det\Gamma_{\mathrm{i}}(\mathbf{p})]\,\delta(\mathbf{p})y_{\mathrm{o}} = [\det\Gamma_{\mathrm{i}}(\mathbf{p})]\,\Gamma_{\mathrm{o}}(\mathbf{p})u. \tag{5.44}$$

Substituting the left hand side of (5.43) in (5.44) yields

$$\delta(\mathbf{p})\det\Gamma_{\mathrm{i}}(\mathbf{p})y_{\mathrm{o}} = \delta(\mathbf{p})\Gamma_{\mathrm{o}}(\mathbf{p})\,\mathrm{adj}\,\Gamma_{\mathrm{i}}(\mathbf{p})y_{\mathrm{i}}. \tag{5.45}$$

Definition 7. Assume that $\det \Gamma_{\rm i}(\mathbf{p})$ is not the zero polynomial. Then, the *transmissibility operator* from $y_{\rm i}$ to $y_{\rm o}$ is the operator

$$\mathcal{T}^{\rm F}_{W_{\rm o},W_{\rm i}|B}(\mathbf{p}) \triangleq \frac{\delta(\mathbf{p})}{\delta(\mathbf{p})\det \Gamma_{\rm i}(\mathbf{p})}\Gamma_{\rm o}(\mathbf{p})\mathrm{adj}\,\Gamma_{\rm i}(\mathbf{p}) = \frac{\delta(\mathbf{p})}{\delta(\mathbf{p})}\Gamma_{\rm o}(\mathbf{p})\Gamma_{\rm i}{}^{-1}(\mathbf{p}). \tag{5.46}$$

Note that (5.46) is independent of the input u and the initial condition $q(0)$ and $\dot{q}(0)$. Using (5.46), the differential equation (5.45) can be written as

$$y_{\rm o} = \mathcal{T}^{\rm F}_{W_{\rm o},W_{\rm i}|B}(\mathbf{p})y_{\rm i}. \tag{5.47}$$

The following theorem shows that the common factor $\delta(\mathbf{p})$ in (5.46) can be cancelled without excluding any solutions of (5.45).

Theorem 4. Assume that $\det \Gamma_{\rm i}(\mathbf{p})$ is not the zero polynomial. Then, $y_{\rm i}$ and $y_{\rm o}$ satisfy

$$y_{\rm o} = \frac{1}{\det \Gamma_{\rm i}(\mathbf{p})}\Gamma_{\rm o}(\mathbf{p})[\mathrm{adj}\,\Gamma_{\rm i}(\mathbf{p})]y_{\rm i} = \Gamma_{\rm o}(\mathbf{p})\Gamma_{\rm i}{}^{-1}(\mathbf{p})y_{\rm i}. \tag{5.48}$$

Proof. See [62]. $\square$

It follows from Theorem 4 that

$$y_{\rm o} = \mathcal{T}^{\rm F}_{W_{\rm o},W_{\rm i}|B}(\mathbf{p})y_{\rm i}, \tag{5.49}$$

where the transmissibility operator (5.46) is redefined as

$$\mathcal{T}^{\mathrm{F}}_{W_{\mathrm{o}},W_{\mathrm{i}}|B}(\mathbf{p}) \triangleq \Gamma_{\mathrm{o}}(\mathbf{p})\Gamma_{\mathrm{i}}{}^{-1}(\mathbf{p}). \tag{5.50}$$

Note that each entry of $\mathcal{T}^{\mathrm{F}}_{W_{\mathrm{o}},W_{\mathrm{i}}|B}(\mathbf{p})$ is a rational operator that is not necessarily proper and whose numerator and denominator are not necessarily coprime.

5.4 Modeling Displacement-Driven Structures

Consider a displacement-driven structure (DDS), where m_k is the driven mass, and thus

$$q_k(t) = q_{k,\mathrm{d}}(t), \tag{5.51}$$

where $q_{k,\mathrm{d}}(t)$ is the prescribed motion of m_k. This prescribed motion requires applying a suitable force as in (5.1). Removing the k^{th} equation from (5.1) yields

$$M_{[k,\cdot]}\ddot{q}(t) + K_{[k,\cdot]}q(t) = 0, \tag{5.52}$$

where $M_{[k,\cdot]} \in \mathbb{R}^{(n-1)\times n}$ and $K_{[k,\cdot]} \in \mathbb{R}^{(n-1)\times n}$ are M and K, respectively, with the k^{th} row removed. It follows that (5.52) can be written as

$$M_{[k,k]}\ddot{q}_{[k]} + K_{[k,k]}q_{[k]} = -K_{[k,\cdot]}e_{k,n}q_{k,\mathrm{d}}, \tag{5.53}$$

where $M_{[k,k]} \in \mathbb{R}^{(n-1)\times(n-1)}$ and $K_{[k,k]} \in \mathbb{R}^{(n-1)\times(n-1)}$ are M and K, respectively, with both the k^{th} row and k^{th} column removed, and $q_{[k]}$ is q with the k^{th} row removed. Writing (5.53) in terms of the differentiation operator $\mathbf{p}$ yields

$$\left(\mathbf{p}^2 M_{[k,k]} + K_{[k,k]}\right) q_{[k]} = -K_{[k,\cdot]}e_{k,n}q_{k,\mathrm{d}}. \tag{5.54}$$

Suppose now that d masses are displacement-driven, where $1 \leq d \leq n-2$, and let $D \triangleq \{k_1, \ldots, k_d\}$ be the set of displacement-driven masses. Then, using the same procedure used to obtain (5.53) we obtain

$$\left(\mathbf{p}^2 M_{[D,D]} + K_{[D,D]}\right) q_{[D]} = -K_{[D,\cdot]} \begin{bmatrix} e_{k_1,n} & \cdots & e_{k_d,n} \end{bmatrix} \begin{bmatrix} q_{k_1,\mathrm{d}} \\ \vdots \\ q_{k_d,\mathrm{d}} \end{bmatrix}, \tag{5.55}$$

where $M_{[D,D]} \in \mathbb{R}^{(n-d)\times(n-d)}$ and $K_{[D,D]} \in \mathbb{R}^{(n-d)\times(n-d)}$ are M and K with rows $k_1, \ldots, k_d$ removed and columns $k_1, \ldots, k_d$ removed, $K_{[D,\cdot]}$ is K with rows $k_1, \ldots, k_d$ removed, and $q_{[D]}$ is q with rows $k_1, \ldots, k_d$ removed.

5.5 SISO Transmissibilities in Displacement-Driven Structures

Define the output

$$q_{\mathrm{d},c|e_{k,n}} \triangleq cI_{n_{[\cdot,k]}} q_{[k]}, \tag{5.56}$$

where $I_{n_{[\cdot,k]}} \in \mathbb{R}^{n\times(n-1)}$ is the identity matrix $I_n \in \mathbb{R}^{n\times n}$ with the k^{th} column removed. Thus, $q_{\mathrm{d},c|e_{k,n}}$ is a linear combination of all position states $q_i, i = 1, \ldots, n, i \neq k$, assuming that the k^{th} mass is displacement-driven. Let $w_{\mathrm{i}}, w_{\mathrm{o}} \in \mathbb{R}^{1\times n}$ and define

$$y_{\mathrm{i,d}} \triangleq q_{\mathrm{d},w_{\mathrm{i}}|e_{k,n}} = w_{\mathrm{i}} I_{n_{[\cdot,k]}} q_{[k]}, \tag{5.57}$$

$$y_{\mathrm{o,d}} \triangleq q_{\mathrm{d},w_{\mathrm{o}}|e_{k,n}} = w_{\mathrm{o}} I_{n_{[\cdot,k]}} q_{[k]}. \tag{5.58}$$

$$\tag{5.59}$$

Following the procedure used to derive (5.12), (5.13) we can show that

$$\delta_{\mathrm{d}}(\mathbf{p})y_{\mathrm{i,d}} = -w_{\mathrm{i}} I_{n_{[\cdot,k]}} \mathrm{adj}\left(\mathbf{p}^2 M_{[k,k]} + K_{[k,k]}\right) K_{[k,\cdot]} e_{k,n} q_{k,\mathrm{d}}, \tag{5.60}$$

$$\delta_{\mathrm{d}}(\mathbf{p})y_{\mathrm{o,d}} = -w_{\mathrm{o}} I_{n_{[\cdot,k]}} \mathrm{adj}\left(\mathbf{p}^2 M_{[k,k]} + K_{[k,k]}\right) K_{[k,\cdot]} e_{k,n} q_{k,\mathrm{d}}, \tag{5.61}$$

where $\delta_{\mathrm{d}}(\mathbf{p}) \stackrel{\triangle}{=} \det\left(\mathbf{p}^2 M_{[k,k]} + K_{[k,k]}\right)$. For convenience, we define the notation

$$G_{\mathrm{d},w_{\mathrm{i}},e_{k,n}}(\mathbf{p}) \stackrel{\triangle}{=} -w_{\mathrm{i}} I_{n_{[\cdot,k]}} \left(\mathbf{p}^2 M_{[k,k]} + K_{[k,k]}\right)^{-1} K_{[k,\cdot]} e_{k,n}, \tag{5.62}$$

$$G_{\mathrm{d},w_{\mathrm{o}},e_{k,n}}(\mathbf{p}) \stackrel{\triangle}{=} -w_{\mathrm{o}} I_{n_{[\cdot,k]}} \left(\mathbf{p}^2 M_{[k,k]} + K_{[k,k]}\right)^{-1} K_{[k,\cdot]} e_{k,n}. \tag{5.63}$$

Using (5.62), (5.63) we can rewrite (5.60), (5.61) as

$$y_{\mathrm{i,d}} = G_{\mathrm{d},w_{\mathrm{i}},e_{k,n}}(\mathbf{p}) q_{k,\mathrm{d}} = \frac{\eta_{\mathrm{i,d}}(\mathbf{p})}{\delta_{\mathrm{d}}(\mathbf{p})} q_{k,\mathrm{d}}, \tag{5.64}$$

$$y_{\mathrm{o,d}} = G_{\mathrm{d},w_{\mathrm{o}},e_{k,n}}(\mathbf{p}) q_{k,\mathrm{d}} = \frac{\eta_{\mathrm{o,d}}(\mathbf{p})}{\delta_{\mathrm{d}}(\mathbf{p})} q_{k,\mathrm{d}}, \tag{5.65}$$

respectively, where

$$\eta_{\mathrm{i,d}}(\mathbf{p}) \stackrel{\triangle}{=} -w_{\mathrm{i}} I_{n_{[\cdot,k]}} \mathrm{adj}\left(\mathbf{p}^2 M_{[k,k]} + K_{[k,k]}\right) K_{[k,\cdot]} e_{k,n}, \tag{5.66}$$

$$\eta_{\mathrm{o,d}}(\mathbf{p}) \stackrel{\triangle}{=} -w_{\mathrm{o}} I_{n_{[\cdot,k]}} \mathrm{adj}\left(\mathbf{p}^2 M_{[k,k]} + K_{[k,k]}\right) K_{[k,\cdot]} e_{k,n}, \tag{5.67}$$

are polynomials in $\mathbf{p}$. It follows from (5.64) and (5.65) that

$$\eta_{\mathrm{o,d}}(\mathbf{p})\delta_{\mathrm{d}}(\mathbf{p}) y_{\mathrm{i,d}} = \eta_{\mathrm{o,d}}(\mathbf{p})\eta_{\mathrm{i,d}}(\mathbf{p}) q_{k,\mathrm{d}},$$

$$\eta_{\mathrm{i,d}}(\mathbf{p})\delta_{\mathrm{d}}(\mathbf{p}) y_{\mathrm{o,d}} = \eta_{\mathrm{i,d}}(\mathbf{p})\eta_{\mathrm{o,d}}(\mathbf{p}) q_{k,\mathrm{d}},$$

and thus

$$\eta_{\mathrm{i,d}}(\mathbf{p})\delta_{\mathrm{d}}(\mathbf{p}) y_{\mathrm{o,d}} = \eta_{\mathrm{o,d}}(\mathbf{p})\delta_{\mathrm{d}}(\mathbf{p}) y_{\mathrm{i,d}}. \tag{5.68}$$

Definition 8. The *transmissibility operator* from $y_{\rm i,d}$ to $y_{\rm o,d}$ is the operator

$$\mathcal{T}^{\rm D}{}_{w_{\rm o},w_{\rm i}|e_{k,n}}(\mathbf{p}) \triangleq \frac{\delta_{\rm d}(\mathbf{p})\eta_{\rm o,d}(\mathbf{p})}{\delta_{\rm d}(\mathbf{p})\eta_{\rm i,d}(\mathbf{p})}.$$

Hence, (5.68) can be written as

$$y_{\rm o,d} = \mathcal{T}^{\rm D}{}_{w_{\rm o},w_{\rm i}|e_{k,n}}(\mathbf{p})y_{\rm i,d}. \tag{5.69}$$

As in Section 5.2, it can be shown that $\delta_{\rm d}(\mathbf{p})$ can be cancelled without excluding any solutions of (5.68), that is, $\mathcal{T}^{\rm D}_{w_{\rm o},w_{\rm i}|e_{k,n}}(\mathbf{p})$ in (5.69) can be redefined as

$$\mathcal{T}^{\rm D}_{w_{\rm o},w_{\rm i}|e_{k,n}}(\mathbf{p}) \triangleq \frac{\eta_{\rm o,d}(\mathbf{p})}{\eta_{\rm i,d}(\mathbf{p})} = \frac{w_{\rm o}I_{n_{[\cdot,k]}}\mathrm{adj}\left(\mathbf{p}^2M_{[k,k]}+K_{[k,k]}\right)K_{[k,\cdot]}e_{k,n}}{w_{\rm i}I_{n_{[\cdot,k]}}\mathrm{adj}\left(\mathbf{p}^2M_{[k,k]}+K_{[k,k]}\right)K_{[k,\cdot]}e_{k,n}}. \tag{5.70}$$

Note that $\mathcal{T}^{\rm D}_{w_{\rm o},w_{\rm i}|e_{k,n}}(\mathbf{p})$ is not necessarily proper, and the polynomials $\eta_{\rm o,d}(\mathbf{p})$ and $\eta_{\rm i,d}(\mathbf{p})$ are not necessarily coprime.

5.6 MIMO Transmissibilities in Displacement-Driven Structures

Consider a DDS, where $m_{k_1},\ldots,m_{k_d}$ are the displacement-driven masses, $1 \le d \le n-2$. Define the output $q_{{\rm d},C|e_{D,n}} \in \mathbb{R}^p$ by

$$q_{{\rm d},C|e_{D,n}} \triangleq CI_{n_{[\cdot,k]}}q_{[D]}, \tag{5.71}$$

where $C \in \mathbb{R}^{p\times n}$, $D \triangleq \{k_1,\ldots,k_d\}$, and $e_{D,n} \triangleq [e_{k_1,n}\ \ldots\ e_{k_d,n}]$. Hence, (5.71) is a vector whose components are linear combinations of all $q_i, i \in \{1,\ldots,n\}\setminus D$. Let

$W_{\rm i} \in \mathbb{R}^{d\times n}, W_{\rm o} \in \mathbb{R}^{(p-d)\times n}$ and define

$$y_{\rm i,d} \stackrel{\triangle}{=} q_{{\rm d},W_{\rm i}|e_{D,n}} = W_{\rm i} I_{n_{[\cdot,D]}} q_{[D]}, \tag{5.72}$$

$$y_{\rm o,d} \stackrel{\triangle}{=} q_{{\rm d},W_{\rm o}|e_{D,n}} = W_{\rm o} I_{n_{[\cdot,D]}} q_{[D]}. \tag{5.73}$$

Following the procedure used to derive (5.12), (5.13) yields

$$\Delta_{\rm d}(\mathbf{p}) y_{\rm i,d} = -W_{\rm i} I_{n_{[\cdot,D]}} {\rm adj}\left(\mathbf{p}^2 M_{[D,D]} + K_{[D,D]}\right) K_{[D,\cdot]} e_{D,n} q_{D,{\rm d}}, \tag{5.74}$$

$$\Delta_{\rm d}(\mathbf{p}) y_{\rm o,d} = -W_{\rm o} I_{n_{[\cdot,D]}} {\rm adj}\left(\mathbf{p}^2 M_{[D,D]} + K_{[D,D]}\right) K_{[D,\cdot]} e_{D,n} q_{D,{\rm d}}, \tag{5.75}$$

where $\Delta_{\rm d}(\mathbf{p}) \stackrel{\triangle}{=} \det\left(\mathbf{p}^2 M_{[D,D]} + K_{[D,D]}\right) \in \mathbb{R}[\mathbf{p}]$ and $q_{D,{\rm d}} \stackrel{\triangle}{=} [q_{k_1} \ \cdots \ q_{k_d}]^{\rm T} \in \mathbb{R}^d$. Using the notation

$$G_{{\rm d},W_{\rm i},e_{D,n}}(\mathbf{p}) \stackrel{\triangle}{=} -W_{\rm i} I_{n_{[\cdot,D]}} \left(\mathbf{p}^2 M_{[D,D]} + K_{[D,D]}\right)^{-1} K_{[D,\cdot]} e_{D,n}, \tag{5.76}$$

$$G_{{\rm d},W_{\rm o},e_{D,n}}(\mathbf{p}) \stackrel{\triangle}{=} -W_{\rm o} I_{n_{[\cdot,D]}} \left(\mathbf{p}^2 M_{[D,D]} + K_{[D,D]}\right)^{-1} K_{[D,\cdot]} e_{D,n}, \tag{5.77}$$

we can rewrite (5.74), (5.75) as

$$y_{\rm i,d} = G_{{\rm d},W_{\rm i},e_{D,n}}(\mathbf{p}) q_{D,{\rm d}}, \tag{5.78}$$

$$y_{\rm o,d} = G_{{\rm d},w_{\rm o},e_{D,n}}(\mathbf{p}) q_{D,{\rm d}}, \tag{5.79}$$

which are interpreted as the differential equations (5.74), (5.75), respectively. Note that (5.78) and (5.79) include the free response due to $q_{[D]}(0)$ and $\dot{q}_{[D]}(0)$ as well as the forced response due to $q_{D,{\rm d}}$. Defining

$$\Gamma_{\rm i,d}(\mathbf{p}) \stackrel{\triangle}{=} -W_{\rm i} I_{n_{[\cdot,D]}} {\rm adj}\left(\mathbf{p}^2 M_{[D,D]} + K_{[D,D]}\right) K_{[D,\cdot]} e_{D,n} \in \mathbb{R}^{d\times d}[\mathbf{p}], \tag{5.80}$$

$$\Gamma_{\rm o,d}(\mathbf{p}) \stackrel{\triangle}{=} -W_{\rm o} I_{n_{[\cdot,D]}} {\rm adj}\left(\mathbf{p}^2 M_{[D,D]} + K_{[D,D]}\right) K_{[D,\cdot]} e_{D,n} \in \mathbb{R}^{(p-d)\times d}[\mathbf{p}], \tag{5.81}$$

we can rewrite (5.74), (5.75) as

$$\Delta_{\rm d}(\mathbf{p}) y_{\rm i,d} = \Gamma_{\rm i,d}(\mathbf{p}) q_{D,{\rm d}}, \tag{5.82}$$

$$\Delta_{\rm d}(\mathbf{p}) y_{\rm o,d} = \Gamma_{\rm o,d}(\mathbf{p}) q_{D,{\rm d}}. \tag{5.83}$$

Multiplying (5.82) by $\operatorname{adj}\Gamma_{\rm i,d}(\mathbf{p})$ from the left yields

$$\operatorname{adj}\Gamma_{\rm i,d}(\mathbf{p})\Delta_{\rm d}(\mathbf{p}) y_{\rm i,d} = \operatorname{adj}\Gamma_{\rm i,d}(\mathbf{p})\Gamma_{\rm i,d}(\mathbf{p}) q_{D,{\rm d}} = \det\Gamma_{\rm i,d}(\mathbf{p}) q_{D,{\rm d}}. \tag{5.84}$$

Next, multiplying (5.83) by $\det\Gamma_{\rm i,d}(\mathbf{p})$ yields

$$[\det\Gamma_{\rm i,d}(\mathbf{p})]\, \Delta_{\rm d}(\mathbf{p}) y_{\rm o,d} = [\det\Gamma_{\rm i,d}(\mathbf{p})]\, \Gamma_{\rm o,d}(\mathbf{p}) q_{D,{\rm d}}. \tag{5.85}$$

Substituting the left hand side of (5.84) into (5.85) yields

$$\Delta_{\rm d}(\mathbf{p}) \det\Gamma_{\rm i,d}(\mathbf{p}) y_{\rm o,d} = \Delta_{\rm d}(\mathbf{p})\Gamma_{\rm o,d}(\mathbf{p}) \operatorname{adj}\Gamma_{\rm i,d}(\mathbf{p}) y_{\rm i,d}. \tag{5.86}$$

Definition 9. Assume that $\det\Gamma_{\rm i,d}(\mathbf{p})$ is not the zero polynomial. The *transmissibility operator* from $y_{\rm i,d}$ to $y_{\rm o,d}$ is the operator

$$\mathcal{T}^{\rm D}{}_{W_{\rm o},W_{\rm i}|e_{D,n}}(\mathbf{p}) \triangleq \frac{\Delta_{\rm d}(\mathbf{p})}{\Delta_{\rm d}(\mathbf{p})\det\Gamma_{\rm i,d}(\mathbf{p})}\Gamma_{\rm o,d}(\mathbf{p})\mathrm{adj}\Gamma_{\rm i,d}(\mathbf{p}) = \frac{\Delta_{\rm d}(\mathbf{p})}{\Delta_{\rm d}(\mathbf{p})}\Gamma_{\rm o,d}(\mathbf{p})\Gamma_{\rm i,d}^{-1}(\mathbf{p}).$$

Hence, (5.86) can be written as

$$y_{\rm o,d} = \mathcal{T}^{\rm D}{}_{W_{\rm o},W_{\rm i}|e_{D,n}}(\mathbf{p}) y_{\rm i,d}. \tag{5.87}$$

As in Section 5.3, it can be shown that $\Delta_{\rm d}(\mathbf{p})$ can be cancelled without excluding any solutions of (5.86), that is, $\mathcal{T}^{\rm D}_{W_{\rm o},W_{\rm i}|e_{D,n}}(\mathbf{p})$ in (5.87) can be redefined as

$$\mathcal{T}^{\rm D}_{W_{\rm o},W_{\rm i}|e_{D,n}}(\mathbf{p}) \stackrel{\triangle}{=} \Gamma_{\rm o,d}(\mathbf{p})\Gamma^{-1}_{\rm i,d}(\mathbf{p}). \tag{5.88}$$

5.7 Equality of Motion Transmissibilities in Force-driven and Displacement-Driven Structures

5.7.1 Equality of SISO Motion Transmissibilities in Force-driven and Displacement-Driven Structures

Define $w_{{\rm o},k}$ and $w_{{\rm i},k}$ to be $w_{\rm o}$ and $w_{\rm i}$, respectively, with the $k^{\rm th}$ component replaced by zero. The following result shows that the SISO transmissbilities of force-driven and displacement-driven structures with identical inputs and outputs and with the force and prescribed motion applied to the same location are identical. This result is somewhat surprising since the specified displacement of a mass could be perceived as introducing a node.

Theorem 5. The SISO force-driven and displacement-driven transmissibilities are equal, that is,

$$\mathcal{T}^{\rm F}_{w_{{\rm o},k},w_{{\rm i},k}|e_{k,n}}(\mathbf{p}) = \mathcal{T}^{\rm D}_{w_{{\rm o},k},w_{{\rm i},k}|e_{k,n}}(\mathbf{p}). \tag{5.89}$$

Proof. It follows from (5.70) that

$$\mathcal{T}^{\rm D}_{w_{\rm o},w_{\rm i}|e_{k,n}}(\mathbf{p}) = \frac{w_{\rm o} I_{n_{[\cdot,k]}} \operatorname{adj}\left(\mathbf{p}^2 M_{[k,k]} + K_{[k,k]}\right) K_{[k,\cdot]} e_{k,n}}{w_{\rm i} I_{n_{[\cdot,k]}} \operatorname{adj}\left(\mathbf{p}^2 M_{[k,k]} + K_{[k,k]}\right) K_{[k,\cdot]} e_{k,n}}. \tag{5.90}$$

Using Proposition B.1 in Appendix B, we have

$$w_{\mathrm{o},k} I_{n_{[\cdot,k]}} \mathrm{adj}\left(\mathbf{p}^2 M_{[k,k]} + K_{[k,k]}\right) K_{[k,\cdot]} e_{k,n} = -w_{\mathrm{o},k} \mathrm{adj}\left(\mathbf{p}^2 M + K\right) e_{k,n}, \tag{5.91}$$

$$w_{\mathrm{i},k} I_{n_{[\cdot,k]}} \mathrm{adj}\left(\mathbf{p}^2 M_{[k,k]} + K_{[k,k]}\right) K_{[k,\cdot]} e_{k,n} = -w_{\mathrm{i},k} \mathrm{adj}\left(\mathbf{p}^2 M + K\right) e_{k,n}. \tag{5.92}$$

Using (5.91) and (5.92), (5.90) yields

$$\mathcal{T}^{\mathrm{D}}_{w_{\mathrm{o},k}, w_{\mathrm{i},k} | e_{k,n}}(\mathbf{p}) = \frac{w_{\mathrm{o},k} \mathrm{adj}\left(\mathbf{p}^2 M + K\right) e_{k,n}}{w_{\mathrm{i},k} \mathrm{adj}\left(\mathbf{p}^2 M + K\right) e_{k,n}}. \tag{5.93}$$

Replacing w_{o}, w_{i}, and b in (5.28) with $w_{\mathrm{o},k}$, $w_{\mathrm{i},k}$, and $e_{k,n}$, respectively, yields

$$\mathcal{T}^{\mathrm{F}}_{w_{\mathrm{o},k}, w_{\mathrm{i},k} | e_{k,n}}(\mathbf{p}) = \frac{w_{\mathrm{o},k} \mathrm{adj}(\mathbf{p}^2 M + K) e_{k,n}}{w_{\mathrm{i},k} \mathrm{adj}(\mathbf{p}^2 M + K) e_{k,n}}. \tag{5.94}$$

Hence, (5.93) and (5.94) yield (5.89). □

5.7.2 Equality of MIMO Motion Transmissibilities in Force-driven and Displacement-Driven Structures

Define $W_{\mathrm{o},D}$ and $W_{\mathrm{i},D}$ to be W_{o} and W_{i}, respectively, with the $k_1^{\mathrm{th}}, \ldots, k_d^{\mathrm{th}}$ columns replaced by zero. The following result shows that the MIMO transmissibilities of force-driven and displacement-driven structures with identical inputs and outputs and with the forces and prescribed motions applied to the same locations are identical.

Theorem 6. The MIMO force-driven and displacement driven transmissibilities are equal, that is,

$$\mathcal{T}^{\mathrm{F}}_{W_{\mathrm{o},D}, W_{\mathrm{i},D} | e_{D,n}}(\mathbf{p}) = \mathcal{T}^{\mathrm{D}}_{W_{\mathrm{o},D}, W_{\mathrm{i},D} | e_{D,n}}(\mathbf{p}). \tag{5.95}$$

Proof. It follows from (5.80), (5.81), and (5.88) that

$$\begin{aligned}\mathcal{T}^{\mathrm{D}}_{W_{\mathrm{o},D},W_{\mathrm{i},D}|e_{D,n}}(\mathbf{p}) &= \Gamma_{\mathrm{o,d}}(\mathbf{p})\Gamma^{-1}_{\mathrm{i,d}}(\mathbf{p}) \\ &= W_{\mathrm{o}} I_{n_{[\cdot,D]}} \mathrm{adj}\left(\mathbf{p}^2 M_{[D,D]} + K_{[D,D]}\right) K_{[D,\cdot]} e_{D,n} \\ &\quad \cdot \left(W_{\mathrm{i}} I_{n_{[\cdot,D]}} \mathrm{adj}\left(\mathbf{p}^2 M_{[D,D]} + K_{[D,D]}\right) K_{[D,\cdot]} e_{D,n}\right)^{-1}. \end{aligned} \tag{5.96}$$

Using Proposition B.2 in Appendix B, we have

$$\begin{aligned} &W_{\mathrm{o}} I_{n_{[\cdot,D]}} \mathrm{adj}\left(\mathbf{p}^2 M_{[D,D]}+K_{[D,D]}\right) K_{[D,\cdot]} e_{D,n} \left(W_{\mathrm{i}} I_{n_{[\cdot,D]}} \mathrm{adj}\left(\mathbf{p}^2 M_{[D,D]} + K_{[D,D]}\right) K_{[D,\cdot]} e_{D,n}\right)^{-1} \\ &\qquad = W_{\mathrm{o},D} \mathrm{adj}\left(\mathbf{p}^2 M + K\right) e_{D,n} (W_{\mathrm{i},D} \mathrm{adj}(\mathbf{p}^2 M + K) e_{D,n})^{-1}. \end{aligned} \tag{5.97}$$

Therefore, (5.96) becomes

$$\mathcal{T}^{\mathrm{D}}_{W_{\mathrm{o},D},W_{\mathrm{i},D}|e_{D,n}}(\mathbf{p}) = W_{\mathrm{o},D} \mathrm{adj}\left(\mathbf{p}^2 M + K\right) e_{D,n} (W_{\mathrm{i},D} \mathrm{adj}(\mathbf{p}^2 M + K) e_{D,n})^{-1}. \tag{5.98}$$

Next, replacing W_{o}, W_{i}, and B in (5.39) and (5.40) with $W_{\mathrm{o},D}$, $W_{\mathrm{i},D}$, and $e_{D,n}$, respectively, (5.50) becomes

$$\begin{aligned}\mathcal{T}^{\mathrm{F}}_{W_{\mathrm{o},D},W_{\mathrm{i},D}|e_{D,n}}(\mathbf{p}) &= \Gamma_{\mathrm{o}}(\mathbf{p})\Gamma^{-1}_{\mathrm{i}}(\mathbf{p}) \\ &= W_{\mathrm{o},D} \mathrm{adj}\left(\mathbf{p}^2 M + K\right) e_{D,n} (W_{\mathrm{i},D} \mathrm{adj}(\mathbf{p}^2 M + K) e_{D,n})^{-1}. \end{aligned} \tag{5.99}$$

Comparing (5.98) with (5.99) yields (5.95). $\square$

5.8 Numerical Examples

In this section we present three examples to illustrate the equality of transmissibilities in force-driven and displacement-driven structures.

Example 5.8.1. Consider the mass-spring system shown in Figure 5.1, where $m_1 = m_2 = m_3 = m_4 = m_5 = m_6 = 1$ kg and $k_{01} = k_{12} = k_{14} = k_{15} = k_{23} = k_{36} = k_{45} = k_{46} = 1$ N/m. We force-drive m_2 and consider the transmissibility from q_1 to q_6. Then we displacement-drive m_2 and consider the transmissibility from q_1 to q_6. Note that $M = I_6$, $M_{[2,2]} = I_5$,

$$K = \begin{bmatrix} 4 & -1 & 0 & -1 & -1 & 0 \\ -1 & 2 & -1 & 0 & 0 & 0 \\ 0 & -1 & 2 & 0 & 0 & -1 \\ -1 & 0 & 0 & 3 & -1 & -1 \\ -1 & 0 & 0 & -1 & 2 & 0 \\ 0 & 0 & -1 & -1 & 0 & 2 \end{bmatrix}, K_{[2,2]} = \begin{bmatrix} 4 & 0 & -1 & -1 & 0 \\ 0 & 2 & 0 & 0 & -1 \\ -1 & 0 & 3 & -1 & -1 \\ -1 & 0 & -1 & 2 & 0 \\ 0 & -1 & -1 & 0 & 2 \end{bmatrix}. \tag{5.100}$$

It follows that

$$\operatorname{adj}\left(\mathbf{p}^2 M + K\right) e_{2,6} = \begin{bmatrix} \mathbf{p}^8 + 9\mathbf{p}^6 + 27\mathbf{p}^4 + 32\mathbf{p}^2 + 14 \\ \mathbf{p}^{10} + 13\mathbf{p}^8 + 61\mathbf{p}^6 + 124\mathbf{p}^4 + 102\mathbf{p}^2 + 25 \\ \mathbf{p}^8 + 11\mathbf{p}^6 + 40\mathbf{p}^4 + 54\mathbf{p}^2 + 22 \\ \mathbf{p}^6 + 8\mathbf{p}^4 + 21\mathbf{p}^2 + 16 \\ \mathbf{p}^6 + 8\mathbf{p}^4 + 19\mathbf{p}^2 + 15 \\ \mathbf{p}^6 + 10\mathbf{p}^4 + 28\mathbf{p}^2 + 19 \end{bmatrix}, \tag{5.101}$$

$$\operatorname{adj}\left(\mathbf{p}^2 M_{[2,2]} + K_{[2,2]}\right) K_{[2,\cdot]} e_{2,6} = -\begin{bmatrix} \mathbf{p}^8 + 9\mathbf{p}^6 + 27\mathbf{p}^4 + 32\mathbf{p}^2 + 14 \\ \mathbf{p}^8 + 11\mathbf{p}^6 + 40\mathbf{p}^4 + 54\mathbf{p}^2 + 22 \\ \mathbf{p}^6 + 8\mathbf{p}^4 + 21\mathbf{p}^2 + 16 \\ \mathbf{p}^6 + 8\mathbf{p}^4 + 19\mathbf{p}^2 + 15 \\ \mathbf{p}^6 + 10\mathbf{p}^4 + 28\mathbf{p}^2 + 19 \end{bmatrix}. \tag{5.102}$$

Next, it follows from (5.28) with $w_{\mathrm{o}} = e_{6,6}^{\mathrm{T}}, w_{\mathrm{i}} = e_{1,6}^{\mathrm{T}}$, and $b = e_{2,6}$ that

$$\mathcal{T}^{\mathrm{F}}_{e_{6,6}^{\mathrm{T}}, e_{1,6}^{\mathrm{T}}|e_{2,6}}(\mathbf{p}) = \frac{\mathbf{p}^6 + 10\mathbf{p}^4 + 28\mathbf{p}^2 + 19}{\mathbf{p}^8 + 9\mathbf{p}^6 + 27\mathbf{p}^4 + 32\mathbf{p}^2 + 14}. \tag{5.103}$$

Similarly, it follows from (5.70) with $w_{\mathrm{o}} = e_{6,6}^{\mathrm{T}}, w_{\mathrm{i}} = e_{1,6}^{\mathrm{T}}$, and $k = 2$ that

$$\mathcal{T}^{\mathrm{D}}_{e_{6,6}^{\mathrm{T}}, e_{1,6}^{\mathrm{T}}|e_{2,6}}(\mathbf{p}) = \frac{\mathbf{p}^6 + 10\mathbf{p}^4 + 28\mathbf{p}^2 + 19}{\mathbf{p}^8 + 9\mathbf{p}^6 + 27\mathbf{p}^4 + 32\mathbf{p}^2 + 14}. \tag{5.104}$$

Hence,

$$\mathcal{T}^{\mathrm{F}}_{e_{6,6}^{\mathrm{T}}, e_{1,6}^{\mathrm{T}}|e_{2,6}}(\mathbf{p}) = \mathcal{T}^{\mathrm{D}}_{e_{6,6}^{\mathrm{T}}, e_{1,6}^{\mathrm{T}}|e_{2,6}}(\mathbf{p}). \qquad \blacksquare$$

Example 5.8.2. Consider a simply supported beam with a uniform density ρ per unit length, modulus of elasticity E, moment of inertia I, length L, and rectangular cross section with area A. We consider first the force-driven case by applying a concentrated transverse force at the location x_{a}, where $0 < x_{\mathrm{a}} < L$. Let $y(t,x)$ denote the displacement of the beam from its equilibrium shape, and let $\delta(x - x_{\mathrm{a}})f(t)$ denote the external force. The beam is modeled by

$$\frac{\partial^4}{\partial x^4} y(t,x) + \frac{\rho A}{EI} \frac{\partial^2}{\partial t^2} y(t,x) = \delta(x - x_{\mathrm{a}}) f(t). \tag{5.105}$$

Let

$$y(t,x) = \sum_{i=1}^{\infty} q_i(t) v_i(x), \tag{5.106}$$

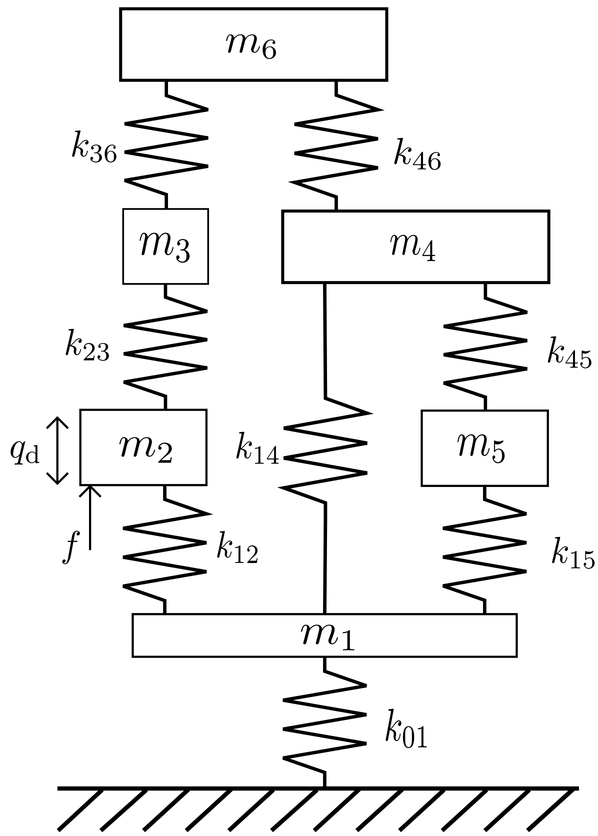

Figure 5.1: Mass-spring system for Example 5.8.1, where $m_1 = m_2 = m_3 = m_4 = m_5 = m_6 = 1$ kg and $k_{01} = k_{12} = k_{14} = k_{15} = k_{23} = k_{36} = k_{45} = k_{46} = 1$ N/m. m_2 is either force-driven by the force f or displacement-driven with the prescribed motion q_d.

where q_i is the modal coordinate corresponding to the mode shape $v_i(x) = \sin(\frac{i\pi x}{L})$. Substituting (5.106) in (5.105) and taking the inner product of both sides of the resulting equation with $v_i(x_\mathrm{a})$ yields

$$\ddot{q}_i(t) + \omega_i^2 q_i(t) = b_i f(t), \ i = 1, 2, 3, \ldots, \tag{5.107}$$

where $\omega_i = \frac{i^2\pi^2}{L^2}\sqrt{\frac{EI}{\rho A}}$ is the modal frequency corresponding to $v_i(x)$ and $b_i \stackrel{\triangle}{=} v_i(x_\mathrm{a})$. Defining

$$q(t) \stackrel{\triangle}{=} \begin{bmatrix} q_1(t) & \cdots & q_r(t) \end{bmatrix}^\mathrm{T}, \ b \stackrel{\triangle}{=} \begin{bmatrix} b_1 & \cdots & b_r \end{bmatrix}^\mathrm{T}, \tag{5.108}$$

it follows from (5.107) that

$$\ddot{q}(t) + \Omega^2 q(t) = bf(t), \tag{5.109}$$

where $\Omega^2 \triangleq \operatorname{diag}(\omega_1^2, \ldots, \omega_r^2)$.

In the displacement-driven case we assume that the interior point x_a moves with the specified displacement $q_\mathrm{d}(t, x_\mathrm{a}) = \sum_{i=1}^r q_i(t) v_i(x_\mathrm{a})$. We define the coordinates

$$\hat{q}(t) \triangleq S^{-\mathrm{T}} q(t), \tag{5.110}$$

where

$$S \triangleq \begin{bmatrix} I_{r-1} & & 0_{(r-1)\times 1} \\ v_1(x_a) & \cdots & v_r(x_a). \end{bmatrix}^{-\mathrm{T}}, \tag{5.111}$$

where to ensure nonsingularity we assume that $v_r(x_a) \neq 0$. Then, the resulting coordinates are

$$\hat{q}(t) = \begin{bmatrix} q_1(t) & \cdots & q_{r-1}(t) & q_\mathrm{d}(t, x_\mathrm{a}) \end{bmatrix}^\mathrm{T}. \tag{5.112}$$

Using (5.110), (5.109) yields

$$\hat{M}\ddot{\hat{q}}(t) + \hat{K}\hat{q}(t) = \hat{B}f(t), \tag{5.113}$$

where $\hat{M} \triangleq SS^\mathrm{T}$, $\hat{K} \triangleq S\Omega^2 S^\mathrm{T}$, $\hat{B} = Sb \triangleq e_{n,n}$.

Driving x_a with a prescribed motion requires applying a suitable force as in (5.105). As in Section 5.4 we remove the r^{th} equation of (5.113) and manipulate the remaining equations to make $q_\mathrm{d}(t, x_\mathrm{a})$ the input. Therefore, (5.113) becomes

$$\hat{M}_{[r,r]}\ddot{q}_{[r]} + \hat{K}_{[r,r]} q_{[r]} = -\hat{K}_{[r,\cdot]} e_{k,n} q_\mathrm{d}(t, x_\mathrm{a}). \tag{5.114}$$

Suppose that $E = 200$ GPa, $L = 100\,\mathrm{mm}$, $h = 10\,\mathrm{mm}$, $w = 1\,\mathrm{mm}$, $x_\mathrm{a} = 83.3\,\mathrm{mm}$, and $x_{\mathrm{s}} = 21.1\,\mathrm{mm}$. The transmissibility from x_{a} to x_{s} for the force-driven beam is given by

$$
\begin{aligned}
\mathcal{T}^{\mathrm{F}}_{v^{\mathrm{T}}(x_{\mathrm{s}},r),v^{\mathrm{T}}(x_{\mathrm{a}},r)|v(x_{\mathrm{a}})} &= \frac{v^{\mathrm{T}}(x_{\mathrm{s}},r)\mathrm{adj}(\mathbf{p}^2\hat{M}+\hat{K})v(x_{\mathrm{a}})}{v^{\mathrm{T}}(x_{\mathrm{a}},r)\mathrm{adj}(\mathbf{p}^2\hat{M}+\hat{K})v(x_{\mathrm{a}})} \\
&= \frac{\mathbf{p}^6 + 156.4\mathbf{p}^4 - 1.814\times 10^4\mathbf{p}^2 + 3.454\times 10^6}{63.38\mathbf{p}^6 + 1.426\times 10^4\mathbf{p}^4 + 8.057\times 10^5\mathbf{p}^2 + 9.591\times 10^6},
\end{aligned}
\tag{5.115}
$$

where $v^{\mathrm{T}}(x_{\mathrm{s}},r)$ and $v^{\mathrm{T}}(x_{\mathrm{a}},r)$ denote $v^{\mathrm{T}}(x_{\mathrm{s}})$ and $v^{\mathrm{T}}(x_{\mathrm{a}})$, respectively, after setting the r^{th} component of $v^{\mathrm{T}}(x_{\mathrm{s}},r)$ and $v^{\mathrm{T}}(x_{\mathrm{a}},r)$ to zero as suggested by Theorem 5. Next, with a prescribed motion at x_{a}, the transmissibility from x_{a} to x_{s} is given by

$$
\begin{aligned}
\mathcal{T}^{\mathrm{D}}_{v^{\mathrm{T}}(x_{\mathrm{s}},r),v^{\mathrm{T}}(x_{\mathrm{a}},r)|v^{\mathrm{T}}(x_{\mathrm{a}},r)} &= \frac{v^{\mathrm{T}}(x_{\mathrm{s}},r)I_{[r,\cdot]}\mathrm{adj}(\mathbf{p}^2\hat{M}_{[r,r]}+\hat{K}_{[r,r]})K_{[r,\cdot]}e^{\mathrm{T}}_{r,r}}{v^{\mathrm{T}}(x_{\mathrm{a}},r)I_{[r,\cdot]}\mathrm{adj}(\mathbf{p}^2\hat{M}_{[r,r]}+\hat{K}_{[r,r]})K_{[r,\cdot]}e^{\mathrm{T}}_{r,r}} \\
&= \frac{\mathbf{p}^6 + 156.4\mathbf{p}^4 - 1.814\times 10^4\mathbf{p}^2 + 3.454\times 10^6}{63.38\mathbf{p}^6 + 1.426\times 10^4\mathbf{p}^4 + 8.057\times 10^5\mathbf{p}^2 + 9.591\times 10^6},
\end{aligned}
$$

which is equivalent to (5.115). ■

Example 5.8.3. Consider the mass-spring system shown in Figure 5.1, where $m_1 = m_2 = m_3 = m_4 = m_5 = m_6 = 1$ kg and $k_{01} = k_{12} = k_{14} = k_{15} = k_{23} = k_{36} = k_{45} = k_{46} = 1$ N/m. We force-drive m_2 and m_3 and consider the transmissibility from $[q_1\ q_4]^{\mathrm{T}}$ to $[q_5\ q_6]^{\mathrm{T}}$. Then we displacement-drive m_2 and m_3 and consider the transmissibility from $[q_1\ q_4]^{\mathrm{T}}$ to $[q_5\ q_6]^{\mathrm{T}}$. Note that $D = \{2,3\}$, $M = I_6$, $M_{[D,D]} = I_4$,

$W_{\rm o} = [e_{5,6}\ e_{6,6}]^{\rm T}$, and $W_{\rm i} = [e_{1,6}\ e_{4,6}]^{\rm T}$. Hence, we have

$$K = \begin{bmatrix} 4 & -1 & 0 & -1 & -1 & 0 \\ -1 & 2 & -1 & 0 & 0 & 0 \\ 0 & -1 & 2 & 0 & 0 & -1 \\ -1 & 0 & 0 & 3 & -1 & -1 \\ -1 & 0 & 0 & -1 & 2 & 0 \\ 0 & 0 & -1 & -1 & 0 & 2 \end{bmatrix}, \quad K_{[D,D]} = \begin{bmatrix} 4 & -1 & -1 & 0 \\ -1 & 3 & -1 & -1 \\ -1 & -1 & 2 & 0 \\ 0 & -1 & 0 & 2 \end{bmatrix}. \quad (5.116)$$

It follows that

$$\begin{aligned}&\operatorname{adj}\left(\mathbf{p}^2 M + K\right)[e_{2,6}\ e_{3,6}] \\ &= \begin{bmatrix} \mathbf{p}^8 + 9\mathbf{p}^6 + 27\mathbf{p}^4 + 32\mathbf{p}^2 + 14 & \mathbf{p}^6 + 8\mathbf{p}^4 + 19\mathbf{p}^2 + 14 \\ \mathbf{p}^{10} + 13\mathbf{p}^8 + 61\mathbf{p}^6 + 124\mathbf{p}^4 + 102\mathbf{p}^2 + 25 & \mathbf{p}^8 + 11\mathbf{p}^6 + 40\mathbf{p}^4 + 54\mathbf{p}^2 + 22 \\ \mathbf{p}^8 + 11\mathbf{p}^6 + 40\mathbf{p}^4 + 54\mathbf{p}^2 + 22 & \mathbf{p}^{10} + 13\mathbf{p}^8 + 61\mathbf{p}^6 + 126\mathbf{p}^4 + 111\mathbf{p}^2 + 30 \\ \mathbf{p}^6 + 8\mathbf{p}^4 + 21\mathbf{p}^2 + 16 & \mathbf{p}^6 + 9\mathbf{p}^4 + 23\mathbf{p}^2 + 18 \\ \mathbf{p}^6 + 8\mathbf{p}^4 + 19\mathbf{p}^2 + 15 & 2\mathbf{p}^4 + 13\mathbf{p}^2 + 16 \\ \mathbf{p}^6 + 10\mathbf{p}^4 + 28\mathbf{p}^2 + 19 & \mathbf{p}^8 + 11\mathbf{p}^6 + 40\mathbf{p}^4 + 55\mathbf{p}^2 + 24 \end{bmatrix}.\end{aligned} \quad (5.117)$$

Using (5.39) and (5.40) we have

$$\begin{aligned}\Gamma_{\rm i}(\mathbf{p}) &= W_{\rm i}\operatorname{adj}\left(\mathbf{p}^2 M + K\right)[e_{2,6}\ e_{3,6}] \\ &= \begin{bmatrix} \mathbf{p}^8 + 9\mathbf{p}^6 + 27\mathbf{p}^4 + 32\mathbf{p}^2 + 14 & \mathbf{p}^6 + 8\mathbf{p}^4 + 19\mathbf{p}^2 + 14 \\ \mathbf{p}^6 + 8\mathbf{p}^4 + 21\mathbf{p}^2 + 16 & \mathbf{p}^6 + 9\mathbf{p}^4 + 23\mathbf{p}^2 + 18 \end{bmatrix}, \quad (5.118) \\ \Gamma_{\rm o}(\mathbf{p}) &= W_{\rm o}\operatorname{adj}\left(\mathbf{p}^2 M + K\right)[e_{2,6}\ e_{3,6}] \\ &= \begin{bmatrix} \mathbf{p}^6 + 8\mathbf{p}^4 + 19\mathbf{p}^2 + 15 & 2\mathbf{p}^4 + 13\mathbf{p}^2 + 16 \\ \mathbf{p}^6 + 10\mathbf{p}^4 + 28\mathbf{p}^2 + 19 & \mathbf{p}^8 + 11\mathbf{p}^6 + 40\mathbf{p}^4 + 55\mathbf{p}^2 + 24 \end{bmatrix}. \quad (5.119)\end{aligned}$$

Moreover,

$$\begin{aligned}
&\operatorname{adj}\left(\mathbf{p}^2 M_{[D,D]} + K_{[D,D]}\right) K_{[D,\cdot]}[e_{2,6}\ e_{3,6}] \\
&\qquad = -\begin{bmatrix} \mathbf{p}^6 + 7\mathbf{p}^4 + 14\mathbf{p}^2 + 8 & \mathbf{p}^2 + 3 \\ \mathbf{p}^4 + 5\mathbf{p}^2 + 6 & \mathbf{p}^4 + 6\mathbf{p}^2 + 7 \\ \mathbf{p}^4 + 6\mathbf{p}^2 + 7 & \mathbf{p}^2 + 5 \\ \mathbf{p}^2 + 3 & \mathbf{p}^6 + 9\mathbf{p}^4 + 23\mathbf{p}^2 + 13 \end{bmatrix}.
\end{aligned} \tag{5.120}$$

It follows from (5.80) and (5.81) that

$$\begin{aligned}
\Gamma_{\mathrm{i,d}} &= -W_{\mathrm{i}} I_{[\cdot,D]} \operatorname{adj}\left(\mathbf{p}^2 M_{[D,D]} + K_{[D,D]}\right) K_{[D,\cdot]}[e_{2,6}\ e_{3,6}] \\
&= \begin{bmatrix} \mathbf{p}^6 + 7\mathbf{p}^4 + 14\mathbf{p}^2 + 8 & \mathbf{p}^2 + 3 \\ \mathbf{p}^4 + 5\mathbf{p}^2 + 6 & \mathbf{p}^4 + 6\mathbf{p}^2 + 7 \end{bmatrix}, \\
\Gamma_{\mathrm{o,d}} &= -W_{\mathrm{o}} I_{[\cdot,D]} \operatorname{adj}\left(\mathbf{p}^2 M_{[D,D]} + K_{[D,D]}\right) K_{[D,\cdot]}[e_{2,6}\ e_{3,6}] \\
&= \begin{bmatrix} \mathbf{p}^4 + 6\mathbf{p}^2 + 7 & \mathbf{p}^2 + 5 \\ \mathbf{p}^2 + 3 & \mathbf{p}^6 + 9\mathbf{p}^4 + 23\mathbf{p}^2 + 13 \end{bmatrix}.
\end{aligned} \tag{5.121}$$

Therefore,

$$\begin{aligned}
\det \Gamma_{\mathrm{i,d}}(\mathbf{p}) \Gamma_{\mathrm{o}}(\mathbf{p}) \operatorname{adj} \Gamma_{\mathrm{i}}(\mathbf{p}) &= \left(\mathbf{p}^{10} + 13\mathbf{p}^8 + 62\mathbf{p}^6 + 133\mathbf{p}^4 + 125\mathbf{p}^2 + 38\right) \\
&\quad \cdot \begin{bmatrix} \mathbf{p}^6 + 8\mathbf{p}^4 + 19\mathbf{p}^2 + 15 & 2\mathbf{p}^4 + 13\mathbf{p}^2 + 16 \\ \mathbf{p}^6 + 10\mathbf{p}^4 + 28\mathbf{p}^2 + 19 & \mathbf{p}^8 + 11\mathbf{p}^6 + 40\mathbf{p}^4 + 55\mathbf{p}^2 + 24 \end{bmatrix} \\
&\quad \cdot \begin{bmatrix} \mathbf{p}^6 + 9\mathbf{p}^4 + 23\mathbf{p}^2 + 18 & -\mathbf{p}^6 - 8\mathbf{p}^4 - 19\mathbf{p}^2 - 14 \\ -\mathbf{p}^6 - 8\mathbf{p}^4 - 21\mathbf{p}^2 - 16 & \mathbf{p}^8 + 9\mathbf{p}^6 + 27\mathbf{p}^4 + 32\mathbf{p}^2 + 14 \end{bmatrix} \\
&= \begin{bmatrix} A_{1,1}(\mathbf{p}) & A_{1,2}(\mathbf{p}) \\ A_{2,1}(\mathbf{p}) & A_{2,2}(\mathbf{p}) \end{bmatrix},
\end{aligned} \tag{5.122}$$

where

$$A_{1,1}(\mathbf{p}) = \mathbf{p}^{22} + 28\mathbf{p}^{20} + 342\mathbf{p}^{18} + 2394\mathbf{p}^{16} + 10611\mathbf{p}^{14} + 31052\mathbf{p}^{12} + 60672\mathbf{p}^{10} + 78167\mathbf{p}^{8} + 63850\mathbf{p}^{6} + 30491\mathbf{p}^{4} + 7184\mathbf{p}^{2} + 532, \tag{5.123}$$

$$A_{1,2}(\mathbf{p}) = A_{1,1}(\mathbf{p}), \tag{5.124}$$

$$A_{2,1}(\mathbf{p}) = -\mathbf{p}^{24} - 31\mathbf{p}^{22} - 426\mathbf{p}^{20} - 3420\mathbf{p}^{18} - 17793\mathbf{p}^{16} - 62885\mathbf{p}^{14} - 153828\mathbf{p}^{12} - 260183\mathbf{p}^{10} - 298351\mathbf{p}^{8} - 222041\mathbf{p}^{6} - 98657\mathbf{p}^{4} - 22084\mathbf{p}^{2} - 1596, \tag{5.125}$$

$$A_{2,2}(\mathbf{p}) = \mathbf{p}^{26} + 33\mathbf{p}^{24} + 487\mathbf{p}^{22} + 4244\mathbf{p}^{20} + 24291\mathbf{p}^{18} + 96077\mathbf{p}^{16} + 268987\mathbf{p}^{14} + 536787\mathbf{p}^{12} + 758045\mathbf{p}^{10} + 740576\mathbf{p}^{8} + 478889\mathbf{p}^{6} + 188907\mathbf{p}^{4} + 38580\mathbf{p}^{2} + 2660. \tag{5.126}$$

Moreover,

$$\begin{aligned}
&\det \Gamma_{\mathrm{i}}(\mathbf{p})\Gamma_{\mathrm{o,d}}(\mathbf{p})\mathrm{adj}\,\Gamma_{\mathrm{i,d}}(\mathbf{p}) \\
&= \left(\mathbf{p}^{14} + 17\mathbf{p}^{12} + 115\mathbf{p}^{10} + 396\mathbf{p}^{8} + 735\mathbf{p}^{6} + 709\mathbf{p}^{4} + 300\mathbf{p}^{2} + 28\right) \\
&\cdot \begin{bmatrix} \mathbf{p}^4 + 6\mathbf{p}^2 + 7 & \mathbf{p}^2 + 5 \\ \mathbf{p}^2 + 3 & \mathbf{p}^6 + 9\mathbf{p}^4 + 23\mathbf{p}^2 + 13 \end{bmatrix} \begin{bmatrix} \mathbf{p}^4 + 6\mathbf{p}^2 + 7 & -\mathbf{p}^2 - 3 \\ -\mathbf{p}^4 - 5\mathbf{p}^2 - 6 & \mathbf{p}^6 + 7\mathbf{p}^4 + 14\mathbf{p}^2 + 8 \end{bmatrix} \\
&= \begin{bmatrix} A_{\mathrm{d},1,1}(\mathbf{p}) & A_{\mathrm{d},1,2}(\mathbf{p}) \\ A_{\mathrm{d},2,1}(\mathbf{p}) & A_{\mathrm{d},2,2}(\mathbf{p}) \end{bmatrix},
\end{aligned} \tag{5.127}$$

where

$$A_{\mathrm{d},1,1}(\mathbf{p}) = \mathbf{p}^{22} + 28\mathbf{p}^{20} + 342\mathbf{p}^{18} + 2394\mathbf{p}^{16} + 10611\mathbf{p}^{14} + 31052\mathbf{p}^{12} + 60672\mathbf{p}^{10} + 78167\mathbf{p}^{8} + 63850\mathbf{p}^{6} + 30491\mathbf{p}^{4} + 7184\mathbf{p}^{2} + 532, \tag{5.128}$$

$$A_{\mathrm{d},1,2}(\mathbf{p}) = A_{\mathrm{d},1,1}(\mathbf{p}), \tag{5.129}$$

$$A_{\mathrm{d},2,1}(\mathbf{p}) = -\mathbf{p}^{24} - 31\mathbf{p}^{22} - 426\mathbf{p}^{20} - 3420\mathbf{p}^{18} - 17793\mathbf{p}^{16} - 62885\mathbf{p}^{14} - 153828\mathbf{p}^{12} - 260183\mathbf{p}^{10} - 298351\mathbf{p}^{8} - 222041\mathbf{p}^{6} - 98657\mathbf{p}^{4} - 22084\mathbf{p}^{2} - 1596, \tag{5.130}$$

$$A_{\mathrm{d},2,2}(\mathbf{p}) = \mathbf{p}^{26} + 33\mathbf{p}^{24} + 487\mathbf{p}^{22} + 4244\mathbf{p}^{20} + 24291\mathbf{p}^{18} + 96077\mathbf{p}^{16} + 268987\mathbf{p}^{14} + 536787\mathbf{p}^{12} + 758045\mathbf{p}^{10} + 740576\mathbf{p}^{8} + 478889\mathbf{p}^{6} + 188907\mathbf{p}^{4} + 38580\mathbf{p}^{2} + 2660. \tag{5.131}$$

Comparing (5.123), (5.124), (5.125), and (5.126) with (5.128), (5.129), (5.130), and (5.131), respectively, yields,

$$A_{1,1} = A_{\mathrm{d},1,1}, \quad A_{1,2} = A_{\mathrm{d},1,2}, \quad A_{2,1} = A_{\mathrm{d},2,1}, \quad A_{2,2} = A_{\mathrm{d},2,2}. \tag{5.132}$$

Therefore, it follows from (5.122) and (5.127) that

$$\det \Gamma_{\mathrm{i,d}}(\mathbf{p})\Gamma_{\mathrm{o}}(\mathbf{p})\mathrm{adj}\,\Gamma_{\mathrm{i}}(\mathbf{p}) = \det \Gamma_{\mathrm{i}}(\mathbf{p})\Gamma_{\mathrm{o,d}}(\mathbf{p})\mathrm{adj}\,\Gamma_{\mathrm{i,d}}(\mathbf{p}). \tag{5.133}$$

That is,

$$\mathcal{T}^{\mathrm{F}}_{W_{\mathrm{o}},W_{\mathrm{i}}|e_{D,n}}(\mathbf{p}) = \mathcal{T}^{\mathrm{D}}_{W_{\mathrm{o}},W_{\mathrm{i}}|e_{D,n}}(\mathbf{p}), \tag{5.134}$$

which confirms Theorem 6.

5.9 Conclusions

We developed a time-domain framework for SISO and MIMO transmissibilities that accounts for nonzero initial conditions for both force-driven and displacement-driven structures. It was shown that if the locations of the forces and prescribed displacements are identical, then the SISO and MIMO force- and displacement-driven transmissibilities are equal. Numerical examples for a mass-spring system and a simply supported beam were presented to illustrate the equality of transmissibilities in force-driven and displacement-driven structures.

The time-domain transmissibility models developed in this chapter are intended to facilitate the use of time-domain identification methods. Preliminary results in this direction are given in [1, 28, 29].

CHAPTER 6

Sensor-to-Sensor Identification of Hammerstein Systems

6.1 Introduction

The usefulness of S2SID depends on the ability to estimate a transfer function independently of the details of the excitation signal. This ability depends on the fact that the input signal is cancelled in the construction of the PTF. As expected, however, this cancellation does not occur in the case of nonlinear systems, which suggests that S2SID is confined to linear systems. However, in the present chapter we consider the case of a Hammerstein system, and we estimate the Markov parameters of a *linear* PTF between the pseudo input and pseudo output despite the fact that these signals are not linearly related. Under these conditions we show that, despite the presence of the input nonlinearities, the estimates of the Markov parameters of the identified PTF are semi-consistent, that is, up to a uniform scale factor, they are asymptotically correct estimates of the Markov parameters of the corresponding PTF of the system in the absence of the input nonlinearities. This statement holds for the case in which both input nonlinearities are nonzero, but otherwise arbitrary.

The contents of the chapter are as follows. In Section 6.2, we formulate the problem. In section 6.3, we define the identification architecture. In section 6.4

we analyze the consistency of the Markov parameters obtained from the proposed method. In section 6.5 we show the numerical examples. We give conclusions in section 6.6.

6.2 Problem Formulation

Consider the block diagram shown in Figure 6.1, where u is the input, $\mathcal{N}_1 : \mathbb{R} \to \mathbb{R}$ and $\mathcal{N}_2 : \mathbb{R} \to \mathbb{R}$ are memoryless nonlinearities, $\mathcal{N}_1(u)$ and $\mathcal{N}_2(u)$ are the intermediate signals, and y_1 and y_2 are the output signals of the asymptotically stable, SISO, linear, time-invariant, causal, discrete-time systems G_1 of order n_1 and G_2 of order n_2, respectively.

Since the input u is not measured, it is not possible to identify the SISO Hammerstein systems $(\mathcal{N}_1, G_1)$ and $(\mathcal{N}_2, G_2)$. Furthermore, because of the presence of the nonlinearities $\mathcal{N}_1$ and $\mathcal{N}_2$, the relationship between y_1 and y_2 is not linear. Nevertheless, for reasons explained in subsequent sections, we identify a linear model whose input and output are the signals y_1 and y_2, respectively, see Figure 6.2. This linear

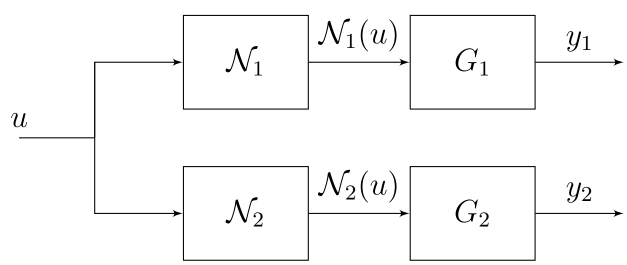

Figure 6.1: SIMO Hammerstein system, $\mathcal{N}_1$ and $\mathcal{N}_2$ represent memoryless nonlinearities, and y_1 and y_2 represent outputs of the linear transfer functions G_1 and G_2, respectively.

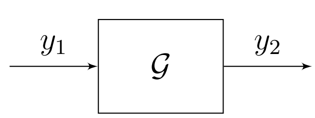

Figure 6.2: The pseudo-transfer function $\mathcal{G}$ is a linear model that is identified based on the input and output signals y_1 and y_2, respectively. This identification does not assume that the relationship between y_1 and y_2 is linear.

model has the form

$$\mathcal{G}(\mathbf{q}) = \frac{B(\mathbf{q})}{A(\mathbf{q})}, \tag{6.1}$$

where $\mathcal{G}$ is the PTF, $\mathbf{q}$ is the forward shift operator, and A and B are polynomials in $\mathbf{q}$. For simplicity, we assume that $\mathcal{G}$ is a finite impulse response (FIR) model, and thus $A(\mathbf{q}) = \mathbf{q}^\mu$ and $B(\mathbf{q}) = \sum_{i=0}^{\mu} H_i \mathbf{q}^i$, where μ is the model order. Consequently, the FIR PTF model $\mathcal{G}$ that relates the pseudo input y_1 to the pseudo output y_2 has the form

$$y_2(k) = \sum_{j=0}^{\mu} H_j y_1(k-j), \tag{6.2}$$

where $H_0, \ldots, H_{\mu-1}$ are the Markov parameters of (6.1).

In order for the PTF to be causal, the relative degree of G_2 must be greater than or equal to the relative degree of G_1. If this is not the case then we delay the pseudo output y_2 as needed.

6.3 Least Squares Identification of the PTF

The FIR model (6.2) can be expressed as

$$y_2(k) = \theta_\mu \phi_\mu(k), \tag{6.3}$$

where

$$\begin{aligned} \theta_\mu &\triangleq \begin{bmatrix} H_0 & \cdots & H_{\mu-1} \end{bmatrix}, \\ \phi_\mu(k) &\triangleq \begin{bmatrix} y_1(k) & \cdots & y_1(k-\mu+1) \end{bmatrix}^{\mathrm{T}}. \end{aligned}$$

The least squares estimate $\hat{\theta}_{\mu,\ell}$ of θ_μ is given by

$$\hat{\theta}_{\mu,\ell} = \arg\min_{\bar{\theta}_\mu} \left\| \Psi_{y_2,\ell} - \bar{\theta}_\mu \Phi_{\mu,\ell} \right\|_{\mathrm{F}}, \tag{6.4}$$

where $\bar{\theta}_\mu$ is a variable of appropriate size, $||\,.\,||_{\mathrm{F}}$ denotes the Frobenius norm,

$$\Psi_{y_2,\ell} \triangleq \begin{bmatrix} y_2(\mu) & \cdots & y_2(\ell) \end{bmatrix},$$
$$\Phi_{\mu,\ell} \triangleq \begin{bmatrix} \phi_\mu(\mu) & \cdots & \phi_\mu(\ell) \end{bmatrix},$$

and ℓ is the number of samples. It follows from (6.4) that

$$\Psi_{y_2,\ell}\Phi_{\mu,\ell}^{\mathrm{T}} = \hat{\theta}_{\mu,\ell}\Phi_{\mu,\ell}\Phi_{\mu,\ell}^{\mathrm{T}}. \tag{6.5}$$

Next, consider the system in Figure 6.3, which represents the system in Figure 6.1 without the Hammerstein nonlinearities $\mathcal{N}_1$ and $\mathcal{N}_2$. Note that y_1' and y_2' represent the outputs of G_1 and G_2, respectively.

Define $H_0', \ldots, H_{\mu-1}'$ to be Markov parameters of the PTF $\mathcal{G}'$ constructed by y_1' and y_2', see Figure 6.4. It follows that

$$\Psi_{y_2',\ell} = \theta_\mu' \Phi_{\mu,\ell}', \tag{6.6}$$

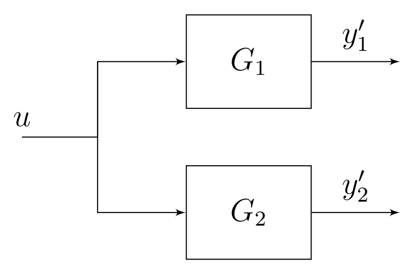

Figure 6.3: y_1' and y_2' are the outputs of the linear transfer functions G_1 and G_2, respectively, with input u. This system does not exist and is used only for analysis

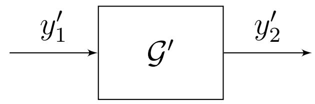

Figure 6.4: The pseudo-transfer function $\mathcal{G}'$ is a linear model that is identified based on the input and output signals y'_1 and y'_2, respectively.

where

$$
\begin{aligned}
\Psi_{y'_2,\ell} &\triangleq \begin{bmatrix} y'_2(\mu) & \cdots & y'_2(\ell) \end{bmatrix}, \qquad (6.7)\\
\theta'_\mu &\triangleq \begin{bmatrix} H'_0 & \cdots & H'_{\mu-1} \end{bmatrix}, \qquad (6.8)\\
\Phi'_{\mu,\ell} &\triangleq \begin{bmatrix} \phi'_\mu(\mu) & \ldots & \phi'_\mu(\ell) \end{bmatrix}, \qquad (6.9)\\
\phi'_\mu(k) &\triangleq \begin{bmatrix} y'_1(k) & \cdots & y'_1(k-\mu+1) \end{bmatrix}^{\mathrm{T}}. \qquad (6.10)
\end{aligned}
$$

Although the PTF $\mathcal{G}'$ is unknown and cannot be identified, the goal is to compare the Markov parameters of the identified FIR PTF $\mathcal{G}$ relating y_1 and y_2 to the Markov parameters of the PTF $\mathcal{G}'$ relating y'_1 to y'_2.

6.4 Consistency Analysis

Assumption 1. u is a realization of a stationary white random process U, and y_1, y_2, y'_1, and y'_2 are realizations of stationary random processes Y_1, Y_2, Y'_1, and Y'_2, respectively.

Assumption 2. For all $k \geq 0$, $\mathcal{N}_1\big(U(k)\big)$, $\mathcal{N}_2\big(U(k)\big)$, $\mathcal{N}_1^2\big(U(k)\big)$, and $\mathcal{N}_1\big(U(k)\big)\mathcal{N}_2\big(U(k)\big)$ have finite mean and variance.

Assumption 3. For all $k \geq 0$, $\mathbb{E}\Big[\mathcal{N}_1\Big(U(k)\Big)\Big] = 0$, $\mathbb{E}\Big[\mathcal{N}_1\Big(U(k)\Big)\mathcal{N}_2\Big(U(k)\Big)\Big] \neq 0$, and $\mathbb{E}\Big[\mathcal{N}_1^2\Big(U(k)\Big)\Big] \neq 0$.

Assumption 4. θ_μ is not zero.

Definition 10. The least squares estimator $\hat{\theta}_{\mu,\ell}$ of θ_μ is a *semi-consistent* estimator of θ'_μ if there exists nonzero $\gamma \in \mathbb{R}$ such that

$$\lim_{\ell\to\infty} \hat{\theta}_{\mu,\ell} \overset{\text{wp1}}{=} \gamma\theta'_\mu.$$

Theorem 7. Let assumptions 1-4 hold. Then $\hat{\theta}_{\mu,\ell}$ is a semi-consistent estimator of θ'_μ.

Proof. Note that,

$$y'_1(k) = \big(u * h_1\big)(k) = \sum_{i=-\infty}^{k} u(i)h_1(k-i), \tag{6.11}$$

$$y'_2(k) = \big(u * h_2\big)(k) = \sum_{i=-\infty}^{k} u(i)h_2(k-i), \tag{6.12}$$

$$y_1(k) = \Big(\mathcal{N}_1\big(u\big) * h_1\Big)(k) = \sum_{i=-\infty}^{k} \mathcal{N}_1\big(u(i)\big)h_1(k-i), \tag{6.13}$$

$$y_2(k) = \Big(\mathcal{N}_2\big(u\big) * h_2\Big)(k) = \sum_{i=-\infty}^{k} \mathcal{N}_2\big(u(i)\big)h_2(k-i), \tag{6.14}$$

where h_1 and h_2 are the impulse response sequences of G_1 and G_2, respectively. Furthermore,

$$y_2(k) = \frac{\alpha(k)}{\beta(k)} y'_2(k), \tag{6.15}$$

where

$$\alpha(k) \triangleq \Big(\mathcal{N}_2(u) * h_2\Big)(k),$$
$$\beta(k) \triangleq \big(u * h_2\big)(k).$$

Therefore,

$$\begin{aligned} \Psi_{y_2,\ell} &= \left[\begin{array}{ccc} \frac{\alpha(\mu)}{\beta(\mu)} y_2'(\mu) & \dots & \frac{\alpha(\ell)}{\beta(\ell)} y_2'(\ell) \end{array} \right] \\ &= \Psi_{y_2',\ell} A_\ell, \end{aligned} \tag{6.16}$$

where

$$A_\ell \triangleq \begin{bmatrix} \frac{\alpha(\mu)}{\beta(\mu)} & & 0 \\ & \ddots & \\ 0 & & \frac{\alpha(\ell)}{\beta(\ell)} \end{bmatrix}. \tag{6.17}$$

Therefore, (6.6) and (6.16) imply that

$$\Psi_{y_2,\ell} = \theta_\mu' \Phi_{\mu,\ell}' A_\ell. \tag{6.18}$$

It follows from (6.5) and (6.18) that $\hat{\theta}_{\mu,\ell}$ satisfies

$$\theta_\mu' \Phi_{\mu,\ell}' A_\ell \Phi_{\mu,\ell}^{\mathrm{T}} = \hat{\theta}_{\mu,\ell} \Phi_{\mu,\ell} \Phi_{\mu,\ell}^{\mathrm{T}}. \tag{6.19}$$

Note that,

$$
\begin{aligned}
&\Phi'_{\mu,\ell} A_\ell \Phi^{\mathrm{T}}_{\mu,\ell} \\
&= \begin{bmatrix} y'_1(\mu) & \cdots & y'_1(\ell) \\ \vdots & & \vdots \\ y'_1(1) & \cdots & y'_1(\ell-\mu+1) \end{bmatrix}
\begin{bmatrix} \frac{y_2(\mu)}{y'_2(\mu)} & & 0 \\ & \ddots & \\ 0 & & \frac{y_2(\ell)}{y'_2(\ell)} \end{bmatrix}
\begin{bmatrix} y_1(\mu) & \cdots & y_1(\ell) \\ \vdots & & \vdots \\ y_1(1) & \cdots & y_1(\ell-\mu+1) \end{bmatrix}^{\mathrm{T}} \\
&= \begin{bmatrix} \displaystyle\sum_{i=\mu}^{\ell} \frac{y'_1(i) y_2(i) y_1(i)}{y'_2(i)} & \cdots & \displaystyle\sum_{i=\mu}^{\ell} \frac{y'_1(i) y_2(i) y_1(i-\mu+1)}{y'_2(i)} \\ \vdots & \ddots & \vdots \\ \displaystyle\sum_{i=\mu}^{\ell} \frac{y'_1(i-\mu+1) y_2(i) y_1(i)}{y'_2(i)} & \cdots & \displaystyle\sum_{i=\mu}^{\ell} \frac{y'_1(i-\mu+1) y_2(i) y_1(i-\mu+1)}{y'_2(i)} \end{bmatrix}.
\end{aligned} \tag{6.20}
$$

Since Y_1, Y_2, Y'_1, and Y'_2 are stationary random processes, it follows that for all $k \geq 0$ we can calculate

$$
\lim_{\ell\to\infty} \frac{1}{\ell} \Phi'_{\mu,\ell} A_\ell \Phi^{\mathrm{T}}_{\mu,\ell} \overset{\mathrm{wp1}}{=} \mathbb{E} \begin{bmatrix} \frac{Y'_1(k) Y_2(k) Y_1(k)}{Y'_2(k)} & \cdots & \frac{Y'_1(k) Y_2(k) Y_1(k-\mu+1)}{Y'_2(k)} \\ \vdots & \ddots & \vdots \\ \frac{Y'_1(k-\mu+1) Y_2(k) Y_1(k)}{Y'_2(k)} & \cdots & \frac{Y'_1(k-\mu+1) Y_2(k) Y_1(k-\mu+1)}{Y'_2(k)} \end{bmatrix}, \tag{6.21}
$$

where (6.21) is independent of k. Moreover, note that,

$$
\begin{aligned}
&\mathbb{E}\left[\frac{Y_1'(k)Y_2(k)Y_1(k)}{Y_2'(k)}\right] \\
&= \mathbb{E}\left[\frac{\sum_{i=-\infty}^{k} U(i)h_1(k-i) \sum_{j=-\infty}^{k} \mathcal{N}_2\big(U(j)\big)h_2(k-j) \sum_{r=-\infty}^{k} \mathcal{N}_1\big(U(r)\big)h_1(k-r)}{\sum_{q=-\infty}^{k} U(q)h_2(k-q)}\right] \\
&= \mathbb{E}\left[\frac{\sum_{i=-\infty}^{k}\sum_{j=-\infty}^{k}\sum_{r=-\infty}^{k} U(i)\mathcal{N}_2\big(U(j)\big)\mathcal{N}_1\big(U(r)\big)h_1(k-i)h_2(k-j)h_1(k-r)}{\sum_{q=-\infty}^{k} U(q)h_2(k-q)}\right].
\end{aligned} \tag{6.22}
$$

Since U is a stationary white random process and $\mathcal{N}_2$ and $\mathcal{N}_1$ are memoryless nonlinearities, it follows that the expectation in (6.22) is nonzero when the arguments i, j, and r are equal and zero otherwise. Therefore, (6.22) can be also written as

$$
\begin{aligned}
&\mathbb{E}\left[\frac{Y_1'(k)Y_2(k)Y_1(k)}{Y_2'(k)}\right] \\
&= \mathbb{E}\left[\frac{\sum_{i=-\infty}^{k} U(i)h_2(k-i) \sum_{j=-\infty}^{k}\sum_{r=-\infty}^{k} \mathcal{N}_2\big(U(j)\big)\mathcal{N}_1\big(U(r)\big)h_1(k-j)h_1(k-r)}{\sum_{q=-\infty}^{k} U(q)h_2(k-q)}\right] \\
&= \mathbb{E}\left[\sum_{j=-\infty}^{k}\sum_{r=-\infty}^{k} \mathcal{N}_2\big(U(j)\big)\mathcal{N}_1\big(U(r)\big)h_1(k-j)h_1(k-r)\right] \\
&= \sum_{j=-\infty}^{k}\sum_{r=-\infty}^{k} \mathbb{E}\left[\mathcal{N}_2\big(U(j)\big)\mathcal{N}_1\big(U(r)\big)\right] h_1(k-j)h_1(k-r) \\
&= \sum_{j=-\infty}^{k} \mathbb{E}\left[\mathcal{N}_2\big(U(k)\big)\mathcal{N}_1\big(U(k)\big)\right] h_1^2(k-j).
\end{aligned} \tag{6.23}
$$

Since $\mathbb{E}\left[\mathcal{N}_2\big(U(k)\big)\mathcal{N}_1\big(U(k)\big)\right]$ is a nonzero constant for all $k \geq 0$ and independent of

j in (6.23), it follows that

$$\mathbb{E}\left[\frac{Y_1'(k)Y_2(k)Y_1(k)}{Y_2'(k)}\right] = \mathbb{E}\left[\mathcal{N}_2\big(U(k)\big)\mathcal{N}_1\big(U(k)\big)\right]\sum_{j=-\infty}^{k} h_1^2(k-j)$$
$$= \mathbb{E}\left[\mathcal{N}_2\big(U(k)\big)\mathcal{N}_1\big(U(k)\big)\right]\sum_{i=0}^{\infty} h_1^2(i), \tag{6.24}$$

for all $k \geq 0$.

Using the same procedure we obtain

$$\lim_{\ell\to\infty}\frac{1}{\ell}\Phi'_{\mu,\ell}A_\ell\Phi^{\mathrm{T}}_{\mu,\ell} \overset{\text{wp1}}{=} \mathbb{E}\left[\mathcal{N}_2\big(U(k)\big)\mathcal{N}_1\big(U(k)\big)\right]\Gamma, \tag{6.25}$$

where

$$\Gamma \triangleq \begin{bmatrix} \sum_{i=0}^{\infty} h_1^2(i) & \cdots & \sum_{i=0}^{\infty} h_1(i)h_1(\mu-1+i) \\ \vdots & \ddots & \vdots \\ \sum_{i=0}^{\infty} h_1(\mu-1+i)h_1(i) & \cdots & \sum_{i=0}^{\infty} h_1^2(i) \end{bmatrix} \in \mathbb{R}^{\mu\times\mu}. \tag{6.26}$$

Likewise,

$$\lim_{\ell\to\infty}\frac{1}{\ell}\Phi_{\mu,\ell}\Phi^{\mathrm{T}}_{\mu,\ell} \overset{\text{wp1}}{=} \mathbb{E}\left[\mathcal{N}_1^2\big(U(k)\big)\right]\Gamma. \tag{6.27}$$

Dividing (6.19) by ℓ and using (6.25) and (6.27) yields

$$\mathbb{E}\left[\mathcal{N}_2\big(U(k)\big)\mathcal{N}_1\big(U(k)\big)\right]\theta'_\mu\Gamma \overset{\text{wp1}}{=} \lim_{\ell\to\infty}\mathbb{E}\left[\mathcal{N}_1^2\big(U(k)\big)\right]\hat{\theta}_{\mu,\ell}\Gamma. \tag{6.28}$$

That is,

$$\Big(\mathbb{E}\left[\mathcal{N}_2\big(U(k)\big)\mathcal{N}_1\big(U(k)\big)\right]\theta'_\mu - \mathbb{E}\left[\mathcal{N}_1^2\big(U(k)\big)\right]\lim_{\ell\to\infty}\hat{\theta}_{\mu,\ell}\Big)\Gamma \overset{\text{wp1}}{=} 0_{1\times\mu}.$$

Since Γ is nonsingular, it follows that

$$\mathbb{E}\left[\mathcal{N}_2\big(U(k)\big)\mathcal{N}_1\big(U(k)\big)\right]\theta'_\mu \overset{\text{wp1}}{=} \mathbb{E}\left[\mathcal{N}_1^2\big(U(k)\big)\right]\lim_{\ell\to\infty}\hat{\theta}_{\mu,\ell}.$$

Finally,

$$\lim_{\ell\to\infty}\hat{\theta}_{\mu,\ell} \overset{\text{wp1}}{=} \frac{\mathbb{E}\left[\mathcal{N}_2\big(U(k)\big)\mathcal{N}_1\big(U(k)\big)\right]}{\mathbb{E}\left[\mathcal{N}_1^2\big(U(k)\big)\right]}\theta'_\mu, \tag{6.29}$$

for all $k \geq 0$. Thus, $\hat{\theta}_{\mu,\ell}$ is a semi-consistent estimator of θ'_μ. □

Example 6.4.1. Let $\mathcal{N}_1(U) = U^3$, $\mathcal{N}_2(U) = U^7$, and let $U(k)$ be uniformly distributed with the density function

$$p(u) = \begin{cases} \frac{1}{2a}, & |u| \leq a, \\ 0, & |u| > a. \end{cases} \tag{6.30}$$

Then,

$$\mathbb{E}\Big[\mathcal{N}_2\Big(U(k)\Big)\mathcal{N}_1\Big(U(k)\Big)\Big] = \frac{1}{2a}\int_{-a}^{a} U^{10}(k)\,dU(k) = a^{10}/11,$$

$$\mathbb{E}\Big[\mathcal{N}_1^2\Big(U(k)\Big)\Big] = \frac{1}{2a}\int_{-a}^{a} U^{6}(k)\,dU = a^{6}/7.$$

Finally, it follows from (6.29) that

$$\lim_{\ell\to\infty}\hat{\theta}_{\mu,\ell} \overset{\text{wp1}}{=} \frac{7a^4}{11}\theta'_\mu.$$

6.5 Numerical Examples

Consider the transfer functions

$$G_1(\mathbf{q}) = \frac{4\mathbf{q}+1}{(\mathbf{q}-0.6)(\mathbf{q}+0.8)(\mathbf{q}-0.9)}, \tag{6.31}$$

$$G_2(\mathbf{q}) = \frac{2\mathbf{q}+5}{(\mathbf{q}-0.55)(\mathbf{q}+0.6)(\mathbf{q}-0.4)}. \tag{6.32}$$

Then, the PTF is

$$\begin{aligned} \mathcal{G}(\mathbf{q}) &= \frac{G_2(\mathbf{q})}{G_1(\mathbf{q})}, \\ &= \frac{(\mathbf{q}-0.6)(\mathbf{q}+0.8)(\mathbf{q}-0.9)(2\mathbf{q}+5)}{(\mathbf{q}-0.55)(\mathbf{q}+0.6)(\mathbf{q}-0.4)(4\mathbf{q}+1)}. \end{aligned} \tag{6.33}$$

It follows from (6.1) that

$$B(\mathbf{q}) = (\mathbf{q}-0.6)(\mathbf{q}+0.8)(\mathbf{q}-0.9)(2\mathbf{q}+5),$$
$$A(\mathbf{q}) = (\mathbf{q}-0.55)(\mathbf{q}+0.6)(\mathbf{q}-0.4)(4\mathbf{q}+1).$$

Define the normalized Markov parameters of the PTF constructed from y_1' and y_2' by

$$H_i'^n \triangleq \frac{H_i'}{H_d'},$$

where H_d' is the first nonzero Markov parameter of the PTF. The estimated Markov parameters $\hat{H}_i$, obtained from $\hat{\theta}_{\mu,\ell}$, are normalized by $\hat{H}_d$ to obtain $\hat{H}_i^n$. The least squares estimates are computed for 200 independent realizations of U. We also define the error metric

$$\varepsilon = \frac{1}{200}\sum_{i=0}^{200}\frac{|H_i'^n - \hat{H}_i^n|}{|H_i'^n|}. \tag{6.34}$$

In the following we show five examples involving both odd, even, and neither odd nor even nonlinearities in both cases of zero mean and nonzero mean for $\mathcal{N}_2(u)$. In example 6.5.2 the term $M(u^2)$ denotes the mean of the realization of the random process U^2 and in example 6.5.5 the term $M(u^2e^u)$ denotes the mean of the realization of the random process U^2e^U.

Example 6.5.1. $\mathcal{N}_1(u) = \text{sign}(u)$, $\mathcal{N}_2(u) = \sin(u)$

Consider the transfer functions G_1 in (6.31) and G_2 in (6.32), and let U be white and have the uniform pdf (6.30) with $a = 5$. Figure 6.5 indicates that the estimates of the Markov parameters H_2, H_3, H_4, and H_5 are semi-consistent.

Example 6.5.2. $\mathcal{N}_1(u) = u^2 - M(u^2)$**,** $\mathcal{N}_2(u) = \cos(u)$

Consider the transfer functions G_1 in (6.31) and G_2 in (6.32), and let U be white and have the Gaussian pdf $N(0,1)$. Figure 6.6 indicates that the estimates of the Markov parameters H_2, H_3, H_4, and H_5 are semi-consistent.

Example 6.5.3. $\mathcal{N}_1(u) = \sinh(u)$, $\mathcal{N}_2(u) = u^3$

Consider the transfer functions G_1 in (6.31) and G_2 in (6.32), and let U be white and have the Gaussian pdf $N(0,1)$. Figure 6.7 indicates that the estimates of the Markov parameters H_2, H_3, H_4, and H_5 are semi-consistent.

Example 6.5.4. $\mathcal{N}_1(u) = \text{sign}(u)$, $\mathcal{N}_2(u) = e^u$

Consider the transfer functions G_1 in (6.31) and G_2 in (6.32), and let U be white and have the uniform pdf (6.30) with $a = 5$. Figure 6.8 indicates that the estimates of the Markov parameters H_2, H_3, H_4, and H_5 are semi-consistent.

Example 6.5.5. $\mathcal{N}_1(u) = u^2e^u - M(u^2e^u)$, $\mathcal{N}_2(u) = \sin(u) + 10$

Consider the transfer functions G_1 in (6.31) and G_2 in (6.32), and let U be white and have the uniform pdf (6.30) with $a = 5$. Figure 6.9 indicates that the estimates of the Markov parameters H_2, H_3, H_4, and H_5 are semi-consistent.

6.6 Conclusions

We used least squares with an FIR model structure to identify a pseudo transfer function for a two-output Hammerstein system. Only output signals of the Hammerstein system were used since the intermediate signals were inaccessible. Despite the presence of the input nonlinearities, we proved that, under certain assumptions, the least squares estimate of the Markov parameters of the PTF is semi-consistent. This method was demonstrated on several numerical examples including odd, even, and neither odd nor even nonlinearities in both cases of zero mean and nonzero mean for the output channel Hammerstein nonlinearity, where the input channel Hammerstein nonlinearity should be of zero mean.

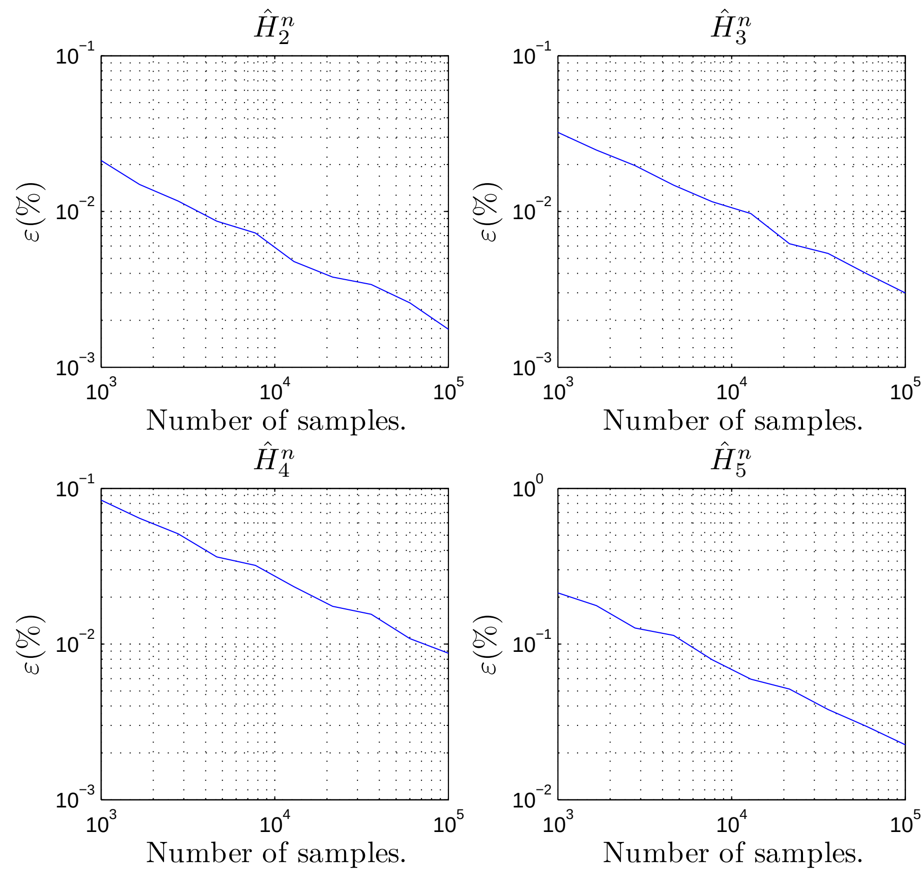

Figure 6.5: Semi-consistency of the estimates of the Markov parameters obtained from the FIR model with the Hammerstein nonlinearities $\mathcal{N}_1(u) = \text{sign}(u)$ and $\mathcal{N}_2(u) = \sin(u)$.

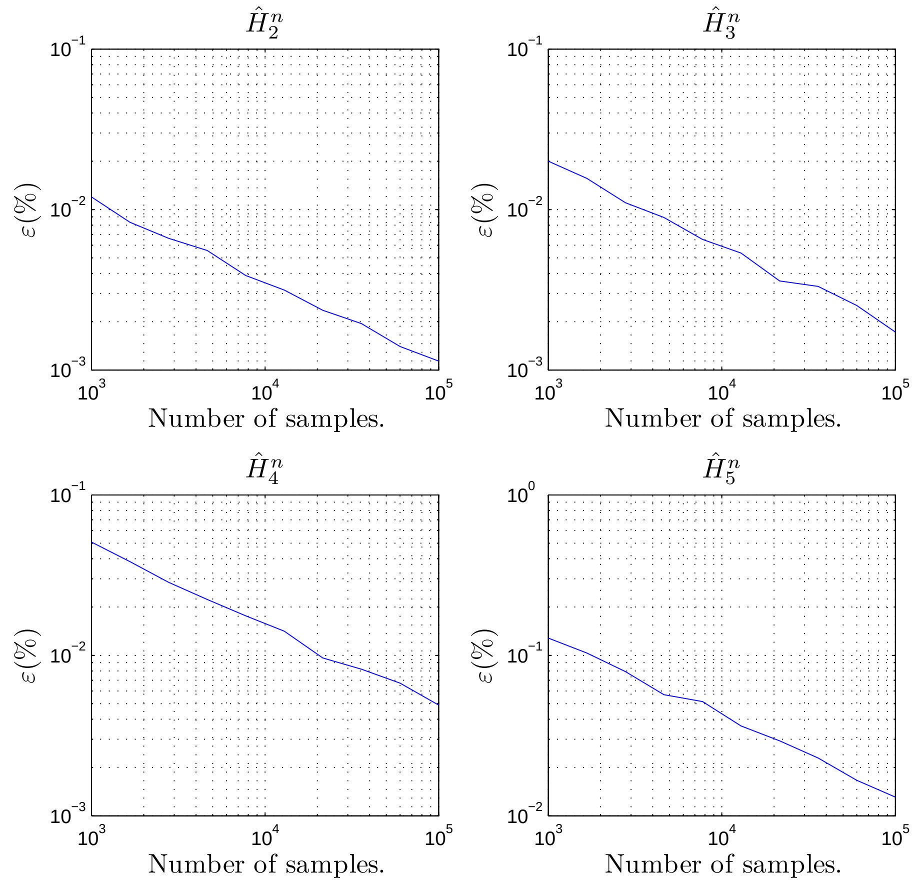

Figure 6.6: Semi-consistency of the estimates of the Markov parameters obtained from the FIR model with the Hammerstein nonlinearities $\mathcal{N}_1(u) = u^2 - M(u^2)$ and $\mathcal{N}_2(u) = \cos(u)$.

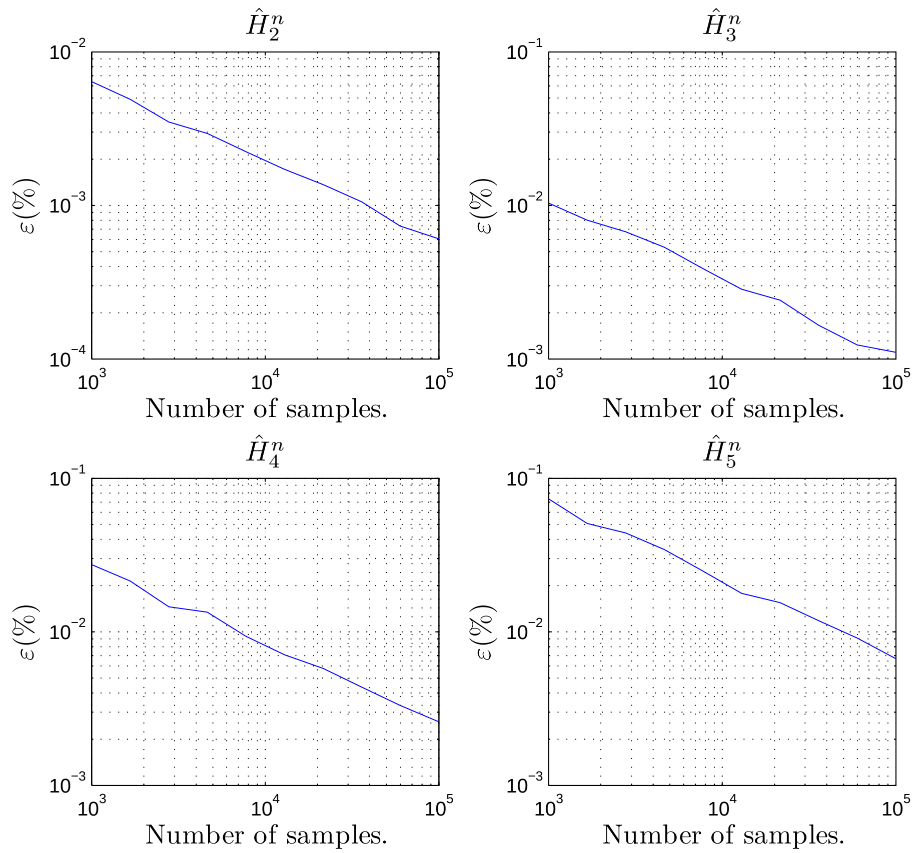

Figure 6.7: Semi-consistency of the estimates of the Markov parameters obtained from the FIR model with the Hammerstein nonlinearities $\mathcal{N}_1(u) = \sinh(u)$ and $\mathcal{N}_2(u) = u^3$.

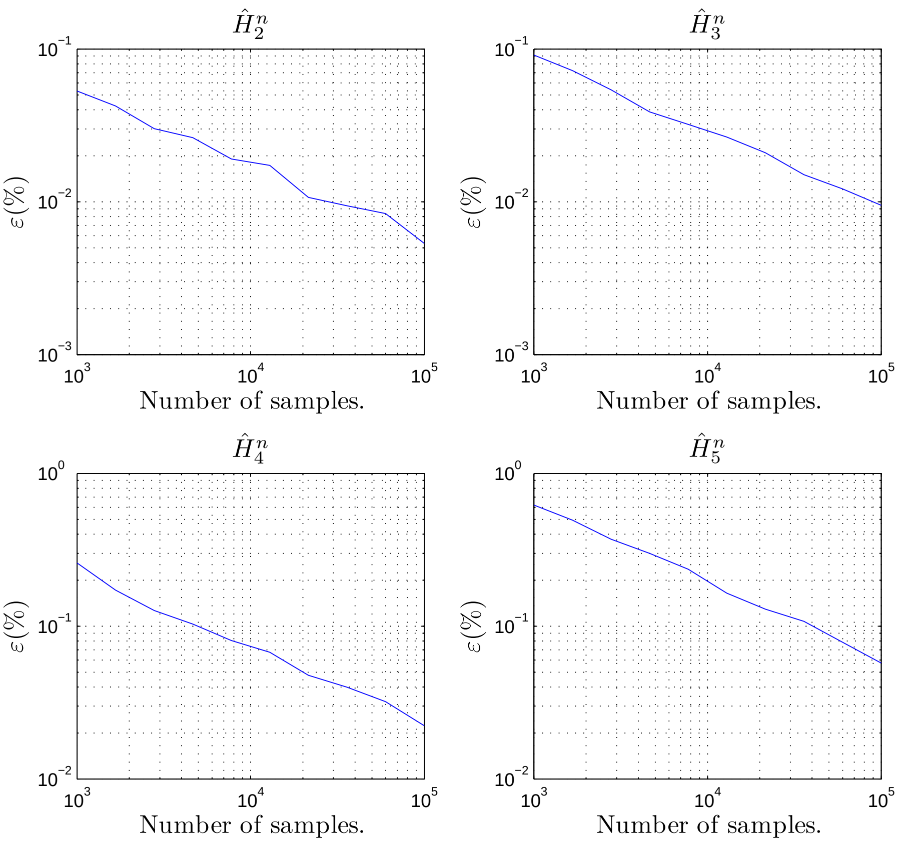

Figure 6.8: Semi-consistency of the estimates of the Markov parameters obtained from the FIR model with the Hammerstein nonlinearities $\mathcal{N}_1(u) = \text{sign}(u)$, $\mathcal{N}_2(u) = e^u$.

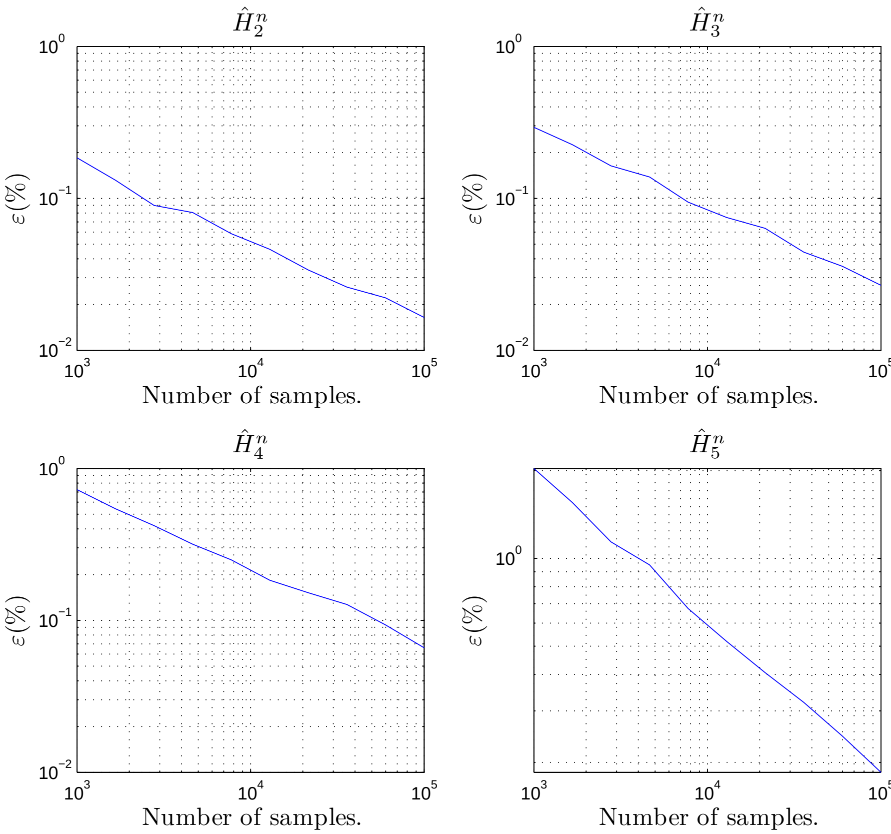

Figure 6.9: Semi-consistency of the estimates of the Markov parameters obtained from the FIR model with the Hammerstein nonlinearities $\mathcal{N}_1(u) = u^2e^u - M(u^2e^u)$ and $\mathcal{N}_2(u) = \sin(u) + 10$.

CHAPTER 7

Conclusions and Future Work

7.1 Conclusions

Transmissibility estimates are traditionally obtained using frequency-domain methods. We showed that ignoring the initial conditions and transient effects can degrade the transmissibility estimates in the frequency-domain. Moreover, we showed that frequency-domain identification techniques cannot give exact estimates with finite data sets. Therefore, we developed continuous time-domain models of transmissibility operators, which model the response of a subset of sensors based on the response of the remaining sensors without knowledge of the driving input. We showed that transmissibility operators account for nonzero initial conditions as well as cancellation of the common factor occurring in the underlying state space model. Moreover, we showed that transmissibility operators are independent of both the initial condition and inputs of the underlying system, which is assumed to be time-invariant.

We showed that transmissibility operators may be unstable, noncausal, and of unknown order. Therefore, to facilitate system identification, we considered a class of models that can approximate transmissibility operators with these properties. This class of models consists of noncausal FIR models based on a truncated Laurent expansion. Connection between transmissibility operators and unstable systems in closed loop was shown. Noncausal FIR models can be used for closed-loop identification of open-loop-unstable plants. To identify the noncausal plant model we delayed the measured output relative to the measured input. We found that the identified noncausal FIR model approximates the Laurent series of the plant inside the annulus of analyticity lying between the disk of stable poles and the punctured plane of unstable poles.

An estimate of the transmissibility operator between pairs or sets of sensors was used to detect faults in the presence of unknown external excitation. The ability to detect faults by exploiting the presence of unknown external excitation is the key difference between this approach and techniques based on residual generation. Transmissibility-based fault detection depends on various assumptions. In particular, this approach assumes that the plant itself does not change between the identification and validation data sets and that the location of the external excitation does not change. By using the estimated transmissibility operator, the residual between pairs or sets of sensors can be used to detect a sensor failure or a change in the dynamics of a system.

We developed a time-domain framework for SISO and MIMO transmissibilities that accounts for nonzero initial conditions for both force-driven and displacement-driven structures. It was shown that if the locations of the forces and prescribed displacements are identical, then the SISO and MIMO force- and displacement-driven transmissibilities are equal.

Finally, since S2SID depends on cancellation of the input, this approach does not extend to nonlinear systems. However, we showed that for the case of a two-output Hammerstein system, the least squares estimate of the PTF is consistent, that is, asymptotically correct, despite the presence of the nonlinearities.

7.2 Future Work

We showed that transmissibility operator between pairs or sets of sensors can be used to detect sensor faults in the presence of unknown external excitation. The characteristic shape of the residual of the transmissibility can be used to infer the type of sensor failure. However, this approach does not identify which sensor has failed. This problem is left for future research. Moreover, the current approach assumes that the underlying system is linear, time invariant and that the location of the external excitation does not change. Future research may consider the effect of nonlinearities as well as extensions to the case of moving loads.

The research objective for S2SID is to develop a technique for obtaining the most accurate estimate of the transmissibility operator possible in the presence of noise on all sensors. System identification with noisy input and output data is a standard problem in system identification known as errors-in-variables (EIV) identification. Since S2SID is based on sensor measurements, all of which may be noisy, the EIV problem is especially relevant. The literature on this problem is extensive [105–108].

Although the idea of a PTF may be unconventional, we have reason to believe that there may be a deep connection between PTF's and behavioral models developed by J. Willems [109, 110]. Unlike traditional input-output techniques, behavioral models focus on terminals and ports, which provide the mechanism for interconnecting physical systems without assigning the attributes of "input" or "output."

Unlike behavioral models, the development of PTF's begins with a causal state space description from which an excitation-independent PTF is derived. At the same time, behavioral models have not been used to provide a time-domain framework for transmissibilities or for sensor fault detection and diagnosis (note that [111] is not based on behaviors in the sense of Willems). Therefore, future research may investigate connections between PTF's and behavioral models and, in so doing, deepen the foundations of both areas. S2SID can also benefit from system identification techniques developed within the context of behavioral models [112], including conditions that guarantee identifiability and persistency [113, 114].

APPENDICES

APPENDIX A

Cancellation of the Common Factor $\delta(\mathbf{p})$ for SISO Transmissibility Operators

Lemmas A.1-A.5 concern SISO transmissibility operators. Lemma A.1 is used to prove Lemma A.2, which in turn is used to prove Lemma A.3 and Lemma A.4. Lemmas A.3 and A.4 are used to prove Lemma A.5, which in turn is used to prove Theorem 1.

Assume that $m = 1$ and $p = 2$ and let (2.20), (2.21), and (2.22) be written as

$$\Gamma_{\mathrm{i}}(\mathbf{p}) = \sum_{j=0}^{n} \beta_{\mathrm{i},j}\mathbf{p}^j, \quad \Gamma_{\mathrm{o}}(\mathbf{p}) = \sum_{j=0}^{n} \beta_{\mathrm{o},j}\mathbf{p}^j,$$
$$\delta(\mathbf{p}) = \mathbf{p}^n + \sum_{j=0}^{n-1} \alpha_j \mathbf{p}^j,$$

respectively, where $\beta_{\mathrm{i},n} = D_{\mathrm{i}}$ and $\beta_{\mathrm{o},n} = D_{\mathrm{o}}$.

Define

$$\alpha \triangleq \begin{bmatrix} \alpha_0 & \alpha_1 & \cdots & \alpha_{n-1} \end{bmatrix}^{\mathrm{T}},$$

$$A_{\mathrm{c}} \triangleq \begin{bmatrix} 0_{(n-1)\times 1} & I_{n-1} \\ \multicolumn{2}{c}{-\alpha^{\mathrm{T}}} \end{bmatrix}, \quad B_{\mathrm{c}} \triangleq e_n^{\mathrm{T}},$$

$$C_{\mathrm{c,i}} \triangleq \begin{bmatrix} \beta_{\mathrm{i},0} & \beta_{\mathrm{i},1} & \cdots & \beta_{\mathrm{i},n-1} \end{bmatrix} - \beta_{\mathrm{i},n}\alpha^{\mathrm{T}},$$

$$C_{\mathrm{c,o}} \triangleq \begin{bmatrix} \beta_{\mathrm{o},0} & \beta_{\mathrm{o},1} & \cdots & \beta_{\mathrm{o},n-1} \end{bmatrix} - \beta_{\mathrm{o},n}\alpha^{\mathrm{T}},$$

where e_i is the i^{th} column of I_n. Consider the state space representation

$$\dot{x}_{\mathrm{c}} = A_{\mathrm{c}} x_{\mathrm{c}} + B_{\mathrm{c}} u, \tag{A.1}$$

$$y_{\mathrm{i}} = C_{\mathrm{c,i}} x_{\mathrm{c}} + D_{\mathrm{i}} u, \tag{A.2}$$

$$y_{\mathrm{o}} = C_{\mathrm{c,o}} x_{\mathrm{c}} + D_{\mathrm{o}} u. \tag{A.3}$$

Note that

$$\Gamma_{\mathrm{i}}(\mathbf{p}) = C_{\mathrm{c,i}} \mathrm{adj}(\mathbf{p}I - A_{\mathrm{c}}) B_c + D_{\mathrm{i}} \delta(\mathbf{p}), \tag{A.4}$$

$$\Gamma_{\mathrm{o}}(\mathbf{p}) = C_{\mathrm{c,o}} \mathrm{adj}(\mathbf{p}I - A_{\mathrm{c}}) B_c + D_{\mathrm{o}} \delta(\mathbf{p}), \tag{A.5}$$

$$\delta(\mathbf{p}) = \det(\mathbf{p}I - A_{\mathrm{c}}), \tag{A.6}$$

That is, (2.23) and (2.24) can be represented by (A.1), (A.2) and (A.1), (A.3), respectively.

For all $j = 0, \ldots, n$, define

$$\chi_j \triangleq \begin{cases} e_{j+1}^{\mathrm{T}}, & 0 \le j \le n-1, \\ -\alpha^{\mathrm{T}}, & j = n. \end{cases}$$

For all $i, j = 0, \ldots, n$, define $f_{i,j} \triangleq \chi_i A_{\mathrm{c}}^j$.

Lemma A.1. For all $i, j = 0, \ldots, n$, $f_{i,j} = f_{j,i}$.

Proof. Note that

$$A_{\mathrm{c}}^j = \begin{cases} I_n, & j = 0, \\ E_j, & 1 \le j \le n-1, \\ \Delta_n, & j = n, \end{cases}$$

where,

$$E_j \triangleq \begin{bmatrix} e_{j+1}^{\mathrm{T}} \\ \vdots \\ e_n^{\mathrm{T}} \\ \Delta_j \end{bmatrix} \in \mathbb{R}^{n \times n}, \quad \Delta_j \triangleq \begin{bmatrix} -\alpha^{\mathrm{T}} \\ \vdots \\ -\alpha^{\mathrm{T}} A_{\mathrm{c}}^{j-1} \end{bmatrix} \in \mathbb{R}^{j \times n}.$$

For all $i = j$, the result holds. For all $0 \le i \le n-1$ and $j = n$, $f_{i,n} = e_{i+1}^{\mathrm{T}} A_{\mathrm{c}}^n = -\alpha^{\mathrm{T}} A_{\mathrm{c}}^i = f_{n,i}$. For all $0 \le i \le n-j-1$ and $0 \le j \le n-1$, $f_{i,j} = e_{i+1}^{\mathrm{T}} E_j = e_{i+j+1}^{\mathrm{T}} = e_{j+1}^{\mathrm{T}} E_i = f_{j,i}$. Finally, for all $n-j \le i \le n-1$ and $0 \le j \le n-1$, $f_{i,j} = e_{i+1}^{\mathrm{T}} E_j = -\alpha^{\mathrm{T}} A_{\mathrm{c}}^{i+j-n} = e_{j+1}^{\mathrm{T}} E_i = f_{j,i}$. $\square$

Define

$$\gamma_{\mathrm{i}}(\mathbf{p}) \triangleq C_{\mathrm{c,i}} \mathrm{adj}(\mathbf{p} I - A_{\mathrm{c}}) B_{\mathrm{c}}, \tag{A.7}$$

$$\gamma_{\mathrm{o}}(\mathbf{p}) \triangleq C_{\mathrm{c,o}} \mathrm{adj}(\mathbf{p} I - A_{\mathrm{c}}) B_{\mathrm{c}}. \tag{A.8}$$

Then, (2.20), (2.21) can be written as

$$\Gamma_{\mathrm{i}}(\mathbf{p}) = \gamma_{\mathrm{i}}(\mathbf{p}) + D_{\mathrm{i}} \delta(\mathbf{p}), \tag{A.9}$$

$$\Gamma_{\mathrm{o}}(\mathbf{p}) = \gamma_{\mathrm{o}}(\mathbf{p}) + D_{\mathrm{o}} \delta(\mathbf{p}). \tag{A.10}$$

Lemma A.2. For all $t \geq 0$,

$$\Gamma_{\mathrm{o}}(\mathbf{p})C_{\mathrm{c,i}}e^{A_{\mathrm{c}}t} = \Gamma_{\mathrm{i}}(\mathbf{p})C_{\mathrm{c,o}}e^{A_{\mathrm{c}}t}, \tag{A.11}$$

$$\gamma_{\mathrm{o}}(\mathbf{p})C_{\mathrm{c,i}}e^{A_{\mathrm{c}}t} = \gamma_{\mathrm{i}}(\mathbf{p})C_{\mathrm{c,o}}e^{A_{\mathrm{c}}t}. \tag{A.12}$$

Proof. Using Lemma A.1 we have

$$\begin{aligned}
\Gamma_{\mathrm{o}}(\mathbf{p})C_{\mathrm{c,i}}e^{A_{\mathrm{c}}t} &= \sum_{i=0}^{n} \beta_{\mathrm{o},i}\mathbf{p}^{i}C_{\mathrm{c,i}}e^{A_{\mathrm{c}}t} \\
&= \sum_{i=0}^{n} \beta_{o,i}C_{\mathrm{c,i}}A_{\mathrm{c}}^{i}e^{A_{\mathrm{c}}t} \\
&= \sum_{i=0}^{n} \beta_{o,i}\left[\sum_{j=0}^{n-1}\left(\beta_{\mathrm{i},j}e_{j+1}^{\mathrm{T}}\right) - \beta_{\mathrm{i},n}\alpha^{\mathrm{T}}\right]A_{\mathrm{c}}^{i}e^{A_{\mathrm{c}}t} \\
&= \sum_{i=0}^{n}\sum_{j=0}^{n} \beta_{\mathrm{o},i}\beta_{\mathrm{i},j}f_{j,i}e^{A_{\mathrm{c}}t} \\
&= \sum_{j=0}^{n}\sum_{i=0}^{n} \beta_{\mathrm{i},j}\beta_{\mathrm{o},i}f_{i,j}e^{A_{\mathrm{c}}t} \\
&= \sum_{j=0}^{n} \beta_{\mathrm{i},j}\left[\sum_{i=0}^{n-1}\left(\beta_{\mathrm{o},i}e_{i+1}^{\mathrm{T}}\right) - \beta_{\mathrm{o},n}\alpha^{\mathrm{T}}\right]A_{\mathrm{c}}^{j}e^{A_{\mathrm{c}}t} \\
&= \sum_{j=0}^{n} \beta_{\mathrm{i},j}\mathbf{p}^{j}C_{\mathrm{c,o}}e^{A_{\mathrm{c}}t} \\
&= \Gamma_{\mathrm{i}}(\mathbf{p})C_{\mathrm{c,o}}e^{A_{\mathrm{c}}t},
\end{aligned}$$

which proves (A.11). To prove (A.12) note that

$$\begin{aligned}
\Gamma_{\mathrm{o}}(\mathbf{p})C_{\mathrm{c,i}}e^{A_{\mathrm{c}}t} &= (\gamma_{\mathrm{o}}(\mathbf{p}) + D_{\mathrm{o}}\delta(\mathbf{p}))C_{\mathrm{c,i}}e^{A_{\mathrm{c}}t} \\
&= \gamma_{\mathrm{o}}(\mathbf{p})C_{\mathrm{c,i}}e^{A_{\mathrm{c}}t} + D_{\mathrm{o}}C_{\mathrm{c,i}}\delta(A_{\mathrm{c}})e^{A_{\mathrm{c}}t} \\
&= \gamma_{\mathrm{o}}(\mathbf{p})C_{\mathrm{c,i}}e^{A_{\mathrm{c}}t},
\end{aligned} \tag{A.13}$$

where δ is the characteristic polynomial of A_{c}, and thus $\delta(A_{\mathrm{c}}) = 0_{n\times n}$. Similarly,

$$\Gamma_{\mathrm{i}}(\mathbf{p})C_{\mathrm{c,o}}e^{A_{\mathrm{c}}t} = \gamma_{\mathrm{i}}(\mathbf{p})C_{\mathrm{c,o}}e^{A_{\mathrm{c}}t}. \tag{A.14}$$

Using (A.11), (A.13) and (A.14) yield (A.12). $\square$

Define

$$y_{\mathrm{i,free}}(t) \triangleq C_{\mathrm{c,i}}e^{A_{\mathrm{c}}t}x_{\mathrm{c}_0}, \quad y_{\mathrm{o,free}}(t) \triangleq C_{\mathrm{c,o}}e^{A_{\mathrm{c}}t}x_{\mathrm{c}_0}. \tag{A.15}$$

Lemma A.3. For all $t \geq 0$,

$$\Gamma_{\mathrm{o}}(\mathbf{p})y_{\mathrm{i,free}}(t) = \Gamma_{\mathrm{i}}(\mathbf{p})y_{\mathrm{o,free}}(t). \tag{A.16}$$

Proof. Using (A.11) of Lemma A.2 we have

$$\begin{aligned}\Gamma_{\mathrm{o}}(\mathbf{p})y_{\mathrm{i,free}}(t) &= \Gamma_{\mathrm{o}}(\mathbf{p})C_{\mathrm{c,i}}e^{A_{\mathrm{c}}t}x_{\mathrm{c}_0}\\ &= \Gamma_{\mathrm{i}}(\mathbf{p})C_{\mathrm{c,o}}e^{A_{\mathrm{c}}t}x_{\mathrm{c}_0} = \Gamma_{\mathrm{i}}(\mathbf{p})y_{\mathrm{o,free}}(t).\end{aligned}$$ $\square$

Define

$$y_{\mathrm{i,forced}}(t) \triangleq \int_0^t C_{\mathrm{c,i}}e^{A_{\mathrm{c}}(t-\tau)}B_{\mathrm{c}}u(\tau)\mathrm{d}\tau + D_{\mathrm{i}}u(t), \tag{A.17}$$

$$y_{\mathrm{o,forced}}(t) \triangleq \int_0^t C_{\mathrm{c,o}}e^{A_{\mathrm{c}}(t-\tau)}B_{\mathrm{c}}u(\tau)\mathrm{d}\tau + D_{\mathrm{o}}u(t). \tag{A.18}$$

Lemma A.4. For all $t \geq 0$,

$$\Gamma_{\mathrm{o}}(\mathbf{p}) y_{\mathrm{i,forced}}(t) = \Gamma_{\mathrm{i}}(\mathbf{p}) y_{\mathrm{o,forced}}(t). \tag{A.19}$$

Proof.

$$\begin{aligned}
\Gamma_{\mathrm{o}}(\mathbf{p}) y_{\mathrm{i,forced}}(t) &= \Gamma_{\mathrm{o}}(\mathbf{p}) \int_0^t C_{\mathrm{c,i}} e^{A_{\mathrm{c}}(t-\tau)} B_{\mathrm{c}} u(\tau) d\tau + D_{\mathrm{i}} \Gamma_{\mathrm{o}}(\mathbf{p}) u(t) \\
&= \Gamma_{\mathrm{o}}(\mathbf{p}) \int_0^t C_{\mathrm{c,i}} e^{A_{\mathrm{c}}(t-\tau)} B_{\mathrm{c}} u(\tau) d\tau + D_{\mathrm{i}} \delta(\mathbf{p}) y_{\mathrm{o,forced}}(t) \\
&= \gamma_{\mathrm{o}}(\mathbf{p}) \int_0^t C_{\mathrm{c,i}} e^{A_{\mathrm{c}}(t-\tau)} B_{\mathrm{c}} u(\tau) d\tau + D_{\mathrm{o}} \delta(\mathbf{p}) \int_0^t C_{\mathrm{c,i}} e^{A_{\mathrm{c}}(t-\tau)} B u(\tau) d\tau \\
&\quad + D_{\mathrm{i}} \delta(\mathbf{p}) \int_0^t C_{\mathrm{c,o}} e^{A_{\mathrm{c}}(t-\tau)} B_{\mathrm{c}} u(\tau) d\tau + D_{\mathrm{i}} D_{\mathrm{o}} \delta(\mathbf{p}) u(t).
\end{aligned} \tag{A.20}$$

Using (A.12) of Lemma A.2 we have

$$\begin{aligned}
\gamma_{\mathrm{o}}(\mathbf{p}) \int_0^t C_{\mathrm{c,i}} e^{A_{\mathrm{c}}(t-\tau)} B_{\mathrm{c}} u(\tau) d\tau &= \gamma_{\mathrm{o}}(\mathbf{p}) C_{\mathrm{c,i}} e^{A_{\mathrm{c}} t} \int_0^t e^{-A_{\mathrm{c}} \tau} B_{\mathrm{c}} u(\tau) d\tau \\
&= \gamma_{\mathrm{i}}(\mathbf{p}) C_{\mathrm{c,o}} e^{A_{\mathrm{c}} t} \int_0^t e^{-A_{\mathrm{c}} \tau} B_{\mathrm{c}} u(\tau) d\tau \\
&= \gamma_{\mathrm{i}}(\mathbf{p}) \int_0^t C_{\mathrm{c,o}} e^{A_{\mathrm{c}}(t-\tau)} B_{\mathrm{c}} u(\tau) d\tau.
\end{aligned} \tag{A.21}$$

Using (A.17), (A.18), and (A.21), (A.20) can be written as

$$\begin{aligned}
\Gamma_{\mathrm{o}}(\mathbf{p})y_{\mathrm{i,forced}}(t) &= \gamma_{\mathrm{i}}(\mathbf{p})\int_0^t C_{\mathrm{c,o}}e^{A_{\mathrm{c}}(t-\tau)}B_{\mathrm{c}}u(\tau)d\tau + D_{\mathrm{o}}\delta(\mathbf{p})\int_0^t C_{\mathrm{c,i}}e^{A_{\mathrm{c}}(t-\tau)}B_{\mathrm{c}}u(\tau)d\tau \\
&\quad + D_{\mathrm{i}}\delta(\mathbf{p})\int_0^t C_{\mathrm{c,o}}e^{A_{\mathrm{c}}(t-\tau)}B_{\mathrm{c}}u(\tau)d\tau + D_{\mathrm{i}}D_{\mathrm{o}}\delta(\mathbf{p})u(t) \\
&= \Gamma_{\mathrm{i}}(\mathbf{p})\int_0^t C_{\mathrm{c,o}}e^{A_{\mathrm{c}}(t-\tau)}B_{\mathrm{c}}u(\tau)d\tau + D_{\mathrm{o}}\delta(\mathbf{p})y_{\mathrm{i,forced}}(t) \\
&= \Gamma_{\mathrm{i}}(\mathbf{p})\int_0^t C_{\mathrm{c,o}}e^{A_{\mathrm{c}}(t-\tau)}B_{\mathrm{c}}u(\tau)d\tau + D_{\mathrm{o}}\Gamma_{\mathrm{i}}(\mathbf{p})u(t) \\
&= \Gamma_{\mathrm{i}}(\mathbf{p})y_{\mathrm{o,forced}}(t). \qquad \square
\end{aligned}$$

Lemma A.5. For all $t \geq 0$,

$$\Gamma_{\mathrm{o}}(\mathbf{p})y_{\mathrm{i}}(t) = \Gamma_{\mathrm{i}}(\mathbf{p})y_{\mathrm{o}}(t). \tag{A.22}$$

Proof. Using Lemmas A.3 and A.4

$$\begin{aligned}
\Gamma_{\mathrm{o}}(\mathbf{p})y_{\mathrm{i}}(t) &= \Gamma_{\mathrm{o}}(\mathbf{p})y_{\mathrm{i,free}}(t) + \Gamma_{\mathrm{o}}(\mathbf{p})y_{\mathrm{i,forced}}(t) \\
&= \Gamma_{\mathrm{i}}(\mathbf{p})y_{\mathrm{o,free}}(t) + \Gamma_{\mathrm{i}}(\mathbf{p})y_{\mathrm{o,forced}}(t) \\
&= \Gamma_{\mathrm{i}}(\mathbf{p})y_{\mathrm{o}}(t). \qquad \square
\end{aligned}$$

APPENDIX B

Adjugate Identities

Let $A \in \mathbb{C}^{n\times n}$, let $A^{\mathrm{A}} \in \mathbb{C}^{n\times n}$ denote the adjugate of A, and let $A_{(i,j)} \in \mathbb{C}$ denote the (i,j) entry of A. Let $D \triangleq \{k_1,\ldots,k_d\}$ where $1 \le d \le n-2$ and $k_i \in \{1,\ldots,n\}$ for all $i = 1,\ldots,d$. Let $A_{[D,\cdot]} \in \mathbb{C}^{(n-d)\times n}$ denote A with rows $k_1,\ldots,k_d$ removed and let $A_{[D,D]} \in \mathbb{C}^{(n-d)\times(n-d)}$ denote A with rows $k_1,\ldots,k_d$ removed and columns $k_1,\ldots,k_d$ removed. Finally, Let $e_{D,n} \triangleq [e_{k_1,n} \ \ldots \ e_{k_d,n}] \in \mathbb{C}^{n\times d}$ where $e_{i,n} \in \mathbb{C}^n$ denotes the i^{th} unit vector. The following proposition is used in the proof of Theorem 5.

Proposition B.1. For all $i \in \{1,\ldots,n\}$,

$$\left[(A^{\mathrm{A}})_{[i,\cdot]} + (A_{[i,i]})^{\mathrm{A}} A_{[i,\cdot]}\right] e_{i,n} = 0_{(n-1)\times 1}. \tag{B.1}$$

Proof. See [115]. □

Next, let $C \in \mathbb{C}^{d\times n}$ and define $R \triangleq A^{\mathrm{A}} e_{D,n} \in \mathbb{C}^{n\times d}$ and $S \triangleq (A_{[D,D]})^{\mathrm{A}} A_{[D,\cdot]} e_{D,\mathrm{n}} \in \mathbb{C}^{(n-d)\times d}$. Let $CR \in \mathbb{C}^{d\times d}$ and $C_{[\cdot,D]}S \in \mathbb{C}^{d\times d}$ be nonsingular where $C_{[\cdot,D]} \in \mathbb{C}^{d\times(n-d)}$ denotes C with columns $k_1,\ldots,k_d$ removed. The following proposition is used in the proof of Theorem 6.

Proposition B.2.

$$I_{n,[D,\cdot]}R(CR)^{-1} = S(C_{[\cdot,D]}S)^{-1}, \tag{B.2}$$

where $I_n \in \mathbb{C}^{n\times n}$ is the identity matrix and $I_{n,[D,\cdot]} \in \mathbb{C}^{(n-d)\times n}$ denotes I_n with rows $k_1, \ldots, k_d$ removed.

BIBLIOGRAPHY

BIBLIOGRAPHY

[1] A. J. Brzezinski, S. L. Kukreja, J. Ni, and D. S. Bernstein, "Sensor-only fault detection using pseudo transfer function identification," in *Proc. Amer. Contr. Conf.*, Baltimore, MD, June 2010, pp. 5433–5438.

[2] A. M. D'Amato, A. J. Brzezinski, M. S. Holzel, J. Ni, and D. S. Bernstein, "Sensor-only noncausal blind identification of pseudo transfer functions," *Proc. IFAC Symp. Sys. Ident. (SYSID)*, pp. 1698–1703, July 2009.

[3] K. F. Aljanaideh, B. J. Coffer, D. S. Dionne, S. L. Kukreja, and D. S. Bernstein, "Sensor-to-sensor identification for the SOFIA testbed," *AIAA Guid. Nav. Contr. Conf.,* Minneapolis, MN, AIAA-2012-4814-770, Aug. 2012.

[4] W. Weijtjens, G. De Sitter, C. Devriendt, and P. Guillaume, "Operational modal parameter estimation of MIMO systems using transmissibility functions," *Automatica*, vol. 50, no. 2, pp. 559–564, 2014.

[5] E. Zhang, R. Pintelon, and J. Schoukens, "Errors-in-variables identification of dynamic systems excited by arbitrary non-white input," *Automatica*, vol. 49, no. 10, pp. 3032–3041, 2013.

[6] D. Hrovat, "Survey of advanced suspension developments and related optimal control applications," *Automatica*, vol. 33, no. 10, pp. 1781–1817, 1997.

[7] A. P. Urgueira, R. A. Almeida, and N. M. Maia, "On the use of the transmissibility concept for the evaluation of frequency response functions," *Mech. Sys. & Sig. Proc.*, vol. 25, no. 3, pp. 940–951, 2011.

[8] C. Devriendt and P. Guillaume, "Identification of modal parameters from transmissibility measurements," *J. Sound & Vib.*, vol. 314, pp. 343–356, 2008.

[9] T. J. Johnson and D. E. Adams, "Transmissibility as a differential indicator of structural damage," *J. Vib. & Acous.*, vol. 124, no. 4, pp. 634–641, 2002.

[10] S. Chesné and A. Deraemaeker, "Damage localization using transmissibility functions: A critical review," *Mech. Sys. & Sig. Proc.*, vol. 38, no. 2, pp. 569–584, 2013.

[11] N. Maia, J. Silva, and A. Ribeiro, "The transmissibility concept in multi-degree-of-freedom systems," *Mech. Sys. & Sig. Proc.*, vol. 15, no. 1, pp. 129–137, 2001.

[12] P. Gajdatsy, K. Janssens, W. Desmet, and H. Van Der Auweraer, "Application of the transmissibility concept in transfer path analysis," *Mech. Sys. & Sig. Proc.*, vol. 24, no. 7, pp. 1963–1976, 2010.

[13] C. W. Da Silva, *Vibration: Fundamentals and Practice.* CRC press, 2007.

[14] C. Devriendt, F. Presezniak, G. De Sitter, K. Vanbrabant, T. De Troyer, S. Vanlanduit, and P. Guillaume, "Structural health monitoring in changing operational conditions using tranmissibility measurements," *Shock & Vib.*, vol. 17, no. 4, pp. 651–675, 2010.

[15] R. Sampaio, N. Maia, A. Ribeiro, and J. Silva, "Damage detection using the transmissibility concept," in *Proc. Int. Cong. Sound Vib. (ICSV), Copenhagen*, 1999, pp. 2559–2568.

[16] ——, "Transmissibility techniques for damage detection," in *Proc. Int. Modal Analysis Conf. (IMAC)*, vol. 2, 2001, pp. 1524–1527.

[17] C. Devriendt, G. De Sitter, and P. Guillaume, "An operational modal analysis approach based on parametrically identified multivariable transmissibilities," *Mech. Sys. & Sig. Proc.*, vol. 24, no. 5, pp. 1250–1259, 2010.

[18] G. Steenackers, C. Devriendt, and P. Guillaume, "On the use of transmissibility measurements for finite element model updating," *J. Sound & Vib.*, vol. 303, no. 3, pp. 707–722, 2007.

[19] A. Ribeiro, N. Maia, and J. Silva, "Experimental evaluation of the transmissibility matrix," *Proc. Int. Modal Analysis Conf. (IMAC), Kissimmee (FL), USA*, pp. 1126–1129, 1999.

[20] ——, "Response prediction from a reduced set of known responses using the transmissibility," in *Proc. Int. Modal Analysis Conf. (IMAC), San Antonio*, 2000, pp. 425–427.

[21] A. Ribeiro, J. Silva, N. Maia, and M. Fontul, "Transmissibility in structural coupling," in *Proc. Int. Conf. on Noise Vib. Eng. (ISMA), Leuven*, 2004.

[22] A. Ribeiro, J. Silva, and N. Maia, "On the generalization of the transmissibility concept," *Mech. Sys. & Sig. Proc.*, vol. 14, no. 1, pp. 29–35, 2000.

[23] C. Devriendt, G. De Sitter, S. Vanlanduit, and P. Guillaume, "Operational modal analysis in the presence of harmonic excitations by the use of transmissibility measurements," *Mech. Sys. & Sig. Proc.*, vol. 23, no. 3, pp. 621–635, 2009.

[24] N. Maia, A. Urgueira, and R. Almeida, "Whys and wherefores of transmissibility," *Vibration Analysis and Control,* Chapter 10, edited by: F. Beltran-Carbajal (Ed.), pp. 197–216, 2011.

[25] M. Norton and D. Karczub, *Fundamentals of Noise and Vibration Analysis for Engineers*. Cambridge University Press, 2003.

[26] E. E. Ungar, "Equality of force and motion transmissibilities," *J. Acous. Soc. of America*, vol. 90, pp. 596–597, 1991.

[27] R. Pintelon and J. Schoukens, *System Identification: A Frequency Domain Approach*. John Wiley & Sons, Ltd., 2012.

[28] A. J. Brzezinski, S. L. Kukreja, J. Ni, and D. S. Bernstein, "Identification of sensor-only MIMO pseudo transfer functions," in *Proc. Conf. Dec. Contr.*, Orlando, FL, Dec. 2011, pp. 1698–1703.

[29] A. M. D'Amato, A. J. Brzezinski, M. S. Holzel, J. Ni, and D. S. Bernstein, "Sensor-only noncausal blind identification of pseudo transfer functions," in *Proc. IFAC Symp. Sys. Ident. (SYSID)*, Saint-Malo, France, July 2009, pp. 1698–1703.

[30] K. F. Aljanaideh, B. J. Coffer, and D. S. Bernstein, "Closed-loop identification of unstable systems using noncausal FIR models," in *Proc. Amer. Contr. Conf.*, Washington, DC, 2013, pp. 1669–1674.

[31] I. Hwang, S. Kim, Y. Kim, and C. E. Seah, "A survey of fault detection, isolation, and reconfiguration methods," *IEEE Trans. Contr. Sys. Tech.*, vol. 18, no. 3, pp. 636–653, 2010.

[32] R. Doraiswami, M. Stevenson, and C. Diduch, *Identification of Physical Systems: Applications to Condition Monitoring, Fault Diagnosis, Soft Sensor, and Controller Design*. Wiley, 2014.

[33] R. Isermann, "Process fault detection based on modeling and estimation methods-a survey," *Automatica*, vol. 20, no. 4, pp. 387–404, 1984.

[34] ——, *Fault-Diagnosis Systems: An Introduction from Fault Detection to Fault Tolerance*. Springer, 2006.

[35] ——, *Fault-Diagnosis Applications: Model-Based Condition Monitoring: Actuators, Drives, Machinery, Plants, Sensors, and Fault-tolerant Systems*. Springer, 2011.

[36] J. J. Gertler, *Fault Detection and Diagnosis in Engineering Systems*. New York, NY: Marcel Dekker Inc., 1998.

[37] V. Venkatasubramanian, R. Rengaswamy, K. Yin, and S. N. Kavuri, "A review of process fault detection and diagnosis: Part I: Quantitative model-based methods," *Comput. Chem. Eng.*, vol. 27, pp. 293–311, 2003.

[38] R. Isermann, "Supervision, fault-detection and fault-diagnosis methods - an introduction," *Contr. Eng. Practice*, vol. 5, no. 5, pp. 639–652, 1997.

[39] R. J. Patton and J. Chen, "Observer-based fault detection and isolation: robustness and applications," *Contr. Eng. Practice*, vol. 5, no. 5, pp. 671–682, 1997.

[40] S. X. Ding, *Model-Based Fault Diagnosis Techniques: Design Schemes, Algorithms, and Tools*. Berlin-Heidelberg, DE: Springer-Verlag, 2008.

[41] L. H. Chiang, E. L. Russell, and R. D. Braatz, *Fault Detection and Diagnosis in Industrial Systems*. London, UK: Springer-Verlag, 2001.

[42] P. M. Frank and X. Ding, "Survey of robust residual generation and evaluation methods in observer-based fault detection systems," *Journal of Process Control*, vol. 7, no. 6, pp. 403–424, 1997.

[43] R. Rengaswamy and V. Venkatasubramanian, "A fast training neural network and its updation for incipient fault detection and diagnosis," *Computers and Chemical Engineering*, vol. 24, no. 2–7, pp. 431–437, 2000.

[44] R. J. Patton, P. M. Frank, and R. N. Clark, *Issues of Fault Diagnosis for Dynamic Systems*. London, UK: Springer-Verlag, 2000.

[45] R. Rajamani and A. Ganguli, "Sensor fault diagnostics for a class of non-linear systems using linear matrix inequalities," *Int. J. Contr.*, vol. 77, no. 10, pp. 920–930, 2004.

[46] P. M. Frank, "Fault diagnosis in dynamic systems using analytical and knowledge-based redundancy: A survey and some new results," *Automatica*, vol. 26, no. 3, pp. 459–474, 1990.

[47] E. Chow and A. S. Willsky, "Analytical redundancy and the design of robust failure detection systems," *IEEE Trans. Autom. Contr.*, vol. 29, no. 7, pp. 603–614, 1984.

[48] M. Staroswiecki and G. Comtet-Varga, "Analytical redundancy relations for fault detection and isolation in algebraic dynamic systems," *Automatica*, vol. 37, no. 5, pp. 687–699, 2001.

[49] J. Chen and R. J. Patton, *Robust Model-Based Fault Diagnosis for Dynamic Systems*. Springer, 2012.

[50] X. Zhang, T. Parisini, and M. M. Polycarpou, "Sensor bias fault isolation in a class of nonlinear systems," *IEEE Trans. Autom. Contr.*, vol. 50, no. 3, pp. 370–376, 2005.

[51] K. F. Martin, "A review by discussion of condition monitoring and fault diagnosis in machine tools," *Int. J. Mach. Tools Manu.*, vol. 34, no. 4, pp. 527–551, 1994.

[52] R. Kothamasu, S. H. Huang, and W. H. VerDuin, "System health monitoring and prognostics - a review of current paradigms and practices," *Int. J. Adv. Manuf. Tech.*, vol. 28, pp. 1012–1024, 2006.

[53] R. Yan and R. X. Gao, "Approximate entropy as a diagnostic tool for machine health monitoring," *Mech. Sys. & Sig. Proc.*, vol. 21, no. 2, pp. 824–839, 2007.

[54] O. Basir and X. Yuan, "Engine fault diagnosis based on multi-sensor information fusion using Dempster-Shafer evidence theory," *Inform. Fusion*, vol. 8, no. 4, pp. 379–386, 2007.

[55] A. J. Brzezinski, L. Li, X. Qiao, and J. Ni, "A new method for grinder dressing fault mitigation using real time peak detection," *Int. J. Adv. Manuf. Tech.*, vol. 45, pp. 470–480, 2009.

[56] M. Basseville, "Detecting changes in signals and systems - a survey," *Automatica*, vol. 24, no. 3, pp. 309–326, 1988.

[57] ——, "On-board component fault detection and isolation using the statistical local approach," *Automatica*, vol. 34, no. 11, pp. 1391–1416, 1998.

[58] M. Basseville and I. V. Nikiforov, *Detection of Abrupt Changes - Theory and Application.* Englewood Cliffs, NJ, USA: Prentice-Hall, 1993.

[59] C. Lo, J. P. Lynch, and M. Liu, "Distributed reference-free fault detection method for autonomous wireless sensor networks," *IEEE Sensors J.*, vol. 13, no. 5, pp. 2009–2019, 2013.

[60] ——, "Pair-wise reference-free fault detection in wireless sensor networks," in *ACM/IEEE Int. Conf. Inform. Proc. Sensor Networks*, 2012, pp. 117–118.

[61] ——, "Reference-free detection of spike faults in wireless sensor networks," in *Int. Symp. Resilient Contr. Sys. (ISRCS)*, 2011, pp. 148–153.

[62] K. F. Aljanaideh and D. S. Bernstein, "Time-domain analysis of sensor-to-sensor transmissibility operators," *Automatica*, vol. 53, pp. 312–319, 2015.

[63] ——, "Aircraft sensor health monitoring based on transmissibility operators," *J. Guid. Contr. Dyn.*, to appear.

[64] ——, "Time-domain analysis of motion transmissibilities in force-driven and displacement-driven structures," *J. Sound & Vib.*, vol. 347, pp. 169–183, 2015.

[65] A. M. Murch, "Flight control system architecture for the NASA AirSTAR flight test infrastructure," *AIAA Guid. Nav. Contr. Conf.,* Honolulu, HI, AIAA-2008-6990, Aug. 2008.

[66] T. L. Jordan and R. M. Bailey, "NASA Langley's AirSTAR testbed–a subscale flight test capability for flight dynamics and control system experiments," *AIAA Guid. Nav. Contr. Conf.,* Honolulu, HI, AIAA-2008-6660, Aug. 2008.

[67] K. F. Aljanaideh, A. A. Ali, M. H. Holzel, S. Kukreja, and D. S. Bernstein, "Sensor-to-sensor identification of Hammerstein systems," in *Proc. Conf. Dec. Contr.*, Maui, HI, Dec. 2012, pp. 2846–2851.

[68] A. J. Brzezinski, "Output-only techniques for fault detection," Ph.D. dissertation, University of Michigan, 2011.

[69] I. Gustavsson, L. Ljung, and T. Söderström, "Identification of processes in closed loop-identifiability and accuracy aspects," *Automatica*, vol. 13, pp. 59–75, 1977.

[70] H. Hjalmarsson, M. Gevers, and F. de Bruyne, "For model-based control design, closed-loop identification gives better performance," *Automatica*, vol. 32, no. 12, pp. 1659–1673, 1996.

[71] I. Landau, "Identification in closed-loop: a powerful design tool (better design models, simple controllers)," *Contr. Eng. Practice*, vol. 9, no. 1, p. 5165, 2001.

[72] T. Söderström and P. Stoica, "Instrumental variable methods for system identification," *Circ. Sys. Sig. Proc.*, vol. 21, no. 1, pp. 1–9, 2002.

[73] ——, "Comparison of some instrumental variable methods-consistency and accuracy aspects," *Automatica*, vol. 17, no. 1, pp. 101–115, 1981.

[74] P. Stoica, T. Söderström, and B. Friedlander, "Optimal instrumental variable estimates of the AR parameters of an ARMA process," *IEEE Trans. Autom. Contr.*, vol. 30, no. 11, pp. 1066–1074, 1985.

[75] L. Ljung, "Prediction error estimation methods," *Circ. Sys. Sig. Proc.*, vol. 21, no. 1, pp. 11–21, 2002.

[76] U. Forssell and L. Ljung, "Closed-loop identification revisited," *Automatica*, vol. 35, no. 7, pp. 1215–1241, 1999.

[77] B. Ho and R. Kalman, "Efficient construction of linear state variable models from input/output functions," *Regelungstechnik*, vol. 14, pp. 545–548, 1966.

[78] J. N. Juang, *Applied System Identification.* Upper Saddle River, NJ: Prentice-Hall, 1993.

[79] B. Recht, M. Fazel, and P. A. Parrilo, "Guaranteed minimum-rank solutions of linear matrix equations via nuclear norm minimization," *SIAM Review*, vol. 52, no. 3, pp. 471–501, 2010.

[80] R. S. Smith, "Frequency domain subspace identification using nuclear norm minimization and Hankel matrix realizations," *IEEE Trans. Autom. Contr.*, vol. 59, no. 11, pp. 2886–2896, 2014.

[81] K. Usevich and I. Markovsky, "Structured low-rank approximation as a rational function minimization," in *Proc. IFAC Symp. Sys. Ident. (SYSID)*, Brussels, Belgium, July 2012, pp. 722–727.

[82] I. Markovsky, "How effective is the nuclear norm heuristic in solving data approximation problems?" in *Proc. IFAC Symp. Sys. Ident. (SYSID)*, Brussels, Belgium, July 2012, pp. 316–321.

[83] H. Hjalmarsson, J. S. Welsh, and C. R. Rojas, "Identification of box-jenkins models using structured ARX models and nuclear norm relaxation," in *Proc. IFAC Symp. Sys. Ident. (SYSID)*, Brussels, Belgium, July 2012, pp. 322–327.

[84] U. Forssell and L. Ljung, "Identification of unstable systems using output error and Box-Jenkins model structures," *IEEE Trans. Autom. Contr.*, vol. 45, no. 1, pp. 137–141, 2000.

[85] H. Hjalmarsson and U. Forssell, "Maximum likelihood estimation of models with unstable dynamics and non-minimum phase noise zeros," in *Proc. IFAC World Congress*, Beijing, China, 1999, pp. 13–18.

[86] U. Forssell and L. Ljung, "A projection method for closed-loop identification," *IEEE Trans. Autom. Contr.*, vol. 45, no. 11, pp. 2101–2106, 2000.

[87] M. Gilson and P. Van den Hof, "Instrumental variable methods for closed-loop system identification," *Automatica*, vol. 41, no. 2, pp. 241–249, 2005.

[88] M. Verhaegen, "Application of a subspace model identification technique to identify LTI systems operating in closed-loop," *Automatica*, vol. 29, no. 4, pp. 1027–1040, 1993.

[89] L. Ljung and T. McKelvey, "Subspace identification from closed-loop data," *Signal processing*, vol. 52, no. 2, pp. 209–215, 1996.

[90] Y. Yamamoto, B. D. Anderson, M. Nagahara, and Y. Koyanagi, "Optimizing FIR approximation for discrete-time IIR filters," *Signal Processing Letters, IEEE*, vol. 10, no. 9, pp. 273–276, 2003.

[91] L. Chai, J. Zhang, C. Zhang, and E. Mosca, "From IIR to FIR digital MIMO models: a constructive hankel norm approximation method," in *Proc. IEEE Conf. Dec. Contr. and Europ. Contr. Conf.*, 2005, pp. 5893–5898.

[92] V. Cerone, D. Piga, and D. Regruto, "Fixed-order FIR approximation of linear systems from quantized input and output data," *Systems & Control Letters*, vol. 62, no. 12, pp. 1136–1142, 2013.

[93] E. Gross, M. Tomizuka, and W. Messner, "Cancellation of discrete time unstable zeros by feedforward control," *J. Dyn. Sys. Meas. Contr.*, vol. 116, no. 1, pp. 33–38, 1994.

[94] L. Hunt, G. Meyer, and R. Su, "Noncausal inverses for linear systems," *IEEE Trans. Autom. Contr.*, vol. 41, no. 4, pp. 608–611, 1996.

[95] B. Widrow and E. Walach, *Adaptive Inverse Control.* Upper Saddle River, NJ: Prentice Hall, 1996.

[96] M. Tomizuka, "Zero phase error tracking algorithm for digital control," *J. Dyn. Sys. Meas. Contr.*, vol. 109, pp. 65–68, 1987.

[97] B. P. Rigney, L. Y. Pao, and D. A. Lawrence, "Nonminimum phase dynamic inversion for settle time applications," *IEEE Trans. Contr. Sys. Tech.*, vol. 17, no. 5, pp. 989–1005, 2009.

[98] T. W. Gamelin, *Complex Analysis.* Springer New York, 2001.

[99] T. Söderström and P. Stoica, *Instrumental variable methods for system identification.* Springer-Verlag Berlin, 1983.

[100] L. Ljung, *System Identification: Theory for the User, 2nd ed.* Upper Saddle River, NJ: Prentice-Hall, 1999.

[101] A. W. Leissa and M. S. Qatu, *Vibration of Continuous Systems.* McGraw Hill, 2011.

[102] K. F. Aljanaideh, A. Xie, S. L. Kukreja, F. Hogan, J. R. Forbes, and D. S. Bernstein, "Numerical and experimental comparison of time-domain techniques for transmissibility identification with multiple drivers," unpublished.

[103] P. Lancaster, *Lambda-Matrices and Vibrating Systems.* Dover Publications, 2002.

[104] C. W. de Silva, *Vibration: Fundamentals and Practice.* CRC press, 2006.

[105] T. Söderström, "Errors-in-variables methods in system identification," *Automatica*, vol. 43, pp. 939–958, 2007.

[106] J. Argüero and G. C. Goodwin, "Identifiability of errors in variables dynamical systems," *Automatica*, vol. 44, pp. 371–382, 2008.

[107] W. X. Zheng, "A Bias Correction Method for Identification of Linear Dynamic Errors-in-Variables Models," *IEEE Trans. Autom. Contr.*, vol. 47, no. 7, pp. 1142–1147, 2002.

[108] P. Stoica and T. Söderström, "Bias correction in least-squares identification," *Int. J. Contr.*, vol. 35, pp. 449–457, 1982.

[109] J. C. Willems, "The behavioral approach to open and interconnected systems," *IEEE Contr. Sys. Mag.*, vol. 27, no. 6, pp. 46–99, 2007.

[110] J. W. Polderman and J. C. Willems, *Exact and Approximate Modeling of Linear Systems: A Behavioral Approach.* Springer, 1998.

[111] B. H. Krogh and L. E. Holloway, "Fault detection and diagnosis in manufacturing systems: a behavioral model approach," in *Proc. Rensselaer Second Int. Conf. Comp. Integ. Mfg.*, 1990, pp. 252–259.

[112] I. Markovsky, J. C. Willems, S. van Huffel, and B. de Moor, *Exact and Approximate Modeling of Linear Systems: A Behavioral Approach.* SIAM, 2008.

[113] M. S. Holzel, A. A. Ali, and D. S. Bernstein, "Input richness and zero buffering in time-domain identification," in *Proc. Amer. Contr. Conf.*, Baltimore, MD, June 2010, pp. 2929–2934.

[114] J. C. Willems, P. Rapisarda, I. Markovsky, and B. L. M. De Moor, "A note on persistency of excitation," *Sys. Contr. Lett.*, vol. 77, no. 4, pp. 325–329, 2005.

[115] K. F. Aljanaideh and D. S. Bernstein, "An adjugate identity," *IMAGE*, vol. 51, p. 35, 2013.